

UNCLASSIFIED

AD NUMBER
AD861165
NEW LIMITATION CHANGE
TO Approved for public release, distribution unlimited
FROM Distribution authorized to U.S. Gov't. agencies and their contractors; Administrative/Operational Use; JUN 1969. Other requests shall be referred to Air Force Flight Dynamics Lab., Attn: FDTC, Wright-Patterson AFB, OH 45433.
AUTHORITY
Air Force Flight Dynamics Lab ltr dtd 4 Feb 1974

THIS PAGE IS UNCLASSIFIED

AFFDL-TR-69-43
VOLUME 1

AD 861165

INVESTIGATION OF JOINTS IN ADVANCED FIBROUS COMPOSITES FOR AIRCRAFT STRUCTURES

JOINT AND ATTACHMENT INVESTIGATION
VOLUME I. TECHNICAL DISCUSSION AND SUMMARY

G. M. Lehman
A. V. Hawley
et al.

TECHNICAL REPORT AFFDL-TR-69-43, VOLUME I
JUNE 1969

This document is subject to special export controls, and each transmittal to foreign governments or foreign nationals may be made only with prior approval of AFFDL (FDTC) Wright-Patterson AFB, Ohio 45433.

Structures Division
Air Force Flight Dynamics Laboratory
Wright-Patterson Air Force Base, Ohio

Reproduced by the
CLEARINGHOUSE
for Federal Scientific & Technical
Information Springfield Va. 22151

NOV 12 1969

240

**INVESTIGATION OF JOINTS
IN ADVANCED FIBROUS COMPOSITES FOR
AIRCRAFT STRUCTURES**

**JOINT AND ATTACHMENT INVESTIGATION
VOLUME I. TECHNICAL DISCUSSION AND SUMMARY**

**G. M. Lehman
A. V. Hawley
et al.**

This document is subject to special export controls, and each transmittal to foreign governments or foreign nationals may be made only with prior approval of AFFDL (FDTC) Wright-Patterson AFB, Ohio 45433.

FOREWORD

This report was prepared by the McDonnell Douglas Corporation, Douglas Aircraft Company, Long Beach, California, under the terms of Air Force Contract F33615-67-C-1582. It is the final report of work completed between 25 April 1967 and 28 March 1969. The contract was administered by the Structures Division, Air Force Flight Dynamics Laboratory (AFFDL). Mr. Elden E. Zink was the Program Manager for AFFDL.

The project was conducted under the direction of Mr. G. E. Anderson, Director of Structural Engineering, Mr. D. G. Smillie, Supervisor of Structural Development and Advanced Design in the Structural Engineering Section, and Mr. D. S. Warren, Supervisor of Research and Development/Analysis Methods in the Structural Mechanics Section. Mr. G. M. Lehman of the Structural Engineering Section was Technical Director. The following Douglas personnel were the principal contributors to the program:

Mr. A. V. Hawley, Structural Design and Weight Analysis

Mr. W. J. Richards and Dr. R. Teodosiadis, Discrete Element Structural Analysis


Mr. M. Ashizawa, Analysis of Parametric Trends

Mr. R. J. Palmer, Materials Research and Process Engineering

Mr. M. Marcoux and Mr. D. E. McCay, Instrumentation and Testing

The manuscript was released for publication in April 1969. The report was prepared under Douglas Report DAC-68498.

This technical report has been reviewed and is approved.



Philip A. Parmley
Chief, Advanced Composites Branch
Structures Division

ABSTRACT

To find ways of efficiently joining composite materials, an investigation was undertaken to explore design philosophies, identify parameters affecting joint strength and life, establish design approaches for aircraft applications, and compile design data. Properties of boron and S-994 fiber glass laminates using Narmco 5505 resin were determined in tension, compression, in-plane shear, interlaminar shear, and pin-bearing tests. In comparing six adhesives, a nylon-epoxy adhesive was found to have the best combination of shear strength and ductility (except in scarf joints, where ductility is less important). Ultimate strength and fatigue data were determined for a variety of bonded joint and bolted joint test specimens. The bonded joint concepts included single and double lap, stepped lap, scarf, and variable stiffness adhesive joints. The bolted joint concepts included laminates with plain holes and with reinforced holes using either composite or steel shim reinforcing or steel bushings. The effects of design parameter variations on joint failure modes were determined, and parametric strength trends were analyzed. Design parameters influencing bonded joint failures the most were adherend and adhesive properties (strength and stiffness), lap length, adherend thickness, and fiber orientation adjacent to the adhesive. Bolted joint failures were most affected by laminate strength and stiffness, edge distance, fastener pitch, laminate thickness, and fastener diameter. A combination bolted-bonded joint performed better than joints employing either bolting or bonding separately because of a fundamental change in failure mode caused by adhesive/fastener interaction. Bolted joints in composites were found to be lighter than comparable joints in aluminum. However, on a weight-efficiency basis, bonded joints were found to be superior to bolted joints. Scarf and stepped lap bonded joints, although more difficult to fabricate than lap joints, showed promise of achieving any desired strength with only a small weight penalty. Linear discrete element analyses (DEA), corrected empirically for adhesive plasticity and nonlinear DEA, yielded good test-theory correlation for bonded joint strength. Load-deformation characteristics of bolted joints were not adequately predicted with linear DEA. Fabrication techniques of the specimens are described in the Appendix. Volume I. Quality control data, engineering drawings of the test specimens, and experimental data plots or tabulations for individual test results are presented in Volume II.

TABLE OF CONTENTS

	Page
I INTRODUCTION	1
II SUMMARY	3
MATERIAL PROPERTIES	3
JOINT INVESTIGATION	3
WEIGHT STUDIES	5
ANALYTICAL STUDIES	5
DESIGN TECHNOLOGY	6
III MATERIAL PROPERTIES	9
LAMINATE PROPERTIES	9
Theoretical Properties	13
Tension Tests	15
Compression Tests	21
In-plane Shear Tests	25
Interlaminar Shear Tests	30
Pin-Bearing Tests	30
ADHESIVE PROPERTIES	40
Adhesive Double Lap Shear Tests	44
Adhesive Flatwise Tension Tests	44
Torsion Ring Shear Tests	49
IV JOINT INVESTIGATION	63
STATIC LOAD TESTS	66
Bonded Joints	67
Bolted Joints	83
PHENOMENOLOGICAL TRENDS IN JOINT FAILURES	96
Bonded Joints	96
Bolted Joints	96
ANALYSIS OF PARAMETRIC TRENDS IN JOINT STRENGTH	104
Bonded Joints	108
Bolted Joints	120
FATIGUE TESTS	140
Screening Tests	140
S-n Data Tests	145
V WEIGHT STUDIES	162
BONDED JOINTS	163
BOLTED JOINTS	170
PANEL and JOINT WEIGHT COMPARISONS	177
VI ANALYTICAL STUDIES	183
LINEAR ANALYSIS OF BONDED JOINTS	183
LINEAR ANALYSIS OF BOLTED JOINTS	189
NONLINEAR ANALYSIS OF BONDED JOINTS	190
Joint Idealization	190
Nonlinear Material Representations	190
Method of Analysis	191
Test-Theory Correlation	193

TABLE OF CONTENTS (Continued)

	Page
VII CONCLUSIONS	195
APPENDIXES	
I. SPECIMEN FABRICATION PROCEDURES	198
II. SHELL 951 ADHESIVE CHARACTERISTICS	215
REFERENCES.....	217
BIBLIOGRAPHY.....	219

LIST OF ILLUSTRATIONS

Figures	Page
1. Basic Filament Patterns for Tension, Shear, and Bearing Specimens	11
2. Basic Filament Patterns for Compression Specimens	11
3. Photomicrograph of Specimen with Al_2O_3/AlN Whiskers at 2 Percent Resin Weight.	12
4. Tensile Test Setup	16
5. Tensile Failure of Specimen Z4824842-507	18
6. Tension Stress-Strain Diagram for Specimen Z4824842-1	19
7. Comparisons of Control Specimen Test Results	20
8. Test Setup and Instrumentation for Compression Specimens.	22
9. Compression Specimen Failures	22
10. Compression Stress-Strain Diagram for Specimen Z3824818-501.	24
11. In-plane Shear Test Setup	26
12. Typical In-plane Shear Specimen Failure	27
13. Shear Stress-Strain Diagram for Specimen Z3824843-1	29
14. Test Setup for Interlaminar Shear Test	31
15. Interlaminar Shear Strength – Whiskered Specimens	33
16. Test Setup for Pin-Bearing Test	34
17. Schematic of Test Fixture for Pin-Bearing Tests	36
18. Hole Condition in Pin-Bearing Specimens Before Test	38
19. Load-Deformation Curves for Pin-Bearing Specimens Z3824815-1	39
20. Load-Deformation Characteristics of Pin-Bearing Specimen Z3824815-1	41
21. Bearing and Shear-Out Failure Specimen Z3824815-1	41

LIST OF ILLUSTRATIONS (Continued)

Figures		Page
22.	Bearing Failure in Z3824815 Specimens	42
23.	Pin Joint Ultimate Strengths - Whiskered Specimens	43
24.	Adhesive Specimen Dimensions	45
25.	Test Setup for Adhesive Double Lap Shear Specimens	46
26.	Enlarged Photo of Bond Failure on Z4824824 - 507 Specimen . .	48
27.	Enlarged Photo of Bond Failure on Z4824824-1 Specimen	48
28.	Adhesive Flatwise Tension Test Setup	50
29.	Typical Core Failure - Adhesive Flatwise Tension Specimen . .	51
30.	Torsion Ring Adhesive Specimen Test Fixture Assembly	53
31.	Torsion Ring Adhesive Test Setup	55
32.	Adhesive Torsion Ring Shear Specimen Bonding Fixture	57
33.	Torsion Ring Adhesive Specimen Failure	60
34.	Bonded Joint Design Concepts	64
35.	Bolted Joint Design Concepts	65
36.	Summary of Repeated Joint Test Results	69
37.	Single Lap Bonded Joint Strength	72
38.	Double Lap Bonded Joint Strength	74
39.	Effect of Et Ratio on Double Lap Adhesive Joint Strength	77
40.	Adhesive Shear Stress-Strain Curves	79
41.	Interfacial Failures in Simple Lap Adhesive Joints (L/t = 12.5)	97
42.	Interlaminar Shear Failure in Adhesive Joints	98

LIST OF ILLUSTRATIONS (Continued)

Figures	Page
43. Adherend Tension Failure in Simple Lap Adhesive Joints ($L/t = 25-50$)	99
44. Boron/Aluminum Eight-Step Lap Joint Failure	99
45. Shear-Out Failures of Bolted Joints ($D = 3/16$ inch)	100
46. Shear-Out Failures of Bushed Holes (Bushing Diameter = $3/16$ inch)	101
47. Combined Tension and Shear-Out Failure of Bolted Joints ($D = 3/16$ inch)	102
48. Bearing Failure of Fiber Glass Laminate ($D = 3/16$ inch)	103
49. Delamination of Fiber Glass Specimen	105
50. Bolted Joint Shear Stress at Failure as a Function of Edge Distance	105
51. Bolted-Bonded Joint Failure in Tension and Interlaminar Shear ($L/t = 12.5$, $e/D = 4$)	106
52. Shim-Reinforced Joint Failure - Complex Mode ($e/D = 1.45$)	107
53. Shim-Reinforced Joint Failure - Tension at Base of Shims	107
54. Bonded Joint Strength Parameter versus Overlap Length - Boron Laminate to Aluminum Alloy	111
55. Bonded Joint Strength Parameter versus Overlap Length - Fiber Glass Laminate to Aluminum Alloy	112
56. Adhesive Shear Strength versus Thickness of Adherend	114
57. Trend of τ_{Test}/τ_{Avg} versus Adhesive Thickness	115
58. Adhesive Shear Strength versus Adhesive Modulus	116
59. Bonded Joint Strength Parameter versus Extensional Stiffness Ratio	118
60. Average Adhesive Shear Stress versus Extensional Stiffness Ratio	119

LIST OF ILLUSTRATIONS (Continued)

Figures	Page
61. Bonded Joint Normalized Strength Parameter versus Overlap Length	12i
62. Bonded Joint – Predicted versus Actual Strength	122
63. Bolted Joint Strength versus Edge Distance Ratio.	124
64. Bolted Joint Strength versus Edge Distance Ratio Normalized for t/D Ratio.	126
65. Bolted Joint Bearing Stress versus Edge Distance Ratio	127
66. Bolted Joint Strength Ratio versus s/D Ratio – $0 < (e/D) < 4$. . .	130
67. Bolted Joint Strength Ratio versus t/D Ratio – $0 < (e/D) < 4$. . .	130
68. Coefficient K_{ϕ} versus Orientation Angle, ϕ – $0 < (e/D) < 4$. . .	132
69. Coefficient K_p versus Percentage of Plies at ± 45 degrees – $0 < (e/D) < 4$	133
70. Coefficient $K_{t/D}$ versus t/D Ratio $(e/D) > 4$	135
71. Coefficient K_p versus Percentage of Plies at ± 45 degrees $(e/D) > 4$	135
72. Bolted Joint Allowable Shear-Out Stress.	136
73. Bolted Joint Correction Factors for s/D and t/D Effects	137
74. Bolted Joint – Predicted versus Actual Strength.	139
75. Fatigue Test Setup	142
76. Bolted Joint – Hole Conditions After Fatigue Cycling.	146
77. Fatigue Performance Comparisons for Composite to Aluminum Alloy Joints.	148
78. Fatigue Data for Adhesive Scarf Joints.	155
79. Fatigue Data for Adhesive Double Lap Joints.	155
80. Fatigue Strength for Adhesive Joints	156

LIST OF ILLUSTRATIONS (Continued)

Figures	Page
81. Fatigue Failure of Aluminum Alloy Adherend – 1.5-Inch Adhesive Scarf Joint.	158
82. Fatigue Failure in Adhesive and Interlaminar Shear – 1.5-Inch Adhesive Scarf Joint.	159
83. Fatigue Failure in Adhesive and Interlaminar Shear – 1-Inch Adhesive Scarf Joint	159
84. Fatigue Failure in Adhesive – 2-Inch Double Lap Joint (Pattern A)	160
85. Fatigue Failure in Interlaminar Shear – 2-Inch Double Lap Joint (Pattern B)	160
86. Fatigue Failure in Adhesive – 1-Inch Double Lap Joint (Pattern A)	161
87. Boron-to-Aluminum Bonded Joint Strengths	165
88. Average Adhesive Shear Stress in Bonded Lap Joints	166
89. Bonded Lap Joint Strengths	166
90. Weight Increments for Bonded Lap Joints	167
91. Weight Increments for Bonded Scarf Joints	169
92. Weight Increments for Stepped Lap Joints in Boron Panels.	172
93. Comparison of Weight Increments for Stepped Lap Joints	173
94. Weight Increments for Bonded Joints in Boron Panels.	174
95. Strength-Weight Relationships for Bolted Joints.	175
96. Weight Increments for Bolted Joints in Boron Panels – Balanced Design.	178
97. Weight Increments for Bolted Single Lap Joints in Boron Panels.	178
98. Weight Increments for Bolted Double Lap Joints in Boron Panels.	179

LIST OF ILLUSTRATIONS (Continued)

		Page
Figures		
99.	Total Weight Comparisons for Panels and Joints	179
100.	Weight of Boron Panels with Double Lap Bolted Joints at Various Load Intensities	180
101.	Comparison of Boron and Aluminum Bolted Joints	180
102.	Idealized Two-Step Lap Joint	185
103.	Stress Distribution in the Adhesive of a Two-Step Lap Joint	186
104.	Fatigue Strength of Bonded Joints	187
105.	Ultimate Strength of Double Lap Bonded Joints	188
106.	Bolted Joint Analysis	189
107.	Nonlinear Material Representation	192
108.	Nonlinear Analysis - 1/2-Inch Double Lap Joint.	194
Appendix Figures		
I-1	Controlled Resin Bleed Layup Detail	200
I-2	Composite - Reinforced Panel Layup Ready for Autoclave Cure	204
I-3	Steel Shim - Reinforced Panel Layup Ready for Autoclave Cure	204
I-4	Edge Details for Steel Shim-Reinforced Specimen	206
I-5	Scarf Joint Machining Setup	206
I-6	Scarf Joint Specimen Details After Machining	207
I-7	Profiling Setup for Fatigue Specimen Machining	208
I-8	Fatigue Specimen Partially Machined.	209
I-9	Finished Details for Stepped-Lap Fatigue Specimen	209
I-10	Edge Detail of Steel Shim Reinforced Fatigue Specimen.	211

LIST OF ILLUSTRATIONS (Continued)

Appendix Figure		Page
I-11	Details of Hole Drilled with Carbide Bit in Steel Shim-Reinforced Specimen.	211
I-12.	Details of Hole Drilled with High Speed Steel Drill in Steel Shim - Reinforced Specimen	212
I-13.	Adhesive Joint Bonding Tools	214

LIST OF TABLES

Table		Page
I	Whisker Dimensional Properties	12
II	Unidirectional Laminate Properties.	14
III	Summary of Theoretical and Experimental Tension Properties	17
IV	Summary of Theoretical and Experimental Compression Properties	23
V	Summary of Theoretical and Experimental In-plane Shear Properties	28
VI	Interlaminar Shear Test Results	32
VII	Pin-Bearing Test Results	37
VIII	Adhesive Double Lap Shear Test Results	47
IX	Adhesive Flatwise Tension Test Results	52
X	Adhesive Torsion Ring Shear Test Results	58
XI	Summary of Shear Strengths for Shell 951 Adhesive with Variations in Strain Rate and Bond-Line Thickness	62
XII	Joint Specimen Laminate Patterns	65
XIII	Summary of Single Lap Bonded Joint Test Results	71
XIV	Summary of Double Lap Bonded Joint Test Results	73
XV	Summary of Double Lap Bonded Joint Test Results for Various Et Ratios	76
XVI	Summary of Double Lap Bonded Joint Test Results with Variable Stiffness Adhesive	80
XVII	Summary of Scarf Bonded Joint Test Results	82
XVIII	Summary of Stepped Lap Bonded Joint Test Results	84
XIX	Summary of Single Lap Bolted Joint Test Results	87
XX	Summary of Double Lap Bolted Joint Test Results	88

LIST OF TABLES (Continued)

Table	Page
XXI Summary of Double Lap Bolted Joint Test Results – Bushed Holes.	89
XXII Summary of Composite-Reinforced Bolted Joint Test Results.	90
XXIII Summary of Shim-Reinforced Bolted Joint Test Results	92
XXIV Summary of Double Lap Bolted and Bonded Joint Test Results	95
XXV Temperature Rise in Fatigue Specimens.	141
XXVI Summary of Bonded Joint Fatigue Test Results	143
XXVII Summary of Bolted Joint Fatigue Test Results.	144
XXVIII Summary of S-n Data Fatigue Test Variables	150
XXIX Summary of Static Test Results on Fatigue Specimen Joint Configurations	151
XXX Summary of S-n Fatigue Data	152
XXXI Material Properties and Allowable Stresses Used in Weight Studies.	164
XXXII Linear Matrix Computer Analyses - Bonded Joints	184
XXXIII Nonlinear Stress-Strain Characteristics Used in Bonded Joint Analysis	192
Appendix	
Table	Page
II-1 Strength Characteristics for Shell 951 Adhesive.	216

LIST OF SYMBOLS

D	bolt diameter	inches
e	edge distance	inches
E	modulus of elasticity	psi
f	applied stress	psi
F	allowable stress	psi
G	shear modulus	psi
L	lap length	inches
N_s	number of shims in reinforced joint	
p	bolt pitch = 2s	inches
P	adhesive strength per bonding surface, load	pounds per inch
s	distance from bolt centerline to side of specimen	inches
S	shear stress	psi
t	laminate thickness	inches
t_a	adhesive thickness	inches
t_l	laminate thickness at reinforced edge	inches
t_s	shim thickness in reinforced joint	inches
Y	shear strain	inches per inch
δ	deflection	inches
ϵ	normal strain	inches per inch
θ	scarf angle	degrees
ρ	density	pounds per cubic inch
σ	normal stress	psi
μ	Poisson's ratio	
τ	shear stress	psi
ϕ	angle between laminate axis, L, and load axis, x	degrees

Subscripts

a adhesive

br bearing

L, T, Z axes along, transverse, and normal to monolayer

so shear out

t, c, s tension, compression, and shear respectively

th tension at section through fastener holes

x, y axes along and transverse to load line

SECTION I

INTRODUCTION

Airframe applications of composite material structures have been investigated for a number of years. With the availability of advanced fibrous reinforcements of high specific strengths and moduli, airframe weight reductions of about 40 percent were frequently predicted. However, as actual development programs were completed it became apparent that weight savings from increased strength and stiffness could be easily offset by weight losses resulting from inefficient joining of these materials.

Eliminating structural joints and cutouts (which are special joint cases if stressed covers are used) is impractical in present-day aircraft because of the requirements for manufacturing breaks, assembly and equipment access, and replacement of damaged structures. Indeed, the trend in modern aircraft is to increase requirements for equipment access as electronic and other subsystems become more complex.

Design policies for joining metal elements are based on years of experience with isotropic and homogeneous materials. Optimum joint proportions have evolved from essentially invariant relationships between tension, shear, and bearing strengths (and moduli) of structural metals. Because of the fundamental differences in properties caused by the anisotropy and inhomogeneity of composites, design policies that were evolved for metal joints cannot be applied directly to composites. The basic strength and modulus relationships on which metal joint technology is based are variables in the composite structural design process. Thus, the design of optimum joints in reinforced composites must start in the selection and arrangement of the basic material constituents.

The objectives of this investigation were to explore design philosophies for joining composite elements, identify the fundamental parameters controlling the strength and life characteristics of such joints, establish design approaches for efficient joining of composites under conditions representative of primary aircraft structures, and compile data for design of efficient structures using these materials.

These objectives were met through a program involving design, fabrication, test, and evaluation of a variety of design data and joint specimens (1438 in all) covering the following variables:

- Material Properties
 - Laminates
 - Adhesives
- Design Concepts
 - Bonded
 - Bolted
 - Combination

- **Joined Materials**

 - Boron-Reinforced Laminates**

 - Fiber glass-Reinforced Laminates**

 - Laminates to Metals**

- **Design Parameters**

 - Laminate Patterns**

 - Joint Geometries**

- **Load Conditions**

 - Static Strength**

 - Constant-Amplitude Fatigue**

Significant variables not investigated in the study include resin and void content variations, elevated and reduced temperature effects, environmental effects, creep phenomena, joint compression and in-plane shear properties, and reversing load fatigue properties.

Results of the study are reported in two volumes:

 - Volume I - Technical Discussion and Summary**

 - Volume II - Engineering Drawings and Experimental Data**

This volume contains the technical discussions and a brief summary (Section II) of the significant results of the program. The balance of the document contains description of test setups and summaries of test results for laminate and adhesive properties, and for bonded and/or bolted joint specimens. Phenomenological trends in joint failures and parametric trends in joint design are analyzed. Optimum joint designs and weight studies are discussed, and the results of linear and nonlinear joint strength analyses are reported. Conclusions drawn from the investigation are presented. Manufacturing and processing techniques used in the fabrication of the specimens are described in the appendix. Quality control data, complete engineering drawings, and individual test results are presented under separate cover in Volume II.

SECTION II

SUMMARY

MATERIAL PROPERTIES

Laminate and adhesive properties were investigated by testing and by theoretical analysis. Fundamental strength and elastic property data specimens were designed in laminates with selected fiber patterns. Specimens were fabricated from boron and S-994 fiber glass filaments in an epoxy resin matrix. Unidirectional laminate data, primarily from published literature, were used to determine the basic monolayer values that were required as input data for theoretical strength and stiffness analyses. The analytical approach, which was based on the distortional energy criterion of failure, predicted initial and final failures for the laminates used in the data specimens when subjected to tension, compression, and shear loading. The agreement between test results and theoretical predictions was good for tension and compression cases, but shear stiffnesses consistently exceeded predicted values. Pin-bearing and interlaminar shear properties were also investigated in the test program. Two pin-bearing specimen configurations were loaded and unloaded in 1000-pound increments to indicate elastic recovery and hysteresis effects of the laminates.

Selected laminates were tested in compression, interlaminar shear, and pin-bearing with small amounts (1 to 2 percent by weight) of whisker additives in the resin. Very high strengths (exceeding predicted values) were achieved with compressive cylinders containing whiskers. Interlaminar shear strength was upgraded from 5 to 24 percent, depending on the laminate pattern and the type and amount of whiskers. No improvement was apparent in pin-bearing specimens, but the shear-out mode of failure was precluded in some cases.

Six adhesives were compared by testing 1/2-inch double lap specimens, by flatwise tension tests on sandwich specimens, and in a torsional ring fixture designed and developed as part of the program. The torsional ring test was devised for the determination of shear strength and modulus of the adhesives, and the salient design features of the fixture are described. The strongest adhesive in this test was AF130, an epoxy novalac with an average ultimate shear stress of 9970 psi, but with brittle failure characteristics. Shell 951, a nylon epoxy adhesive, was selected for further investigation. Its average ultimate shear strength was 6100 psi, but because of its considerable ductility it proved to be nearly five times as strong as AF130 in the lap tests. The effects of bond line thickness and strain rate were investigated for Shell 951 adhesive using the torsional ring test.

JOINT INVESTIGATION

A test program was conducted on boron and fiber glass flat laminate specimens of bonded and bolted joint configurations. The basic types of bonded joints included single and double lap, scarf, and stepped lap designs.

External scarf and variable adhesive joint configurations were also tested, but these did not show significant strength advantages over the other joint types. Variations in fiber pattern and lap length were investigated for composite-to-composite and composite-to-metal joints. Metal adherends included aluminum, titanium, and stainless steel. The strongest joints were obtained when the extensional stiffnesses of the adherends on each side of the joint were equal. Double lap joints were more than twice as strong as single lap joints of the same lap length because the symmetry of the configuration reduced bending in the adherends and transverse stresses across the adhesive. The bending in the adherends did not prevent them from approaching their maximum tensile strengths at failure. The scarf and stepped lap configurations have the capability of scale-up to transmit a load of any magnitude, providing that the lap length is not restricted. The scarf joint was difficult to fabricate, especially in achieving a high quality bond of uniform thickness. The stepped lap design achieved higher average shear stresses than the scarf. The strength of the stepped lap joint was not very sensitive to the number of steps when total lap length was constant. Interlaminar shear was the predominant failure mode in many of the bonded joints.

The bolted joints included single and double lap configurations. The single lap joints strengths were not greatly penalized by the joint eccentricity. Various types of reinforcement at the bolt hole were investigated with the double-lap configuration. The use of bushings reduced the joint weight efficiency. The insertion of metal shims and thickened-end designs resulted in weight-effective joints. The shimmed joint was more difficult to fabricate but produced a very compact, high-strength joint. The thickened-end configuration was a good general purpose design. The addition of adhesive bonding to a bolted joint gave strengths that were greater than similar joints using bonding or bolting separately. Shear-out failures were prevalent in all bolted joints except for the shim-reinforced and combination bolted-bonded joints. Although whiskers improved the laminate properties, joint strengths were not increased by their use as a resin additive.

Constant-amplitude fatigue tests (at a stress ratio of +0.05) were conducted on the various configurations for screening joint concepts. In these tests laminate failures occurred in single lap bolted joints and in combination bolted-bonded joints. In double lap bolted joints, fatigue failures occurred in the aluminum joint members, and in adhesive joints the failures were associated with the adhesive or the resin adjacent to the adhesive. Two joint concepts (double lap adhesive and scarf adhesive) were selected for the generation of S-n curves at constant amplitude. The scarf joints sustained stress levels approximately three times greater than those of the double lap joints.

Phenomenological trends in joint failure modes were analyzed in terms of basic joint design parameter variations. Significant parameters were identified, and strength prediction methods were evolved for the design of statically loaded tension joints. Details of processing and fabrication of the specimens and physical property data are included in the appendixes and in Volume II.

WEIGHT STUDIES

The strength prediction methods evolved in the joint investigation were used to design minimum weight joints. A boron laminate with a $0^\circ/45^\circ/-45^\circ/0^\circ$ pattern was used in the study, and the derived weights were compared to aluminum alloy joints of equivalent strength. Weight increments were calculated with respect to a basic panel, the thickness of which was based on its required tensile strength. In bonded joints, the scarf and stepped lap configurations were lighter in weight than the lap joints at all load levels. Boron had a smaller weight increment than aluminum alloy for all joints except the scarf joint when scarf length was constrained by practical considerations.

The thickened-end configuration was used in the study of single and double lap bolted joints. A balanced design, in which all possible failure modes occurred simultaneously, was investigated and found to yield a weight greater than minimum. A procedure for the design of optimum joints was developed, and examples for boron and aluminum joints were evaluated. Weights considerably less than those for a balanced design were achieved.

The significance of the joint weight increments was illustrated by considering joints associated with panels typical of aircraft applications. Boron panels were approximately half the weight of aluminum panels for the same tensile loads. The weight increment of the scarf and stepped lap joints was so small in comparison with the panel weights that there was little difference between them on the basis of total weight. The boron stepped lap joint resulted in the smallest total weight. In this joint, weight was reduced by increasing the number of steps, but because the joint weight was such a small percentage of total panel weight there was negligible gain from the use of more than four steps.

ANALYTICAL STUDIES

The basic joint configurations in the experimental program were studied analytically to evaluate available analysis methods and to provide insight into the trends in the experimental data. Linear and nonlinear behaviors were analyzed, primarily using lumped parameter modeling and matrix computer methods.

Results of linear analyses of double lap, bonded joints were modified by an approximate method of accounting for plasticity. The results agreed very well with experimental data for both adhesive and adherend failures.

Load-deformation characteristics of bolted joints were not adequately predicted by linear analysis. Agreement between test and linear theory for the basic fastener-sheet assembly was poor. The discrepancy was probably caused by nonlinear behavior due to local filament buckling and matrix plasticity caused by high bearing stresses in the laminate. An extremely sophisticated nonlinear analysis capability is required to account for these mechanisms.

Double lap bonded joints were analyzed by a nonlinear digital method, and the results are summarized in this document. The agreement with test data was excellent. This approach offers the potential of reliable prediction of shear failures in the adhesive and of sheet tension or interlaminar shear failures of the adherends.

Results of linear analyses of bonded joints are in good agreement with fatigue data from the screening tests. Test-theory comparisons are included for (1) single lap, double lap, stepped lap, and scarf joint configurations, and (2) boron composite, fiber glass composite, and aluminum adherends.

DESIGN TECHNOLOGY

On a weight-efficiency basis, bonded joints were found to be superior to bolted joints, and, therefore, they are recommended for permanent-joint applications. Bolted joints will continue to be required for demountable assemblies and for numerous stressed and non-stressed access door installations. Although bolted joints are heavier than bonded joints, bolted joints in composites are lighter than comparable joints in aluminum alloy for the same design conditions.

Laminate shear was the failure mode in most joint failures, both in interlaminar shear of bonded joints and in shear-out of bolted joints. In bonded lap joints, when a good balance was achieved between lap length and adherend thickness (to balance adhesive shear strength and adherend tensile strength) the resin between laminate layers failed in interlaminar shear. In bolted joints, conventional shear-out failures were observed in most of the specimens, even when joint proportions were selected to produce bearing failures.

The simplest bonded joint was the single lap, in which the two members being joined were merely overlapped and bonded together. For small overlap lengths, the adhesive approached its full shear strength. As lap length was increased, joint strength increased at a decreasing rate. The strength of the joint was increased considerably by using a double shear configuration with a faying surface on each side of the center adherend. For a given lap length the adhesive area was double that of a single lap joint, but the strength was more than double because the symmetry of the joint reduced bending in the adherends and peel stresses in the adhesive. The adherends for both single and double lap joints approached their predicted tensile strengths at failure despite bending effects. For loads greater than the strength capacity of lap joints, it was necessary to use a joint configuration in which the strains in the adherends were more compatible. Of the types investigated, the scarf and the stepped lap joints both showed promise of achieving any desired strength with a small weight penalty. The manufacture of each introduced more difficulty in fabrication.

The choice of adhesive may be influenced by practical reasons, such as temperature and pressure requirements during the cure cycle. Residual thermal stresses are particularly important when joining materials of different thermal expansions. A low-temperature-cure adhesive would be advantageous in such cases. Similarly, an adhesive that does not require high bonding pressures or close contact of adherends would considerably reduce fabrication difficulties.

For highly loaded joints, mechanical properties of the adhesive are of prime importance. However, it was found that ultimate shear strength alone was not a good criterion for selection of an adhesive. Where there was

some incompatibility of strain in the adherends, it was demonstrated that improved strength was obtained using an adhesive that exhibited considerable ductility. Of the adhesives tested, AF130 was the strongest with an ultimate tensile strength of 9970 psi. Shell 951 had a strength of 6100 psi but sustained a very large strain before failure. When used in 0.5-inch double lap specimens, the average failure stresses obtained with AF130 and Shell 951 were 1125 and 5556 psi, respectively, indicating the considerable advantage of ductility. An exception to this rule was noted in the case of the scarf joint using AF130 adhesive. Because of the improved strain compatibility of the adherends, stress concentration in the adhesive was reduced to such a level that AF130 produced a stronger joint despite its brittle stress-strain characteristics in shear.

Design parameters having the greatest influence on bonded joint failures were lap length, adherend thickness, and fiber orientation adjacent to the adhesive. In single and double lap joints, short lap lengths and thick adherends ($L/t = 12.5$) tended to produce adhesive failures or interfacial failures between resin and fibers in the first layer of the laminate. Long lap lengths and thin adherends ($L/t = 50$) tended to produce tension failures in the adherends. Between these two extremes ($L/t = 25$), interlaminar shear failures were prevalent. Interlaminar shear failures were also observed near the fiber ends in scarf adhesive joints, and near the step ends of stepped lap joints. The interlaminar shear failures were usually associated with layers oriented at 45 degrees to the load axis, particularly when such layers were adjacent to the adhesive.

Single and double lap joints attained maximum strengths when the extensional stiffnesses of the adherends at both ends of the joint were equal. Extensional stiffness is proportional to the product of Young's modulus and adherend thickness. Balancing the extensional stiffnesses of the adherends equalized peak stresses at each end of the bond line and produced the highest average adhesive shear stresses.

Adhesive joints tested in constant-amplitude fatigue (at a stress ratio of +0.05) achieved runout conditions when the maximum shear stress in the adhesive was restricted to approximately the proportional limit stress of the adhesive in shear. Thus, the scarf joints achieved runout stresses about 3.5 times greater than those of double lap joints. Adhesive shear stresses above the proportional limit caused fatigue cracks in the adhesive (or in the resin adjacent to the adhesive) that propagated through the joint and caused failure. Residual strength of the runout specimens usually exceeded static strength values.

The presence of the fastener hole was a critical factor in each mode of failure observed in the bolted joints. Stress concentration factors caused by the hole ensured that failure would not occur in the basic laminate section or in the fastener unless the joint area was reinforced in some manner (i. e., metal shim inserts, edge buildup, etc.).

Design parameters having an influence on mechanical joint failures were laminate properties, laminate patterns, edge distance, fastener pitch, laminate thickness, and fastener diameter. Within the range of variation of these

parameters in the present program, the shear-out mode predominated in the joint failures. Shear stresses that developed at failure (for a number of laminate thicknesses and edge distances) decreased as edge distance increased. Thus, increasing edge distance was found to be an inefficient method of increasing joint strength. For a given edge distance, joint strength increased approximately linearly with composite thickness until bolt bending effects reversed this trend.

Edge distances of 4.5 times the fastener diameter were required to achieve a balance between shear-out and bearing strengths of the laminates used in the test specimens. Tensile failures through the fastener holes were precluded by a side distance of twice the fastener diameter. A thickness-to-diameter ratio of 0.8 resulted in maximum bearing strength. Above this ratio, bolt bending effects reduced the average bearing stresses, particularly in the stiffer boron composites. Maximum shear-out stresses were developed in a laminate containing 0- and 45-degree layers when 2/3 of the layers were oriented at 45 degrees to the load axis.

Bolted joints with steel bushings (at the t/D ratios investigated during the program) were considerably weaker than similar composite joints without bushings.

The combination bolted-bonded joint performed better than joints employing either bolting or bonding separately. The strength of this joint was improved due to a fundamental change in failure mode caused by the adhesive. The mode of failure for this joint was a combination of tension through a section at the fastener and interlaminar shear in the composite. If this joint had been either bolted or bonded, it would have failed in a lower-strength shear-out mode (if bolted) or an interfacial shear mode (if bonded). The addition of adhesive bonding in the bolted joint resulted in a large increase in strength for a negligible weight increase.

The steel shim-reinforced specimens failed in a variety of complex modes involving bolt shear, tension through a section at the fastener hole, tension in the basic laminate section, and delamination of the specimen at the shim-to-resin interface. These joints produced bolt failures in double shear at edge distances of about five times the bolt diameter. Strength-weight relationships comparable to all composite bolted joints were produced with edge distances of about twice the bolt diameter.

SECTION III

MATERIAL PROPERTIES

Data specimens were fabricated and tested to determine engineering properties of the laminates and adhesives used in the joint tests. These data specimens, together with test methods and results, are described in this section under the headings Laminate Properties and Adhesive Properties. Engineering drawings showing design details of the data specimens are included in Volume II.

LAMINATE PROPERTIES

To establish an engineering data base for the composite materials being used in the joint tests, analytical and experimental investigations were conducted to determine laminate response under the following loads:

- Tension
- Compression
- In-plane shear
- Interlaminar shear
- Pin-bearing

Stress-strain data were measured for the compound multilayered laminates used in the joint specimens for uniaxial tension and compression, and for in-plane shear. Unidirectional laminate properties were also determined for longitudinal and transverse tension and for in-plane shear. Stress-strain curves for each of the tension, compression, and in-plane shear specimens are included in Volume II.

All data specimens, and subsequently all joint specimens, were made from prepregged, "B" staged boron tapes or S-994 fiber glass roving using the Narmco 5505 epoxy resin system. The boron tapes were purchased under material specification DMS 1919, "Boron Filament Tape, Organic Resin Impregnated," from the Whittaker Corporation, Narmco Materials Division. This specification is included in Volume II. The S-994 fiber glass roving was impregnated by the U.S. Polymeric Company using bulk 5505 resin purchased from Narmco. A specification was not established for this material, but incoming inspection tests were conducted on each shipment of material before it was used in specimens. These inspection records are also included in Volume II.

Two basic laminate patterns that result in a combination of axial and shear properties were selected for the tension, shear (both in-plane and interlaminar), and bearing specimens. These properties are required in varying degrees in practically all aircraft components. The selected laminate patterns are illustrated in Figure 1. Each arrow represents an oriented monolayer of reinforcement applied in the numbered sequence. The specimen walls were built up by repeating these basic patterns. For the

compression specimens, the first laminate pattern was retained, but the second was changed to a pattern regarded as more suitable for a compression member.

Specimen configurations were fabricated in both boron and S-994 high-tensile-strength (HTS) fiber glass reinforcements. One of the boron patterns contained a 90°-oriented ply of S-994 HTS fiber glass as shown in Figure 2. This ply was included to improve the transverse properties and enhance the micromechanical behavior of the longitudinal plies in compression. This pattern was more suitable for a structural member loaded primarily in compression; e. g., a landing gear strut.

The specimen laminate patterns were chosen so that corresponding specimens in boron and fiber glass had the same percentages of longitudinal, circumferential, and oblique angle plies and the same nominal wall thicknesses. Because of the difference in ply thickness between boron tape (about 0.005 inch) and fiber glass roving (about 0.010 inch), the number of layers in similar specimens did not correspond.

A second difference in the tension, compression, and shear specimens should be noted. The specimens containing only boron reinforcement were fabricated using 3-inch-wide pregregged (Narmco 5505 resin) tape including a layer of 104 glass scrim cloth. The boron specimens with the transverse plies of S-994 HTS fiber glass were fabricated using 1/8-inch pregregged boron tape excluding the glass scrim cloth.

Some configurations of the compression, interlaminar shear, and pin-bearing specimens contained small amounts of whisker additions to the resin. Two types of whisker mixtures were used, as specified in Table I. These specimens were included in the test program to indicate the effects of resin additives on compression, interlaminar shear, and bearing properties of the composites. The strength effects of these whisker additions are discussed under the appropriate specimen headings.

After test, one whiskered specimen was sectioned, polished, etched, and photographed at a magnification of 500X (Figure 3) to check the dispersion of whiskers due to resin flow during cure. The specimen contained the Al_2O_3/AlN whisker mixture at 2 percent of the resin weight. Thus, the laminate contained fibers of the following diameters:

Boron	0.004 inch
Fiber Glass	0.00037 inch
Al_2O_3/AlN Whiskers	0.00012 inch

The dispersion of whiskers through the laminate was quite uniform, as shown in Figure 3.

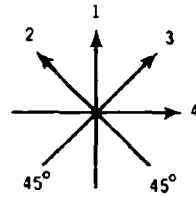
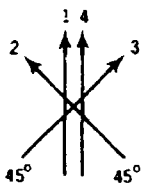
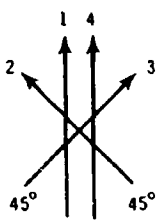
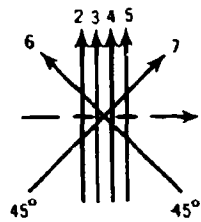


FIGURE 1. BASIC FILAMENT PATTERNS FOR TENSION, SHEAR, AND BEARING SPECIMENS



(BORON-TYPICAL-SOLID LINE)



(S-994 HTS GLASS-DASH LINE)

FIGURE 2. BASIC FILAMENT PATTERNS FOR COMPRESSION SPECIMENS

TABLE I
WHISKER DIMENSIONAL PROPERTIES

TYPE	DIAMETER RANGE	LENGTH RANGE	ASPECT RATIO
MIXED WHISKERS AlN - Al ₂ O ₃	3-30 MICRONS 0.00012 - 0.0012 INCHES	30-600 MICRONS 0.0012 - 0.024 INCHES	10-200
MIXED WHISKERS SiC - Al ₂ O ₃	2-30 MICRONS 0.00008 - 0.0012 INCHES	20-1000 MICRONS 0.0008 - 0.040 INCHES	10-500

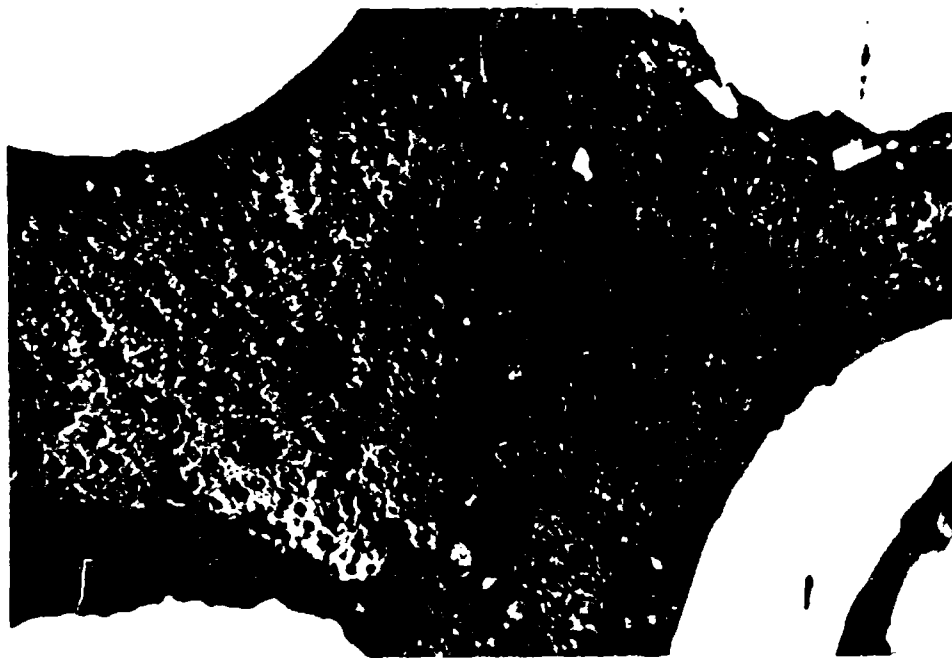


FIGURE 3. PHOTOMICROGRAPH OF SPECIMEN WITH Al₂O₃/AlN WHISKERS AT 2 PERCENT RESIN WEIGHT

Theoretical Properties

In the initial stages of analysis, it was considered worthwhile to demonstrate the extent to which the behavior of the multidirectional material could be predicted when subjected to uniaxial loading. This enabled the strength of the adherends to be considered, together with the bolt or bond strength, in the joint analysis.

Theoretical properties of the data specimens were predicted using the strength analysis approach of Tsai (Reference 1), based on the distortional energy criterion of continued deformation of anisotropic materials postulated by Hill (Reference 2). This approach was applied to the compound multi-layered laminates used in the data specimens to predict stress-strain behavior to ultimate strength. Based on monolayer properties, the elastic properties and stress distributions of the laminate under the applied loads were computed, and each layer was checked against the distortional energy criterion of failure. When the applied load was large enough, one layer of the laminate satisfied the failure criterion and "first failure" was considered to have occurred. That layer was then taken out of action for subsequent calculations. As each layer "failed," the remaining layers of the laminate were used to recalculate the elastic properties and internal stress distributions. This process was repeated until the ultimate strength of the laminate was determined.

This analytical approach was programmed for computer analysis by Schofield (Reference 3). This program performed a strength analysis of balanced multilayered laminates for stress-strain behavior up to ultimate load. The program input data included uniaxial properties as noted in Table II. The uniaxial properties were determined initially from published literature (References 4 through 6). Because of the dearth of information on S-994 fiber glass-Narmco 5505 laminates, properties for this system were approximated using data from Reference 4 for fiber glass/828-1031 BDMA-MNA resin, except that transverse tensile strength (F_{Tt}) was increased to represent the Narmco 5505 resin properties more accurately. For boron-Narmco 5505 laminates, elastic properties and longitudinal strengths were obtained from Reference 5. Transverse properties were selected from a compendium of composite data (Reference 6) in which recent published test results were summarized. Subsequent testing indicated that the selected transverse properties were representative, but somewhat conservative as shown in Table II.

Uniaxial laminate properties were determined in the program for tension and in-plane shear. These properties are also summarized in Table II, and are reported in detail in subsequent sections. Experimental results for longitudinal strengths and elastic properties were significantly less than those obtained in References 4 and 5. However, correlation of analytical and experimental results for the patterned (e.g., $0^\circ/45^\circ/-45^\circ/0^\circ$) specimens was superior when the published uniaxial data were used in analysis rather than the uniaxial test results.

**TABLE II
UNIDIRECTIONAL LAMINATE PROPERTIES**

	S-994 FIBER GLASS		BORON	
	NARMCO 5505 RESIN	828-1031 BDMA-MNA RESIN	NARMCO 5505 RESIN	
	EXPERIMENT	LITERATURE*	EXPERIMENT	LITERATURE*
ELASTIC PROPERTIES				
E_L (10^6 PSI)	5.85 - 9.30	7.65 (1)	24.8 - 29.6	30.00(2)
E_T (10^6 PSI)	1.59 - 2.25	2.24 (1)	1.90 - 2.21	3.00(2)
G_{LT} (10^6 PSI)	0.84 - 1.43	0.78 (1)	0.73 - 0.88	1.10(2)
μ_{LT}	0.248 - 0.308	0.270(1)	0.163 - 0.266	0.380(2)
μ_{TL}	0.027 - 0.075	0.079 (1)	0.018 - 0.029	0.038(2)
STRENGTH PROPERTIES				
F_{L_t} (10^3 PSI)	175.3 - 242.0	264.0 (1)	152 - 190.7	200.0(2)
F_{L_c} (10^3 PSI)	-	173.0 (1)	-	250.0(2)
F_{T_t} (10^3 PSI)	7.96 - 9.60	7.5 (3)	6.80 - 8.37	7.0(3)
F_{T_c} (10^3 PSI)	-	29.0 (1)	-	20.0(3)
F_s (10^3 PSI)	9.62 - 13.58	8.5 (1)	11.04 - 15.00	12.0(3)

(1) DATA FROM REFERENCE 4, PAGE 239. FIBER GLASS/828-1031 BDMA-MNA LAMINATE.

(2) DATA FROM REFERENCE 5.

(3) DATA ESTIMATED FROM REFERENCE 6.

*DATA FROM LITERATURE WERE USED IN ANALYSIS. THESE GAVE BETTER CORRELATION OF PREDICTED PROPERTIES WITH TEST RESULTS FOR MULTIDIRECTIONAL LAMINATES USED IN SPECIMENS.

The program conducts a strength analysis for both stress-free (unrestrained) and strain-free (restrained) boundary conditions. In this study the tensile and compression specimens were analyzed for stress-free boundaries. The shear specimens were analyzed with strain-free boundaries because these boundary conditions were considered more representative of the "picture frame" shear test setup.

Predicted stress-strain behavior for the strength and elastic property specimens are indicated on the data plots in Volume II. The points of first failure in the laminate and ultimate failure of the composite are indicated. Failure conditions were usually induced initially in transverse plies, causing a slope change in the stress-strain curve. This transverse failure implied crazing or yielding of matrix material. As external loads increased, failure conditions were satisfied successively in the remaining layers of the laminate until complete failure was induced in the fibers of a critical layer. At this point the ultimate strength of the laminate was considered to have been achieved.

Tension Tests

The tension tests were performed on IITRI-type coupons (Drawing Z4824842, Volume II) in a Riehle test machine. Test loads were introduced through bonded gripping tabs using serrated machine grips. Loads were applied at a crosshead rate of 0.05 inches per minute. Axial and transverse strains were recorded using standard strain gages to provide modulus of elasticity and Poisson's ratio data. The test setup and instrumentation are shown in Figure 4.

Stress-strain plots were obtained for both unidirectional and multidirectional laminates. Test results are summarized in Table III. Figure 5 illustrates the failure of a -507 specimen with a $0^\circ/45^\circ/-45^\circ/0^\circ$ pattern. The 45-degree plies failed transversely in the resin, and the zero-degree plies failed in axial tension. The theoretical analysis predicted transverse failure in the 45-degree plies (first failure) at 19.6-ksi composite stress and ultimate failure at 101.5 ksi. The actual stress-strain response of the specimens was in excellent agreement with the prediction, as shown in Figure 6.

In addition to tests on the laminate property tensile specimens, tension tests were conducted on IITRI-configuration control specimens made from selected laminates used in adhesive joint and pin-bearing specimens. These tests were conducted to check the consistency of laminate quality during the specimen fabrication phase. The laminates were cured in six separate panels from which either one or two control specimens were machined. Each specimen was instrumented with an axial and a transverse strain gage to provide modulus of elasticity and Poisson's ratio data. The specimens were loaded at a rate of 0.05 inch per minute through bonded gripping tabs using serrated machine grips. The test results are summarized in Table III and compared graphically in Figure 7. Laminates of $0^\circ/45^\circ/-45^\circ/0^\circ$ patterns attained actual tensile stresses in excess of 122 ksi in some of the joint specimens compared to an average of 99.3 ksi for the control specimens. This may have been a gage-length effect since the joint specimens had an unsupported length of only 1/4 inch in contrast with the 6-inch gage-length of the control specimens.

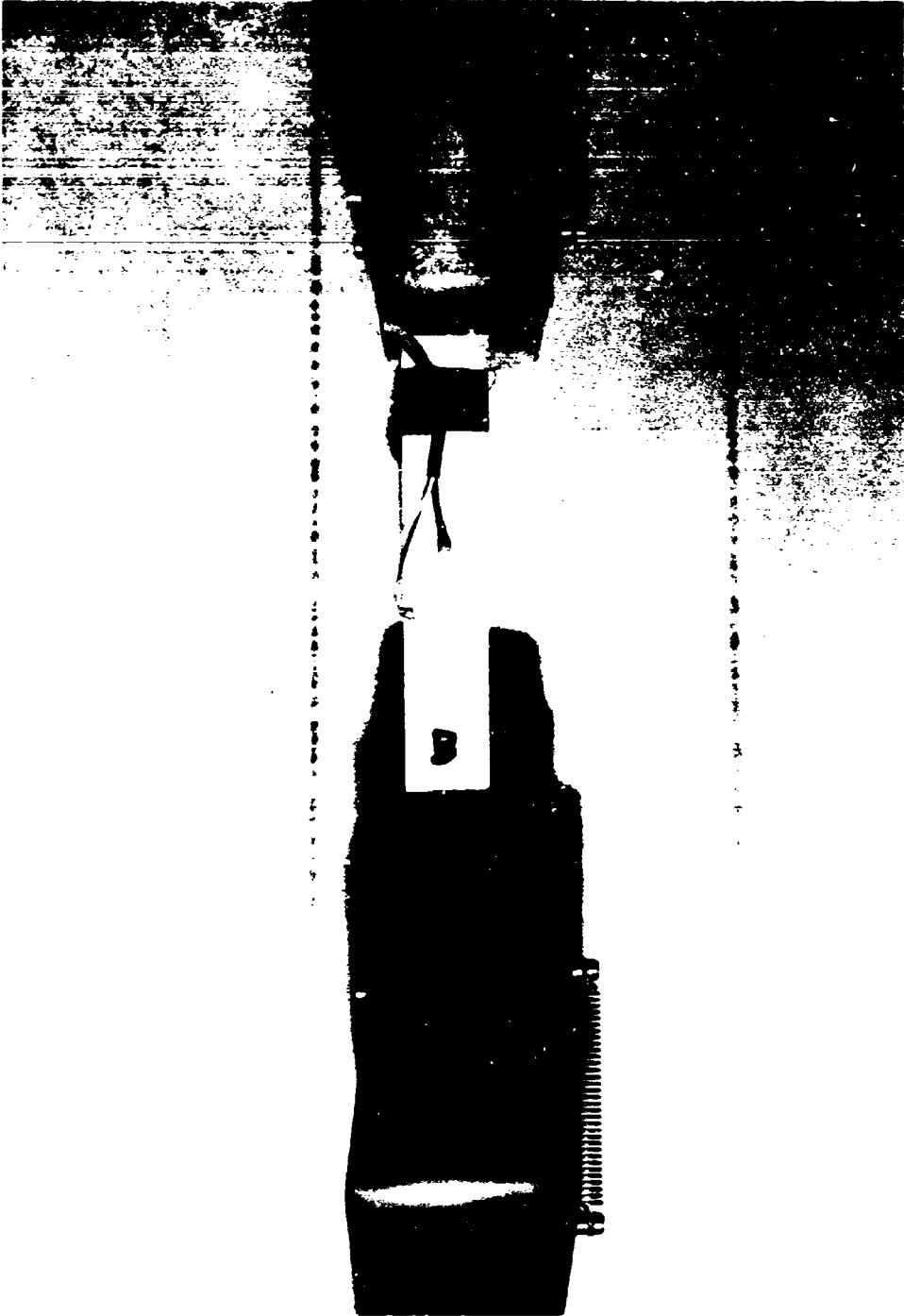


FIGURE 4. TENSILE TEST SETUP

**TABLE III
SUMMARY OF THEORETICAL AND EXPERIMENTAL TENSION PROPERTIES**

SPECIMEN DESCRIPTION	LAMINATE PATTERN	LAMINATE THICKNESS	ELASTIC CONSTANTS				STRENGTH PROPERTIES			VOLUME FRACTIONS			
			PREDICTED		ACTUAL		PREDICTED		ACTUAL	FILAMENT	RESIN	VOIDS	
			E_x (10 ⁶ PSI)	μ_{xy}	E_x (10 ⁶ PSI)	μ_{xy}	FIRST FAILURE STRESS (KSI)	ULTIMATE STRESS (KSI)	ULTIMATE STRESS (KSI)				
BORON/MARMC 5505	Z4824842 511	ALL 0°	0.030			25.50	0.250			158.5	0.595	0.381	0.024
						24.80	0.241			158.5			
					27.20	0.266			171.0				
					25.80	0.164			190.7				
					27.60	0.167			180.0				
					29.60	0.163			152.0				
					AVG 26.75	AVG 0.209			AVG 168.5				
	Z4824842 513	ALL 90°	0.050			2.21	0.018			7.15	0.621	0.324	0.055
						2.03	0.029			8.80			
					1.90	0.021			8.37				
				AVG 2.05	AVG 0.023			AVG 7.44					
Z4824842 1	0°/45°/45°/90°	0.040			16.80	0.722			95.0	0.636	0.332	0.032	
					16.50	0.714			99.5				
				17.40	0.745			88.0					
				17.13	0.688	AVG 16.90	AVG 0.727	94.0	101.5	AVG 94.2			
CONTROL SPECIMENS FROM Z3824828	0°/45°/45°/90°	0.040			14.8	0.704			100.0	0.545	0.412	0.043	
					15.7	0.706			95.0				
				17.13	0.688	AVG 15.3	AVG 0.705	94.0	101.5	AVG 97.5			
CONTROL SPECIMENS FROM Z3824827 AND Z3824854	0°/45°/45°/90° 45°/90°/90°/45°	0.080			15.1	0.710			98.2	0.537	0.436	0.027	
					14.7	0.616			102.5				
				17.13	0.688	AVG 14.9	AVG 0.663	94.0	101.5	AVG 100.4			
CONTROL SPECIMENS FROM Z3824815-1	0°/45°/45°/90°	0.120			17.0	0.687			102.0	0.612	0.342	0.046	
					16.7	0.720			104.3				
				17.13	0.688	AVG 16.9	AVG 0.704	94.0	101.5	AVG 103.2			
CONTROL SPECIMENS FROM Z3824829	0°/45°/45°/90°	0.160			17.2	0.777			93.3	0.597	0.330	0.073	
					17.0	0.700			98.5				
				17.13	0.688	AVG 17.1	AVG 0.736	94.0	101.5	AVG 95.9			
Z482484 501	0°/45°/45°/90°	0.040			11.5	0.331			60.0	0.602	0.342	0.056	
					11.5	0.312			43.8				
				11.2	0.329			53.8					
				11.87	0.336	AVG 11.4	AVG 0.324	31.1	66.4	AVG 52.5			
CONTROL SPECIMENS FROM Z3824815 503	0°/45°/45°/90°	0.120			10.8	0.394			66.0	0.609	0.346	0.045	
					9.7	0.200			57.4				
				11.87	0.336	AVG 10.3	AVG 0.298	31.1	66.4	AVG 61.7			
S-994 FIBERGLASS/MARMC 5505	Z4824842 503	ALL 0°	0.060			7.70	0.308				0.548	0.411	0.005
						7.80	0.248						
				0.030		9.30	0.263						
						5.85	0.266			175.3			
					6.56	0.288			203.3				
					6.40	0.260			242.0				
					AVG 7.27	AVG 0.272			AVG 206.8				
	Z4824842 505	ALL 90°	0.060			2.20	0.075			7.48	0.548	0.411	0.005
						2.19	0.068			8.00			
				0.050		2.25	0.063			8.17	0.594	0.401	0.005
			1.84	0.027			7.96						
				1.59	0.071			9.60					
				AVG 2.01	AVG 0.061			AVG 8.24					
Z4824842 507	0°/45°/45°/90°	0.080			4.55	0.581			120.0				
					4.06	0.575			143.4				
				5.77	0.577			137.0					
				5.10	0.453	AVG 4.79	AVG 0.581	19.6	115.3	AVG 133.4			
Z4824842 509	0°/45°/45°/90°	0.080			3.66				62.6				
					3.80				56.4				
				3.75				57.3					
				3.92	0.308	AVG 3.74		6.6	65.3	AVG 58.4			



FIGURE 5. TENSILE FAILURE OF SPECIMEN Z4824842-507

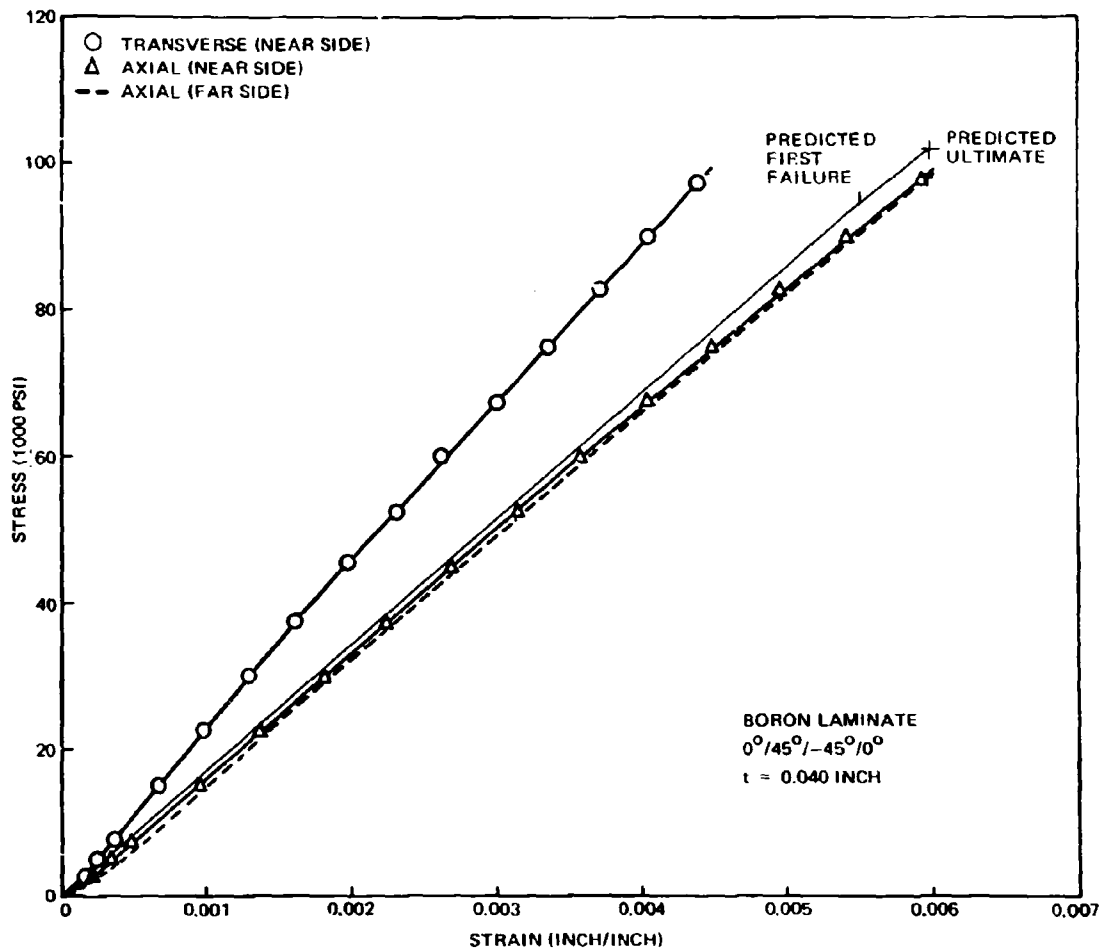


FIGURE 6. TENSION STRESS-STRAIN DIAGRAM FOR SPECIMEN Z4824842-1

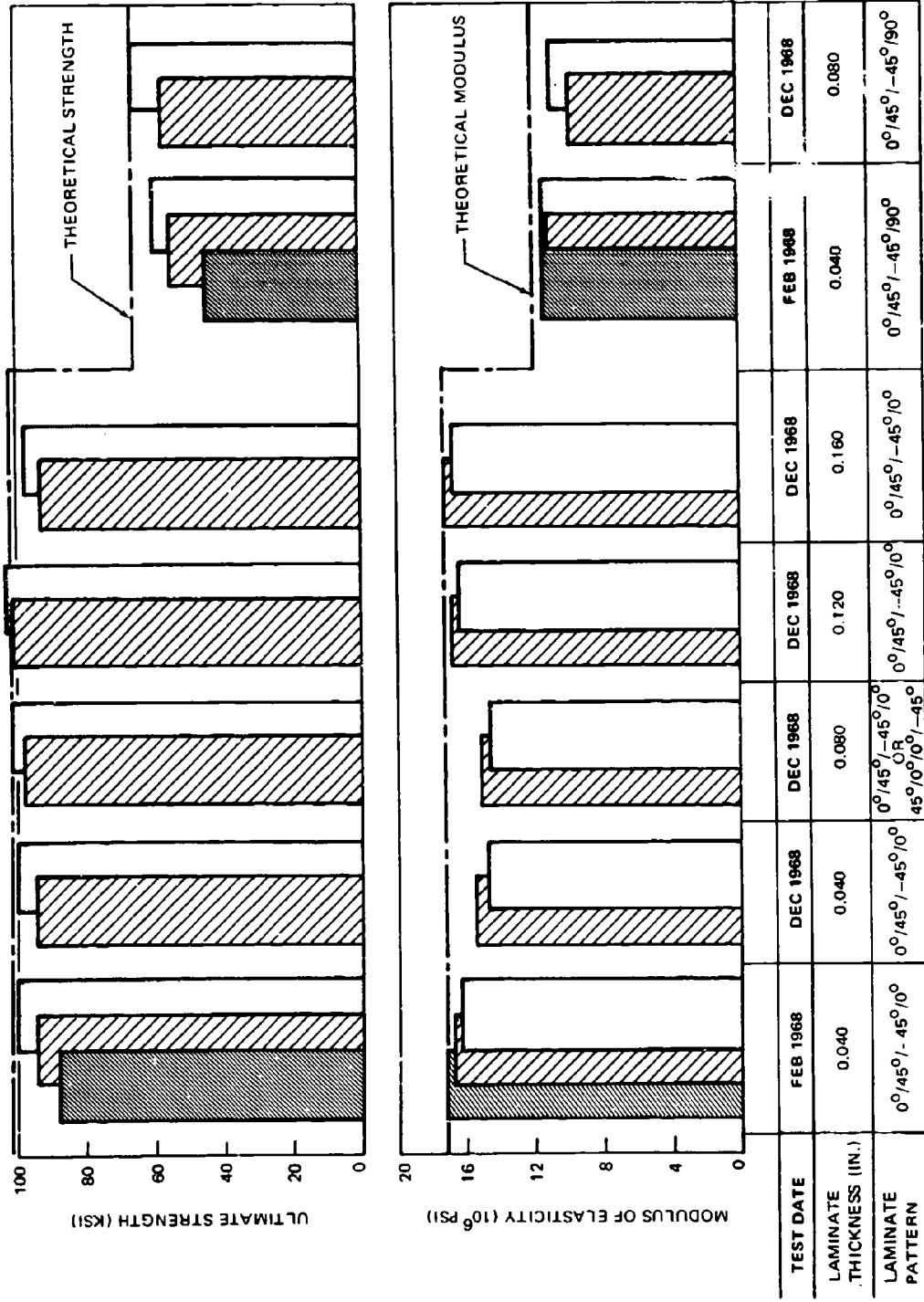


FIGURE 7. COMPARISONS OF CONTROL SPECIMEN TEST RESULTS

BARS REPRESENT ONE SPECIMEN EACH - SIMILAR SHADING IN THE ULTIMATE STRENGTH AND MODULUS OF ELASTICITY PLOTS INDICATES DATA OBTAINED FROM THE SAME SPECIMEN.

Resin contents in Table III were lower than anticipated. These were determined using a vacuum pyrolysis technique described in Section III, Volume II. Control of resin content was not attempted during the program, other than by purchase of the prepregged tape by specification (DMS 1919) and by consistent processing. The laminate cure cycle was used consistently throughout the program and the resin content depended, therefore, on the resin content in the prepregged tape and the amount of bleed obtained during the cure cycle.

Test results from the control specimens indicated that the more recently made laminates had lower fiber volumes, slightly lower modulus values (averaging about 4 percent), and a modest strength improvement (averaging about 5 percent) due primarily to one relatively low strength specimen for each pattern in the original specimen group. Corresponding test results from the pin-bearing and adhesive joint specimens are presented subsequently under the appropriate headings.

Compression Tests

A tubular specimen configuration was selected for compression testing to provide an inherently stable cross section and to avoid the problem of cut plies at the edges of a flat specimen. The tubes were sized for length, diameter, and wall thickness to preclude the occurrence of local macro-mechanical instabilities prior to ultimate material rupture.

A specially designed test fixture was used for the compression tests. The test setup is shown in Figure 8. The loaded edges of the compression specimens were retained in Cerro-Tru metal (a 260°F melting-point alloy) to preclude local brooming failure at the bearing surface. To minimize the effects of radial frictional restraint at the tube ends, the compression load was introduced through a cone-shaped retaining ring and bearing plate. Thus, a radial component of the applied compression load caused radial straining of the retaining ring, which reduce the "barreling" tendency of the specimen. Typical failures are shown in Figure 9. The basic specimen configuration and the assembly of the specimen and retaining rings are also illustrated in Figure 9.

A strain-gaged load cell was placed between each specimen assembly and a steel loading block in a Baldwin test machine as shown in Figure 8. Shims were applied between the block and the machine table to provide parallel surfaces between the machine compression head and the top surface of the specimen. Load was applied to the specimen through the loading block at the rate of 10,000 pounds per minute.

Strains were measured with an extensometer/compressometer as shown in Figure 8. This instrument provided continuous strain readings in both the longitudinal and circumferential directions. Strains along the longitudinal axes of the specimens were measured through the movement of a differential transformer. The diametral strain, orthogonal to the axial strains, was determined from the movement of strain-gaged flexural strips. Loads were read directly from the load cell. Test results are summarized in Table IV, and a typical stress-strain plot is shown in Figure 10.

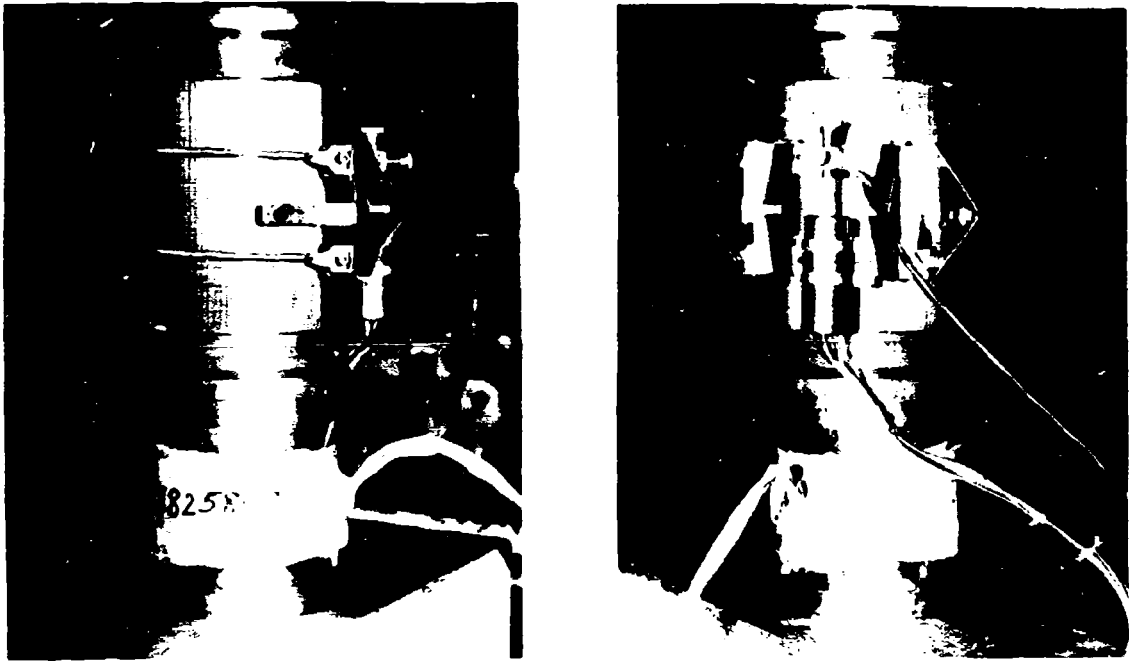


FIGURE 8. TEST SETUP AND INSTRUMENTATION FOR COMPRESSION SPECIMENS

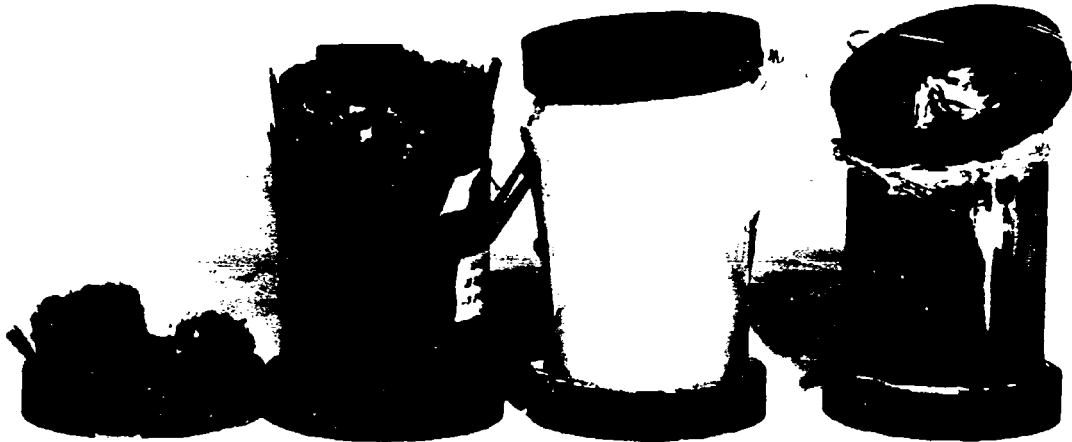


FIGURE 9. COMPRESSION SPECIMEN FAILURES

TABLE IV
SUMMARY OF THEORETICAL AND EXPERIMENTAL COMPRESSION PROPERTIES

CONFIGURATION Z3624818	SPECIMEN NUMBER	ELASTIC CONSTANTS				STRENGTH PROPERTIES				REMARKS
		ELASTIC MODULUS, E (10 ⁶ PSI)		POISSON'S RATIO, μ_{xy}		PREDICTED		ACTUAL		
		PREDICTED	ACTUAL	PREDICTED	ACTUAL	FIRST FAILURE STRESS (KSI)	ULTIMATE STRESS (KSI)	ULTIMATE STRESS (KSI)	ACTUAL ULTIMATE STRESS (KSI)	
0°/45°/-45°/0° t = 0.120 INCH BORON/NARMCO 5505	1	17.1	17.0	0.688	0.638	95.2	134.8	134.8	94.4	SECOND LOADING
	2	17.1	16.1	0.688	0.950	95.2	134.8	134.8	—	
	3	17.1	17.4	0.688	0.169	95.2	134.8	134.8	100.9	
-501 0°/45°/-45°/0° t = 0.120 INCH S-994/NARMCO 5505	1	5.1	5.0	0.453	0.130	37.4	86.5	86.5	86.0	
	2	5.1	5.0	0.453	0.095	37.4	86.5	86.5	89.3	
	3	5.1	4.12	0.453	0.118	37.4	86.5	86.5	89.5	
-503 PATTERN NOTED t = 0.100 INCH BORON/NARMCO 5505 AND NOTED	1	19.7	14.3	0.439	0.063	150.0	176.0	176.0	166.8	PATTERN CONSISTED OF 20% CIRCULAR, 20% AT ±45°, AND 60% LONGITUDINAL - CIRCUL- LAR WRAPS WERE S-994
	2	19.7	19.8	0.439	0.093	150.0	176.0	176.0	185.0	
	3	19.7	24.7	0.439	0.055	150.0	176.0	176.0	171.4	
-505 PATTERN NOTED t = 0.100 INCH S-994/NARMCO 5505	1	5.65	6.5	0.247	0.065	46.5	110.7	110.7	99.0	PATTERN CONSISTED OF 20% CIRCULAR, 20% AT ±45°, AND 60% LONGITUDINAL
	2	5.65	5.0	0.247	0.065	46.5	110.7	110.7	98.5	
	3	5.65	4.76	0.247	0.051	46.5	110.7	110.7	71.3	
-507 0°/45°/-45°/0° t = 0.120 INCH BORON/NARMCO 5505 + NOTED WHISKERS	1	17.1	20.0	0.688	0.173	96.2	134.8	134.8	154.8	SIC - AI N WHISKERS ADDED TO LAMINATE AT 2% OF RESIN WEIGHT
	2	17.1	15.14	0.688	0.100	96.2	134.8	134.8	135.7	
	3	17.1	17.24	0.688	0.160	96.2	134.8	134.8	137.7	
-508 0°/45°/-45°/0° t = 0.120 INCH BORON/NARMCO 5505 + NOTED WHISKERS	1*	17.1	11.10	0.688	0.111	95.2	134.8	134.8	137.3*	SIC - AI N WHISKERS ADDED TO LAMINATE AT 1% OF RESIN WEIGHT
	2	17.1	14.10	0.688	0.138	96.2	134.8	134.8	161.6	
	3	17.1	12.20	0.688	0.171	95.2	134.8	134.8	169.9	
-511 0°/45°/-45°/0° t = 0.120 INCH BORON/NARMCO 5505 + NOTED WHISKERS	1	17.1	16.2	0.688	0.155	95.2	134.8	134.8	170.3	Al ₂ O ₃ - AI N WHISKERS ADDED TO LAMINATE AT 2% OF RESIN WEIGHT
	2	17.1	18.8	0.688	0.188	95.2	134.8	134.8	124.2	
	3	17.1	13.2	0.688	0.139	95.2	134.8	134.8	165.3	

*RETAINING RING FAILED

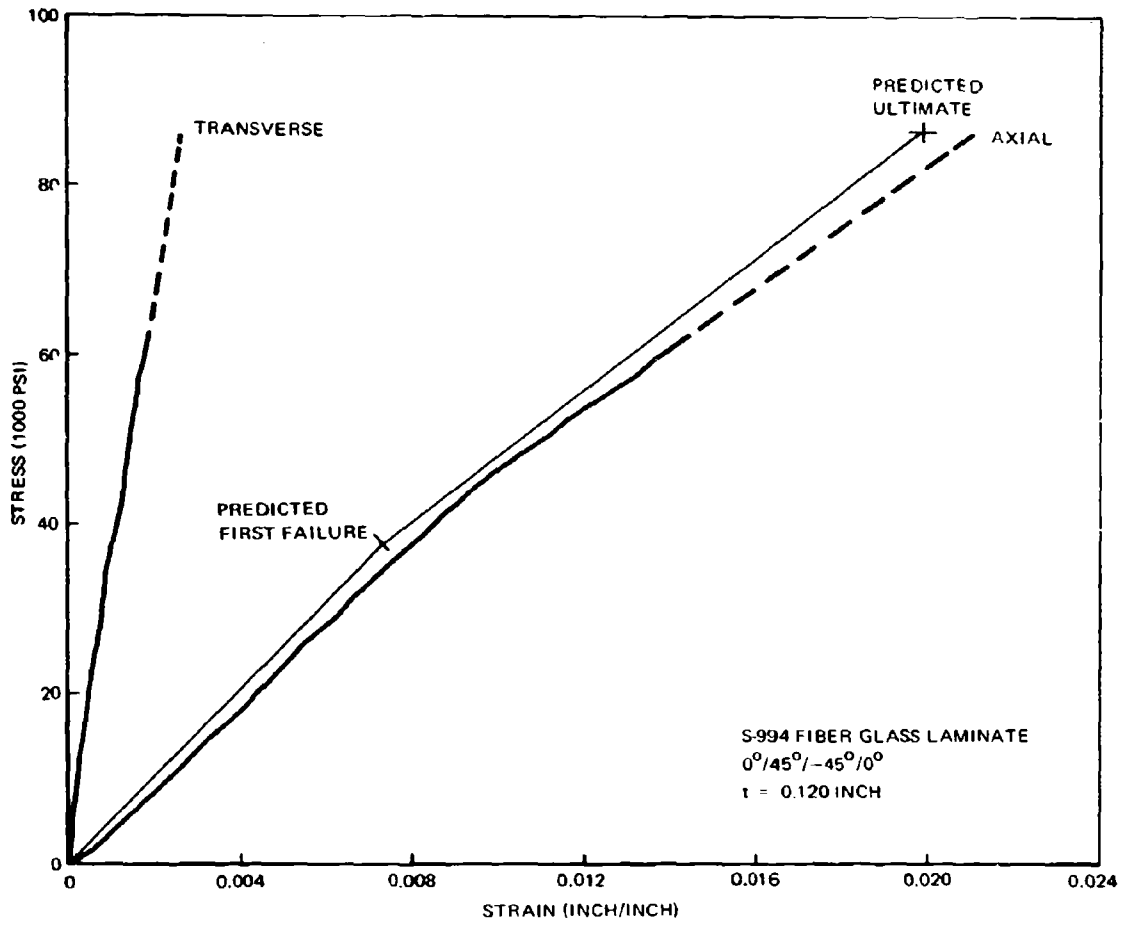


FIGURE 10. COMPRESSION STRESS-STRAIN DIAGRAM FOR SPECIMEN Z3824818-501

An appreciable amount of strain energy was released at ultimate failure of the cylinders. Therefore, after the first test, the compressometer was removed at a stress level varying from about 70,000 to 120,000 psi (depending on specimen configuration) to prevent damage to the instrument at failure. Thus, the compression stress-strain relationships of Volume II were extrapolated to the actual failure stress as indicated by the dashed lines on the plots.

The addition of whiskers as resin additives produced cylinders of very high strength. Their ultimate strengths exceeded the predicted values as noted in Table IV. Erratic stress-strain curves were recorded for most of these cylinders, due in part to slippage of the compressometer gage points in the extremely hard composites. For the -507 specimen, whisker additions to the resin apparently increased the extensional modulus to greater than theoretical levels; i. e., 20 million actual versus 17.1 million predicted.

For the specimen configurations with circumferential overwraps, predicted strength levels were very nearly attained. For the balance of the cylinders with neither whisker additives nor circumferential overwraps, the ultimate stresses attained in test were bracketed by the predicted stresses for first failure and ultimate failure. This behavior suggested that after first failure, local instabilities at the micromechanical level precipitated complete failure before the predicted strength could be achieved. The addition of whiskers and/or circumferential overwraps apparently stabilized the internal fibers and matrix until ultimate strength was attained.

In general, the correlation of theoretical and experimental data was quite good. Stress and longitudinal strain data compared very well with predictions, but diametral strains were much lower than predicted. Since the observed diametral strains were very consistent throughout the testing and no errors were found in the instrumentation setup, it was theorized that the 7075-T6 retaining rings inhibited diametral straining of the specimens.

In-plane Shear Tests

In-plane shear properties were determined using a picture-frame shear jig as shown in Figure 11. The four corners of the square jig frame were pinned to permit the frame and specimen to assume a rhombic shape under load. Test loads were introduced to the frame using a clevis-and-pin arrangement at two opposite corners of the frame. The shear loads were transferred to the specimen through eight equally torqued, 1/4-inch-diameter bolts through the four jig frame members and the specimen edges. A typical specimen failure is shown in Figure 12.

In-plane shear strengths were determined for both unidirectional and multi-directional laminates. Unidirectional laminate properties were determined from flat laminate panels of 0.100 inch nominal thickness. Multidirectional laminates were tested as the face sheets of honeycomb sandwich specimens. The boron and fiber glass laminates had nominal thicknesses of 0.020 and 0.040 inch, respectively. Design details of the specimens are shown on Drawing Z3824843, Volume II.

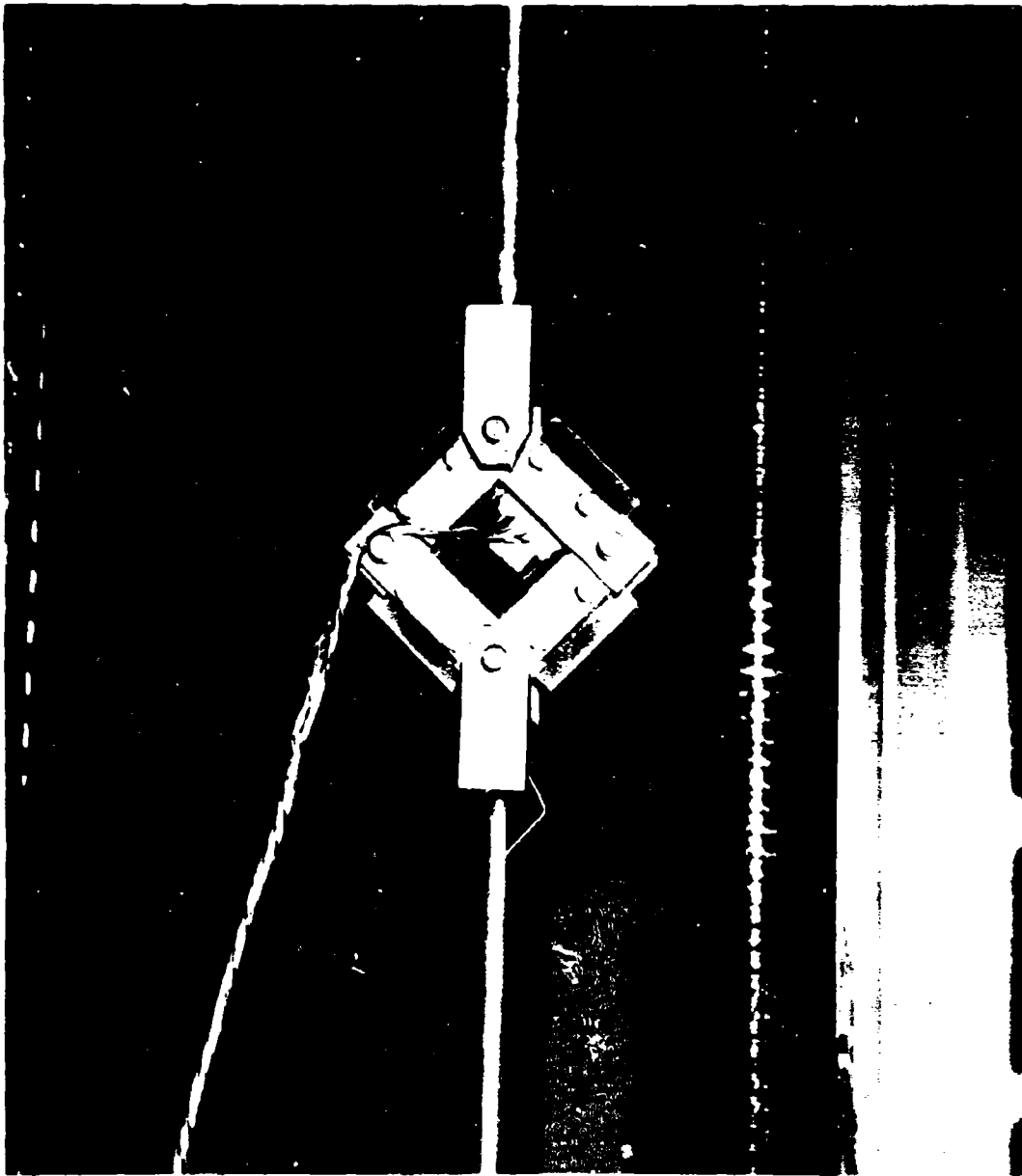


FIGURE 11. IN-PLANE SHEAR TEST SETUP

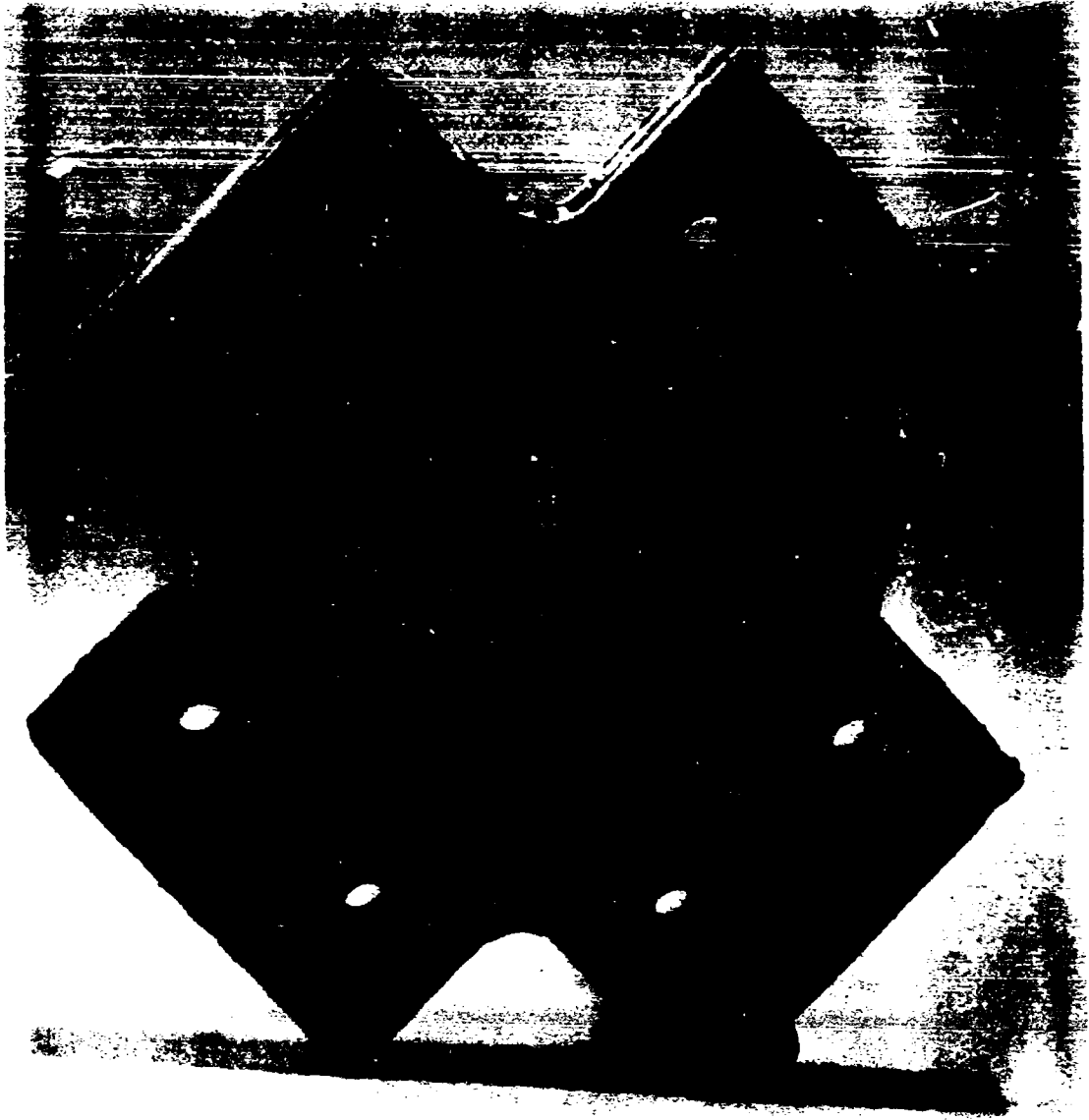


FIGURE 12. TYPICAL IN-PLANE SHEAR SPECIMEN FAILURE

TABLE V.
SUMMARY OF THEORETICAL AND EXPERIMENTAL IN PLANE SHEAR PROPERTIES

MATERIALS	PATTERN	THICKNESS (IN.)	ELASTIC CONSTANTS		STRENGTH PROPERTIES				VOLUME FRACTIONS		
			SHEAR MODULUS, G		PREDICTED		ACTUAL		FILAMENTS	RESIN	VOIDS
			PREDICTED (10 ⁶ PSI)	ACTUAL (10 ⁶ PSI)	FIRST FAILURE STRESS (KSI)	ULTIMATE STRESS (KSI)	FIRST FAILURE STRESS (KSI)	ULTIMATE STRESS (KSI)			
S-954/NARI/MCO 5505	ALL 0°	0.100	—	1.43	8.3	13.58	0.627	0.365	0.006		
				0.91	7.1	11.0					
				0.34	6.0	9.62					
				AVG 1.06	AVG 7.1	AVG 11.40					
	0°/±45°/90°			1.52	2.03	46.6	34.5				
					1.79		42.1				
				1.50		34.9					
			AVG 1.77	—	AVG 37.2						
0°/±45°/90°			1.52	2.08	46.6	34.8					
				2.24		34.2					
				1.93		33.7					
			AVG 2.08	10.7	46.6	AVG 34.2					
BORON/NAR/MCO 5505	ALL 0°	0.100	—	0.88	NONE	15.00	0.589	0.367	0.044		
				0.77	6.9	12.50					
				0.73	7.3	11.04					
				AVG 0.79	AVG 7.1	AVG 12.94					
	0°/±45°/0°			4.45	6.22	52.0	46.0				
					6.17		41.3				
				6.05		41.0					
			AVG 6.15	20.4	52.0	AVG 42.7					
0°/±45°/90°			4.45	5.48	52.0	31.7					
				6.23		33.8					
				5.80		33.7					
			AVG 5.84	20.4	52.0	AVG 33.1					

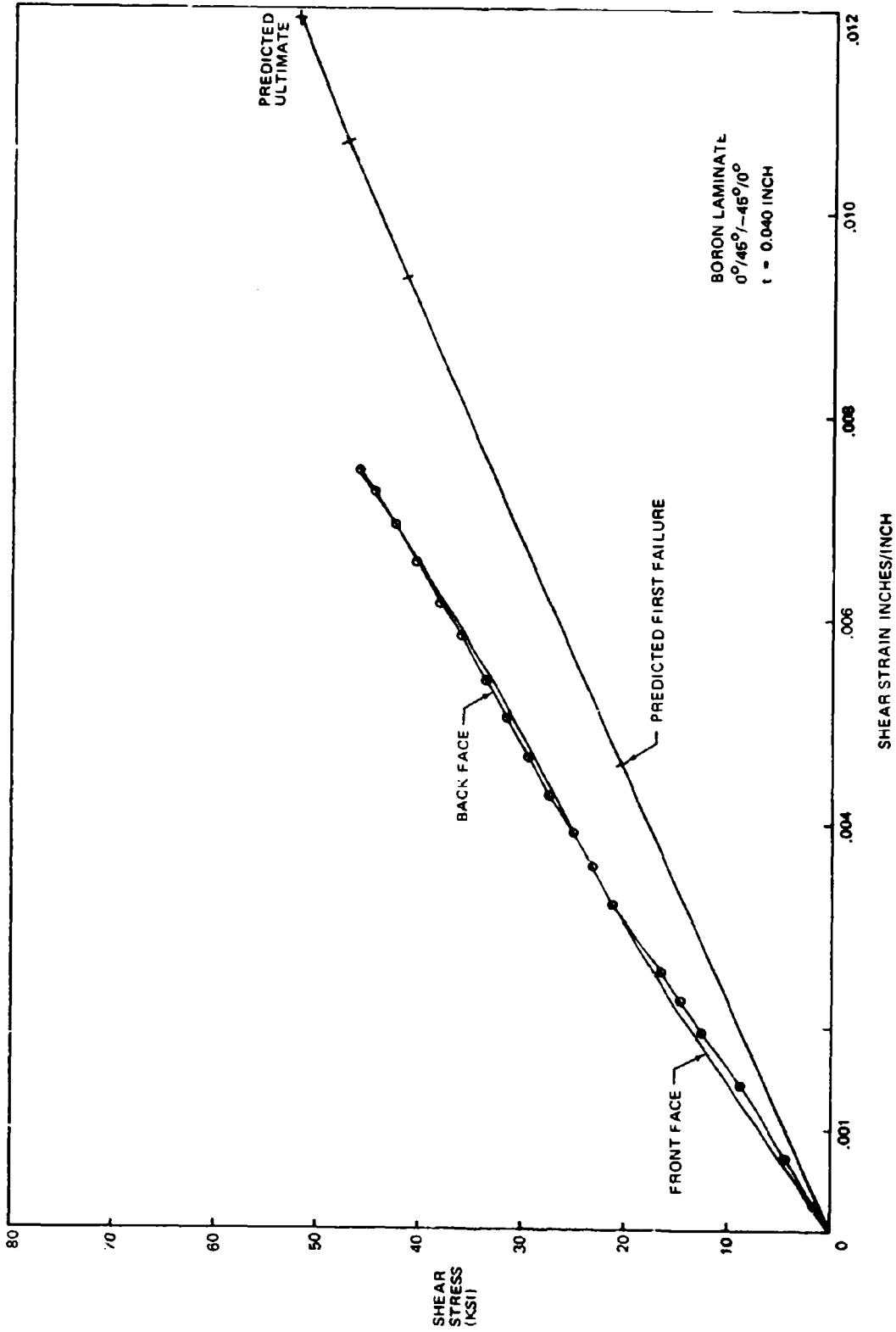


FIGURE 13. SHEAR STRESS-STRAIN DIAGRAM FOR SPECIMEN Z3824843-1

Two strain gages were mounted orthogonally near the center of each specimen to measure tension and compression strain data, which were reduced to shear strains. Test loads and strains were recorded continuously until failure. Test results are summarized in Table V, and a typical stress-strain curve is plotted in Figure 13.

Interlaminar Shear Tests

The interlaminar shear properties were determined on a small simple-beam specimen (Drawing Z4824816, Volume II). The test setup is illustrated in Figure 14. The specimens were simply supported by two 0.250-inch-diameter dowel pins, located in machined grooves 0.5 inch apart, on the test fixture. An alignment groove, centrally located between the pins, was used to position the test fixture under the 0.250-inch-diameter loading nose. The specimens were placed on the dowel pins with equal overhang at each end. Load was applied in the Riehle test machine at the rate of 0.05 inch per minute until failure occurred. Failure was indicated by an abrupt relaxation of the load input.

Test results are summarized in Table VI. The interlaminar shear stress, τ , was computed using the equation

$$\tau = 3P/4wt$$

where

P = Ultimate Load (pounds)

w = Specimen Width (inches)

t = Specimen Thickness (inches)

Tests results indicate interlaminar shear stress levels between 6850 and 13,425 psi, depending on fiber material patterns and resin additives. The addition of the Al_2O_3/SiC whisker mixture, at about 2 percent of resin weight, upgraded the interlaminar shear stress by about 24 percent as shown in Figure 15.

Pin-Bearing Tests

The pin-bearing specimens were fabricated in accordance with Drawing Z3824815, Volume II. The specimen proportions for pin diameter ($D = 1/4$ inch), laminate thickness ($t = 0.120$ inch), edge distance ratio ($e/D = 4 1/2$), and side distance ratio ($S/D = 3$) were chosen to produce bearing failure in the specimens. However, observed failure modes and subsequent analysis of bolted joint test results (see Section IV) indicated that an interaction of bearing and shear-out stresses caused failure in most cases.

The specimens were installed in the test fixture and mounted in a Riehle test machine. The load was introduced into the specimen through a 1/2-inch-diameter pin as shown in Figure 16. This self aligning method was used to avoid slippage of conventional grips, because unsymmetrical slippage would introduce (and magnify) errors in the deformation measurement.

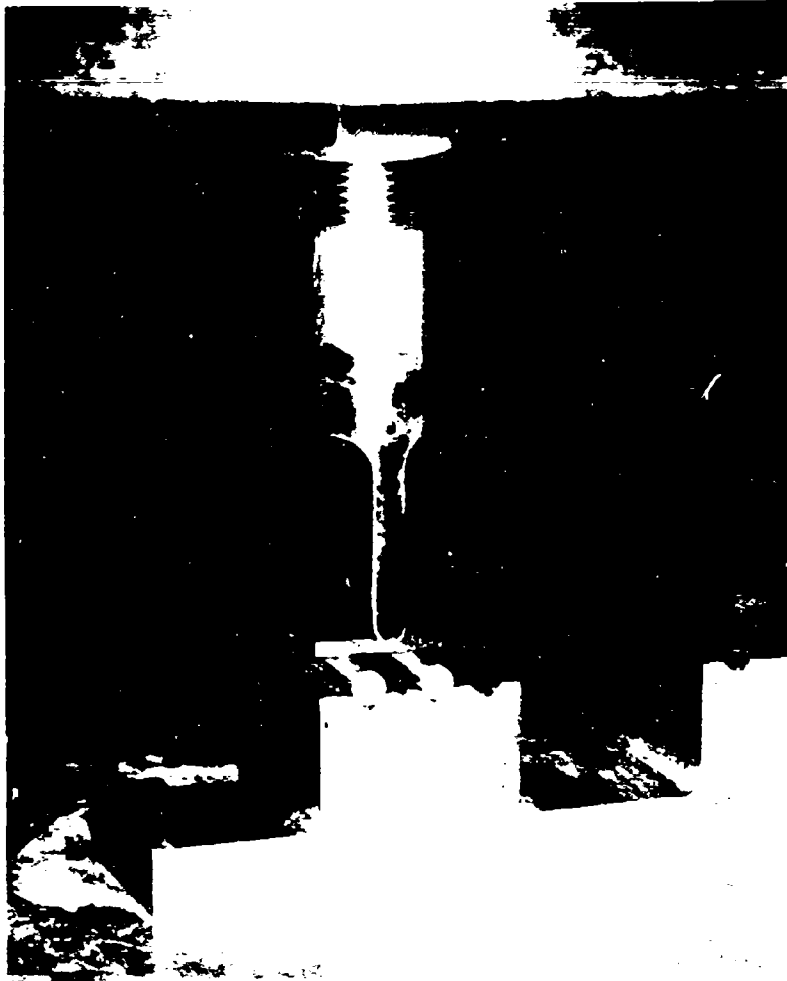


FIGURE 14. TEST SETUP FOR INTERLAMINAR SHEAR TEST

**TABLE VI
INTERLAMINAR SHEAR TEST RESULTS**

CONFIGURATION	SPECIMEN MATERIALS AND FIBER PATTERN	GAGE (IN.)	WIDTH (IN.)	AREA A, (SQ IN.)	FAILURE LOAD P, (LB)	INTERLAMINAR SHEAR STRENGTH = P/A (PSI)
-1	BORON/NARMCO 5505 0°/45°/-45°/0°	0.1203	0.4248	0.0511	715	10,480
		0.1194	0.4156	0.0496	657	9,940
		0.1158	0.4323	0.0501	683	10,200
-501	S-994 GLASS/NARMCO 5505 0°/45°/-45°/0°	0.1364	0.3625	0.0494	790	12,000
		0.1283	0.3720	0.0477	795	12,500
		0.1384	0.3690	0.0511	845	12,400
-503	BORON/NARMCO 5505 0°/45°/-45°/90°	0.1179	0.3988	0.0470	488	7,780
		0.1280	0.3950	0.0477	518	8,150
		0.1217	0.3906	0.0475	570	9,000
-505	S-994 GLASS/NARMCO 5505 0°/45°/-45°/90°	0.1370	0.4007	0.0549	501	6,850
		0.1373	0.3648	0.0501	526	7,875
		0.1278	0.3900	0.0498	519	7,805
-507	BORON/NARMCO 5505 SiC-Al ₂ O ₃ WHISKERS AT 2% OF RESIN WEIGHT 0°/45°/-45°/0°	0.1152	0.3422	0.0394	705	13,425
		0.1201	0.3620	0.0435	712	12,250
		0.1189	0.3651	0.0434	721	12,450
-509	BORON/NARMCO 5505 SiC-Al ₂ O ₃ WHISKERS AT 1% OF RESIN WEIGHT 0°/45°/-45°/0°	0.1181	0.3509	0.0414	680	12,300
		0.1173	0.3548	0.0416	669	12,040
		0.1162	0.3532	0.0410	671	12,250
-511	BORON/NARMCO 5505 AlN-Al ₂ O ₃ WHISKERS AT 2% OF RESIN WEIGHT 0°/45°/-45°/0°	0.1190	0.3689	0.0439	629	10,720
		0.1242	0.3681	0.0457	661	10,830
		0.1233	0.3678	0.0453	640	10,600

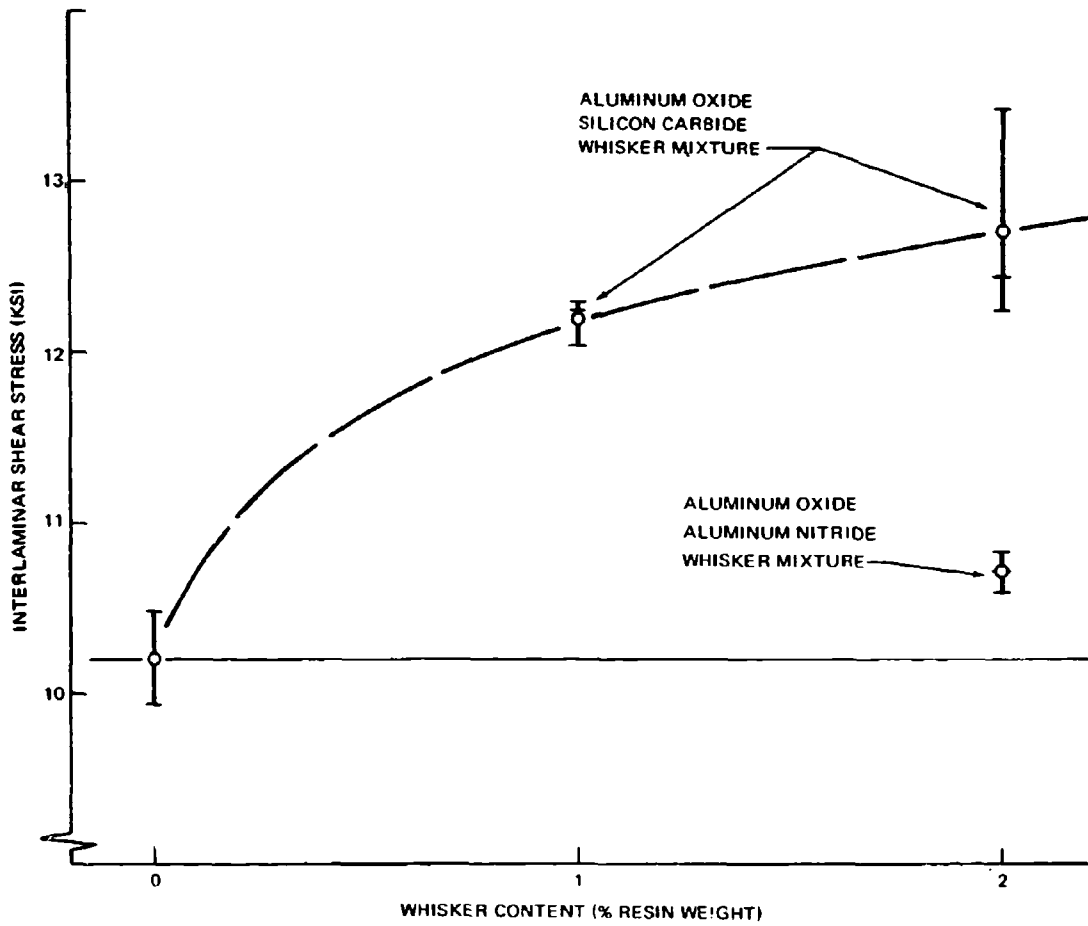


FIGURE 15. INTERLAMINAR SHEAR STRENGTH - WHISKERED SPECIMENS

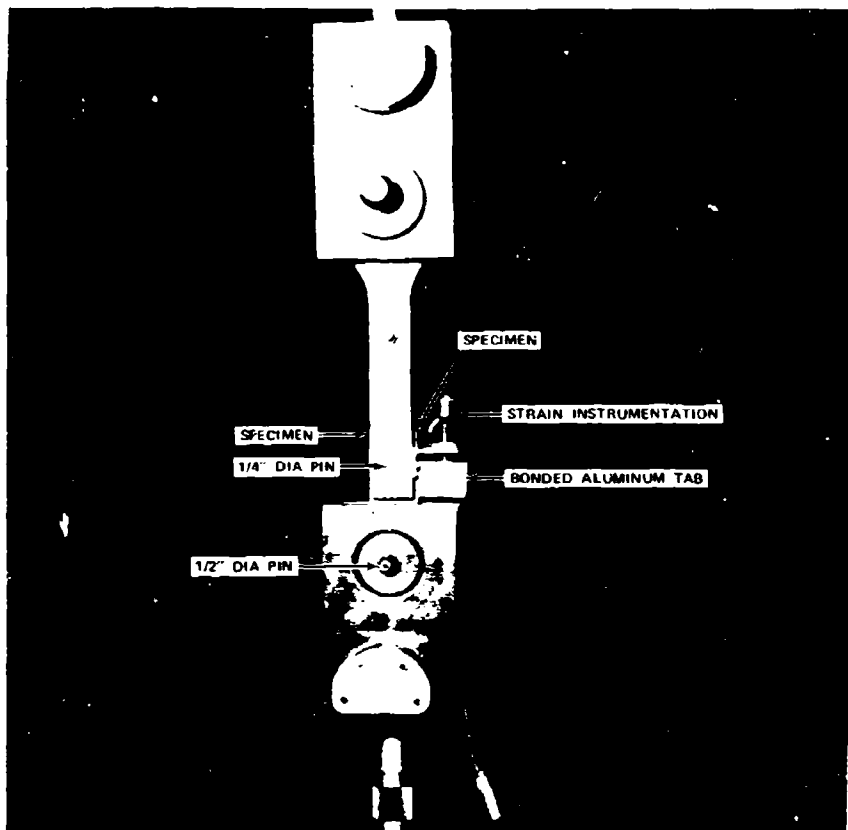


FIGURE 16. TEST SETUP FOR PIN-BEARING TEST

A differential transformer was mounted to the fixture, and hole deformation was measured by employing an aluminum tab bonded to the specimen as shown in Figure 17. The deformation data were measured at the upper edge of the bearing hole only, so deformations occurring at the 1/2-inch-diameter hole, through which the load was introduced, did not affect the recorded data. The load was applied continuously at a crosshead feed rate of 0.05 inch per minute, and data were read out on a microformer recorder. It provided direct and continuous recording of load versus deformation. The test results were summarized in Table VII.

The bearing test holes were drilled in the composite using a 1/4-inch-diameter, water-cooled, diamond-core drill. The resulting holes ranged in diameter from 0.255 to 0.264 inch. Figure 18 is an enlarged photograph of the hole edge and bearing surface conditions of a typical hole.

The initial tests were accomplished using 125,000- to 145,000-psi heat-treated steel pins ground to diameters of 0.257, 0.261, and 0.263 inch. These pins were used selectively to provide a pin fit in the composite hole ranging from a slight interference fit to a 0.004 inch clearance. As noted in Table VII, two pin bearing specimen configurations (-507 and -509) were tested using pins with slight interference fits in the composite. As a result, the load-deformation plots were erratic, indicating negative deformations in some cases. It was theorized that the interference-fit pins at low load levels caused sufficient friction at the bearing surface to prevent alignment of the specimen axis with the load line. When frictional effects were overcome by load buildup, rotation of the specimen caused erroneous deformation measurements.

A pin clearance of about 0.0005 to 0.0010 inch on the diameter yielded more repeatable test results. This amount of clearance did not noticeably inhibit specimen-centering, and it minimized the nonlinear load-deformation characteristics at low load levels while the pin was seating in the composite. A typical load-deformation plot is shown in Figure 19.

In subsequent pin-bearing tests (designated Series 2 in Table VII) additional load-deflection plots were generated on Specimens 3824815-1, -503, and -511. Three specimens of each configuration were loaded continuously to failure, and an additional three specimens each of the -1 and -503 configurations were loaded and unloaded in 1000-pound increments to failure. The latter tests were conducted to indicate elastic recovery and hysteresis characteristics of the laminates.

Based on previous experience, these later tests were conducted using high heat treat (160,000 to 180,000 psi) steel pins with a 0.0005- to 0.0010-inch pin clearance on the hole diameter. The increased-strength pins reduced bending effects, while the specified pin clearance yielded more repeatable load-deflection plots. Loads were applied at a crosshead feed rate of 0.05 inch per minute for all specimens. As shown in Table VII, the second-series test results were very consistent and in fair agreement with previous results. In the later tests, the -503 configuration consistently achieved higher bearing stresses at failure. Shear failures were prevalent in the -511 configuration (boron/epoxy with $AIN-Al_2O_3$ whiskers) at the low end of the strength range of the previous tests.

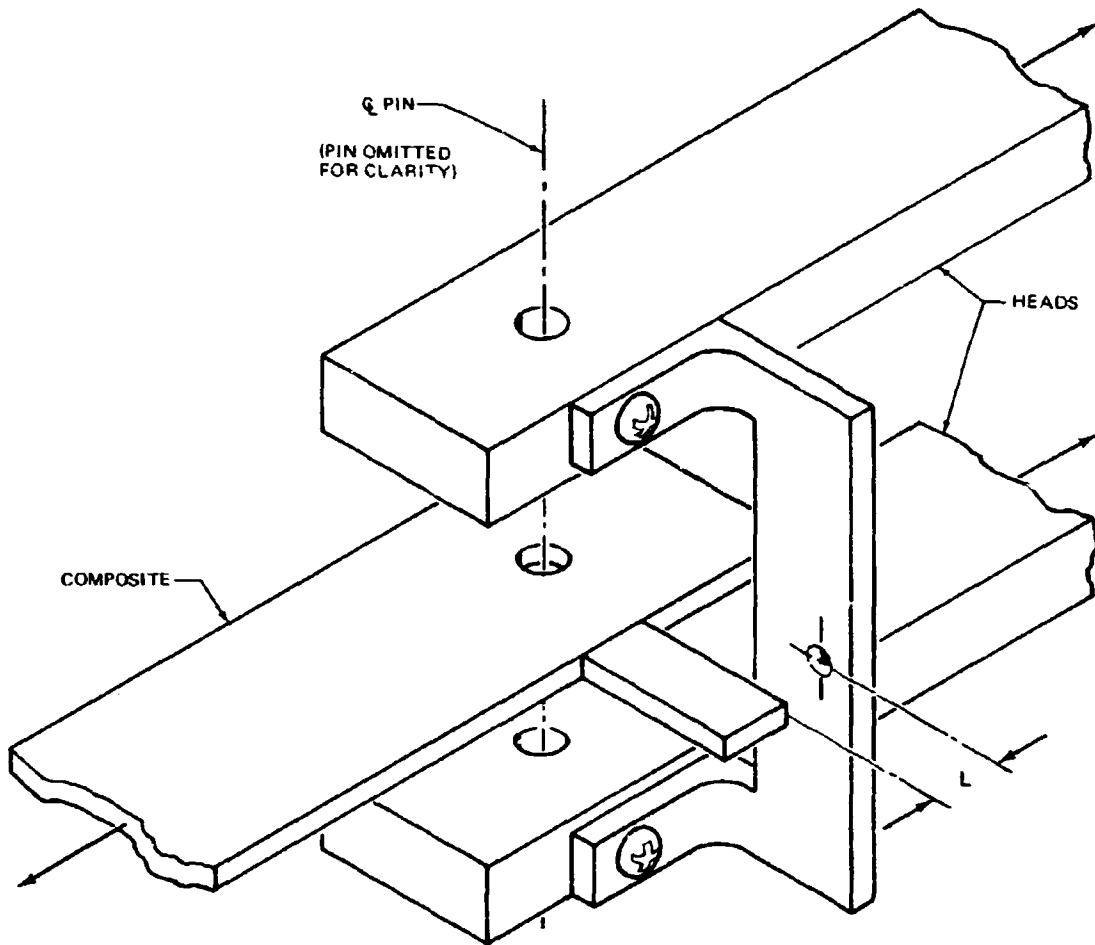


FIGURE 17. SCHEMATIC OF TEST FIXTURE FOR PIN-BEARING TESTS

TABLE VII
PIN-BEARING TEST RESULTS

CONFIGURATION	SPECIMEN MATERIALS AND FIBER PATTERNS	GAGE (IN.)	HOLE DIA (IN.)	PIN DIA (IN.)	BEARING AREA (SQ IN.)	ULTIMATE LOAD (LBS)	AVERAGE STRESS AT FAILURE		BEARING STRESS AT 4% OF PSEY (PSI)	FAILURE MODE	TEST DATE
							BEARING (PSI)	SHEAR-OUT (PSI)			
Z3824815-1	BORON/NARMCO 5505 DP/ASP/ASP/POP	0.1200	0.258	0.257	0.0308	4,440	144,000	14,800	121,000	COMBINED SHEAR AND BEARING	7/67
		0.1200	0.260	0.257	0.0308	3,620	117,500	12,100	72,700	SHEAR-OUT	
		0.1198	0.2569	0.257	0.0308	4,230	137,500	14,100	136,500	COMBINED SHEAR AND TENSION	
Z3824815-1 SERIES 2		0.1295	0.2567	0.256	0.0330	3,582	108,000	11,000	58,000	SHEAR-OUT	12/68
		0.1286	0.2564	0.256	0.0328	3,773	113,500	11,500	62,400		
		0.1286	0.2566	0.256	0.0329	3,580	109,000	11,100	57,200		
Z3824815-1 LOADED INCREMENTALLY SERIES 2		0.1260	0.2562	0.2540	0.0320	3,686	112,000	11,400	-	SHEAR-OUT	12/68
		0.1293	0.2566	0.2560	0.0331	3,686	110,800	11,300	-		
		0.1254	0.2563	0.2560	0.0320	3,570	111,500	11,300	-		
Z3824815-501	S-994 GLASS/NARMCO 5505 DP/ASP/ASP/POP	0.1308	0.256	0.2560	0.0349	1,800	53,100	5,300	48,000	BEARING	10/67
		0.1260	0.256	0.2560	0.0321	1,960	60,760	6,200	29,900		
		0.1320	0.254	0.2530	0.0334	1,980	59,600	6,040	41,400		
Z3824815-503	BORON/NARMCO 5505 DP/ASP/ASP/POP	0.1200	0.260	0.2570	0.0308	3,580	116,500	12,000	95,500	BEARING	7/67
		0.1200	0.260	0.2570	0.0308	3,640	118,100	12,100	76,000		
		0.1200	0.264	0.2630	0.0316	3,800	120,000	12,700	49,500		
Z3824815-503 SERIES 2		0.1150	0.2556	0.2560	0.0293	4,146	141,300	14,400	119,400	BEARING	12/68
		0.1150	0.2546	0.2540	0.0292	4,256	146,700	14,800	113,000		
		0.1190	0.2560	0.2540	0.0302	4,086	134,300	13,600	-		
Z3824815-503 LOADED INCREMENTALLY SERIES 2		0.1182	0.2562	0.2540	0.0300	3,718	123,900	12,800	-	BEARING	12/68
		0.1171	0.2560	0.2540	0.0298	4,116	138,000	14,000	-		
		0.1182	0.2551	0.2540	0.0302	3,780	126,000	12,700	-		
Z3824815-506	S-994 GLASS/NARMCO 5505 DP/ASP/ASP/POP	0.1260	0.256	0.2560	0.0319	1,986	61,650	6,300	25,200	BEARING	10/67
		0.1380	0.256	0.2560	0.0354	2,210	62,600	6,360	46,200		
		0.1380	0.256	0.2560	0.0347	2,186	63,000	6,430	57,600		
Z3824815-507	BORON/NARMCO 5505 SiC-Al ₂ O ₃ WHISKERS AT 2% OF RESIN WEIGHT DP/ASP/ASP/POP	0.1215	0.2569	0.2570	0.0313	2,980	98,600	9,770	56,000	COMBINED SHEAR AND BEARING	12/67
		0.1212	0.2569	0.2570	0.0312	4,500	144,200	14,800	136,800	BEARING (AT 1/2 DIAMETER LOADING PIN)	
		0.1212	0.2580	0.2580	0.0313	3,620	115,900	11,900	81,000	COMBINED SHEAR AND TENSION	
Z3824815-508	BORON/NARMCO 5505 SiC-Al ₂ O ₃ WHISKERS AT 1% OF RESIN WEIGHT DP/ASP/ASP/POP	0.1186	0.2569	0.2570	0.0306	3,710	121,800	12,500	90,600	BEARING	12/67
		0.1188	0.2568	0.2560	0.0304	3,910	128,600	13,200	38,700	COMBINED SHEAR AND BEARING	
		0.1182	0.2668	0.2560	0.0302	3,670	121,300	12,400	118,800	COMBINED SHEAR AND BEARING	
Z3824815-511	BORON/NARMCO 5505 AlN-Al ₂ O ₃ WHISKERS AT 2% OF RESIN WEIGHT DP/ASP/ASP/POP	0.1200	0.2610	0.2610	0.0313	4,200	134,100	14,000	79,500	BEARING	7/67
		0.1200	0.2610	0.2570	0.0308	4,060	131,500	13,500	98,800	BEARING	
		0.1200	0.2630	0.2630	0.0315	3,880	-	-	85,000	SHEAR (AT 1/2 DIAMETER LOADING PIN)	
Z3824815-511 SERIES 2		0.1183	0.2570	0.2560	0.0298	3,880	129,500	13,300	124,000	SHEAR-OUT	12/68
		0.1163	0.2564	0.2560	0.0298	3,775	126,600	13,000	117,200		
		0.1170	0.2560	0.2560	0.0298	4,080	136,500	13,800	115,400		

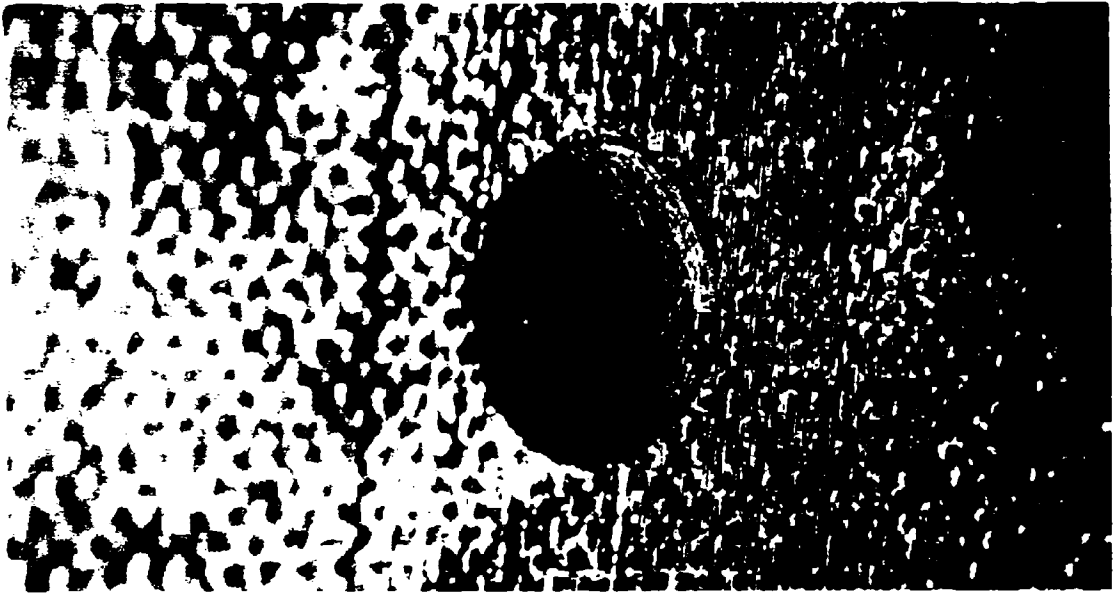


FIGURE 13. HOLE CONDITION IN PIN-BEARING SPECIMENS BEFORE TEST

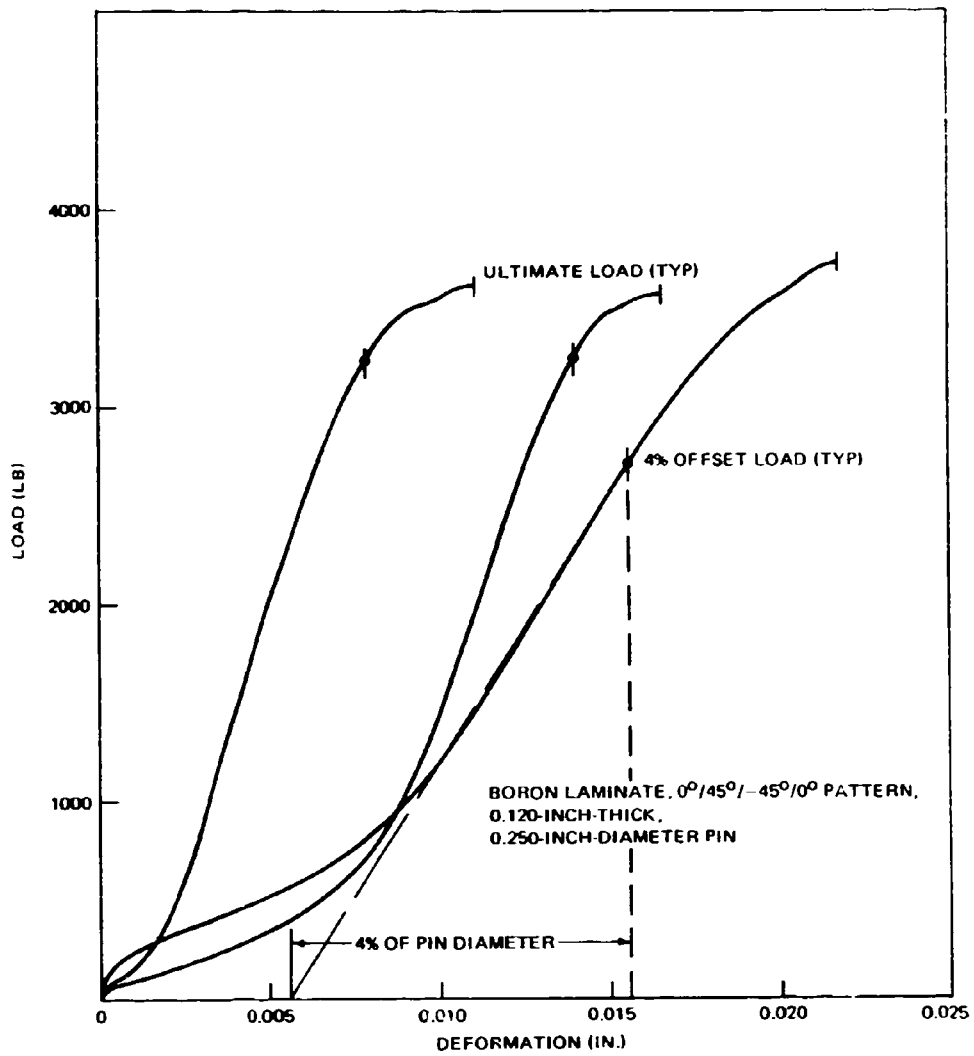


FIGURE 19. LOAD-DEFORMATION CURVES FOR PIN-BEARING SPECIMENS Z3824815-1

A typical load-deformation plot from one of the specimens that was loaded and unloaded incrementally is shown in Figure 20. This plot indicates that a considerable amount of plastic deformation occurred in the first 1000-pound load increment. Approximately 30 percent of the deformation at a 1000-pound load was not recovered elastically. Load-deformation plots for the other pin-bearing specimens are included in Volume II. Each of these curves indicates that some of the strain from the first 1000-pound load was not recovered elastically. The amounts varied between tests since the initial slope of each load-deformation plot depended on the specimen alignment characteristics as the pin was seating in the composite. The plots indicate that from 30 to 80 percent of the deformation may result from plasticity and/or other nonlinear characteristics (e. g., buckling of fiber ends).

The 4-percent bearing yield stresses were determined using ASTM Test Method D953-54. This method determined the load at which a tangent to the load-deformation curve intersected the zero load axis at a deformation of 4 percent of the original hole diameter. This point is indicated on the load-deformation plot in Figure 19 and on the similar plots in Volume II.

Figures 21 and 22 are photographs of typical specimen failures. As shown in Figure 21, the -1 specimens failed in a combined bearing and shear mode. The initial -511 specimen configuration was identical to the -1, except for the addition of an Al_2O_3/AlN whisker mixture as a resin additive (2 percent of the resin weight). These specimens and the -503 specimens failed in a true bearing mode as shown in Figure 22. The whisker additions in the -511 specimen upgraded the resin shear strength sufficiently to preclude a shear-out failure.

The addition of whiskers did not appear to upgrade the ultimate bearing stress of the composite, as shown in Figure 23. The range of bearing stresses between otherwise identical specimens indicated 126.6 to 131.5 ksi for the -511 whiskered specimens and up to 144 ksi for the similar -1 specimen in which bearing failure was significant.

ADHESIVE PROPERTIES

Strength and modulus data were determined for six adhesives in the material properties tests. Strength comparisons were based on lap shear tests and flatwise tension tests on a honeycomb core. Stress-strain data in shear were determined using a torsion ring shear test apparatus developed as part of the program.

Adhesives covering a range of strength and modulus properties were chosen for evaluation. Only those with considerable production history were considered, so batch variables and material aging effects were minimized. Selected adhesives were the following:

- AF130, Epoxy Novalac
- AF110B, Epoxy Nitrile
- Narmco 252, 250°F Cure

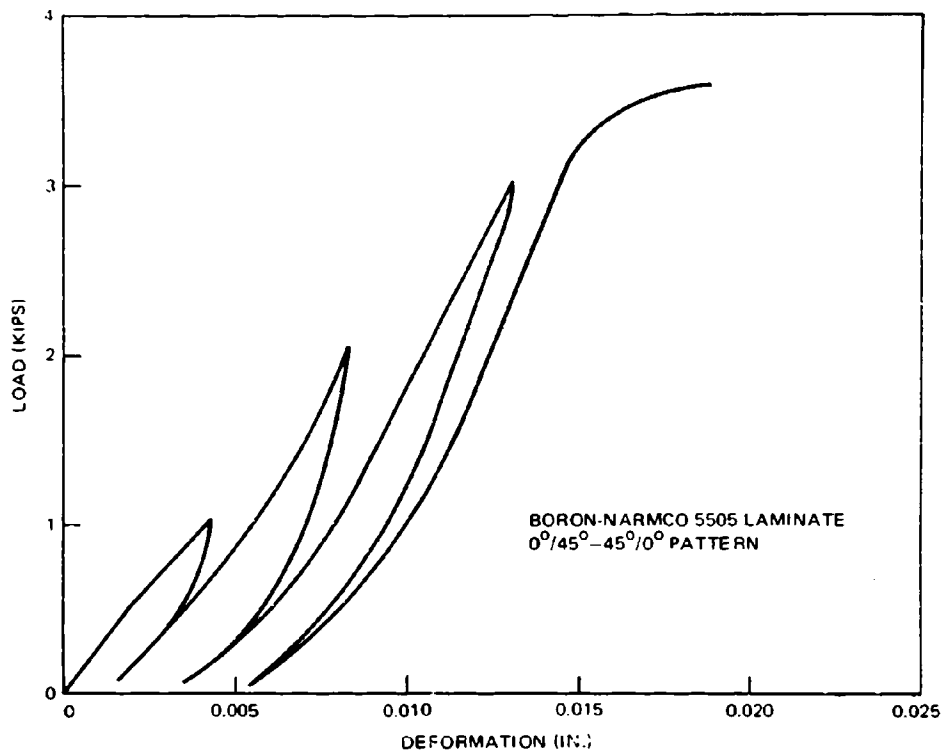


FIGURE 20. LOAD-DEFORMATION CHARACTERISTICS OF PIN-BEARING SPECIMEN Z3824815-1

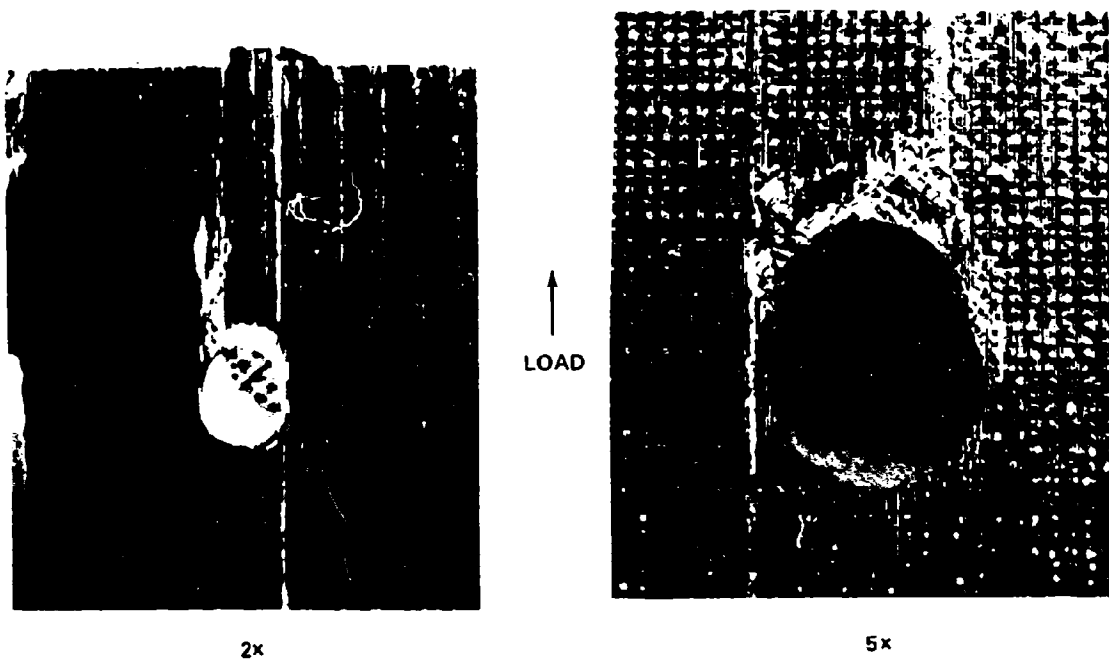


FIGURE 21. BEARING AND SHEAR-OUT FAILURE IN SPECIMEN Z3824815-1



5x

↑
LOAD



5x

FIGURE 22. BEARING FAILURES IN Z3824815 SPECIMENS

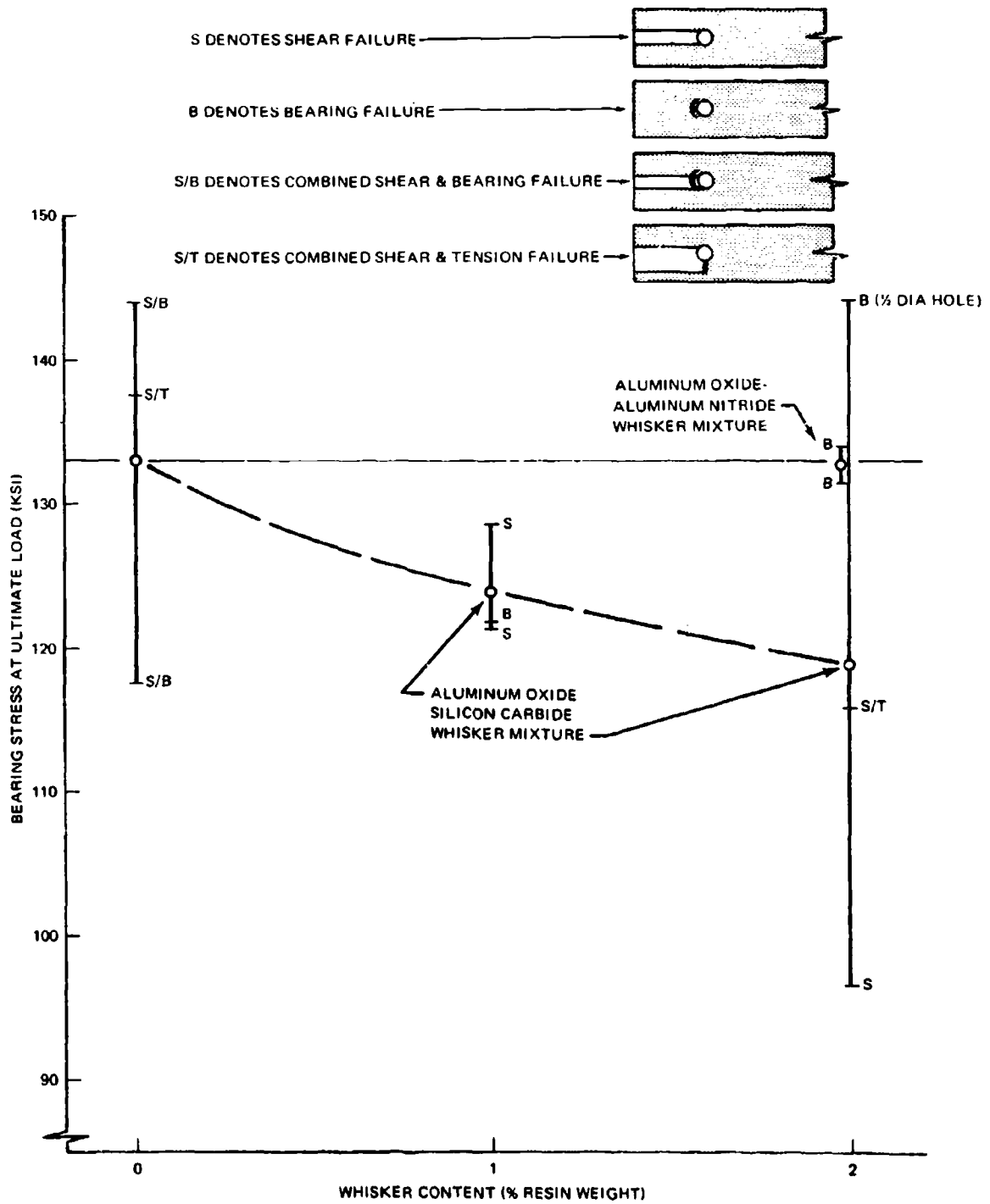


FIGURE 23. PIN JOINT ULTIMATE STRENGTHS - WHISKERED SPECIMENS

- HT424, Epoxy Phenolic
- Shell 951, Nylon Epoxy
- Lefkoweld 109, Cold-Set Epoxy

Adhesive Double Lap Shear Tests

The specimens were fabricated in a double lap configuration as shown in Figure 24. The specimen assemblies were installed in an Instron test machine as shown in Figure 25. Load was applied through mechanical grips at a crosshead rate of 0.05 inch per minute to failure. The specimens were gripped in standard serrated grips. Shims of equivalent thickness to the combined thickness of the composite specimen and bond were inserted between the aluminum adherends to provide a means of gripping the aluminum without inducing stresses in the bond.

The method of gripping proved satisfactory for all but the higher strength adhesives. Two of the -507 specimens (Shell 951 adhesive) were tested successfully. However, two specimens failed in the grips at a composite stress level of about 84,000 psi. (The calculated ultimate strength of this laminate was greater than 100,000 psi.) One of these latter specimens and the remaining untested specimen were then fitted with bonded aluminum alloy gripping tabs. On the second load application, the salvaged specimen failed at 2790 pounds at an average adhesive shear stress of 3470 psi. This bond line sustained 5450 psi in shear on the first load application. In subsequent fatigue testing, it was theorized that damage was sustained by the adhesive when local stresses exceeded the proportional limit stress of the adhesive. In this case, the entire bond line was stressed beyond the proportional limit, and therefore it is assumed that damage to the adhesive had reduced the effective bond area on the second load application. The untested specimen failed in tension through the basic composite section at 4590 pounds. The composite stress level at this load was 98,000 psi, and the average shear stress in the adhesive was 5950 psi when the laminate failed.

Test results for the double lap shear specimens were summarized in Table VIII. The higher strength materials tended to fail in an adhesive/cohesive manner as shown in Figure 26, while the lower strength materials tended toward a resin/fiber interfacial failure in the first layer in the laminate, as shown in Figure 27.

Adhesive Flatwise Tension Tests

The objective of the adhesive flatwise tension tests was to determine the adhesives' capacities to meet or exceed requirements to bond the honey-comb sandwich core to the composite face sheet. The specimen design is shown in Drawing Z4824825, Volume II.

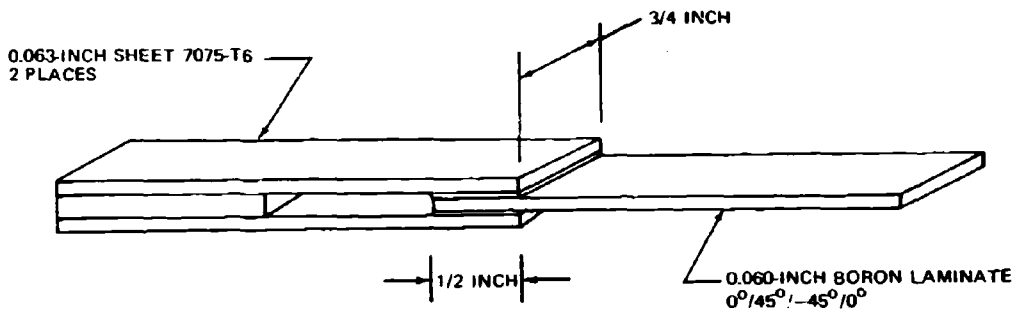


FIGURE 24. ADHESIVE SPECIMEN DIMENSIONS

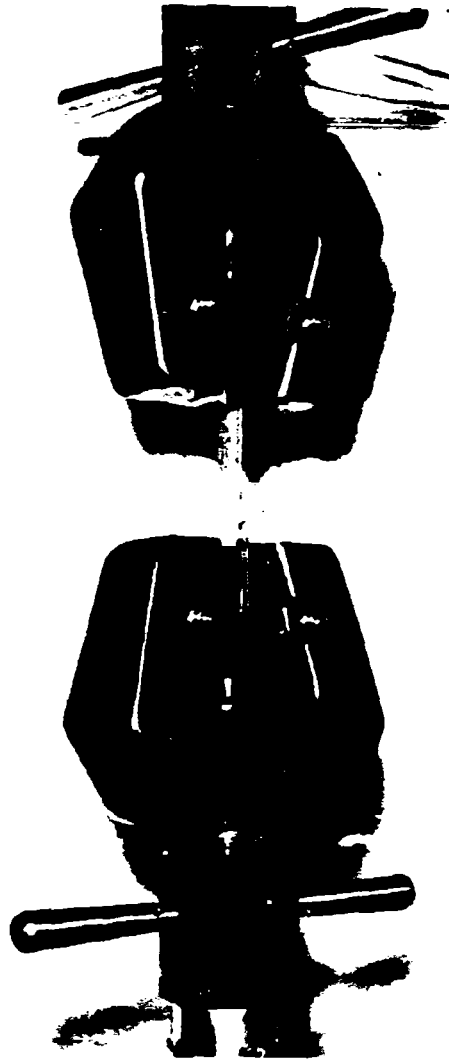


FIGURE 25. TEST SETUP FOR ADHESIVE DOUBLE LAP SHEAR SPECIMENS

TABLE VIII
ADHESIVE DOUBLE LAP SHEAR TEST RESULTS

(Specimen No. Z 4824824)

Dash No.	Specimen No.	Adhesive	Bond Line Data				Ultimate Load (Lb)	Adhesive Average Shear Stress (Psi)	Type of Failure
			Average Thickness (In.)	Width (In)	Overlap (In)	Area (Sq In.)			
-1	1	AF 130	0.0033	0.769	0.570	0.877	880	1,004	Failure was 100% between the boron fibers and resin in first ply of laminate, both sides of specimen
	2		0.0038	0.768	0.490	0.743	925	1,245	
	3		0.0038	0.764	0.550	0.840	960	1,142	
	4		0.0030	0.784	0.570	0.884	960	962	
	5		0.0038	0.786	0.530	0.833	1,060	1,272	
-501	1	Narmco 252	0.0006	0.778	0.510	0.784	3,920	4,940	Glass scrim side - 50% adhesion to laminate surface area 50% laminate resin to boron fibers Opposite side - 100% adhesive to laminate.
	2		0.0006	0.781	0.500	0.781	3,925	5,026	
	3		0.0005	0.771	0.470	0.726	2,925	4,036	
	4		0.0007	0.760	0.460	0.698	3,925	5,614	
	5		0.0008	0.775	0.530	0.822	3,795	4,620	
-503	1	AF 1108	0.0025	0.770	0.500	0.770	3,650	4,740	Glass scrim side - 75% cohesion, 25% resin to boron Opposite side - 75% cohesive, 25% adhesive to laminate.
	2		0.0033	0.766	0.610	0.760	3,476	4,463	
	3		0.0020	0.768	0.520	0.798	3,225	4,038	
	4		0.0035	0.771	0.510	0.766	3,485	4,432	
	5		0.0030	0.771	0.500	0.771	*3,380	(4,390)	
-506	1	Bloomingdale HT 424	0.0075	0.788	0.500	0.788	1,075	1,364	Glass scrim side - 50% adhesive to laminate, 50% resin to boron. Opposite side - mainly between resin and boron fiber.
	2		0.0080	0.782	0.540	0.845	1,725	2,043	
	3		0.0075	0.760	0.540	0.821	875	1,068	
	4		0.0090	0.769	0.520	0.789	1,040	1,317	
	5		0.0080	0.767	0.560	0.859	1,435	1,670	
-507	1	Shell 951	0.0033	0.769	0.470	0.723	4,175	5,775	Glass scrim side - 90% between laminate resin and boron. Opposite side - 50% cohesive, 50% adhesive to laminate.
	2		0.0033	0.780	0.520	0.811	4,370	5,387	
	3		0.0035	0.780	0.500	0.780	*4,075	(5,220)	
	4		0.0033	0.770	0.500	0.770	4,590**	(5,950)	
	5		0.0030	0.789	0.610	0.804	*4,370†	(5,450)	
-508	1	Leikoweld 108	0.0020	0.766	0.520	0.797	1,500	1,893	50% adhesive to laminate, 50% adhesive to aluminum.
	2		0.0020	0.792	0.530	0.840	1,475	1,758	
	3		0.0018	0.774	0.520	0.806	1,575	1,956	
	4		0.0013	0.785	0.530	0.832	1,300	1,562	
	5		0.0015	0.782	0.520	0.813	1,825	2,244	

* Failed in Grip.

** This specimen was tested with A1 alloy gripping tabs bonded to the composite. The specimen failed in tension through the basic section at a composite stress level of 98,000 psi.

† This specimen was salvaged with A1 alloy gripping tabs bonded to the composite and retested. Bond failed in shear at load of 2790 pounds during retest.

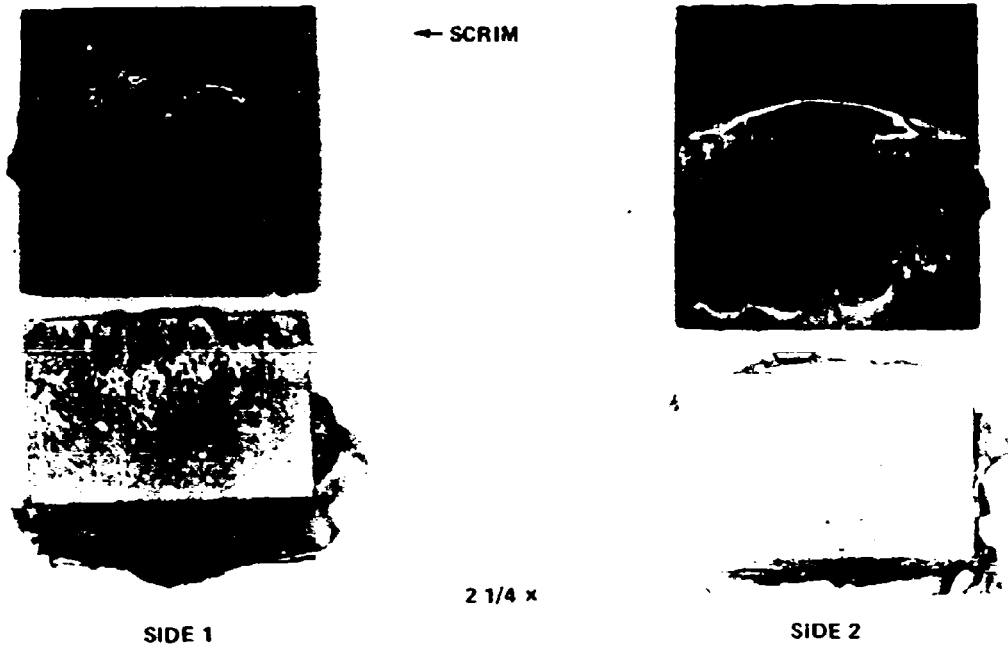


FIGURE 26. ENLARGED PHOTO OF BOND FAILURE ON Z4824824-507 SPECIMEN

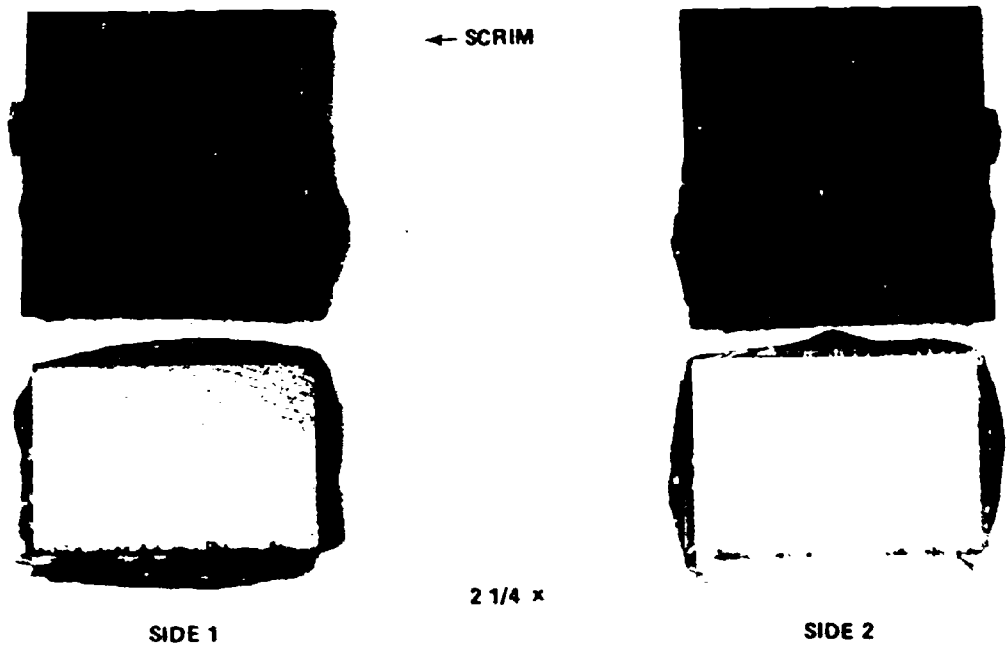


FIGURE 27. ENLARGED PHOTO OF BOND FAILURE ON Z4824824-1 SPECIMEN

After fabrication, standard aluminum alloy loading blocks were bonded to each face of the specimens using Lefkowitz 109 cold-set adhesive. The specimens were installed in a Baldwin test machine as shown in Figure 28. Load was applied at a crosshead rate of 0.05 inch per minute to failure. Most of the adhesives had sufficient strength to produce tensile failures in the aluminum honeycomb core (3/16-5052-001N). A typical failure is shown in Figure 29. Test results are summarized in Table IX.

Torsion Ring Shear Tests

An accurate knowledge of adhesive shear strength and modulus is a prerequisite to efficient design of bonded joints. These properties were determined in the present study using a torsion ring shear test similar to the test method described by Lunsford in Reference 7. The torsion ring approach eliminated the large stress concentration and secondary peeling effects observed in conventional overlap shear specimens.

Torsion ring adhesive specimens were fabricated and tested to evaluate the stress-strain properties in shear of the six adhesives used in the program. After this evaluation, the specimen was modified to permit control of bond line thickness, and the effects of bond line thickness and strain-rate were studied for Shell 951 adhesive.

Design and fabrication of the test apparatus and specimens are discussed in this section, together with test methods and results. Details of the test apparatus, specimens, and instrumentation are shown in Drawing Z5824822, Z3824821, and Z5824826, respectively, in Volume II.

The torsion ring shear test was designed for accurate determination of the stress-strain characteristics of the adhesives in shear without the stress magnification effects of conventional flat lap shear specimens. The fixture was designed with the objective of applying a pure torsional strain with negligible translational strain. The instrumentation had sufficient accuracy to measure torsional deflections less than 0.0001 inch to generate a stress-strain curve within a total deflection of approximately 0.001 inch.

The basic test apparatus is illustrated in Figure 30 together with details of the specimen installation and chucking methods. This design afforded the following advantages:

- It required a simple coupon that was prebonded independently. Thus, a number of coupons were prepared in advance and tested at one setup of the testing machine.
- Specimen halves were aligned by use of a single central hole.
- The coupon was accurately measured before and after bonding for precise determination of bond line thickness. Access to both sides of the adhesive bond line was provided so excess adhesive could be removed to maintain a constant bond line dimension.



FIGURE 28. ADHESIVE FLATWISE TENSION TEST SETUP

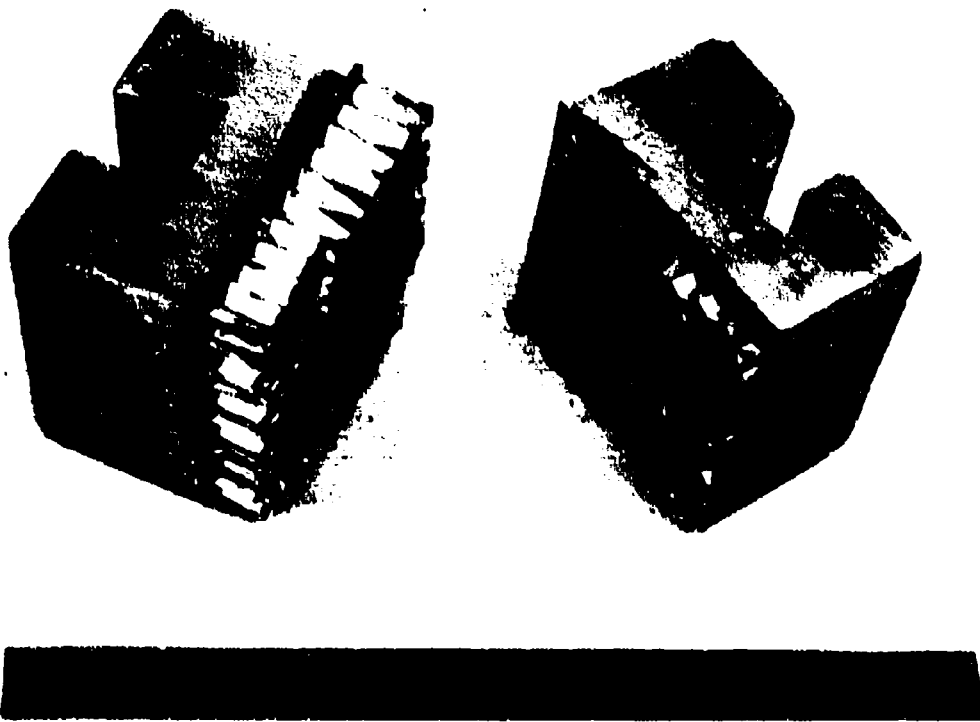


FIGURE 29. TYPICAL CORE FAILURE – ADHESIVE FLATWIRE TENSION SPECIMEN

**TABLE IX
ADHESIVE FLATWISE TENSION TEST RESULTS**

ADHESIVE	ULTIMATE LOAD (LB)	ADHESIVE STRESS (PSI)	AVERAGE STRESS (PSI)	TYPE FAILURE
AF-130	2745	686	648	ALUMINUM HOLDING FIXTURE TO BORON SKIN
3-M	2790	698		
(-1)	2330	583		
	2495	624		
252	2990	748	753	ADHESIVE 80% CORE 20%
NARMCO	3005	751		CORE 100%
(-501)	2515	629*		BORON SKIN TO ALUMINUM BLOCK*
	2992	748		CORE 100%
	3060	765		CORE 100%
AF-1108	2970	743	747	CORE 100%
3-M	3066	766		CORE 50% BORON SKIN 50%
(-503)	3020	755		CORE 100%
	2890	723		CORE 100%
HT-424	1040	251	337	ADHESIVE TO BORON
BLOOMINGDALE	1530	382		ADHESIVE 50%
(-605)	1280	320		ADHESIVE TO BORON
	1685	398		ADHESIVE 20%
951	2940	735	721	CORE 100%
SHELL	2460	615*		BORON SKIN TO ALUMINUM BLOCK*
(-507)	2863	716		CORE 100%
	2755	689		CORE 100%
	2980	745		SKIN DELAMINATION
109	2245	561	492	BORON SKIN
LEFKOWELD	2717	679		BORON 50% CORE 50%
(-509)	2060	515		CORE 100%
	857	214		BORON SKIN

*NOT INCLUDED IN AVERAGE. FAILED AT SKIN-TO-TEST BLOCK INTERFACE.

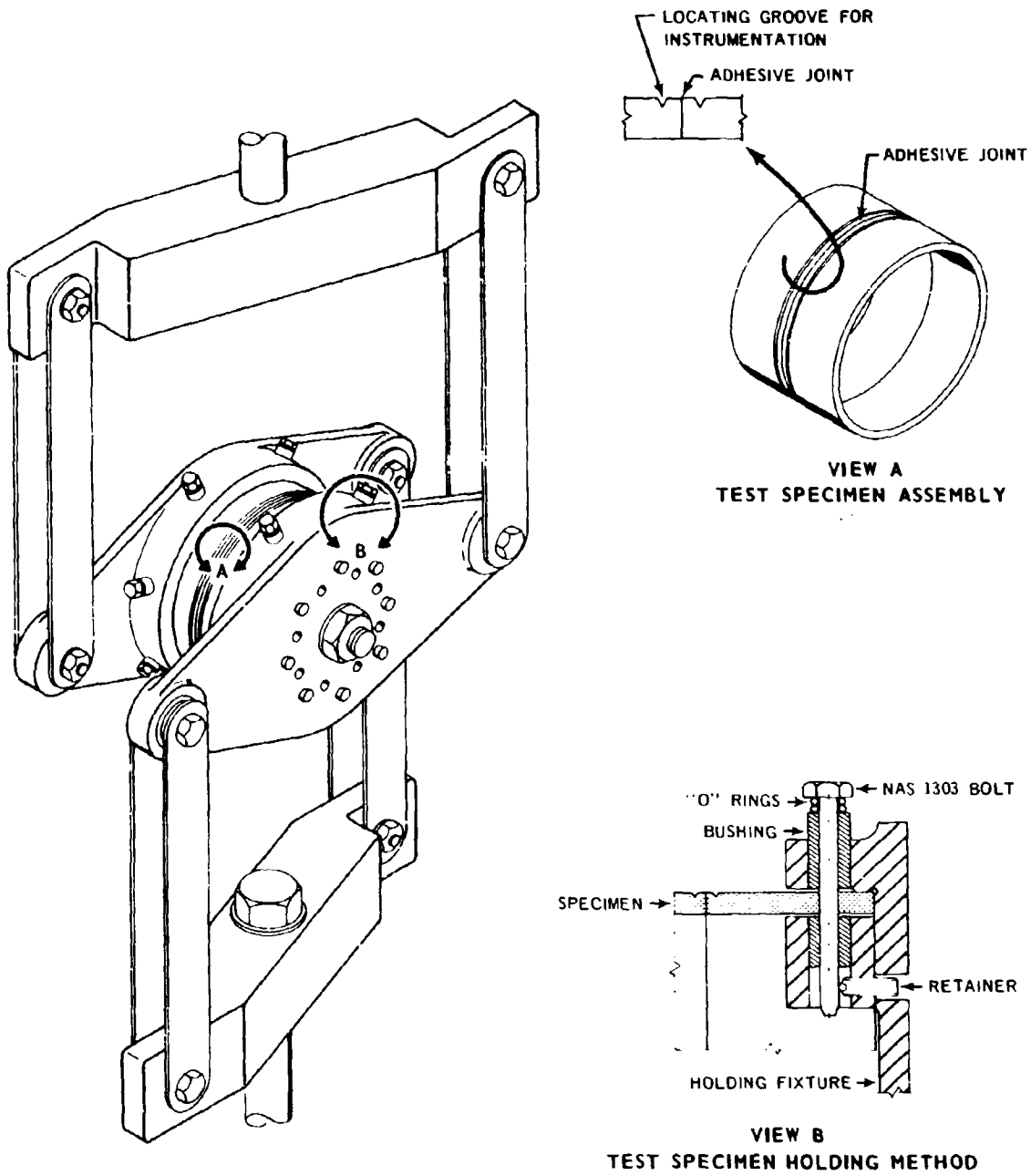
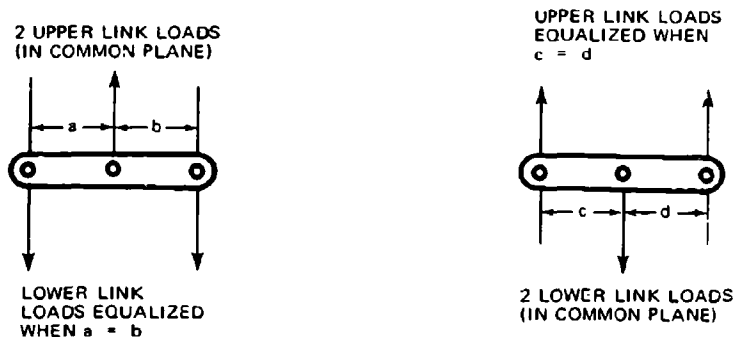


FIGURE 30. TORSION RING ADHESIVE SPECIMEN TEST FIXTURE ASSEMBLY

- Torque was applied through a linkage system that eliminated a rotating central bearing, thus eliminating friction and translational shear in the bond due to bearing tolerances.
- The specimen was held tightly in the fixture without inducing prestresses in the bond line due to mechanical gripping.

The overall test setup is shown in Figure 31. The specimen axis was in a horizontal position, and the arms on the chucks were connected by tension links to the upper and lower crossheads of a tensile testing machine. The links were installed so that the right arm of the forward chuck was connected to the upper crosshead, and the left arm was connected to the lower crosshead. Opposite connections were used on the rear chuck, so motion of the crossheads induced torque in the tubular specimen and torsional shear in the adhesive bond. Both ends of each link were connected by means of spherical roller bearings to provide a precise point of load application, to minimize friction, and to maintain pure tension (i. e., no bending or torsion) in the links. The spherical bearings also provided load equalization in the tension links within the dimensional accuracy of the bearing center locations in the chucks. The lower link loads were balanced about the diagonal axis through the spherical bearing centers for the upper links. In a similar way, the upper link loads were balanced. The balancing effect resulted from the double whiffle-tree linkage arrangement shown schematically in the following sketch.



With equal link loads, equal torque on the two chucks was dependent only on the links being parallel and equally spaced. Because the links were accurately spaced by the chuck arms at one end and the test machine mounting brackets at the other, dimensional errors of a few thousandths of an inch constituted a very small percentage of error in the geometry. An error of 0.005 inch in the chuck arm length would produce an error in the value of the torsional couple of only 0.05 percent.

This arrangement was not sensitive to the location of the coupon center relative to the linkage attachment points. The coupon center could be off the true center location in any direction without changing the torque applied to the specimen, provided that the plane of the bond line was parallel to the plane of the torque-producing couple.



FIGURE 31. TORSION RING ADHESIVE TEST SETUP

The shear strains were measured using a linear transducer supported on two rings that clamped to the specimen. The transducer core was attached to one ring and clamped on the specimen adjacent to the bond line. The transducer coil was attached to the second ring and clamped to the specimen on the other side of the adhesive. Thus, the transducer measured bond line deformations under virtually pure torsional shear. This instrumentation installation is shown in Figure 31. Resolution of the linear transducer was stepless (infinite) and was resolved to within 0.1 percent of the full linear range (0.050 inch) by a null-balance indicating system. Thus, accurate deflection data to 0.00005 inch were recorded. Loads measured on the testing machine and the deflections measured by the transducers were corrected for the geometrical relationships of the load linkage and instrumentation mountings during data reduction for the plotting of stress-strain curves.

Alignment of the tubular specimen halves of the torsion ring shear specimen during curing of the adhesive was maintained by the simple fixture shown in Figure 32 (Drawing Z3824823, Volume II). It consisted of a rectangular aluminum block with two corners machined parallel, two circular springs made of flat spring-steel strip stock, and two machined cover plates. The following assembly sequence was used.

The lower tube half was placed on the lower cover plate, and the rectangular block and one spring were placed inside the tube. Releasing the spring aligned the inside wall of the tube against the corners of the block. The adhesive was placed on the top edge of the lower tube. The upper tube was positioned on the adhesive and the second spring installed. Release of the spring pulled the upper tube against the corners of the same block and thus aligned the upper and lower specimen halves. The top cover plate was installed and the assembly was vacuum bagged and cured in an autoclave. The autoclave pressure was adjusted to maintain the desired pressure on the bond line during cure. The tube alignment was maintained by the spring forces during the curing cycle.

The tests were conducted on a Baldwin test machine with the loads applied at a crosshead rate of 0.05 inch per minute. The test data were summarized in Table X. The load measured on the testing machine (P_M) and the deflections measured by the transducer (δ_M) were corrected for the geometrical relationships of the load linkage and instrumentation mountings. Accordingly, the shear stress (τ) and the shear strain (γ) were calculated as follows:

$$\tau = 0.75 P_M \text{ (psi)}$$

$$\gamma = \frac{0.67\delta_M}{t_a} \text{ (in./in.)}$$

where t_a is the adhesive thickness.

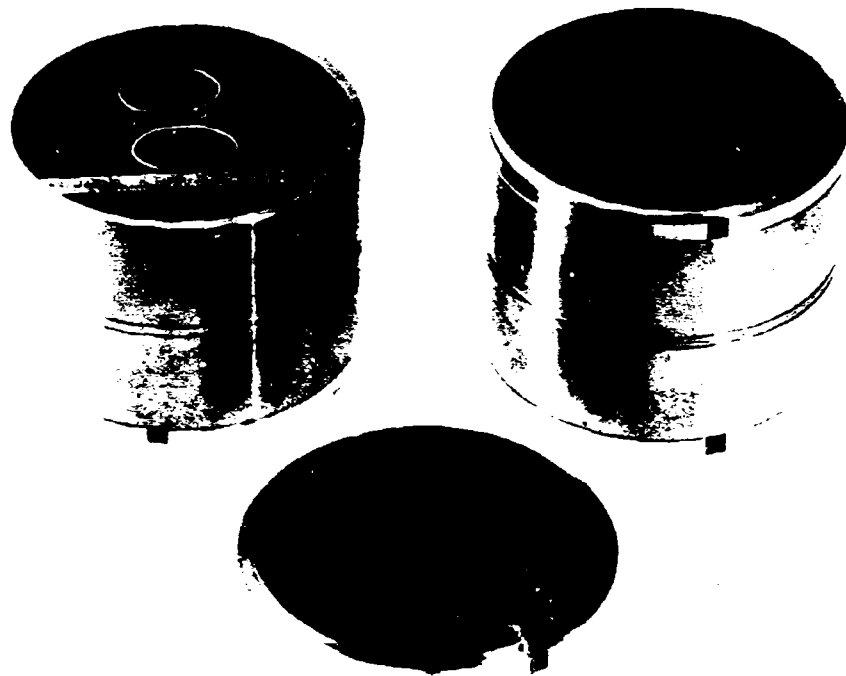


FIGURE 32. ADHESIVE TORSION RING SHEAR SPECIMEN BONDING FIXTURE

TABLE X
ADHESIVE TORSION RING SHEAR TEST RESULTS

CONFIGURATION	ADHESIVE TYPE	ADHESIVE THICKNESS (IN.)	ULTIMATE LOAD (LB)	ULTIMATE SHEAR STRESS (PSI)	SHEAR STRAIN RATE (IN./IN./MIN)	ULTIMATE SHEAR STRAIN (IN./IN.)
-1	3M AF130	0.0038	13,850	10,400	12.1	-
		0.0037	13,750	10,313	12.4	0.688
		0.0032	14,050	10,520	14.4	0.125
		0.0034	10,825	8,120	13.5	-
		0.0025	14,000	10,500	18.4	0.042
-501	NARMCO 252	0.0111	4,410	3,305	4.15	-
		0.0089	4,200	3,150	5.17	0.950
		0.0113	4,100	3,075	4.07	0.836
		0.0150	2,230	1,672	3.07	0.469
		0.0140	1,910	1,430	3.28	0.215
-506	BLOOMINGDALE HT424	0.015	6,850	5,140	3.07	-
		0.013	5,530	4,150	3.54	-
		0.013	6,150	4,640	3.54	-
		0.014	3,930	2,945	3.29	0.158
		0.012	3,640	2,730	3.84	-
-507	SHELL 951	0.0050	9,620	7,220	9.2	1.930
		0.0075	7,830	5,870	6.14	1.783
		0.0048	9,180	6,885	9.6	2.315
		0.0036	6,185	4,640	12.8	1.950
		0.0047	7,850	5,890	9.8	0.941
-509	LEFKOWELD 109	0.0018	5,680	4,260	25.6	-
		0.0010	2,400	1,800	46.0	0.503
		0.0026	4,710	3,530	17.7	0.825
		0.0018	2,300	1,725	25.6	0.798
		0.0090	1,370	1,028	5.11	0.159

The specimens (excepting the -503 configuration) exhibited good failure characteristics, with virtually 100 percent cohesive failures as shown in Figure 33. This figure illustrates a typical failure of the Shell 951 adhesive. The -503 specimens (AF 110B adhesive) failed at low loads and did not provide usable stress-strain data. Ultimate stresses for Narmco 252 (averaging 3250 psi), were less than the average stresses obtained in the lap shear test (4036 to 5614 psi). AF 130 adhesive attained the highest ultimate shear stress, averaging 9970 psi in the torsion ring tests, approximately nine times the average of lap shear tests.

Stress-strain curves were nonlinear, and in the case of AF130 they were inconsistent, making the estimation of shear modulus difficult. Narmco 252 and Shell 951 yielded smooth curves and good ductility in shear. The modulus values in some cases were difficult to assess because fixture effects appeared to modify the initial stress-strain relationships at the lower ends of the curves. The stress-strain curves are included in Volume II.

After completion of the stress-strain tests of the six candidate adhesives, the torsion ring test specimen was modified for a study of thickness and strain-rate effects on shear properties. Shell 951 adhesive was used in this investigation.

The test procedure used previously was modified to produce nominal adhesive shear-strain rates of 10, 30, and 50 radians per minute for each adhesive thickness range. These strain rates were maintained by adjusting the crosshead rate on the testing machine in the range of 0.05 to 0.83 inch per minute, depending on adhesive thickness. Considering the linkage geometry in the test apparatus, strain rate ($\dot{\gamma}$) was related to crosshead rate (\dot{m}) by the equation

$$\dot{\gamma} = 0.92 \dot{m}/t_a \text{ (radians/minute)}$$

Thickness control of the adhesive was maintained by the use of a machined shoulder on each specimen half in conjunction with precision-machined spacers (Drawing Z2828871) that were removed from the specimen assembly after the adhesive was cured. Dimensional details of the spacers are shown in Volume II. The details were machined for nominal bond line thicknesses of 0.005, 0.010, and 0.015 inch, each with a tolerance of ± 0.0015 inch.

Because the normal pressure on the bond surface was relieved by the mechanical stops during cure, some porosity was observed in the cured adhesive, particularly in the thicker bond lines. After curing, the excess adhesive flash was removed, and bond lines were measured optically using a Balphot metalograph machine. The bond lines were generally thicker than the nominal dimensions, and in some cases they slightly exceeded the anticipated tolerances. However, the bond lines fell into three distinct thickness ranges, so the method of thickness control was considered successful.



FIGURE 33. TORSION RING ADHESIVE SPECIMEN FAILURE

Test results are summarized in Table XI. Although the scatter of data tended to obscure results, the following trends were observed.

- Ultimate shear stress and strain and elastic shear modulus decreased as adhesive thickness increased.
- Ultimate shear stress and elastic shear modulus increased and ultimate shear strain decreased as strain-rate increased.

The increased shear strength and modulus of thinner bond lines has been observed by other investigators. Franzblau and Rutherford (Reference 8) discussed the effects of interfacial zones in the adhesive near the interfaces with the adherends. Reasons for the existence of these zones are not well established at the present time, but they may be caused by restraint of the adhesive by the stiffer adherends, changes in the molecular structure at the interface, or residual stresses caused by thermal effects during cool-down from the curing temperature.

Franzblau and Rutherford (Reference 8), using Epon 828/Versamid, found that the elastic modulus of a very thin film was 630,000 to 721,000 psi compared to a bulk modulus of 330,000 psi. From the apparent modulus observed in test of a joint with a thin bond line, they estimate the thickness of the interfacial zone at 1.5 ± 0.5 mils. Thus, in a joint with a bond line of 5 mils thickness, approximately 60 percent of the adhesive could be regarded as interfacial zones.

TABLE XI.
SUMMARY OF SHEAR STRENGTHS FOR SHELL 951 ADHESIVE WITH
VARIATIONS IN STRAIN-RATE AND BOND-LINE THICKNESS

SHEAR STRAIN RATE (RADIAN/MIN.)	ADHESIVE THICKNESS (IN.)	ULTIMATE SHEAR STRESS (PSI)	ULTIMATE SHEAR STRAIN (IN./IN.)
10	0.0067	4320	1.80
10	0.0072	4875	1.80
10	0.0123	5420	1.07
12	0.0057	4860	2.71
30	0.0053	5330	2.12
30	0.0057	4900	2.18
50	0.0053	2925	1.80
50	0.0053	4560	1.00
50	0.0067	5620	0.91
10	0.0117	3405	1.60
10	0.0123	3323	1.50
30	0.0100	3885	2.00
30	0.0103	3400	1.79
30	0.0110	3780	1.16
30	0.0117	3255	1.52
50	0.0117	3450	1.12
50	0.0117	3605	1.07
50	0.0133	4220	0.43
10	0.0143	5085	0.22
10	0.0160	2925	1.53
10	0.0163	2756	1.28
10	0.0167	2715	1.50
30	0.0150	2925	1.13
35	0.0157	2895	1.12
50	0.0160	3065	1.00
50	0.0163	2960	1.36
50	0.0167	5015	0.18

SECTION IV

JOINT INVESTIGATION

The joint specimens were designed to provide experimental data for a variety of design variables, including the following:

Joint Concepts

- Bolted
- Bonded
- Combination

Joined Materials

- Boron Laminates
- Fiber Glass Laminates
- Laminates to Metals

Design Parameters

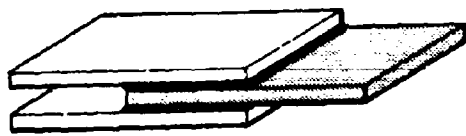
- Laminate Patterns
- Joint Geometry

Load Conditions

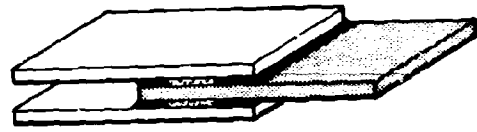
- Static
- Fatigue

The joint concepts are illustrated in Figures 34 and 35 for the bonded and bolted joints, respectively. Epoxy resin composites of S-994 fiberglass or boron filaments were joined to similar composites or to metal elements. Narmco 5505 epoxy resin was used in all laminates. In each specimen configuration a basic ply pattern of $0^\circ/\pm 45^\circ/0^\circ$ was used. (The angles refer to individual ply orientations with respect to the load axis.) This pattern has general applicability to airframes because it combines good axial and in-plane shear properties in both strength and modulus (Tables III through V in Section III).

In addition to the basic pattern, a pattern appropriate to each joint concept was selected as an alternative. The fiber patterns used in the specimens are identified in Table XII. These designations will be used subsequently to describe the patterns. For patterns A, B, and C, specimen thicknesses were built up by repeating the specified pattern. Each specimen was constructed symmetrically about the midplane of the laminate to avoid warpage due to differential thermal expansions during cure.



DOUBLE LAP



VARIABLE STIFFNESS ADHESIVE



SINGLE LAP



EXTERNAL SCARF



STEPPED LAP



SCARF

FIGURE 34. BONDED JOINT DESIGN CONCEPTS

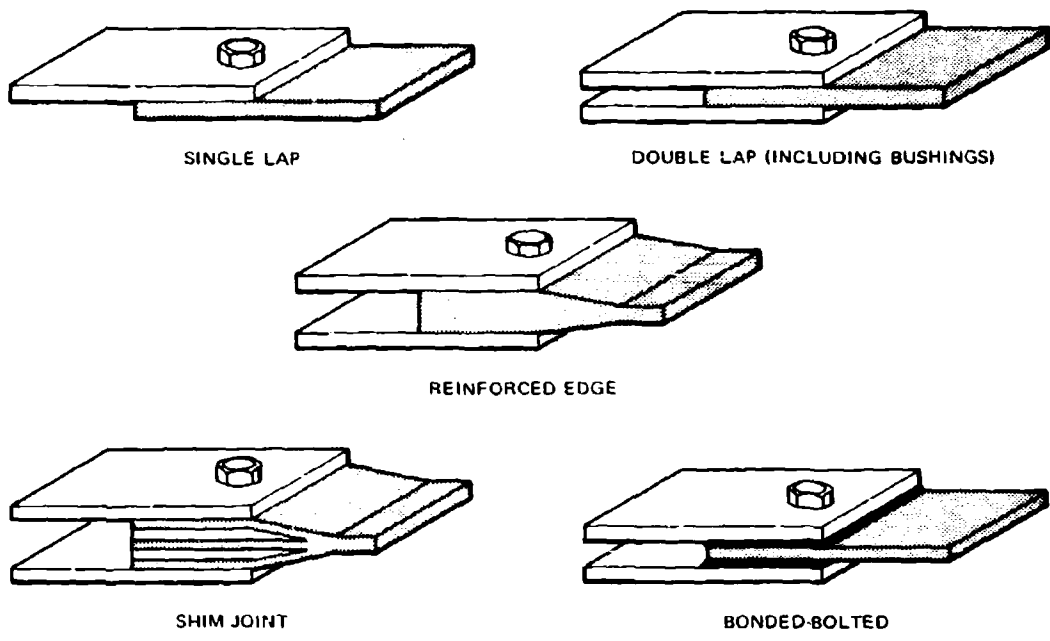


FIGURE 35. BOLTED JOINT DESIGN CONCEPTS

TABLE XII
JOINT SPECIMEN LAMINATE PATTERNS

LAMINATE PATTERN	PATTERN DESIGNATION	PERCENT OF PLYS AT $\pm 45^\circ$
$0^\circ/\pm 45^\circ/0^\circ$	A	50
$+45^\circ/0^\circ/0^\circ/-45^\circ$	B	50
$\pm 15^\circ$	C	0
$\pm 45^\circ/\pm 45^\circ/0^\circ$ (16 LAYERS)/ $\pm 45^\circ/\pm 45^\circ$	D	33-1/3
$\pm 45^\circ/\pm 45^\circ/0^\circ$ (24 LAYERS)/ $\pm 45^\circ/\pm 45^\circ$	E	25
$\pm 45^\circ/0^\circ$ (8 LAYERS)/ $\pm 45^\circ$	F	33-1/3
$\pm 45^\circ/0^\circ$ (12 LAYERS)/ $\pm 45^\circ$	G	25

The second pattern was chosen to exhibit a laminate characteristic different from the first. Laminate modulus was known to be a significant variable, but this was investigated by testing both boron and fiber glass-reinforced composites. As an alternative for bonded joints, the modulus of the laminate was retained, but the arrangement of the layer directions within the laminate was changed. This variation had particular significance in bonded joints when the layer next to the bond was considered. Since the modulus ratio of 0° to 45° layers was about 10 to 1, significant differences in bond strength were expected to result from selecting these orientations as the outermost layers. Gross laminate strength and stiffness were not affected, so the joint strength effects of the pattern were isolated. For this reason, the $45^\circ/0^\circ/0^\circ/-45^\circ$ pattern was selected as the alternative for the bonded lap joints where the first angle represents the outermost layer. For bolted joints, D, E, F, and G were selected as alternative patterns. The basic variation in these patterns was the percentage of layers at $\pm 45^\circ$ to the load axis. A specimen width of 1 inch was selected to minimize the effects on joint strength of cut fibers at the specimen edges.

The joint specimens were designed in general to the strength levels anticipated in the adhesives or fasteners. In specimens where adhesives or fasteners were not expected to be critical, the metal or composite elements were sized for an ultimate load intensity of 12,000 pounds per inch. This load intensity was arbitrarily selected because it typifies load requirements for many primary aircraft structures. Because a study of parametric trends was an objective of the program, adhesive or fastener strength were not always consistent with the strengths of the joined elements as dimensions of the specimens were varied. Thus, a variety of failure modes and joint strengths were produced.

Specimen design details, test results, failure modes, and strength trends are discussed in this section under the headings Static Load Tests and Fatigue Tests. Engineering drawings of all joint specimens are included in Volume II.

STATIC LOAD TESTS

The joint concepts included basic lap joints of bolted and bonded configurations and design variations of each to improve static load capacity. For the bonded joints, design variations included variable stiffness adhesive, scarf, and stepped-lap joints. The variable stiffness adhesive joint was intended to reduce stress concentrations in the bond line by the use of a ductile adhesive at the extremities of the joint. The scarf and stepped lap designs were intended to reduce joint eccentricity and stress concentrations in the adhesive through improved strain compatibility of the adherends. For bolted joints the design variations included reinforcement of the hole with steel bushings, laminate edge buildups, and metal shims in the laminate. A combination bolted and bonded joint was also included.

The specimens were each loaded to failure through serrated machine grips in a Riehle test machine at a crosshead rate of 0.05 inch per minute. The laminate details were protected with bonded aluminum gripping tabs to avoid stress risers and premature failures in the laminates from the serrated grips.

Bonded Joints

The basic parametric variations for the composite joint investigation were chosen using design principles of metal joint technology. The ranges of parameter variations were selected after reviewing recent published data for composite joints (References 8 through 15).

An ultimate load intensity of 12,000 pounds per inch was chosen as a design target. In the single and double lap joint configurations, this strength was not expected to be attained in the adhesive, so the specimen thicknesses were designed around the anticipated bond line strengths.

The specimen thicknesses were chosen to transmit the loads that the adhesive was capable of transferring at about 1 inch lap length. Thickness was kept constant for joints of the same type regardless of lap length. In the case of single lap specimens, the thickness was chosen as 0.040 inch, which at 1 inch width and an ultimate tensile stress of 100,000 psi allowed a maximum load of 4000 pounds in the laminate. Non-uniform stresses in the laminate due to bending and stress concentrations were expected to cause failure at a lower average stress level. Hence, 0.040-inch thickness was selected to transfer the maximum expected strength of the bond at all overlap lengths. Similarly, with a double overlap the laminate thickness was chosen as 0.080 inch.

Shell 951 adhesive was selected as the primary bonding agent on the basis of the adhesive evaluation tests (Table VIII). This was the strongest of six adhesives tested, averaging 5750 pounds/inch on 1/2-inch double overlap joints. There was no test evidence to show the variation of strength with overlap length, but analytical studies on joints using MB408 adhesive, which has a similarly low modulus, suggested that at a 2-inch overlap the strength was increased by only about 20 percent. Further increases in overlap did not significantly increase the strength. AF130 adhesive was also used in some of the joints when the application required a stronger or stiffer adhesive and the reduced ductility did not adversely affect joint design.

For bonded joints the ratio L/t is a commonly used design parameter involving lap length and adherend thicknesses. Single lap joints in the experimental program were fabricated with lap lengths of 1/2 inch, 1 inch, and 2 inches that, together with a nominal laminate thickness of 0.040 inch, resulted in L/t ratios of 12.5, 25, and 50, respectively. The same lap lengths were used for the double lap joints in conjunction with a nominal laminate thickness of 0.080 inch. The resulting L/t ratios were 6.25, 12.5, and 25, respectively.

During the course of the program, a number of single lap, double lap, and variable stiffness adhesive joints were remade and retested. These specimens were fabricated to repeat tests where prior test data did not agree with strength trends and to provide a check on the consistency of processing methods and laminate quality throughout the specimen fabrication period.

Graphic comparisons of test results between the original and remade specimens are shown in Figure 36. Test results are also summarized in Tables XIII through XVI and reported in detail in Volume II.

The remade specimens were generally equal in strength or stronger than their original counterparts, although failure modes did not always correspond for a given specimen configuration. Failure modes did correspond for specimens Z3824827-507 (Pattern B, boron-to-aluminum, double lap), each group failing in tension through the basic laminate. However, the remade specimens were considerably stronger than the original group (118.7 ksi vs 104 ksi ultimate). Failure modes were also in agreement for specimens Z3824828-525 (Pattern A, boron-to-aluminum, single lap), each group failing in an adhesive mode with minor indications of interlaminar shear involvement. The remade specimens indicated higher average shear stresses than the original group (3016 vs 2480 psi). Although this variation was more than anticipated, the failure modes, the appearance of the failures, and the scatter of data (Figure 36) were consistent, so the original test results were not discounted. Specimens Z3824828-501 (Pattern A, boron-to-boron, single lap) also failed consistently in interlaminar shear. However, the original specimens indicated higher strength than the repeat specimens.

In the balance of the repeat specimen tests, the remade specimens failed in a different mode than the original specimens, so direct comparisons could not be made. It was determined from test results, however, that stress levels at failure in tension and interlaminar shear were similar.

The second group of boron-to-aluminum double lap specimens employing fiber Pattern A (Z3824827-501 and Z3824854-1) failed in tension in the laminate at an average stress level of 122 ksi and in interlaminar shear at an average stress of 4400 psi. The corresponding specimens in the original group failed primarily in interlaminar shear, also at an average stress of 4400 psi. None of the original specimens failed in tension, although one specimen sustained a tensile stress of 117 ksi before failing in interlaminar shear.

The second group of variable stiffness adhesive, boron-to-aluminum double lap specimens employing fiber Pattern B (Z3824854-505) were significantly stronger in tension than their original counterparts. Remade laminates failed at an average tensile stress level of 119 ksi versus 108.5 ksi for the original group. Four of the remade specimens failed in interlaminar shear at an average stress level of 4600 psi. Although none of the original specimens failed in interlaminar shear, they did sustain stresses of about this magnitude before failing in tension.

The test results for the remade 3824827-523 specimens (Pattern A, boron-to-titanium, double lap) indicated substantially higher ultimate loads than the original tests. These tests were repeated because the original specimens failed prematurely in the grips. The test results for the remade laminates indicated tensile failures at stresses of 112 to 122 ksi. These results were consistent with the tensile failures for similar boron-to-aluminum double lap specimens.

Overall comparisons of test results indicated that the original laminates were of good quality, and the test results were valid except in cases where the specimen failed in the test machine grips. Failure modes for corresponding configurations of the 1-inch lap joints did not always agree. This was probably because the 1-inch joint was almost equally susceptible to laminate tensile or interlaminar shear failures.

Single Lap Joints

The static test results for single lap adhesive joints (Drawing Z3824828) in boron and glass laminates are summarized in Table XIII. Average values are plotted in Figure 37 as functions of lap length. A nominal ultimate adhesive stress of 6000 psi was used as a tangent line. This was the order of shear strength achieved by Shell 951 adhesive in the evaluation tests. Where the curves lie on this line, it is assumed that plasticity effects in the adhesive effectively equalized shear stresses over the joint.

A number of failures occurred within the laminates, a result that was not indicated by linear elastic analysis. It was concluded that the adhesive was sufficiently more ductile than the epoxy matrix, causing the matrix material to reach failure strains first. This type of failure resulted in delamination within the first few layers of composite adjacent to the bond.

Seven of the boron specimens (Pattern B) failed in tension across the laminate at stresses between 87,500 and 114,000 psi. These stresses are in rough agreement with theoretical results for tensile specimens of these patterns, indicating that the boron laminate was stressed quite uniformly at failure and that bending effects were not pronounced. No tension failures of fiberglass or aluminum occurred in the single lap tests.

The composite-to-composite joints gave higher strengths than those joining composite to aluminum. Residual thermal stresses from adhesive curing may have influenced the bond strength in the latter specimens.

Test results for the single-lap external scarf joints (Drawing Z3824828-547 and -549) are given in Table XIII. The results indicate a slight strength improvement over the corresponding simple lap joints (Z3824828-525 and -537, respectively). The average stress in the adhesive was improved 8 percent in the boron laminate-to-aluminum joint and 3.3 percent in the S-994 fiber glass laminate-to-aluminum joint.

Double Lap Joints

The static test results for the double lap adhesive joints (Z3824827) are summarized in Table XIV and Figure 38 for both boron and fiber glass specimens. The boron double lap specimens achieved a higher average bond stress than the single lap specimens, indicating that bending effects and adhesive peel stresses were less pronounced. The fiber glass specimens did not show this effect. In Pattern B the double lap adhesive stresses were lower than those for the single lap, and strengths were less than those of Pattern A for both boron and fiber glass. Failures within the laminates appeared to be associated principally with the 45-degree layers.

Strengths of the double lap boron specimens were higher than expected. At 2-inch lap lengths, failures occurred in both the aluminum adherends and in the laminates. Boron laminate tensile strengths as high as 122,000 psi were achieved without failure. The fiber glass specimens showed a tendency to reduced strengths when lap length exceed 1.5 inches.

TABLE XIII
SUMMARY OF SINGLE LAP BONDED JOINT TEST RESULTS

JOINT DESCRIPTION MATERIALS, AND GAGES	P A T T E R N	NOMINAL LAP LENGTH (IN.)	AVERAGE ADHESIVE THICKNESS (IN.)	ULTIMATE STATIC LOAD (LB)	AVERAGE ADHESIVE SHEAR STRESS AT FAILURE*	AVERAGE ADHEREND TENSILE STRESS AT FAILURE			FAILURE MODES**
						COMPOSITE (PSI)	ALUMINUM (PSI)	ALUMINUM (PSI)	
SINGLE LAP BORON (0.040)/ BORON (0.040)	A	0.50	0.0029	2905	5722	72,500	NOT APPLICABLE		(1)
	A	1.00 1	0.0010	3908	3875	97,700			(2)
	A	1.00 11	0.0034	3385	3336	84,000			(2)
	A	2.00	0.0024	3859	1957	99,000			(2)
	B	0.50	0.0019	2362	4678	99,000			(2)
	B	1.00	0.0020	3898	2155	97,500			(2)
SINGLE LAP FIBERGLASS (0.040)/ FIBERGLASS (0.040)	B	2.00	0.0019	4209	2155	105,000			(3)
	A	0.50	0.0017	2648	5087	65,300	NOT APPLICABLE		(1)
	A	1.00	0.0014	3538	3424	88,500			(1)
	A	2.00	0.0020	3650	1794	91,300			(1)
	B	0.50	0.0010	2486	5056	62,400			(1), (2)
	B	1.00	0.0010	2719	2665	68,000			(1), (2)
SINGLE LAP BORON (0.040)/ 7075-T6 (0.063)	B	2.00	0.0021	3708	1839	92,700			(1), (2)
	A	0.50	0.0019	2416	4738	60,400	39,300		(1), (2)
	A	1.00	0.0019	2514	2480	62,700	39,900		(1), (2)
	A	1.00 11	0.0030	3040	3016	75,800	48,300		(1), (2)
	A	2.00	0.0020	3670	1832	91,600	58,300		(1), (2)
	B	0.50	0.0013	2009	3570	50,200	31,900		(2)
SINGLE LAP FIBERGLASS (0.040)/ 7075-T6 (0.063)	B	1.00	0.0022	3645	3630	91,200	58,000		(2)
	B	2.00	0.0019	3780	1928	94,500	60,000		(2), (3)
	A	0.50	0.0016	2006	3958	50,100	31,800		(1)
	A	1.00	0.0030	2318	2729	58,000	36,800		(1)
	A	2.00	0.0026	2463	1226	61,500	39,100		(1)
	B	0.50	0.0034	2121	4100	53,000	33,700		(1)
SINGLE LAP BORON (0.040)/ 7075-T6 (0.063) EXTERNAL SCARF	B	1.00	0.0030	2553	2589	64,800	41,000		(1)
	B	2.00	0.0022	3094	1560	77,300	49,000		(1)
	A	1.00	0.0054	2781	2677	69,500	44,200		(1)
	A	1.00	0.0035	2383	2306	59,500	37,900		(1)
	A	1.00	0.0035	2383	2306	59,500	37,900		(1)
	A	1.00	0.0035	2383	2306	59,500	37,900		(1)

* AVERAGE OF FIVE TESTS
** (1) ADHESIVE
(2) INTERLAMINAR SHEAR
(3) TENSION IN BASIC LAMINATE SECTION

1 TESTED IN JANUARY 1968
11 TESTED IN DECEMBER 1968

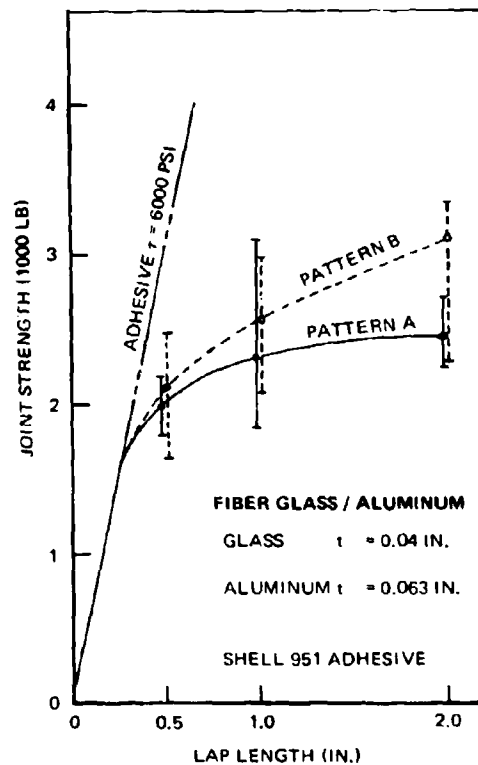
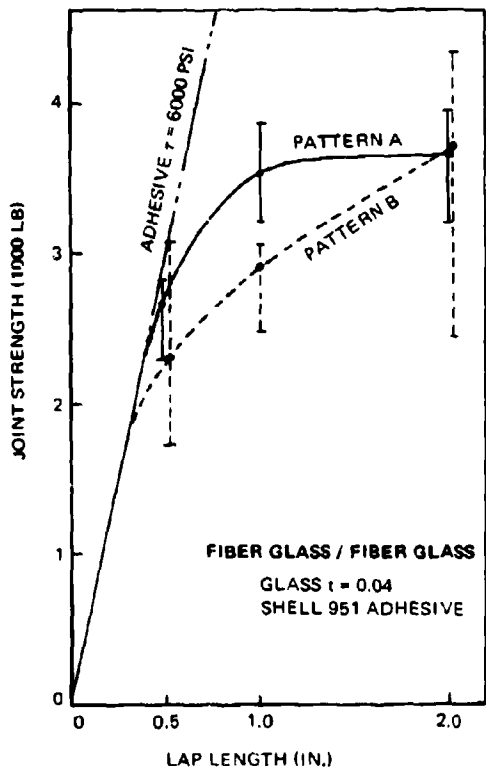
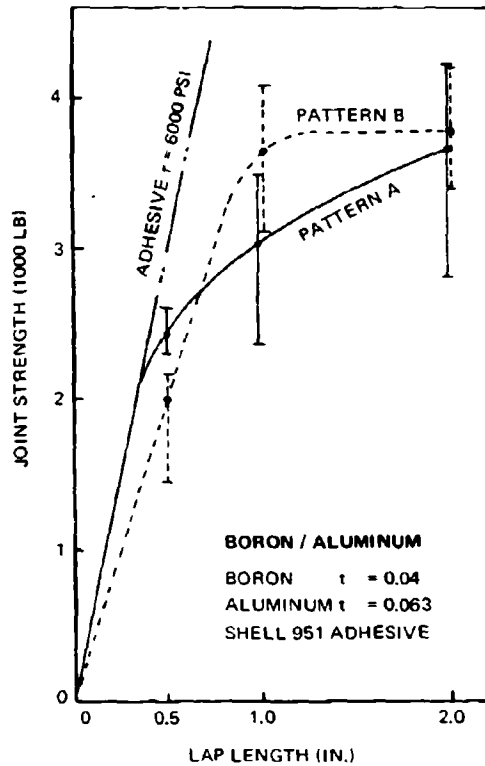
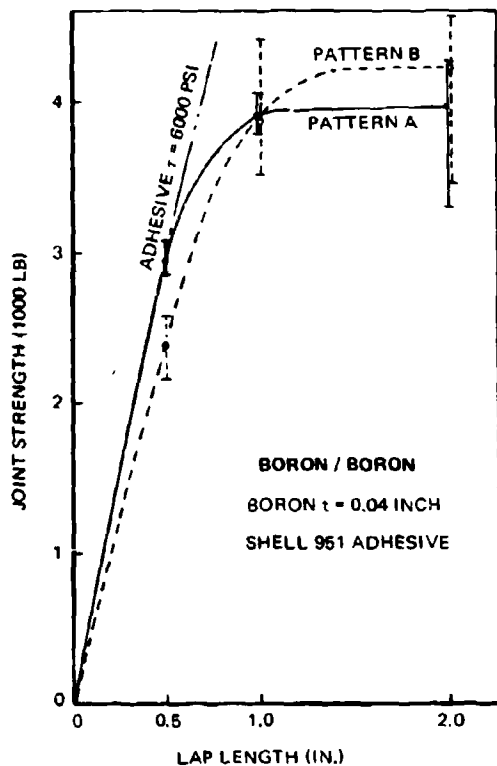


FIGURE 37. SINGLE LAP BONDED JOINT STRENGTH

TABLE XIV
SUMMARY OF DOUBLE LAP BONDED JOINT TEST RESULTS (1-INCH SPECIMEN WIDTH)

JOINT DESCRIPTION MATERIALS, AND GAGES (IN.)	P A T T E R N	NOMINAL LAP LENGTH (IN.)	AVERAGE ADHESIVE THICKNESS (IN.)	ULTIMATE STATIC LOAD (LB)	AVERAGE ADHESIVE SHEAR STRESS AT FAILURE* (PSI)	AVERAGE ADHEREND TENSILE STRESSES AT FAILURE		FAILURE MODES**
						COMPOSITE (PSI)	ALUMINUM (PSI)	
DOUBLE LAP BORON (0.080)/7075-T6 (0.126)	A	0.50	0.0011	5769	5625	72,000	45,700	(1), (2)
	A	1.00 †	0.0012	9104	4406	113,600	72,200	(2), (3)
	A	1.00 ††	0.0020	9746	4482	122,000	77,300	(3)
	A	2.00	0.0010	9378	2340	117,000	74,500	(1), (4)
	B	0.50	0.0015	5982	5783	74,700	47,500	(1), (2)
	B	1.00 †	0.0012	8327	4160	104,000	66,000	(3)
	B	1.00 ††	0.0026	9502	4751	118,700	75,400	(3)
	B	2.00	0.0014	6180	1540	77,200	49,000	(2), (3)
DOUBLE LAP FIBER GLASS (0.080)/7075-T6 (0.126)	A	0.50	0.0025	5038	4986	63,000	40,000	(1)
	A	1.00	0.0033	5713	2743	71,500	45,400	(1), (2)
	A	2.00	0.0034	5297	1347	66,200	42,000	(1), (2)
	B	0.50	0.0019	4059	4008	50,900	32,200	(2)
	B	1.00	0.0023	4530	2257	56,600	36,000	(2)
	B	2.00	0.0025	4551	1110	57,100	36,200	(2)

* AVERAGE OF FIVE TESTS

† TESTED IN FEBRUARY 1968

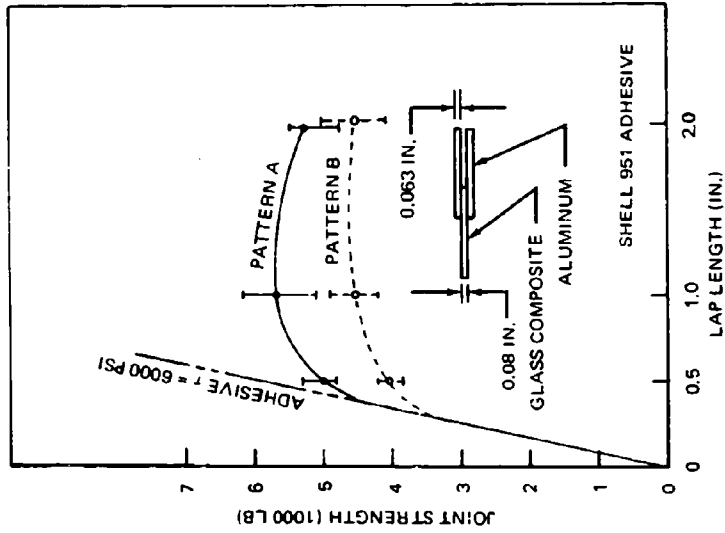
†† TESTED IN DECEMBER 1968

** (1) ADHESIVE

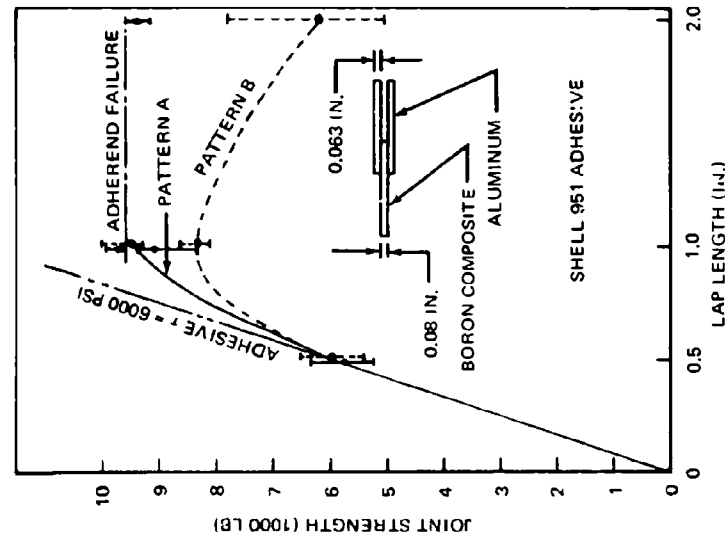
(2) INTERLAMINAR SHEAR

(3) TENSION IN BASIC LAMINATE SECTION

(4) TENSION IN BASIC ALUMINUM SECTION



a. BORON



b. FIBER GLASS

FIGURE 38. DOUBLE LAP BONDED JOINT STRENGTH

For adhesive lap joints, it was beneficial to balance the extensional stiffnesses of the adherends for equalization of the stress peaks in the adhesive. This stiffness is proportional to the product of modulus of elasticity and thickness (Et) of the adherends. Analysis showed that the peak stresses in the adhesive at each end of the lap were equal and had minimum values when Et was the same for both adherends in the joint. The Et ratio was defined as the smaller Et value divided by the larger.

Double lap adhesive specimens joining composite adherends to titanium alloy and to stainless steel were fabricated and tested to supplement the composite-to-aluminum alloy joints of Table XIV. The results are shown in Table XV. Average adhesive stress was plotted against the Et ratio in Figure 39. This figure is based on the 1-inch overlap specimens of Drawing Z3824827, Volume II, which vary only in adherend material and thickness. The elastic moduli used in the preparation of Figure 39 are as follows:

	E(psi)	α (in./in./ $^{\circ}$ F)
Boron/Epoxy	17.1×10^6	3.0×10^{-6} *
S-994 Fiber Glass/Epoxy	5.1×10^6	2.8×10^{-6} *
Aluminum Alloy	10.3×10^6	13.5×10^{-6}
Titanium Alloy	15.5×10^6	5.7×10^{-6}
Stainless Steel	29.0×10^6	6.1×10^{-6}

*Unidirectional laminate.

Boron and S-994 fiber glass-reinforced composites were bonded to each of the three metals. Test results showed a general increase in strength as the Et ratio approached a value of one. Maximum strength was achieved when the two sides of the joint had the same Et value. There was some variation about the general trend due to the interfacial conditions of the adherends being joined. Boron laminate specimens appeared to have slightly decreasing strengths when joined to aluminum, titanium, and stainless steel in that order. When bonded to fiber glass laminates, the strength trend for these metals was reversed. All results shown are for $0^{\circ}/\pm 45^{\circ}/0^{\circ}$ laminates bonded with Shell 951 adhesive and having a zero-degree layer next to the bond. The effects of Et ratio are discussed further in Analysis of Parametric Trends in Joint Strength, presented subsequently in this section.

Variable Stiffness Adhesive Joints

The variable stiffness adhesive specimens (Z3824854) were designed using a ductile adhesive (Shell 951) at the joint extremities and a high-strength adhesive (AF130) in the joint center. This configuration is similar in concept to the joint tested by Clark (Reference 9), but using different adhesives. These adhesives were chosen both for their engineering properties and their common curing cycles (i. e., 50 psi, 350 $^{\circ}$ F for one hour).

TABLE XV
SUMMARY OF DOUBLE LAP BONDED JOINT TEST RESULTS FOR VARIOUS Et RATIOS

JOINT MATERIALS AND GAGES (IN.)	P A T T R N	NOMINAL LAP LENGTH (IN.)	AVERAGE ADHESIVE THICKNESS (IN.)	ULTIMATE STATIC LOAD (LB)	AVERAGE ADHESIVE SHEAR STRESS AT FAILURE (PSI)	AVERAGE ADHEREND TENSILE STRESSES AT FAILURE		FAILURE MODES**
						COMPOSITE (PSI)	METAL (PSI)	
BORON (0.080)/ S STL (0.040)	A	1.00	0.0016	8065	4040	101,000	202,000	(1), (2), (3)
BORON (0.080)/ S STL (0.050)	A	1.00	0.0020	8650	4325	108,000	173,000	(1), (2), (3)
BORON (0.080)/ S STL (0.064)	A	1.00	0.0045	7290	3645	91,200	114,000	(1), (3)
BORON (0.080)/ TI (0.064)	A	1.00	0.0042 0.0036	6600 † 9530 ††	3148 4746	82,500 119,000	103,000 149,000	(1), (2), (3)
BORON (0.080)/ TI (0.090)	A	1.00	0.0032 0.0030	8760 †† 8812 †	4380 4375	110,000 109,500	98,000 97,300	(2), (3)
BORON (0.080)/ TI (0.126)	A	1.00	0.0040	8100	4088	101,500	64,300	(3)
FIBER GLASS (0.080)/ S STL (0.040)	A	1.00	0.0012	6575	3287	82,300	164,500	(1), (2)
FIBER GLASS (0.080)/ S STL (0.050)	A	1.00	0.0016	6460	3230	80,750	129,000	(1), (2)
FIBER GLASS (0.080)/ S STL (0.064)	A	1.00	0.0010	6235	3115	78,000	97,500	(1), (2)
FIBER GLASS (0.080)/ TI (0.064)	A	1.00	0.0042	5957	2952	74,500	93,000	(1)
FIBER GLASS (0.080)/ TI (0.090)	A	1.00	0.0027	5815	2838	72,600	64,500	(1), (2)
FIBER GLASS (0.080)/ TI (0.126)	A	1.00	0.0045	5608	2691	70,200	44,500	(1), (2)

* AVERAGE OF FIVE TESTS

† TESTED IN MAY 1968

†† TESTED IN JANUARY 1969

** (1) ADHESIVE

(2) INTERLAMINAR SHEAR

(3) TENSION IN BASIC LAMINATE SECTION

(4) TENSION IN BASIC METAL SECTION

△ S STL = STAINLESS STEEL

GAGES NOTED FOR METALS INCLUDE THOSE FOR BOTH METAL ADHERENDS

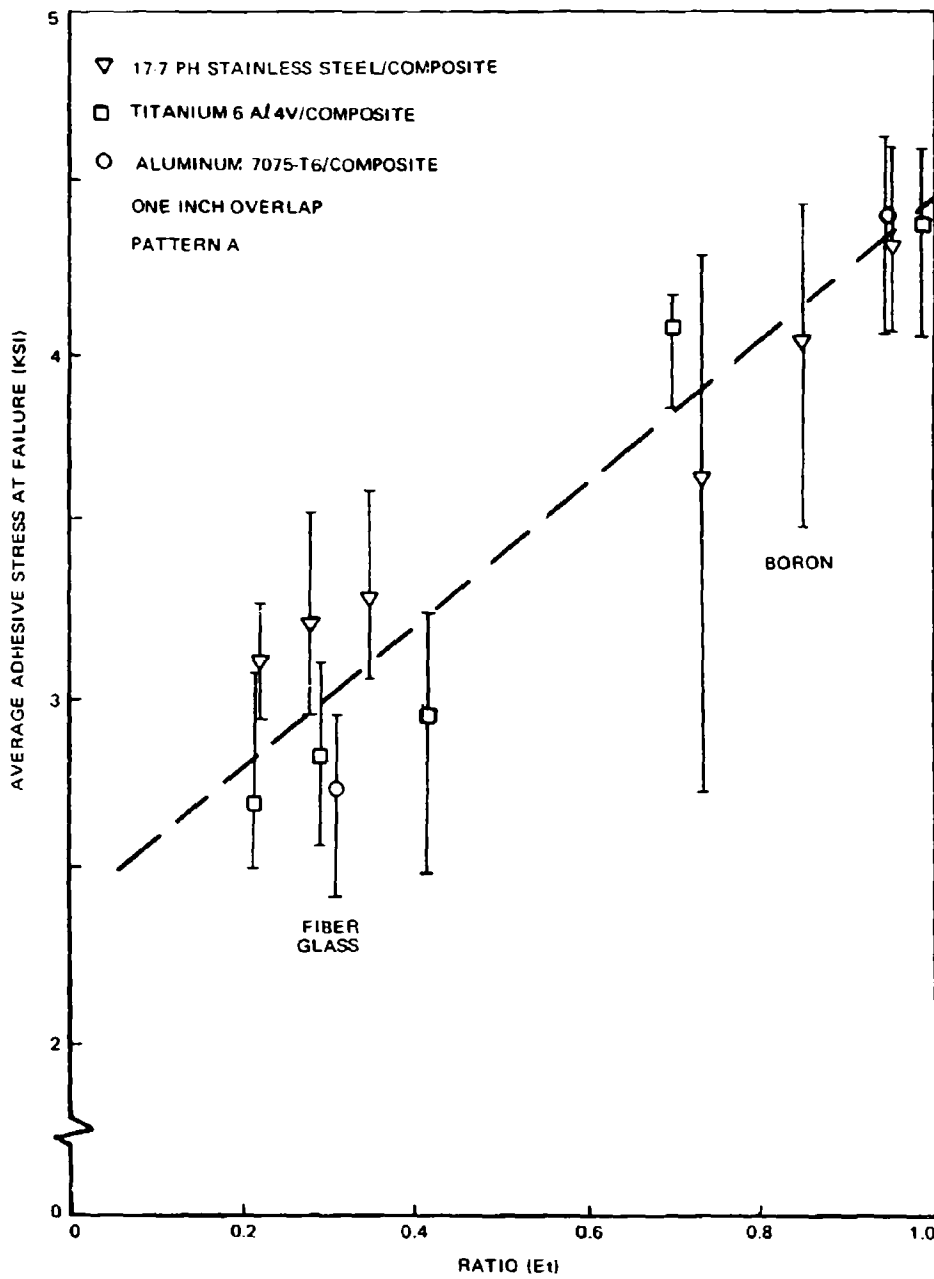


FIGURE 39. EFFECT OF E_t RATIO ON DOUBLE LAP ADHESIVE JOINT STRENGTH

Shell 951 was selected as the basic adhesive for the bonded specimens because it gave the highest strengths in the double lap shear tests. Subsequent testing with the torsion ring assembly showed that Shell 951 had an ultimate shear stress only slightly higher than the average stress achieved in the 1/2-inch double lap test. This high average stress was achieved because the ductility of this adhesive reduced the stress concentrations until a state of nearly uniform shear stress existed at failure. A typical stress/deflection curve is shown in Figure 40. It shows that the shear deflection at failure is approximately twice the adhesive thickness. For comparison, a similar curve was drawn for AF130 adhesive, which has a higher ultimate stress but a much lower shear deflection at failure. The effects of adhesive ductility were apparent from the fact that AF130 developed an average shear stress (in the 1/2-inch double lap tests) of little more than 10 percent of its ultimate shear strength from the torsion ring tests.

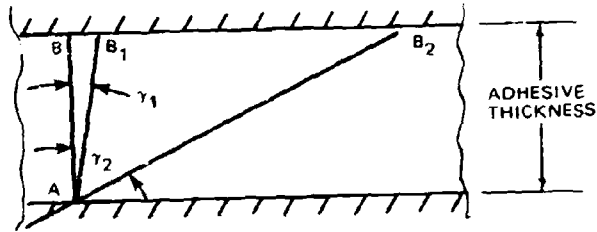
The test results are summarized in Table XVI. In general, the higher strengths were achieved with the ductile adhesive alone. The variable stiffness adhesive did result in an 8 to 18 percent strength improvement when used with boron laminates with 45-degree layers in contact with the adhesive (Pattern B). These strength improvements correspond to lap lengths of 1 and 2 inches, respectively. For the 1-inch lap length, the strength comparison was not conclusive because the Shell 951 specimens all failed in the boron laminates. For the two-inch lap length, the average strength of the variable stiffness joint was improved primarily by two specimens which sustained loads of more than 10,000 pounds. The other three specimens developed strengths comparable to the corresponding specimens using Shell 951 alone.

Scarf Joints

The scarf joint approached the ideals of strain compatibility in the adherends and uniform stress in the adhesive. It was anticipated that the shear stress would be of the order of 10,000 psi and that approximately 8000 psi would be achieved in the joint specimens. The joint strength design goal was 12,000 pounds, so a scarf length of 1-1/2 inches was chosen for the boron specimens. Fiber glass laminates were expected to be slightly stronger, so the same dimension was used. In joints where the composite was joined to aluminum alloy, the latter material controlled the specimen thickness since the allowable stresses were lower. Because alloy 7075-T6 was selected for the specimens, a section 0.160 inch thick (at an allowable stress of 75 ksi) was needed to attain the target load intensity of 12,000 pounds per inch. To simplify the specimen design and fabrication, the composite thickness was also set at 0.160 inch for the scarf joints. Overlap lengths of 1/2, 1, and 1-1/2 inches were selected, yielding scarf angles of about 18, 9, and 6 degrees, respectively.

After completion of the scarf specimen design, shear strength of Shell 951 adhesive was found to average about 6100 psi from the torsion ring shear tests (Specimen Z3824821). Thus, the scarf specimens attained only about 2/3 of the target load intensity at 1-1/2 inch length.

SUBSCRIPT 1 DENOTES AF 130 ADHESIVE
 SUBSCRIPT 2 DENOTES SHELL 951 ADHESIVE



SHEAR STRAINS AT FAILURE TO SCALE

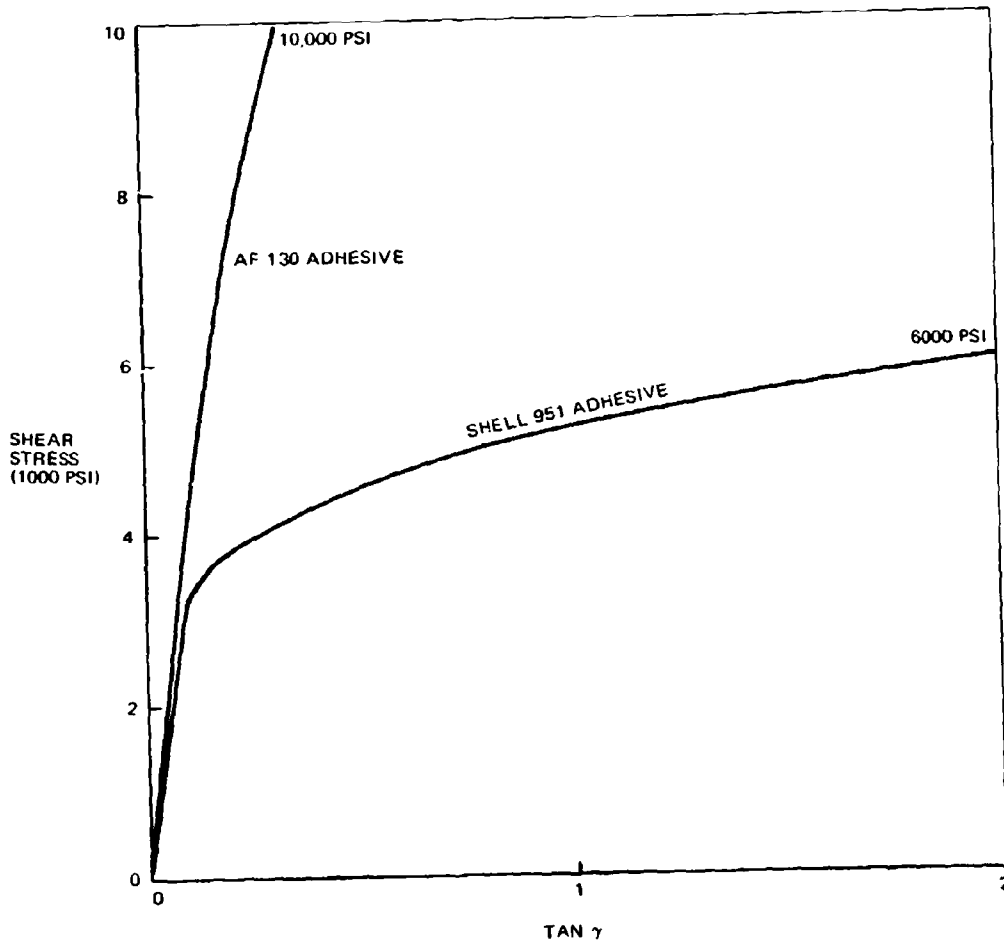


FIGURE 40. ADHESIVE SHEAR STRESS-STRAIN CURVES

TABLE XVI
SUMMARY OF DOUBLE LAP BONDED JOINT TEST RESULTS WITH VARIABLE STIFFNESS ADHESIVE

JOINT DESCRIPTION MATERIALS, AND GAGES (IN.)	P A T T E R N	NOMINAL LAP LENGTH (IN.)	AVERAGE ADHESIVE THICKNESS (IN.)	ULTIMATE STATIC LOAD (LB)	AVERAGE ADHESIVE SHEAR STRESS AT FAILURE* (PSI)	AVERAGE ADHEREND TENSILE STRESSES AT FAILURE		FAILURE MODES**
						COMPOSITE (PSI)	ALUMINUM (PSI)	
DOUBLE LAP BORON (0.080)/7075-T6 (0.126)	A	0.50	0.0034	5360	5215	67,000	42,600	(4)
	A	1.00 †	0.0052	7230	3615	95,000	57,400	(1)
	A	1.00 ††	0.0034	8658	4372	108,300	68,800	(1)
	A	1.50	0.0044	7297	2433	91,300	58,000	(1)
	A	2.00	0.0048	7583	1894	95,000	60,300	(1)
	B	0.50	0.0022	5254	5065	65,500	41,700	(4)
	B	1.00 †	0.0012	9055	4527	113,300	72,000	(1), (2)
	B	1.00 ††	0.0022	9100	4640	113,600	72,200	(1)
	B	1.50	0.0042	8708	2920	108,900	69,100	(1)
	B	2.00	0.0042	7295	1820	91,200	57,900	(1), (3)
DOUBLE LAP FIBER GLASS (0.080)/7075-T6 (0.126)	A	1.00	0.0070	4845	2303	60,600	38,500	(4)
	A	1.50	0.0060	4765	1561	59,600	37,900	(4)
	A	2.00	0.0060	5085	1267	63,600	40,400	(4)
	B	1.00	0.0064	3027	1488	37,900	24,100	(2), (4)
	B	1.50	0.0056	3022	1004	37,800	24,000	(2)
	B	2.00	0.0056	3133	784	39,100	24,900	(2)

* AVERAGE OF 5 TESTS

- ** (1) TENSILE FAILURE IN BORON ADHEREND
- (2) INTERLAMINAR FAILURE
- (3) TENSILE FAILURE IN ALUMINUM ADHEREND
- (4) ADHESIVE FAILURE

† TESTED IN JUNE 1968

†† TESTED IN DECEMBER 1968

Static test results for the scarf joints are given in Table XVII. The longer scarf joints developed average adhesive shear stresses of about 5000 psi. Considering the tension component across the bond line, the principal shear stresses in the adhesive were about 5 percent greater than the average values noted in Table XVII. Using 5000 psi as an allowable stress, a scarf angle of 3 degrees would be required to provide bond strength consistent with the basic laminate strength, assuming the laminate has an ultimate allowable stress of 100,000 psi. Although a 3-degree scarf angle is considered to be below practical limits, raising the allowable adhesive stress would increase the required scarf angle.

A scarf joint using AF130 adhesive (Z3824829-547) produced a significant improvement in ultimate strength by comparison with a joint of identical geometry using Shell 951 adhesive. The AF130 joint developed an average adhesive stress level at failure that was 18.5 percent greater than the Shell 951 joint. This result indicates that adhesive ductility is relatively less important in the scarf joint because stress concentrations in the adhesive are not as severe as in other bonded joint configurations.

The methods of machining and bonding the scarf surface in the composite may have contributed to the reduced load capacity of the scarf joint. The composite adherends for the scarf joints were machined using a diamond-impregnated disc. This cutting method may have broken some of the filament ends and reduced the number of continuous filaments being bonded. Because of the specimen configuration, it was difficult to maintain pressure on the bondline during the adhesive cure cycle, particularly for the smaller lap lengths. Bond line thicknesses ranged up to 0.014 inch for the scarf joints, compared to an average of about 0.002 inch for the other types of adhesive joints. Additional scarf joints were fabricated later in the program as part of the fatigue tests (see S-n Data Tests). These specimens had uniform bond lines of 0.003-inch thickness and indicated an average improvement of 13.5 percent in the adhesive shear stress at static failure.

There were some fiber failures within the laminates adjacent to the bond line, particularly in the 45-degree layers. Fiber glass joints were slightly stronger than boron joints, but there was little strength difference due to the pattern or between composite-to-composite and composite-to-aluminum bonds.

The external scarf specimen discussed previously was designed with the bond area on the outside surface of the laminate to be joined. This design retained the strain compatibility of the scarf but introduced the offset load path of the single lap. The quality of the bond was expected to be improved because pressure was applied more readily during cure, and the faces being joined were flat and unmachined, with the filament layers parallel to the bond face. However, as noted previously, the strength performance of the external scarf joint was only slightly better than a simple lap joint of similar geometry.

Stepped Lap Joints

The stepped lap joints were included in the test program because they approximate the strain compatibility of the scarf joint but obviate

TABLE XVII
SUMMARY OF SCARF BONDED JOINT TEST RESULTS (1-INCH SPECIMEN WIDTH)

JOINT DESCRIPTION MATERIALS AND GAGES (IN.)	P A T T E R N	NOMINAL LAP LENGTH (IN.)	AVERAGE ADHESIVE THICKNESS (IN.)	ULTIMATE STATIC LOAD (LBS)	AVERAGE ADHESIVE SHEAR STRESS AT FAILURE* (PSI)	AVERAGE ADHEREND TENSILE STRESSES AT FAILURE		FAILURE MODES**
						COMPOSITE AND ALUMINUM (PSI)		
SCARF BORON (0.160)/ BORON (0.160)	A	0.50	0.0063	2137	4190		13,400	(1)
	A	1.00	0.0027	5233	5105		32,700	(1)
	A	1.50	0.0050	7672	5110		48,000	(1), (2)
	C	0.50	0.0057	1475	2705		9,200	(1)
	C	1.00	0.0057	3410	3275		31,300	(1)
	C	1.50	0.0063	6525	4335		40,800	(1), (2)
SCARF FIBER GLASS (0.160)/ FIBER GLASS (0.160)	A	0.50	0.0133	2050	3745		12,800	(1)
	A	1.00	0.0053	5582	5205		34,900	(1), (2)
	A	1.50	0.0067	9565	5560		59,800	(1), (2)
	C	0.50	0.0123	2442	4375		15,300	(1)
	C	1.00	0.0123	5458	5010		34,200	(1)
	C	1.50	0.0087	9537	5610		59,500	(1)
SCARF BORON (0.160)/ 7075-T6 (0.160)	A	0.50	0.0067	1688	3400		10,500	(1)
	A	1.00	0.0053	4683	4930		29,300	(1), (2)
	A	1.50	0.0053	6863	4955		43,500	(1), (2)
	C	0.50	0.0100	1890	3685		11,700	(1)
	C	1.00	0.0053	4877	5015		30,500	(1), (2)
	C	1.50	0.0073	6528	4610		41,400	(1), (2)
SCARF FIBER GLASS (0.160)/ 7075-T6 (0.160)	A	0.50	0.0063	2613	4790		16,300	(1)
	A	1.00	0.0053	5463	5020		34,100	(1)
	A	1.50	0.0063	6808	4355		42,500	(1)
	C	0.50	0.0043	2810	5275		17,500	(1)
	C	1.00	0.0037	5877	5455		36,700	(1)
	C	1.50	0.0040	8083	5265		50,500	(1)
SCARF BORON (0.160) 7075-T6 (0.160) AF130 ADHESIVE	A	1.50	0.003	8530	5758		53,300	

*AVERAGE OF THREE TESTS.

** (1) ADHESIVE
(2) INTERLAMINAR SHEAR

machining the composite bonding surface. For the joint specimens, step lengths of 1, 1/2, and 1/4 inch were chosen, each with a total overlap length of 2 inches.

The stepped lap joints produced the highest average adhesive shear stresses, indicating that static strength was not sensitive to the number of steps. The test data are summarized in Table XVIII. The four-step joint gave slightly higher load capacities, but because only 2-inch lap lengths were tested, optimum step length could be about 0.5 inch. Boron joints were considerably stronger than glass joints. Average stresses close to 6000 psi were frequently achieved with boron specimens.

Failures were complex, involving some adhesive, some adherend failures in tension through the steps, and some delamination of the laminates. Interlaminar failures from the inside corners of the laminate steps were observed in some specimens. This type of failure was anticipated from the high shear stresses in the resin as indicated by discrete element analysis.

Bolted Joints

The strength of bolted joints in composite laminates depends on the geometrical parameters (e/D , s/D , and t/D), the laminate constituents, and the layup pattern. Before the bolted specimen designs were completed, an investigation was made of available test results for boron laminates. Test data were obtained from published results of C. R. Rogers, et. al., (References 5 and 10), F. Wilson (Reference 11), V. H. Saffire (Reference 12), and from initial tests performed in this program.

Very few of the test failures were attributable solely to bearing stresses. Although there was a bearing stress beyond which loading was not possible, this limit varied from pattern to pattern and was seldom achieved in test. Edge and side distances must be large to develop the bearing strength of the composites. It was observed that laminates composed of $\pm \phi$ layers generally failed along filament lines, indicating that the inter-filament strength of the matrix was a limiting factor. Laminates with 50 percent of the layers at zero degrees and 50 percent at $\pm \phi$ usually failed along zero-degree and 90-degree lines from the sides of the hole. When ϕ approached zero, failure was usually by cleavage, the whole laminate splitting along its length.

TABLE XVIII
SUMMARY OF STEPPED LAP BONDED JOINT TEST RESULTS (1-INCH SPECIMEN WIDTH)

JOINT DESCRIPTION MATERIALS, AND GAGES (IN.)	P A T T E R N	STEPS	LAP LENGTH (IN.)	AVERAGE ADHESIVE THICKNESS (IN.)	ULTIMATE STATIC LOAD (LB)	AVERAGE ADHESIVE SHEAR STRESS AT FAILURE* (PSI)	AVERAGE ADHEREND TENSILE STRESS AT FAILURE COMPOSITE AND ALUMINUM (PSI)	FAILURE MODES**
STEPPED LAP BORON (0.160)/7075-T6 (0.160)	A	2	2.00	0.0024	10,880	5,483	68,000	(2)
	A	4		0.0026	11,874	6,017	74,100	(1), (2)
	A	8		0.0024	11,379	5,767	71,000	(1), (3)
	C	2		0.0024	11,053	5,583	69,000	(1), (2)
	C	4		0.0026	11,670	5,925	73,000	(1), (2)
	C	8		0.0026	11,560	5,880	72,200	(1), (2), (3)
STEPPED LAP FIBERGLASS (0.160)/ 7075-T6 (0.160)	A	2	2.00	0.0034	7,386	3,744	46,000	(2)
	A	4		0.0036	8,800	4,480	55,000	(2)
	A	8		0.0030	6,972	3,534	43,500	(2)
	C	2		0.0034	9,052	4,582	56,500	(2)
	C	4		0.0034	8,100	4,037	50,600	(2)
	C	8		0.0038	6,810	3,772	42,500	(2)

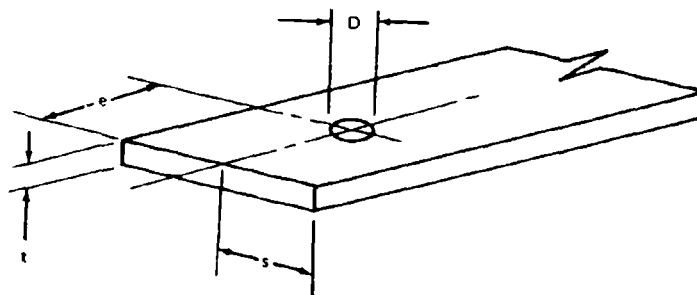
*AVERAGE OF FIVE TESTS

** (1) ADHESIVE

(2) INTERLAMINAR SHEAR

(3) TENSION IN ALUMINUM SECTION

Design variables selected for the composite joint specimens were edge distance (e), side distance (s), fastener diameter (D), laminate thickness (t), and laminate pattern. The commonly used design parameters for mechanical joints in metal structures are e/D , s/D , and t/D . If properly chosen these parameters provide a balanced joint design in shear, tension, and bearing strengths, respectively. In composite joints, the choice of laminate pattern was an added design parameter because it changed the relative proportions of laminate strength in shear, tension, and bearing. Thus, optimum joint proportions in composites will vary with the choice of laminate patterns.



Bolted (rather than simply pinned) joints were selected, so the effects of bolt clamping friction are included in the test data. These specimens provided data more representative of aircraft joints. Consistent surface conditions and bolt torques were maintained on the specimens to minimize data scatter caused by frictional effects. Standard installation torques were used, resulting in bolt tensile stresses between 30 and 40 ksi.

Specimen width was selected to preclude premature failures in tension through the bolt holes. The standard specimen width was 1 inch, giving s/D ratios of 2.63 and 2.00, respectively, for 3/16- and 1/4-inch diameter bolts. A specimen width of 3/4 inch was selected for the reinforced bolted joints using a 3/16-inch diameter bolt ($s/D = 2.00$).

Test results (from References 10 through 12) indicated that the full bearing stress would not be developed if D/t exceeded a value of about two. Hence, a nominal laminate thickness of 0.120 inch and a pin diameter of 3/16 inch were chosen to give D/t equal to 1.58. A standard pin diameter (0.190 inch) was selected for the specimen construction. A high heat treat steel fastener (180,000 psi minimum) was chosen to give a shear strength greater than the expected range of failure loads. The minimum strength of this bolt is 3062 pounds in single shear. At this load the composite bearing stress was calculated at 139,000 psi, so bolt failures were not likely to occur before the ultimate bearing load. For double lap specimens in which the bolt was in double shear, a laminate 0.160-inch nominal thickness was also selected. In double lap composite-to-aluminum alloy specimens, the laminate was the center member of the joint.

Published test results suggested that bearing stress increased with e/D until a ratio of about five was reached. The selected values of e for the specimens were 1/2, 3/4, and 1-1/4 inches, giving e/D ratios of 2.63, 3.95, and 6.58, respectively.

The design approach for the bolted specimens with reinforced edges was to develop the bolt strength in the joint. Two bolt diameters (3/16- and 1/4-inch nominal) were included in these specimens. The reinforced composite joints were designed to produce a balance between bearing strength and tensile strength through the net tension section at the fastener hole. Edge distance (shear-out strength) was varied to bracket the bolt strength in double shear.

Bolted Lap Joints

Static test results for single and double lap bolted specimens are summarized in Tables XIX and XX, respectively. Laminate patterns for these joints consisted of Pattern A and an alternative pattern in some cases, consisting primarily of zero-degree plies with a few plies at ± 45 degrees. These specimens failed primarily in the shear-out mode, although a study of results indicates that at e/D ratios greater than about five, bearing stresses contributed significantly to failure. Bearing strengths of about 150,000 psi and 130,000 psi were attained in the boron and fiber glass laminates, respectively, up to t/D ratios of about 0.8. Beyond this ratio, bolt bending effects tended to reduce average bearing stresses.

Strength was generally reduced when the percentage of 45-degree layers was reduced from 50 percent. The addition of whiskers did not improve joint strength of these specimens.

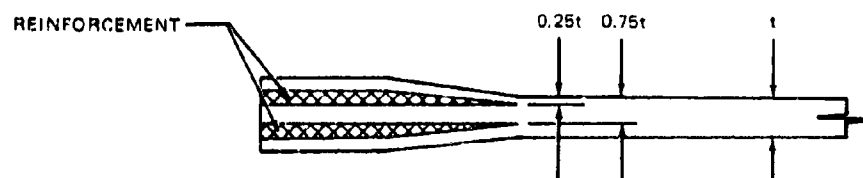
Bolted Joints with Bushed Holes

The specimens were prepared with a hole diameter that afforded a snug fit rather than a force fit on the bushings. Each bushing was filed for a net fit in the laminate to assure good specimen alignment after the bolts and nuts were installed and torqued. The test results are summarized in Table XXI.

These specimens failed primarily in the shear-out mode and developed lower stresses at failure than did the plain bolted specimens. The test results confirmed the reduced weight efficiency predicted for bushed joints.

Bolted Joints with Composite Reinforced Edges

Bolted joints in which the specimen edges were locally reinforced with a laminate buildup were tested with both 0.190- and 0.250-inch-diameter bolts. Static test results are given in Table XXII. The reinforcement was added at two places in the specimen, at 25 and 75 percent of the thickness of the basic pattern as shown in the following sketch. Pattern A was used in each of the two reinforced areas to a thickness of 0.080 inch for the 0.190-inch-diameter bolts and 0.100 inch for the 0.250-inch-diameter bolts. The resulting specimen nominal thicknesses at the joint were 0.280 and 0.360 inch, respectively. The corresponding percentages of filaments at ± 45 degrees are noted in Table XXII.



Shear-out failures predominated, but some tension and bearing failures also occurred. The tension failure through the hole was dependent on the tensile strength of the basic laminate and the stress concentration factor due to the presence of the hole. Although this concentration factor was a function of the diameter-to-width ratio of the specimen, it was reasonably constant in the dimensional range of the specimens tested. When widths and edge distances were large, bearing failures occurred. In glass specimens there was a considerable amount of delamination around the hole but no failure to the edge of the specimens. In boron specimens, bearing deformation was localized around the loaded edge of the hole. For laminates with 50 percent of the layers at ± 45 degrees, the highest bearing stresses recorded were 139,000 psi for fiber glass and 157,200 psi for boron-reinforced laminates. As the percentage of ± 45 -degree layers

TABLE XIX
SUMMARY OF SINGLE LAP BOLTED JOINT TEST RESULTS (1-INCH SPECIMEN WIDTH)*

JOINT DESCRIPTION AND MATERIALS	LAMINATE THICKNESS (IN.)	ULTIMATE STATIC LOAD** (LB)	AVERAGE LAMINATE STRESSES AT FAILURE			FAILURE MODE
			SHEAR-OUT (PSI)	TENSION (PSI)	BEARING (PSI)	
SINGLE LAP FIBER GLASS/7075-T6	0.112	2523	15,200	28,030	119,920	SHEAR-OUT
SINGLE LAP BORON/7075-T6	0.116	2823	16,160	29,640	127,740	SHEAR-OUT
SINGLE LAP FIBER GLASS/FIBER GLASS	0.114	2087	12,430	23,580	98,120	SHEAR-OUT
SINGLE LAP BORON/BORON	0.116	2560	14,720	27,210	115,240	SHEAR-OUT

*0.190-INCH BOLT DIAMETER, 0.750-INCH EDGE DISTANCE, PATTERN A
**AVERAGE OF FIVE TESTS

TABLE XX.
SUMMARY OF DOUBLE LAP BOLTED JOINT TEST RESULTS (1-INCH SPECIMEN WIDTH)

JOINT AND MATERIALS	LAMINATE THICKNESS (IN.)	EDGE DISTANCE (IN.)	PATTERN †	ULTIMATE STATIC LOAD, AVERAGE OF 5 TESTS (LBS)	AVERAGE LAMINATE STRESSES AT FAILURE				FAILURE MODE*
					SHEAR-OUT (PSI)	TENSION (PSI)	BEARING (PSI)		
DOUBLE LAP FIBER GLASS/7075-T6	0.100	0.50	A	1862	18,600	23,000	98,000	(1), (4)	
	0.102	0.75	A	2359	15,400	26,600	122,000	(1), (4)	
	0.104	1.25	A	2583	9,900	30,700	131,000	(3), (4)	
	0.110	0.50	F	1133	10,300	12,800	54,200	(1), (4)	
	0.102	0.75	F	1630	10,600	19,700	84,000	(1), (4)	
	0.108	1.25	F	2226	8,200	25,400	108,500	(1), (4)	
	0.148	0.50	A	2559	17,300	21,300	91,000	(1), (4)	
	0.138	0.75	A	3244	15,700	29,000	123,000	(1), (4)	
	0.146	1.25	A	3782	10,400	32,000	136,500	(3), (4)	
	0.138	0.50	G	1340	9,700	12,000	51,100	(1), (4)	
	0.151	0.75	G	2302	10,200	18,900	80,000	(1), (4)	
	0.143	1.25	G	2600	7,300	22,400	95,500	(1), (4)	
	DOUBLE LAP BORON/7075-T6	0.128	0.50	A	2189	17,100	21,200	90,000	(1)
		0.117	0.75	A	3028	17,200	32,000	136,000	(1)
		0.120	1.25	A	3420	11,400	35,200	150,000	(1), (2), (4)
0.133		0.50	D	1524	11,500	14,200	60,600	(1)	
0.115		0.75	D	2059	11,900	22,100	94,500	(1)	
0.116		1.25	D	3107	10,700	33,000	141,000	(1)	
0.168		0.50	A	2621	15,600	19,200	82,000	(1)	
0.160		0.75	A	4214	17,500	32,600	138,700	(1), (2)	
0.163		1.25	A	4756	11,700	36,000	154,000	(1), (2), (4)	
0.166		0.50	E	1648	9,900	12,300	52,100	(1)	
0.157		0.75	E	2604	11,000	20,500	87,500	(1)	
0.165		1.25	E	4317	10,500	32,300	138,000	(1)	

* (1) SHEAR-OUT
(2) TENSION AT SECTION THROUGH BOLT HOLE
(3) BEARING
(4) INTERLAMINAR SHEAR

† SEE TABLE XII
** THESE STRESSES COMPUTED AS THOUGH ADHESIVE WAS NOT INCLUDED.

TABLE XXI
SUMMARY OF DOUBLE LAP BOLTED JOINT TEST RESULTS - BUSHED HOLES

JOINT DESCRIPTION MATERIALS AND SPECIMEN WIDTH	LAMINATE THICKNESS (IN.)	BOLT DIAMETER (IN.)	EDGE DISTANCE (IN.)	PATTERN	FIBER AT $\pm 45^\circ$ (%)	ULTIMATE STATIC LOAD AVERAGE OF 5 TESTS (LB)	AVERAGE LAMINATE STRESSES AT FAILURE			FAILURE MODES*
							SHEAR-OUT (PSI)	TENSION (PSI)	BEARING (PSI)	
DOUBLE LAP BORON/ALUMINUM 1.250-IN. SPECIMEN WIDTH	0.171	0.3125	1.0	A	50	4773	11,690	24,670	74,800	(1)
	0.171	0.3125	1.5	A	50	4524	8,820	27,930	84,640	(2)
	0.176	0.3125	2.0	A	50	4585	6,480	27,360	83,020	(1), (2)
	0.127	0.3125	1.0	A	50	3595	13,460	28,820	86,100	(1), (2)
	0.126	0.3125	1.5	A	50	3865	10,220	32,340	98,000	(1), (2)
	0.127	0.3125	2.0	A	50	4683	9,230	38,240	118,240	(1), (2)
DOUBLE LAP FIBER GLASS/ALUMINUM 1.250-IN. SPECIMEN WIDTH	0.167	0.3125	1.0	A	50	4253	12,710	26,860	81,380	(1)
	0.166	0.3125	1.5	A	50	4889	9,820	31,490	94,280	(3)
	0.146	0.3125	2.0	A	50	5001	8,590	37,210	110,000	(3)
	0.128	0.3125	1.0	A	50	3487	13,660	29,190	87,480	(1)
	0.122	0.3125	1.5	A	50	3825	10,480	33,740	100,540	(3)
	0.121	0.3125	2.0	A	50	4174	8,810	37,120	110,200	(3)

- (1) SHEAR-OUT
(2) TENSION AT SECTION THROUGH BOLT HOLE
(3) BEARING FAILURE

TABLE XXII
SUMMARY OF COMPOSITE-REINFORCED BOLTED JOINT TEST RESULTS

JOINT DESCRIPTION MATERIALS AND SPECIMEN WIDTH	LAMINATE THICKNESS (IN.)	BOLT DIAMETER (IN.)	EDGE DISTANCE (IN.)	PATTERN †	FIBER AT ±45° (%)	ULTIMATE STATIC LOAD AVERAGE OF 5 TESTS (LB)	AVERAGE LAMINATE STRESSES AT FAILURE			FAILURE MODES*
							SHEAR-OUT (PSI)	TENSION (PSI)	BEARING (PSI)	
DOUBLE LAP BORON/STEEL** 0.750-IN. SPECIMEN WIDTH	0.278	0.190	0.50	A	50	4,602	16,500	28,600	87,300	(1)
	0.279	0.190	0.75	A	50	6,910	16,500	44,300	130,000	(1), (3)
	0.279	0.190	1.25	A	50	7,215	10,400	45,900	137,000	(1), (3)
	0.292	0.190	0.50	D	43	3,885	13,300	23,500	70,000	(1)
	0.301	0.190	0.75	D	43	6,785	15,000	39,700	118,500	(1)
DOUBLE LAP FIBER GLASS/ STEEL** 0.750-IN. SPECIMEN WIDTH	0.289	0.190	1.25	D	43	7,140	9,900	43,600	130,000	(1)
	0.283	0.190	0.50	A	50	5,975	21,100	37,500	111,000	(1), (2)
	0.268	0.190	0.75	A	50	6,390	15,800	42,400	125,500	(1), (2)
	0.275	0.190	1.25	A	50	6,725	9,800	42,900	129,000	(1), (2)
	0.257	0.190	0.50	F	43	4,763	18,500	33,300	97,500	(1), (2)
DOUBLE LAP BORON/STEEL** 1-IN. SPECIMEN WIDTH	0.274	0.190	0.75	F	43	6,470	15,700	41,800	124,000	(1), (2)
	0.257	0.190	1.25	F	43	6,420	10,000	44,600	131,000	(1), (2)
	0.366	0.250	0.75	A	50	9,179	16,700	33,500	100,000	(1)
	0.378	0.250	1.00	A	50	11,914	15,800	42,000	126,000	(1), (3)
	0.361	0.250	1.50	A	50	12,021	11,100	44,400	133,000	(1), (3)
DOUBLE LAP FIBER GLASS/ STEEL** 1-IN. SPECIMEN WIDTH	0.346	0.250	0.75	E	39	6,284	12,100	24,200	72,500	(1)
	0.373	0.250	1.00	E	39	10,715	14,400	38,300	115,000	(1)
	0.343	0.250	1.50	E	39	10,300	10,000	40,000	120,000	(1)
	0.381	0.250	0.75	A	50	10,796	18,900	37,700	113,000	(1), (2)
	0.351	0.250	1.00	A	50	11,200	15,900	42,500	127,700	(1), (2)
DOUBLE LAP FIBER GLASS/ STEEL** 1-IN. SPECIMEN WIDTH	0.324	0.250	0.75	G	39	7,463	15,300	30,700	92,000	(1), (2)
	0.342	0.250	1.00	G	39	8,742	12,800	34,100	102,000	(1), (2)
	0.353	0.250	1.50	G	39	10,430	9,800	39,500	118,000	(1), (2)

† SEE TABLE XII

* (1) SHEAR-OUT
(2) INTERLAMINAR SHEAR
(3) TENSION AT SECTION THROUGH BOLT HOLE
** RIGID TEST FIXTURE

decreased, the bearing stresses decreased also. Thus, no direct relationship between allowable bearing stress and ultimate tensile stress was observed. At 25 percent ± 45 -degree layers, the highest bearing stresses were 121,400 psi for fiber glass and 151,500 psi for boron-reinforced laminates.

Bolted Joints with Steel Shim Reinforcement

The joints reinforced with steel shims (17-7PH stainless) were included to reduce the edge distances needed to develop the bolt strengths. In designing these joints, empirical equations for critical failure modes were developed from similar work reported by the Bendix Corporation (Reference 13). The equations used to design the shim joint specimens in the present study were the following:

- Tension Strength Across Holes

$$P_{th} = \left[N_s t_s F_s + t F_{tx} \right] K_{th} (p - D) \quad (\text{pounds/bolt})$$

where

$$K_{th} = \frac{79.327}{143.75 - 100 D/p}$$

F_s = ultimate tensile strength of shim material (psi)

- Pin Bearing Strength

$$P_{br} = 1.5D \left[N_s t_s F_s (1 - 0.010D/t_s) + t F_{tx} \right] \quad (\text{pounds/bolt})$$

- Hoop Tension Strength

$$P_{ht} = 2.6D \left(\frac{e/D - 0.5}{e/D + 0.4} \right) (N_s t_s F_s + t F_{ty}) \quad (\text{pounds/bolt})$$

- Shear-out Strength

$$P_{so} = 2e (0.6 N_s t_s F_s + t F_{so}) \quad (\text{pounds/bolt})$$

- Adhesive Bond Strength (shim-to-laminate)

$$P_a = 2N_s F_a p \quad (\text{pounds/inch})$$

Shim joint static test results are presented in Table XXIII. The 17-7PH stainless steel shims were installed in a manner similar to the composite reinforcement described previously. Shim thicknesses of 0.036 inch were used with 0.190-inch-diameter bolts, and 0.050-inch shims were used with 0.250-inch-diameter bolts. The resulting nominal specimen thicknesses were 0.192 and 0.260 inch, respectively.

TABLE XXIII
SUMMARY OF SHIM-REINFORCED BOLTED JOINT TEST RESULTS

JOINT DESCRIPTION, MATERIALS, AND SPECIMEN WIDTH	LAMINATE THICKNESS (IN.)	BOLT DIAMETER (IN.)	EDGE DISTANCE (IN.)	PATTERN 1	ULTIMATE STATIC LOAD AND NO. TESTS (LB.)	AVERAGE LAMINATE STRESSES AT FAILURE			FAILURE MODES*
						SHEAR-OUT (PSI)	TENSION (PSI)	BEARING (PSI)	
DOUBLE LAP BORON/STEEL** 0.750-IN SPECIMEN WIDTH	0.192	0.190	0.375	A	6,938 (5)	49,100	64,500	191,000	(2), (3), (4)
	0.192	0.190	0.500	A	6,670 (4)	34,700	62,000	184,000	(2), (3), (4)
	0.192	0.190	1.000	A	7,813 (5)	20,400	72,600	215,000	(2), (7)
	0.192	0.190	0.375	D	6,883 (5)	47,800	64,000	189,500	(2), (3)
	0.192	0.190	0.500	D	7,690 (5)	40,000	71,500	212,000	(2), (3)
DOUBLE LAP FIBER GLASS/ STEEL** 0.750-IN SPECIMEN WIDTH	0.192	0.190	1.000	D	8,360 (4)	21,800	77,800	230,000	(1), (3)
	0.192	0.190	0.375	A	4,550 (4)	31,600	42,400	125,000	(2), (3)
	0.192	0.190	0.500	A	5,300 (5)	27,600	49,400	146,000	(2), (3)
	0.192	0.190	1.000	A	5,006 (5)	13,000	46,500	137,500	(2), (3)
	0.192	0.190	0.375	F	4,070 (5)	28,200	37,900	112,000	(2), (3), (4)
DOUBLE LAP BORON/STEEL** 1-IN SPECIMEN WIDTH	0.260	0.250	0.500	F	5,254 (5)	27,900	49,800	147,400	(2)
	0.260	0.250	1.000	F	5,316 (5)	13,800	49,400	146,000	(2), (3)
	0.260	0.250	0.4375	A	11,905 (5)	52,500	61,300	184,000	(4)
	0.260	0.250	0.500	A	12,820 (5)	49,400	65,800	197,000	(4), (5)
	0.260	0.250	0.750	A	12,800 (4)	32,800	65,700	197,100	(4)
DOUBLE LAP FIBER GLASS/ STEEL** 1-IN SPECIMEN WIDTH	0.260	0.250	0.4375	E	10,800 (3)	47,500	55,500	166,000	(6)
	0.260	0.250	0.500	E	11,815 (5)	45,500	60,600	184,000	(3), (4)
	0.260	0.250	0.750	E	14,300 (5)	38,200	76,500	229,000	(2), (3), (4)
	0.260	0.250	1.250	E	14,850 (2)	22,800	76,200	228,000	(1)
	0.260	0.250	0.500	A	7,172 (5)	77,600	36,800	110,000	(3), (4)
DOUBLE LAP FIBER GLASS/ STEEL** 1-IN SPECIMEN WIDTH	0.260	0.250	0.750	A	8,888 (5)	22,800	45,500	137,000	(3)
	0.260	0.250	0.500	G	7,100 (5)	27,400	36,500	108,400	(3)
	0.260	0.250	0.750	G	7,392 (5)	18,900	37,900	113,700	(3)
DOUBLE LAP FIBER GLASS/ STEEL** 1-IN SPECIMEN WIDTH	0.260	0.250	1.250	G	8,142 (5)	12,500	41,700	125,000	(3), (4)

* SEE TABLE XII

1. BOLT SHEAR
 2. TENSION IN LAMINATE AT BASE OF SHIMS
 3. SHIM DELAMINATION AND LAMINATE SHEAR-OUT
 4. TENSION IN LAMINATE AND SHIM OF SECTION THROUGH FASTENER HOLE
 5. TENSION IN LAMINATE AND ONE SHIM, TENSION AND SHEAR-OUT IN SECOND SHIM
 6. SHEAR-OUT OF LAMINATE AND ONE SHIM, TENSION IN SECOND SHIM
 7. TENSION IN OUTER PLYS OF LAMINATE AT BASE OF SHIMS AND AT SECTION THROUGH FASTENER HOLE IN PLYS BETWEEN SHIMS; PARTIAL DELAMINATION OF SHIMS.
- **RIGID TEST FIXTURE

The joints were designed to have strengths equal to the double shear strengths of the bolts when the longer edge distances were used. These strengths were 7280 and 12,970 pounds for the 0.190- and 0.250-inch-diameter bolts, respectively. Some of the boron specimens exceeded these values, even at the shortest edge distances, and the bolts, although severely deformed, did not fail in shear.

The types of failure modes are indicated in Table XXIII. A number of the specimens failed in the basic unreinforced laminate region, generally at the base of the shims. Most of these failures were in the specimens with 0.190-inch-diameter bolts. The change in slope of the laminate layers at the shims introduced bending stresses in the filaments and a change of directional load that tended to delaminate the layers in a tension joint. An additional factor was that the transfer of load from the shims into the laminate introduced peak interlaminar shear stresses in this region of the specimen. These failures usually occurred simultaneously with one or more other modes and, hence, may have been secondary failures. Efficiency factors (joint strength/basic laminate strength) ranging from 72 to 91 and 38 to 48 percent were recorded for boron and fiber glass, respectively. These factors were computed using theoretical laminate strengths and actual joint strengths from Volume II.

On the basis of test results attained in the shim-reinforced specimens, the following modifications to the Bendix equations are recommended:

- Tension Strength Across Holes — The design equation was satisfactory but the expression for calculating K_{th} gave unconservative results. Better correlation with test results was achieved when values of 0.40 and 0.285 were used for K_{th} of boron and fiber glass laminates, respectively.
- Pin Bearing Strength — The second term of this equation ($1.5 Dt F_{tx}$) represents the contribution of the laminate to bearing strength. This term was replaced by one developed in this study (see Analysis of Parametric Trends in Joint Strength). The latter term is $(Dt F_{br})$. Thus, the recommended equation for pin-bearing strength is:

$$P_{br} = D [N_s t_s F_s (1.5 - 0.015 D/t_s) + t F_{br}]$$

- Hoop Tension Strength — No failures of this type occurred in the specimens. This mode of failure was precluded by the shear-out criterion.
- Shear-Out Strength — The design equation for shear-out strength was found to be satisfactory. As in the case of pin-bearing strength, F_{s0} for the laminate was evaluated using an expression developed in this study (see Analysis of Parametric Trends in Joint Strength).

- Adhesive Bond Strength (shim-to-laminate) — Interfacial adhesive failure between the shim and the laminate occurred in several specimens. The shims were bonded to the matrix during the cure. The minimum bond stresses developed between boron laminates and stainless steel shims were 1420, 1340, and 1350 psi, respectively, for shims of 1-9/16, 1-15/16, and 2-3/4 inches length. Corresponding stresses between fiber glass laminates to stainless steel shims were 940, 860, and 740 psi, respectively, for shims of 1-7/16, 1-15/16, and 2-3/4 inches length. The highest average interfacial stresses achieved in test were 1947 psi for boron laminates and 1373 psi for fiber glass laminates. Although these results, particularly for glass, were lower than anticipated this type of joint shows considerable promise for carrying the high loads expected in primary structural joints.

Bolted-Bonded Joints

Test results for joints that were both bolted and bonded are presented in Table XXIV. These joints produced results that were better than similar bolted or bonded joints tested separately. The corresponding bolted joints without bonding were less than one-third as strong in fiber glass laminates and less than one-fifth as strong in boron laminates. Based on a nominal 3 square inches of bond area, the average bond shear stresses were 2717 and 4300 psi for fiber glass and boron specimens, respectively. Interpolation for a lap length of 1.5 inches for the similar bonded double lap joints gave corresponding values of about 1800 and 3300 psi. Allowing for the geometrical differences, it is apparent that the presence of the bolt enhanced the performance of the bond, and vice versa.

TABLE XXIV
SUMMARY OF DOUBLE LAP BOLTED AND BONDED JOINT TEST RESULTS

JOINT AND MATERIALS	LAMINATE THICKNESS (IN.)	EDGE DISTANCE (IN.)	PATTERN	ULTIMATE STATIC LOAD, AVERAGE OF 5 TESTS (LB)	AVERAGE LAMINATE STRESSES AT FAILURE			FAILURE MODE*
					SHEAR-OUT (PSI)	TENSION (PSI)	BEARING (PSI)	
DOUBLE LAP FIBERGLASS/7075-T6 BOLTED AND BONDED	0.120	0.75	A	7470	41,500**	77,000**	328,000**	(1), (2)
DOUBLE LAP BORON/7075-T6 BOLTED AND BONDED	0.120	0.75	A	12,875	71,500**	132,000**	564,000**	(1), (2)

*(1) TENSION AT SECTION THROUGH BOLT HOLE

(2) INTERLAMINAR SHEAR

** THESE STRESSES COMPUTED AS THOUGH ADHESIVE WAS NOT INCLUDED.

PHENOMENOLOGICAL TRENDS IN JOINT FAILURES

The joints in composite materials failed in the modes associated with joints in homogeneous structural materials and also in modes caused by the relatively low shear strength of the laminates.

Bonded Joints

Bonded joints in reinforced epoxy laminates were observed to fail in the following modes:

- Cohesive Failure from Combined Stresses (predominantly shear) in the Adhesive
- Adhesive Failure at the Resin/Adhesive Interface
- Adhesive Failure at the Resin/Fiber Interface in the First Layer of the Laminate
- Interlaminar Shear (combined with some fiber breakage) within the Laminate
- Tension (or compression) in the Adherends

These modes are illustrated in Figures 41 through 43.

Design parameters having the greatest influence on bonded joint failures were lap length, adherend thickness, and fiber orientations adjacent to the adhesive. In single and double lap joints, short lap lengths and thick adherends ($L/t = 12.5$) tended to produce Failure Modes 1, 2, 3, depending on fiber orientations. Long lap lengths and thin adherends ($L/t = 50$) tended to produce failures in the adherends (Mode 5). Between these two extremes ($L/t = 25$), interlaminar shear failures were observed. Interlaminar shear failures were also observed near the fiber ends in scarf adhesive joints as shown in Figure 42, and near the step ends of stepped lap joints as shown in Figure 44.

Bolted Joints

Possible failure modes for bolted joints in composite laminates were the following:

- Shear-out of the Laminate
- Combined Tension and Shear-out at the Edge of the Fastener Hole
- Tension (or compression) of the Laminate at the Minimum Section through the fastener hole
- Bearing in the Laminate

These modes are illustrated in Figures 45 through 48.

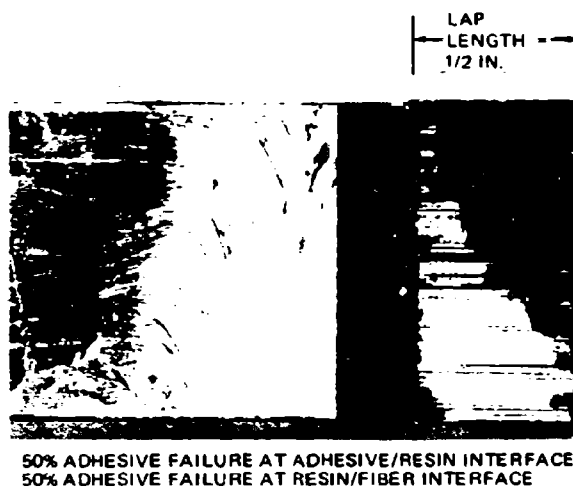
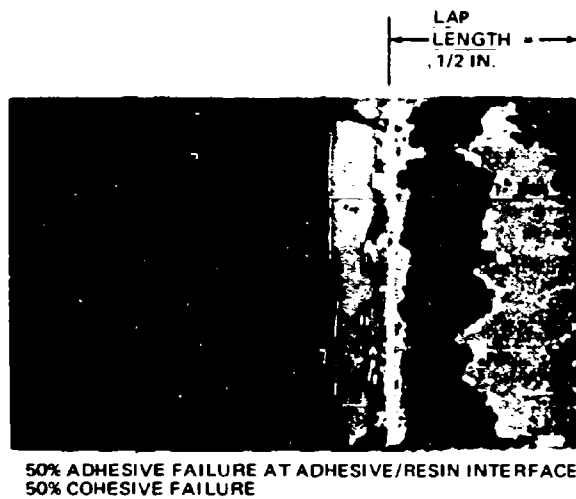
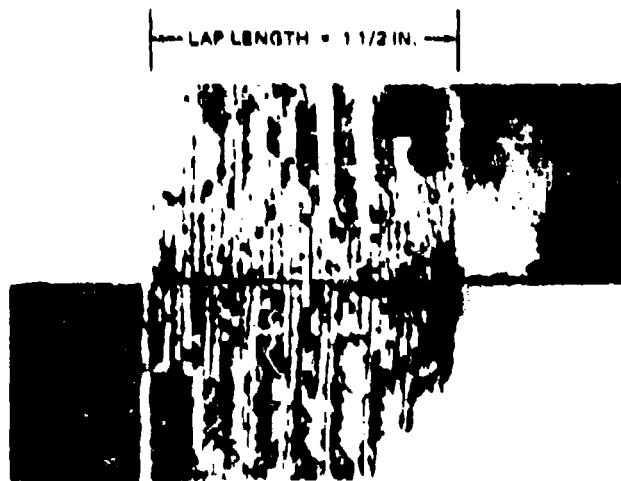


FIGURE 41. INTERFACIAL FAILURES IN SIMPLE LAP ADHESIVE JOINTS ($L/t = 12.5$)



SIMPLE LAP JOINT ($L/t = 28$)



SCARF JOINT

FIGURE 42. INTERLAMINAR SHEAR FAILURE IN ADHESIVE JOINTS



FIGURE 43. ADHEREND TENSION FAILURE IN SIMPLE LAP ADHESIVE JOINTS ($L/t = 25-50$)

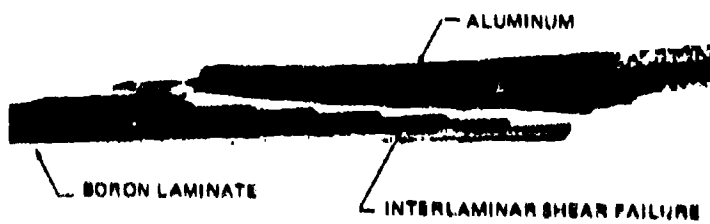


FIGURE 44. BORON/ALUMINUM EIGHT-STEP LAP JOINT FAILURE

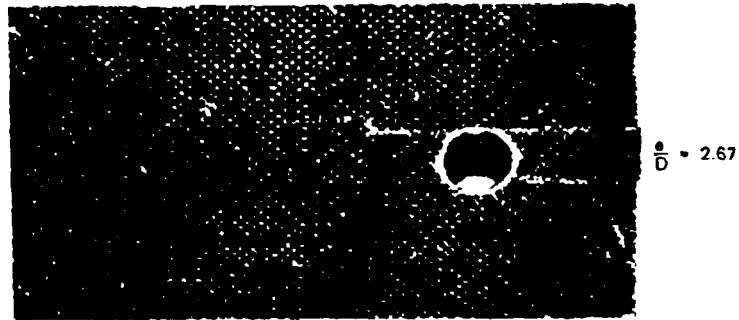


FIGURE 45. SHEAR-OUT FAILURES OF BOLTED JOINTS (D = 3/16 INCH)

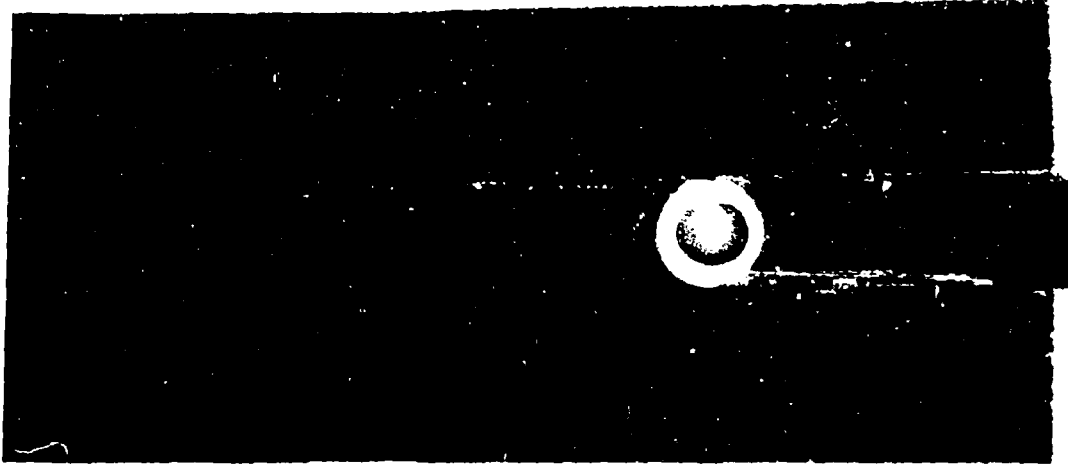
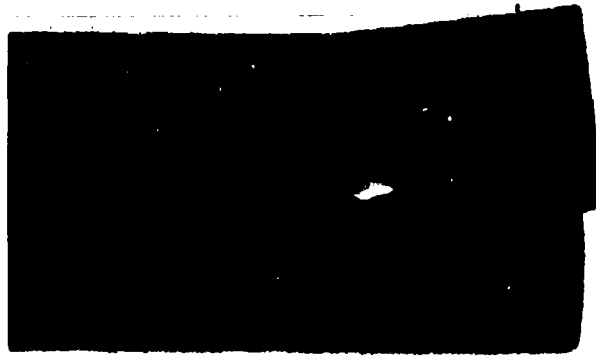
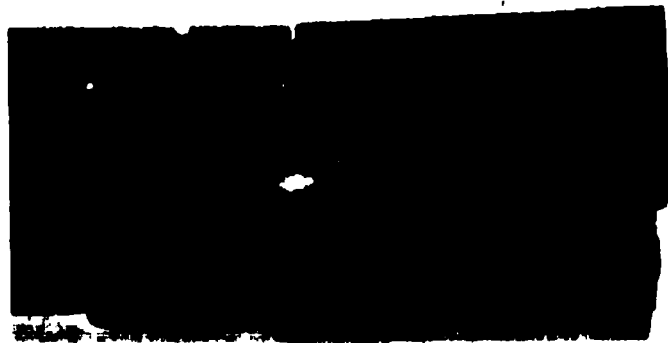


FIGURE 40. SHEAR-OUT FAILURES OF PUSHED HOLES (BUSHING DIAMETER = 5/16 INCH)



$\frac{b}{D} = 4$



$\frac{b}{D} = 0.67$

FIGURE 47. COMBINED TENSION AND SHEAR-OUT FAILURE OF BOLTED JOINTS (D = 3/16 INCH)

SPECIMEN Z3824833-601 (2.8x)

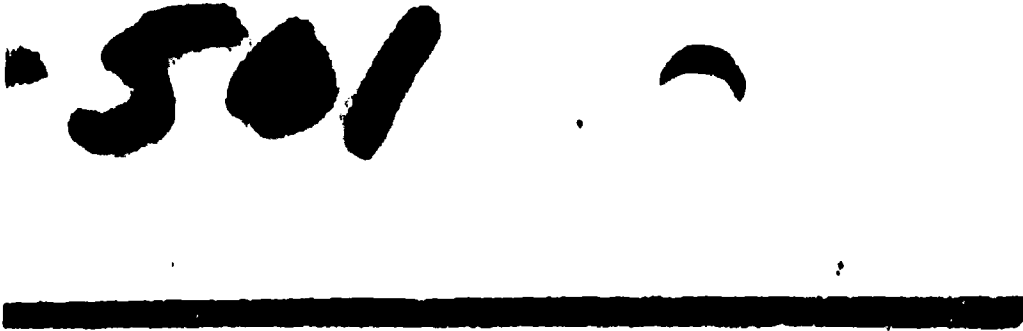


FIGURE 48. BEARING FAILURE OF FIBER GLASS LAMINATED (D = 3/16 INCH)

The presence of the fastener hole was a critical factor in each mode of failure observed in the bolted joints. Stress concentration factors caused by the hole ensured that failure would not occur in the basic laminate section or in the fastener unless the joint area was reinforced in some manner (i. e., metal shim inserts, edge buildup, etc).

An examination of failure modes indicated a basic difference between boron and glass laminate behavior. Gross laminate failures occurred in the boron specimens, either in the tension mode (at 90 degrees to the load line) or in a conventional shear-out mode. These failures are illustrated in Figure 47. The glass specimens, however, appeared to fail in the individual lamina along filament lines. These failures were characterized by delaminations as shown in Figure 49, which probably resulted from interlaminar shear failures of the resin between the relative flexible glass fibers.

Design parameters having an influence on the mechanical joint failures were edge distance, side distance (specimen width), laminate thickness, and fastener diameter. Within the range of variation of these parameters in the present program, the shear-out mode predominated in joint failures. The shear stresses developed at failure for a number of laminate thicknesses and edge distances, are summarized in Figure 50. It was postulated that the stress concentration at the edge of the hole along the shear-out planes was not a sensitive function of edge distance, because the average shear stress at failure decreased as edge distance increased. The increasing bearing stresses also contributed to initiation of failures at the larger edge distances. Thus, increasing edge distance was an inefficient method of increasing the joint strength. For a given edge distance, joint strength increased approximately linearly with composite thickness.

The combination bolted-bonded joint performed better than joints employing either bolting or bonding separately. The strength of this joint was improved due to a failure mode change caused by the presence of the adhesive. As shown in Figure 51, the mode of failure was a combination of tension through a section at the fastener and interlaminar shear in the composite. If this joint had been either bolted or bonded separately, it would probably have failed in shear-out (bolted) or an interfacial shear mode (bonded).

The steel shim-reinforced specimens failed in a variety of complex modes involving bolt shear, tension through a section at the fastener hole, tension in the basic laminate section, and delamination of the specimen at the shim-to-resin interface. Examples of these failures are shown in Figures 52 and 53.

ANALYSIS OF PARAMETRIC TRENDS IN JOINT STRENGTH

Test data may be analyzed mathematically, graphically, or with a semi-empirical approach combining the two techniques. The latter approach is advantageous in identifying parametric trends when the number of experimental variables is large and when adequate experimental data are available. The semi-empirical analysis technique was used in the present program to evaluate the effects of design variables on the strength performance of the fundamental double lap joints, both bonded and bolted.

SPECIMEN Z3924833-1 (2.3x)



FIGURE 49. DELAMINATION OF FIBER GLASS SPECIMEN

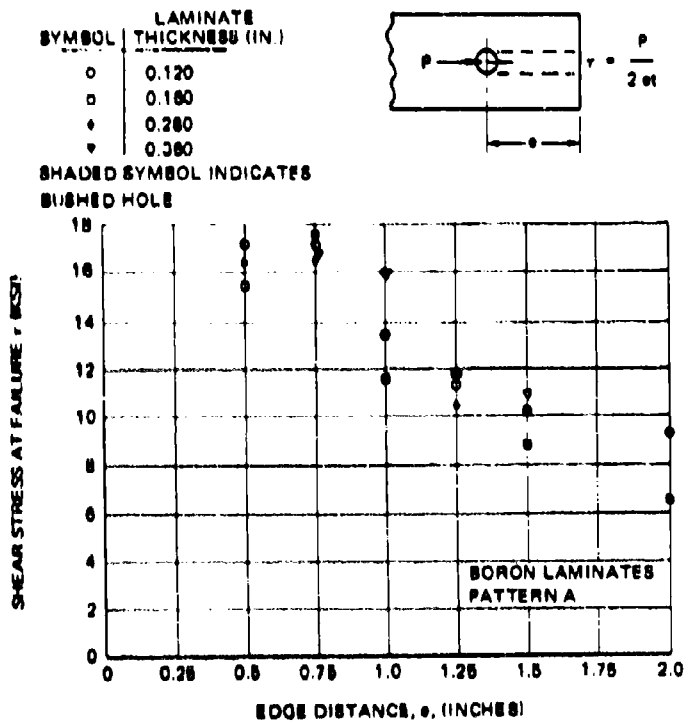
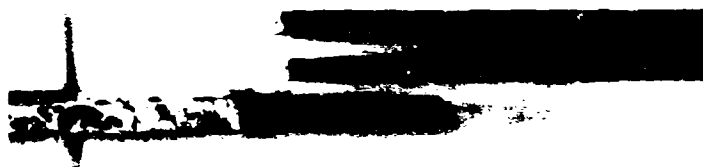


FIGURE 50. BOLTED JOINT SHEAR STRESS AT FAILURE AS A FUNCTION OF EDGE DISTANCE

LAP LENGTH = 1 1/2 IN.



EDGEVIEW

BORON/EPOXY COMPOSITE



ALUMINUM ALLOY

PLANVIEW

FIGURE 51. BOLTED-BONDED JOINT FAILURE IN TENSION AND INTERLAMINAR SHEAR
($L/r = 12.5$, $e/D = 4$)



FIGURE 52. SHIM-REINFORCED JOINT FAILURE – COMPLEX MODE ($e/D = 1.45$)



FIGURE 53. SHIM-REINFORCED JOINT FAILURE – TENSION AT BASE OF SHIMS

The analyses were conducted in four steps as follows:

- Design variables were selected that were independent of one another and that influenced joint strength.
- The number of independent variables was reduced to fewer non-dimensional parameters by dimensional analysis.
- The relationships between dependent and independent variables were evaluated from test data. These relationships were expressed in terms involving the geometric parameters (edge distance, lap length, thickness, etc) or in terms of coefficients involving parameters other than geometric (ply orientations and arrangements).
- The coefficients and mathematical expressions were formulated into general equations and design charts for calculating joint strengths.

In addition to the experimental data generated in the present program, data on comparable bolted joints from References 9 through 14 were evaluated in the parametric analysis.

As the effects of the design parameters were identified and normalized, the scatter of experimental data was methodically reduced. When the effects of all the study parameters were normalized, the agreement between predicted loads and test data was very good.

Bonded Joints

The following variables in the bonded joint study were selected as significant:

t_1, t_2 = Thickness of Adherends

t_a = Thickness of Adhesive

L = Length of Overlap

w = Width of Overlap

p_n = Parameters (or coefficients) Defining Fiber Pattern and Percentage of Plies at Various Orientations

E_1, E_2 = Young's Moduli of Adherends

G = shear Modulus of Adhesive

F_{tu} = Tensile Strength of Weaker Adherend

F_{su}^a = Shear Strength of Adhesive

Processing variables were significant to both adherend and adhesive strengths, but since laminating and bonding processes were not varied in the specimen preparation, the effects of processing variables were assumed to be negligible.

Bonded joint failures occurred in the adhesives and/or the adherends depending on loads, fiber patterns, and joint geometry. In the present analysis, joint failure was considered to have occurred when the applied tension stress in the laminate or shear stress in the adhesive reached ultimate, whichever occurred first. These criteria of failure may be stated mathematically as follows:

Adherend Failure

$$\left(\frac{t}{L}\right)F_{tu} \leq \frac{N}{L}x < F_{su}^a$$

Adhesive Failure

$$\left(\frac{t}{L}\right)F_{tu} > \frac{N}{L}x \geq F_{su}^a$$

In the case of adhesive failure, the average shear stress in the adhesive (τ_{avg}) was related to the ultimate shear strength of the adhesive (F_{su}^a) by the expression

$$\tau_{avg} = \eta F_{su}^a = \frac{N}{L}x \quad (1)$$

where η is the reciprocal of the stress concentration factor in the adhesive. Thus in a joint in which the adhesive is in the plastic range, the prediction of joint strength depended on defining the value of η , assuming that adhesive failure was critical.

The reduction of variables by dimensional analysis was accomplished using the dimensionless parameter η as the dependent variable. The independent variables t_1 , t_2 , t_a , and L have fundamental length units (L), and the moduli E_1 , E_2 , and G have units FL^{-2} where F denotes force. (Force may be treated as a fundamental unit in this study because none of the significant variables involves mass units.) The independent variable p_n is dimensionless.

In functional notation, the equation for η was expressed as

$$\eta = f(E_1^a, t_1^b, t_a^c, L^d, G^e, E_2^f, t_2^g, p_n^h) \quad (2)$$

In dimensional form, Equation (2) was written

$$0 = f' \left[(FL^{-2})^a, (L)^b, (L)^c, (L)^d, (FL^{-2})^e, (FL^{-2})^f, (L)^g \right] \quad (3)$$

From Equation (3) the following two equations were obtained.

$$-2a + b + c + d - 2e - 2f + g = 0$$

$$a + e + f = 0$$

Solving for a and b, and rewriting Equation (1),

$$\eta = f \left[(E_1)^{-e-f}, (t_1)^{-c-d-g}, (t_2)^c, (L)^d, (G)^e, (E_2)^f, (t_2)^g \right]$$

Collecting terms,

$$\eta = f \left[\left(\frac{t_2}{t_1} \right)^c, \left(\frac{L}{t_1} \right)^d, \left(\frac{G}{E_1} \right)^e, \left(\frac{E_2}{E_1} \right)^f, \left(\frac{t_2}{t_1} \right)^g \right]$$

From the experimental data it was concluded that $f = g$, so the latter two terms were combined into

$$\left(\frac{E_2 t_2}{E_1 t_1} \right)^f$$

In the analysis of parametric trends, interlaminar shear failures of the resin were treated in the same fashion as adhesive failures. Values of η were determined from experimental data for both types of failure with acceptable results in predicting joint strengths. Better definition of failure criteria for interlaminar shear is required for distinguishing between these two modes (i. e., adhesive or interlaminar shear) exclusively by analytical methods.

For Shell 951 adhesive, the ultimate shear strength averaged 6100 psi in the torsional ring shear tests. Adhesive thicknesses for these tests were roughly comparable to those measured in the joint specimens. Substituting this value in Equation (1), the equation for η became

$$\eta = \frac{N_x / L}{6100}$$

Using this equation, plots of η versus overlap length were prepared for the double lap joints tested in the experimental program. These plots are shown in Figures 54 and 55, respectively, for boron and fiber glass laminates.

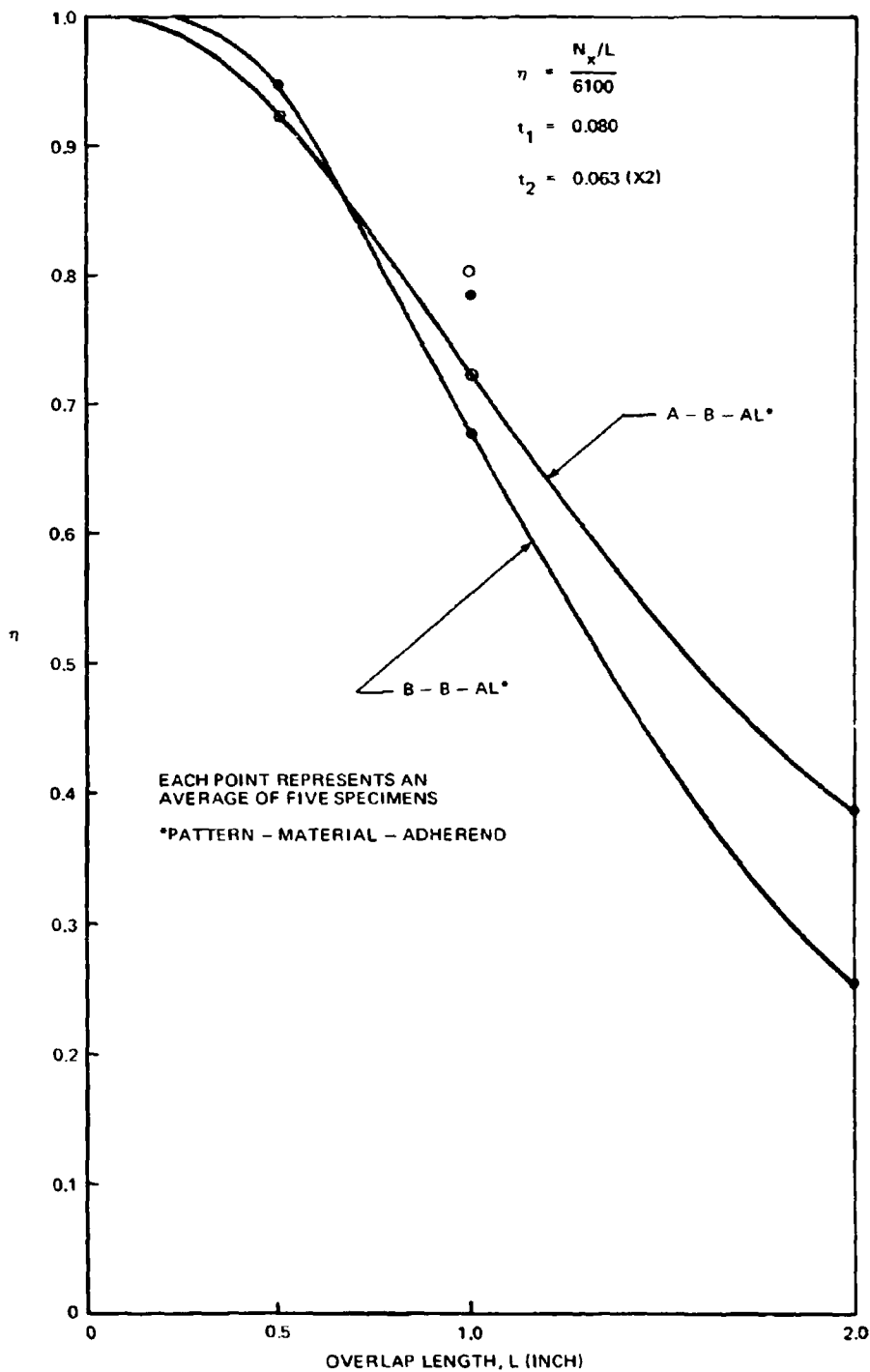


FIGURE 54. BONDED JOINT STRENGTH PARAMETER VERSUS OVERLAP LENGTH - BORON LAMINATE TO ALUMINUM ALLOY

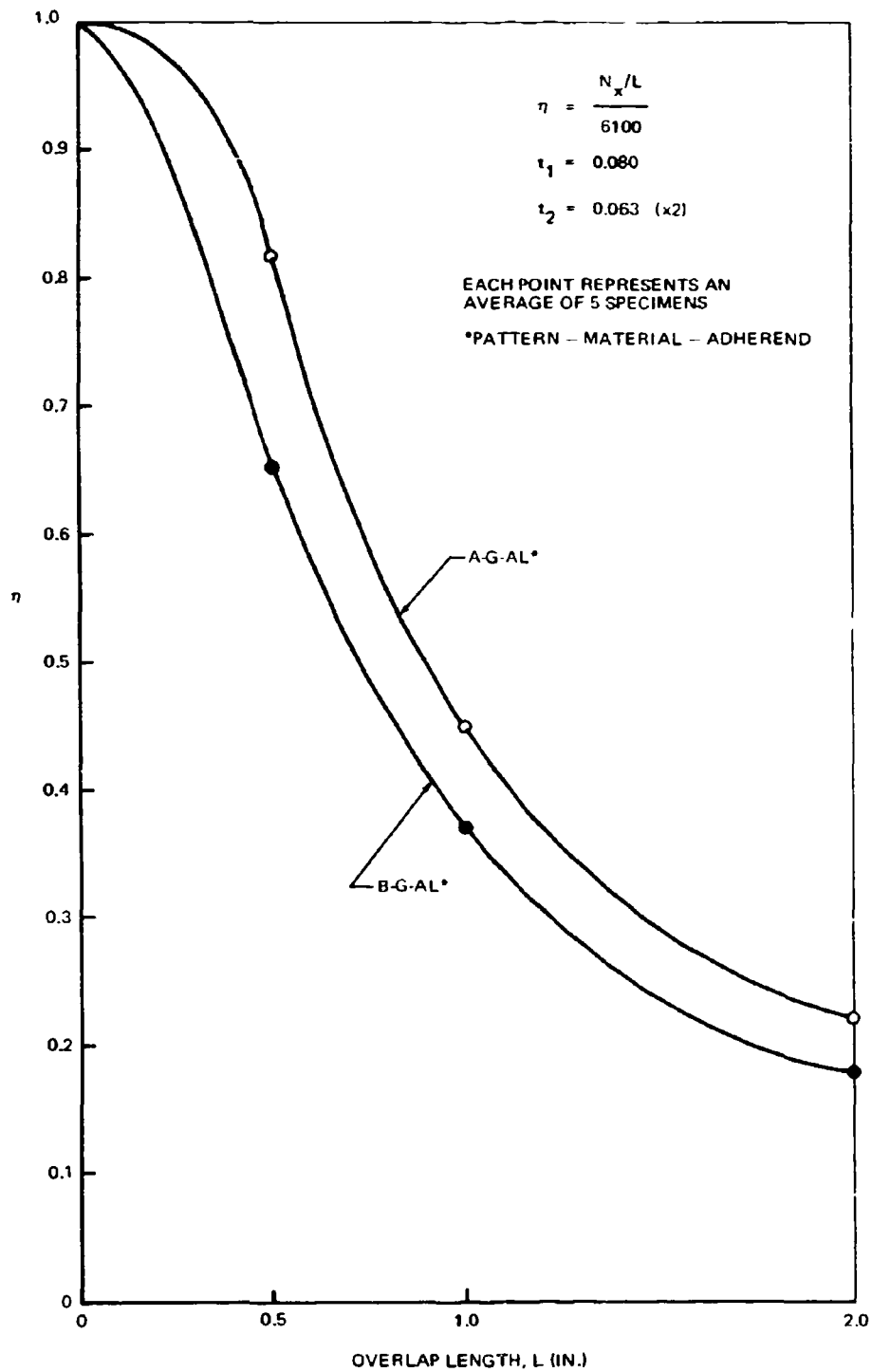


FIGURE 55. BONDED JOINT STRENGTH PARAMETER VERSUS OVERLAP LENGTH - FIBER GLASS LAMINATE TO ALUMINUM ALLOY

Overlap length, L , was plotted along the abscissa rather than (L/t_1) because laminate thicknesses were not varied in the specimens. However, laminate thickness has been recognized as an important design parameter. Figure 56 was plotted from data obtained by Kutscha and Hofer (Reference 14) for Scotchply XP-251S laminates and Metalbond 400 adhesive. Conclusions drawn from the plot were that (1) average adhesive shear strength increased as adherend thickness increased, and (2) average adhesive shear strength approached a limit as (L/t) increased. These trends were expected, because adherend stiffness increased linearly with thickness and improved strain compatibility; i. e., reduced stress concentration in the adhesive. This effect was less pronounced when adherend thicknesses were relatively large with respect to lap length.

To evaluate η as a function of the parameter (L/t) by semi-empirical methods, additional experimentation is needed in which the laminate thicknesses are varied together with the lap lengths. As additional experimental points are obtained, appropriate coefficients can be determined by curve fitting techniques to define the mathematical relationship between η and (L/t) .

Joint width, w , was held constant in the experimental program, and thus it was not included in the analysis of strength trends. Nadler and Yoshino (Reference 15) indicated that increased joint width appeared to have an adverse effect on joint efficiency in a design application. Comparisons of coupon results with those obtained from a 54-inch-diameter monocoque cylinder indicated an appreciable scale effect (25 to 30 percent), adversely affecting joint strength. This effect should also be investigated further.

The evaluation of adhesive thickness effects was based on Figure 57. The ratios of shear stresses attained in individual tests to average shear stress were plotted against actual adhesive thicknesses. These data were obtained from Z3824827 double lap specimens in which the rest of the independent variables were held constant. Adhesive thicknesses varied from 0.001 to about 0.006 inch. Although the scatter of results may have obscured trends, no distinct strength trend was apparent for this range of adhesive thicknesses. Thus, the joint strength effects of adhesive thickness variations were considered negligible in the evaluation of the bonded joint tests.

Over a larger range of adhesive thicknesses, shear strength and modulus variations were significant. This observation was based on the results of torsional ring adhesive shear tests in which the adhesive thickness was controlled over the range of 0.0050 to 0.0165 inch. These test results are discussed in Section III, Material Properties.

Shell 951 was selected as the adhesive to be used in the data specimens, and, therefore, variations in the parameter (G/E) were not investigated in the present study. Some insight into the effect of adhesive shear modulus in joint strength was obtained from test data in Reference 14. Figure 58 is a plot of adhesive shear strength developed by composite joints as a function of Young's Modulus (E) of the adhesive. Because the adhesives were homogeneous and isotropic materials, shear modulus (G) and Young's modulus

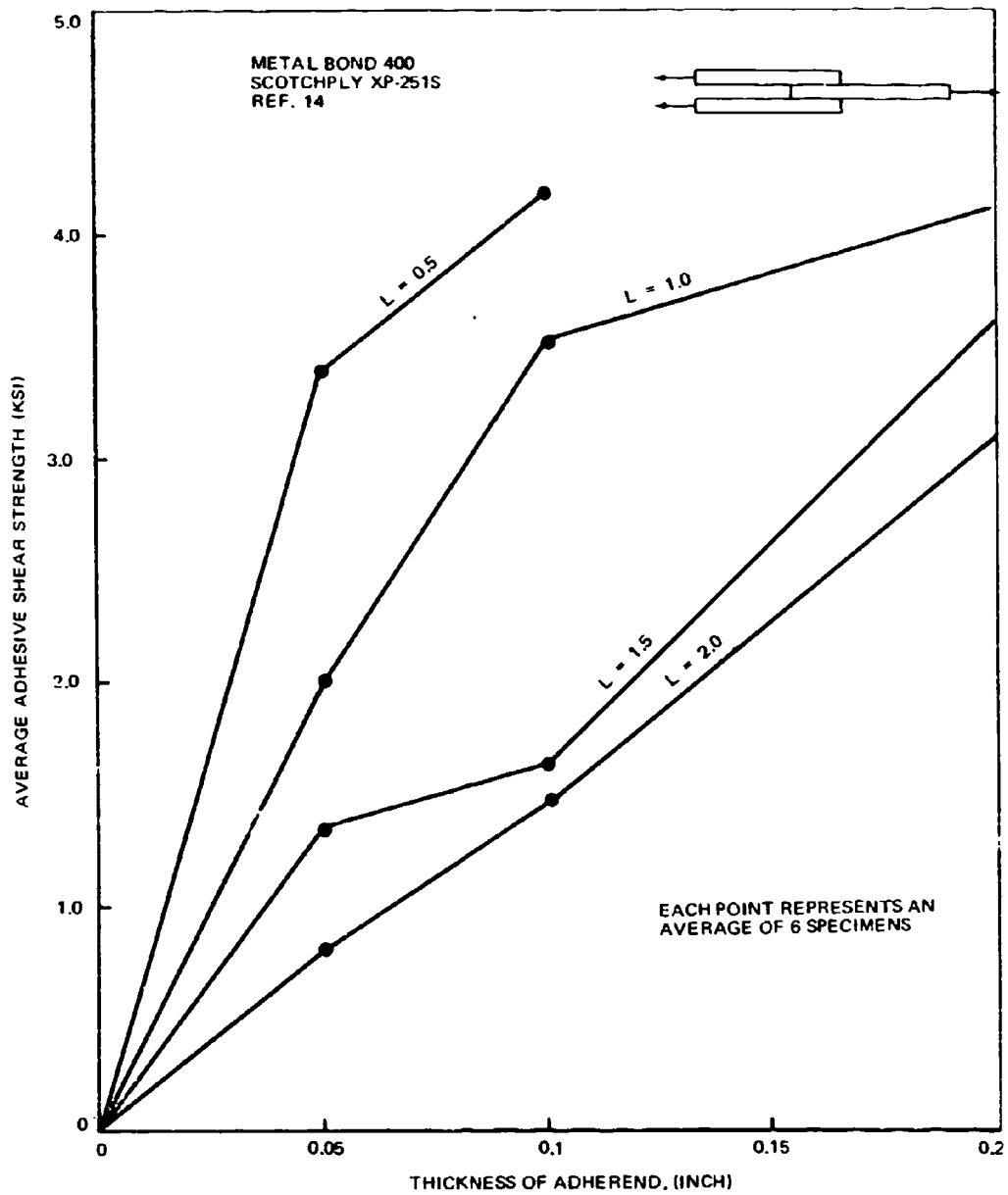


FIGURE 56. ADHESIVE SHEAR STRENGTH VERSUS THICKNESS OF ADHEREND

- | | |
|---------|---------|
| ◆ - 1 | ▽ - 519 |
| ⊠ - 505 | ◇ - 521 |
| □ - 511 | △ - 523 |
| ○ - 513 | ◻ - 525 |
| △ - 515 | ○ - 535 |
| ◇ - 517 | ◻ - 537 |

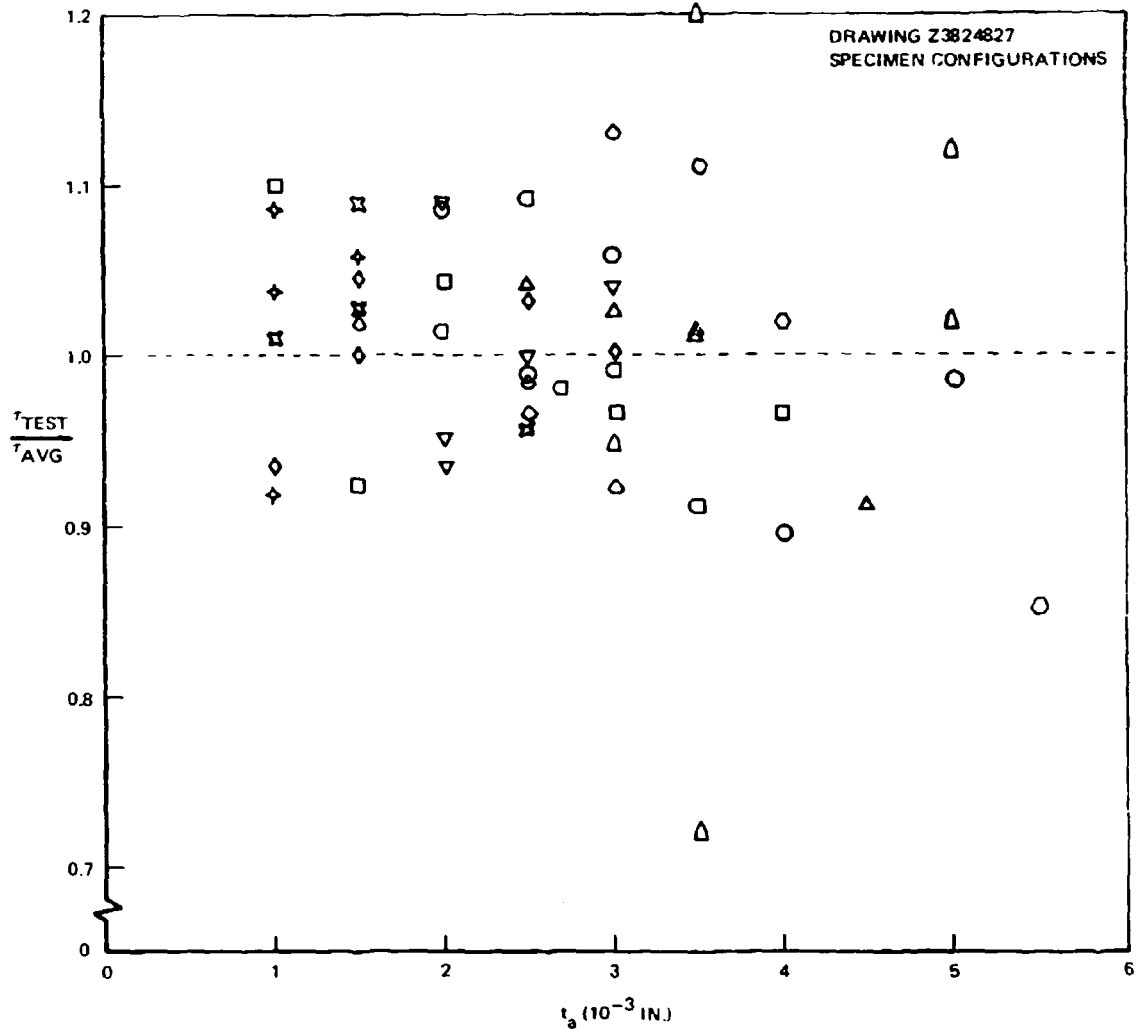


FIGURE 57. TREND OF $\frac{\tau_{TEST}}{\tau_{AVG}}$ VERSUS ADHESIVE THICKNESS

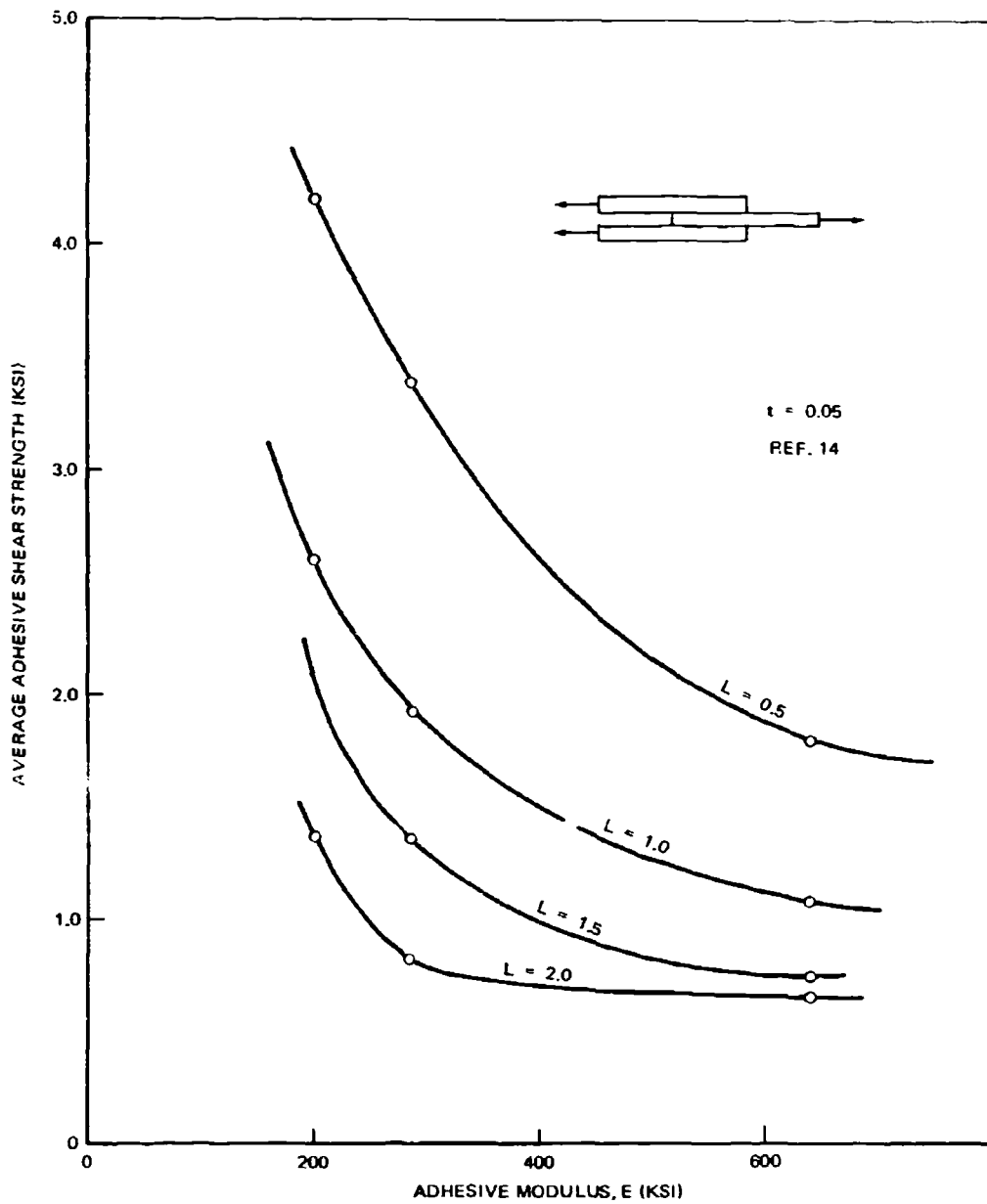


FIGURE 58. ADHESIVE SHEAR STRENGTH VERSUS ADHESIVE MODULUS

were related by the familiar equation, $G = E/2(1 + \mu)$. As modulus decreased, joint strength increased, so high adhesive strengths were believed to be less of an asset than low moduli (and ductile behavior). The lower modulus adhesives alleviated the peak stresses in the adhesives at the ends of the lap length, resulting in higher average stresses.

Discrete element analysis showed that the peak stresses in the adhesive at each end of the lap were equal and of minimum value when the adherend extensional stiffness ratio (E_1t_1/E_2t_2) was unity. This ratio was defined as the smaller value of Et divided by the larger. In designing single and double lap joints, it is recommended that the extensional stiffnesses of the adherends be balanced for maximum strength. However, in many design problems the matching of stiffnesses is not possible because of other design requirements.

Figure 59 indicates the effects of variations in extensional stiffness ratios for double lap joints (of 1-inch lap length) tested in the program. In this plot, extensional stiffness ratio was plotted against a parameter β

where

$$\beta = \frac{\eta_1}{\eta_2}$$

and

$$\eta_1 = \frac{(N_x/L)_1}{6100} \text{ for } (Et) \text{ ratios other than unity}$$

$$\eta_2 = \frac{(N_x/L)_2}{6100} \text{ for } (Et) \text{ ratios equal to unity.}$$

Further examination of the test data indicated that lap length and the (Et) ratio were not independent variables but interacted in a variable fashion to influence average adhesive shear stress at failure. This relationship is shown graphically in Figure 60. The limiting value, τ_{max} , was intuitively set at the ultimate shear stress of the adhesive as lap length approached zero. If the length of overlap was very small and τ_{avg} approached τ_{max} , the difference in magnitude of the peak stresses would be practically insensitive to (Et) variations. On the contrary, for large overlap lengths (i. e., small values of η) the difference in the magnitude of peak stresses was quite sensitive to (Et) ratio. The degree of sensitivity of (Et) is indicated in Figure 60 by the slopes of the lines of constant lap length. For example, as lap length approached zero, the slope approached zero. Under these circumstances, τ_{avg} approached τ_{max} regardless of (Et) ratio. As lap length increased, the slopes of the lines increased, indicating increased sensitivity to changes in (Et) ratio.

The test data for 2-inch lap lengths were inconclusive because adherend failures were experienced for the larger (Et) ratios. However, it was felt that at longer lap lengths, the sensitivity of average shear stress to (Et) ratio would approach a limit, and hence the slope of the line for a 2-inch lap

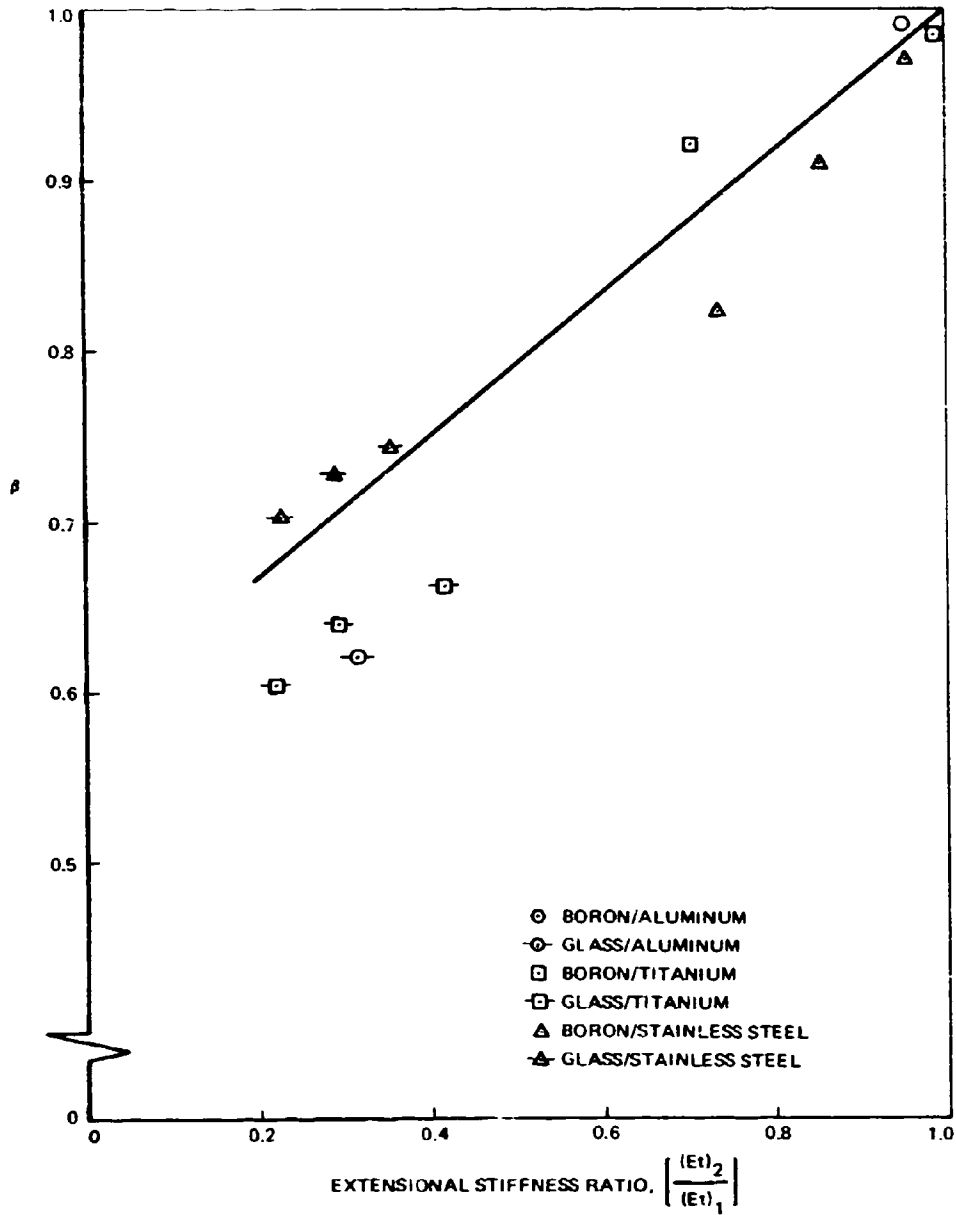


FIGURE 59. BONDED JOINT STRENGTH PARAMETER VERSUS EXTENSIONAL STIFFNESS RATIO

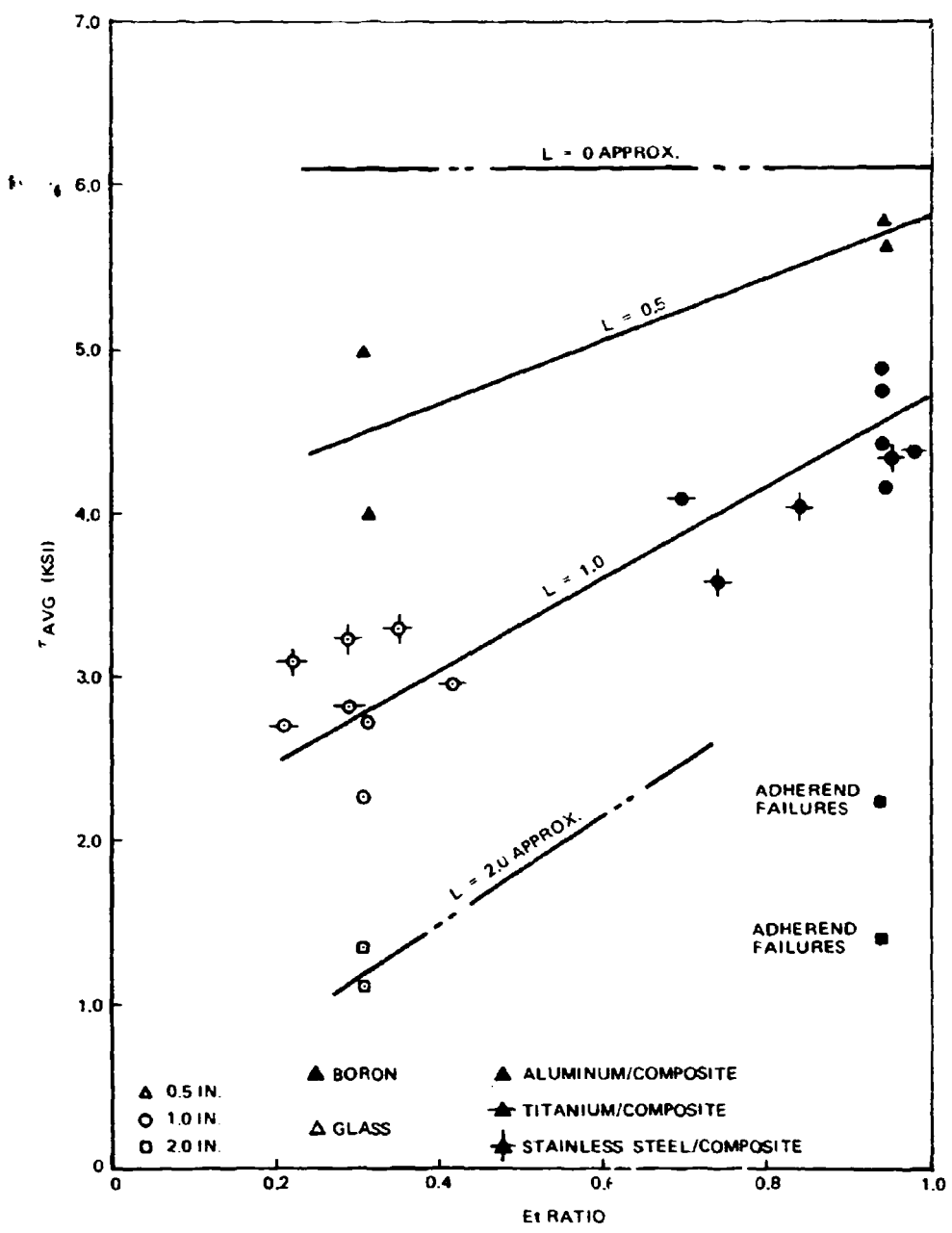


FIGURE 60. AVERAGE ADHESIVE SHEAR STRESS VERSUS EXTENSIONAL STIFFNESS RATIO

length was intuitively set at a value only slightly greater than the line of 1-inch lap length. These intuitive concepts should be checked with additional experimental data.

By using Figure 60, the parameter η was normalized for the effects of (Et) ratio using the relationship

$$\eta_{(Et)} = \eta / \beta$$

Results are plotted in Figure 61.

The double lap joint strengths were calculated using data from Figures 59 and 61 and the failure criteria stated at the beginning of this section. Comparisons of the predicted and test loads are plotted in Figure 62.

Predicted loads were determined in six steps as follows:

1. The Et ratio was calculated
2. β was determined from Figure 59, and $\eta_{(Et)}$ was determined from Figure 61.
3. η was calculated from the equation $\eta = \beta \eta_{(Et)}$.
4. Critical N_x for the adhesive was calculated from the equation $N_x = \eta (F_{su}^a) L$.
5. Critical N_x for the adherends was calculated from the equation $N_x = F_{tu} t$

where

- Ftu = 75 ksi for 7075-T6 aluminum alloy
- = 110 ksi for boron laminates of Pattern A (average value attained in test specimens)
- = 130 ksi for 6Al-4V titanium alloy
- = 130 ksi for S-994 fiber glass laminates (Pattern A)
- = 210 ksi for 17-7PH stainless steel

6. The lesser value of N_x was chosen as the critical load intensity for the joint.

Bolted Joints

Variables in the bolted joint study selected as significant are the following:

P, Joint Strength

D, Diameter of the Fastener

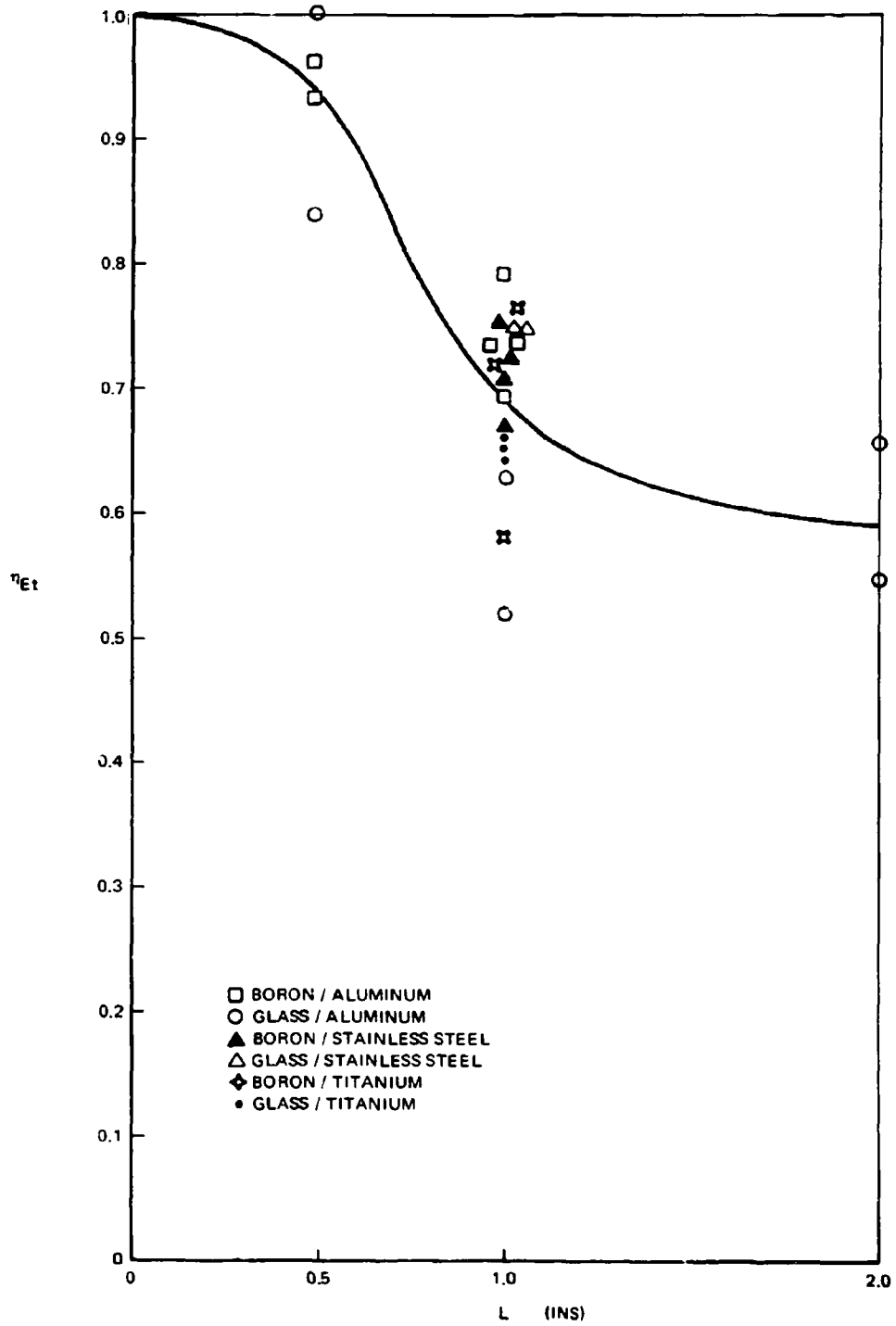


FIGURE 61. BONDED JOINT NORMALIZED STRENGTH PARAMETER VERSUS OVERLAP LENGTH

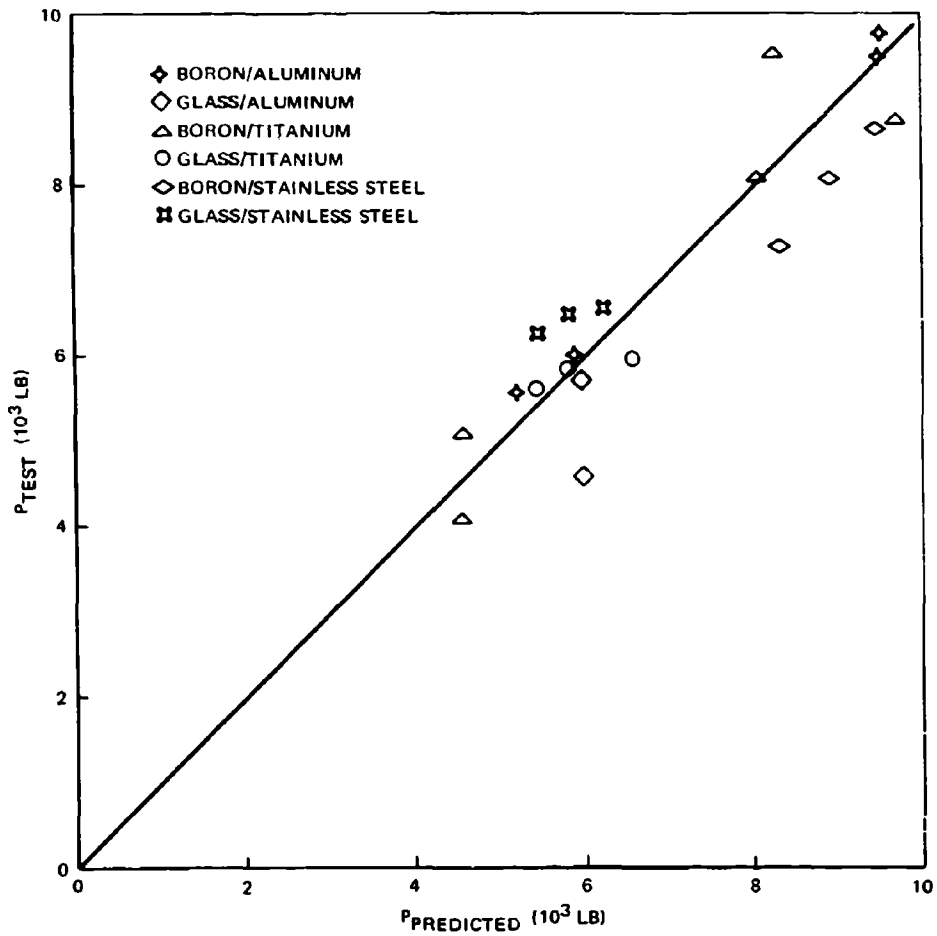


FIGURE 62. BONDED JOINT - PREDICTED VERSUS ACTUAL STRENGTH

e, Edge Distance

t, Laminate Thickness

s, Side Distance

ϕ , Orientation Angle of Layers (other than 0°) with Respect to Load Axis

p, Percentage of Layers at $\pm \phi$

The dependent variable, P, has the fundamental unit of force (F). The independent variables D, e, t, and s have the fundamental unit of length (L), and ϕ and p are dimensionless.

In functional notation, the equation for joint strength is expressed as

$$P = f(D^a, e^b, t^c, s^d, \phi^m, p^n) \quad (4)$$

In dimensional form, Equation (4) becomes

$$F = f'(L^a, L^b, L^c, L^d) \quad (5)$$

The variables ϕ and p are dimensionless and are thus excluded from Equation (5).

From Equation (5),

$$a + b + c + d = 0$$

$$a = -b -c -d$$

Rewriting Equation (4) and gathering terms,

$$P = f(D^{-b-c-d}, e^b, t^c, s^d)$$

$$P = f\left[\left(\frac{e}{D}\right)^b, \left(\frac{t}{D}\right)^c, \left(\frac{s}{D}\right)^d\right]$$

Thus, the ratios (e/D), (t/D), and (s/D) were used to determine the relationships between dependent and independent variables.

Joint strengths from the specimen tests are plotted against the ratio (e/D) in Figure 63. Each data point represents the average of five specimen tests. The data points represent both boron and fiber glass-reinforced specimens with an (s/D) ratio of 2.67 and having 50 percent of the layers at zero degrees and 50 percent at ± 45 degrees to the load axis. With other variables held constant, the load P increased linearly with respect to (e/D)

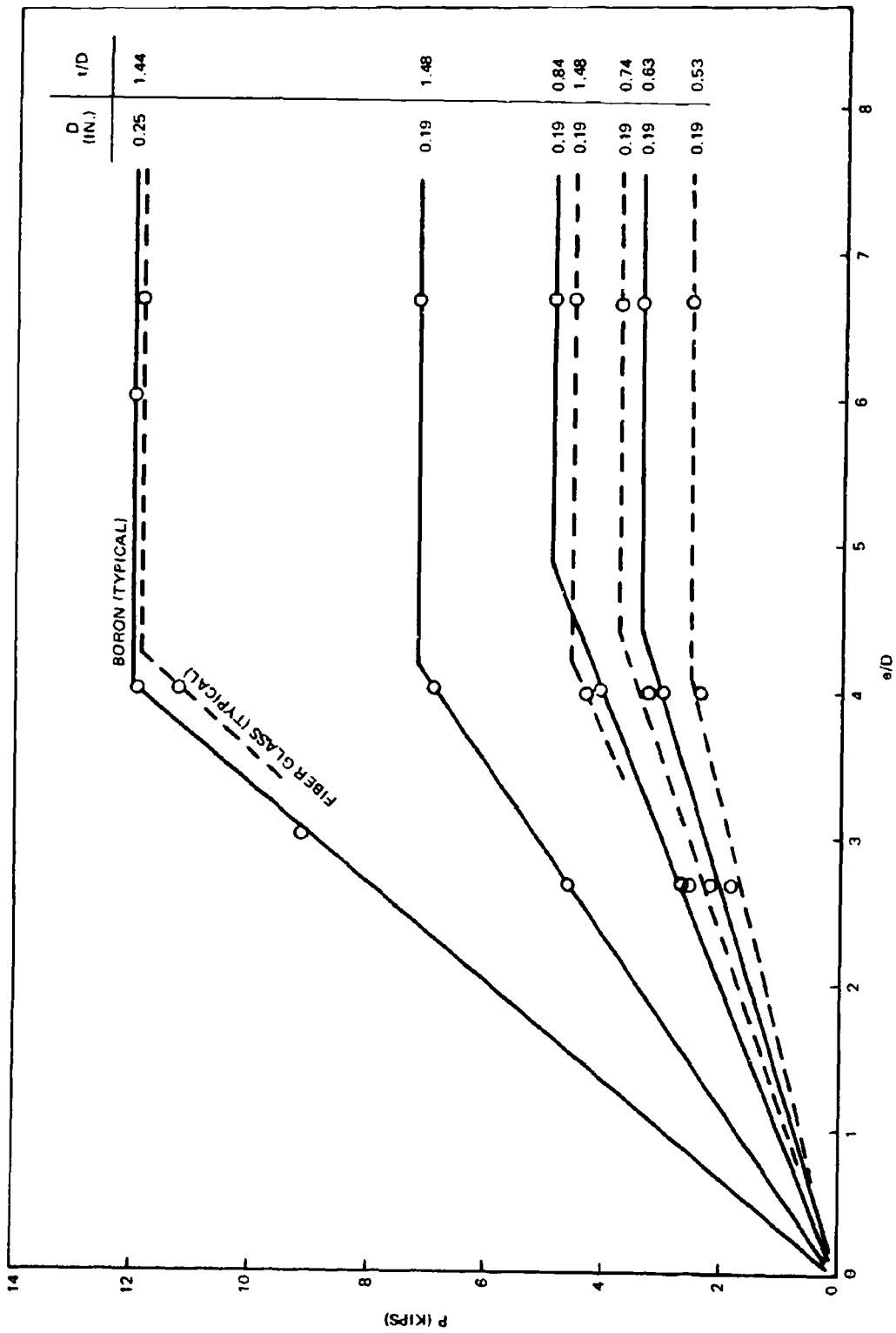


FIGURE 63. BOLTED JOINT STRENGTH VERSUS EDGE DISTANCE RATIO

up to a value of about four. Beyond this value, increasing the (e/D) ratio did not appreciably increase joint strength.

From Figure 63 it was observed that in the range $0 < e/D < 4$, the slope of the lines (for a given fastener diameter) increased as the ratio t/D increased, regardless of filament material. To normalize this effect, the same data were plotted in Figure 64 with $P(D/t)$ and e/D as the ordinate and abscissa, respectively. Published data from General Dynamics (Reference 10) and Whittaker (Reference 11) for similar specimens are also included in Figure 64. The Whittaker data apply to specimens with a fiber pattern of $0^\circ/45^\circ/-45^\circ$ and an s/D ratio of three. These properties approximate the characteristics of the rest of the specimens under consideration and were used to supplement the test data from the program for the 0.25-inch-diameter bolt. Note that the five curves in Figure 63 representing the bolt diameter of 0.19 inch are adequately represented by one line on Figure 64.

From Figure 64 it was observed that the slopes of the lines increased as bolt diameter increased. In the range of interest ($0 < e/D < 4$), the lines were each represented mathematically with an equation of the form

$$P\left(\frac{D}{t}\right) = m \left(\frac{e}{D}\right) + b \quad (6)$$

where m is the slope of the line and b is the vertical axis intercept. The constant b in each case equals zero because each line must go through the origin. From Figure 64 the slopes were determined as follows:

$$m = 1.20 \text{ for } D = 0.190$$

$$m = 2.09 \text{ for } D = 0.250$$

To normalize the diameter effect, the slopes were divided by the bolt diameter with various exponents (i. e., the value of m/D^n was determined for several values of n). From this study, the proper normalizing factor was determined as D^2 . Thus, Equation (6) was rewritten,

$$P\left(\frac{D}{t}\right)\left(\frac{1}{D^2}\right) = \frac{m}{D^2} \left(\frac{e}{D}\right)$$

$$\left(\frac{P}{Dt}\right) = m_1 \left(\frac{e}{D}\right) \quad 0 < \frac{e}{D} < 4$$

where

$$m_1 \cong \frac{1.20}{(0.19)^2} \cong \frac{2.09}{(0.25)^2} = 34 \text{ ksi}$$

The test data are replotted in Figure 65 with P/Dt as a function of the ratio e/D .

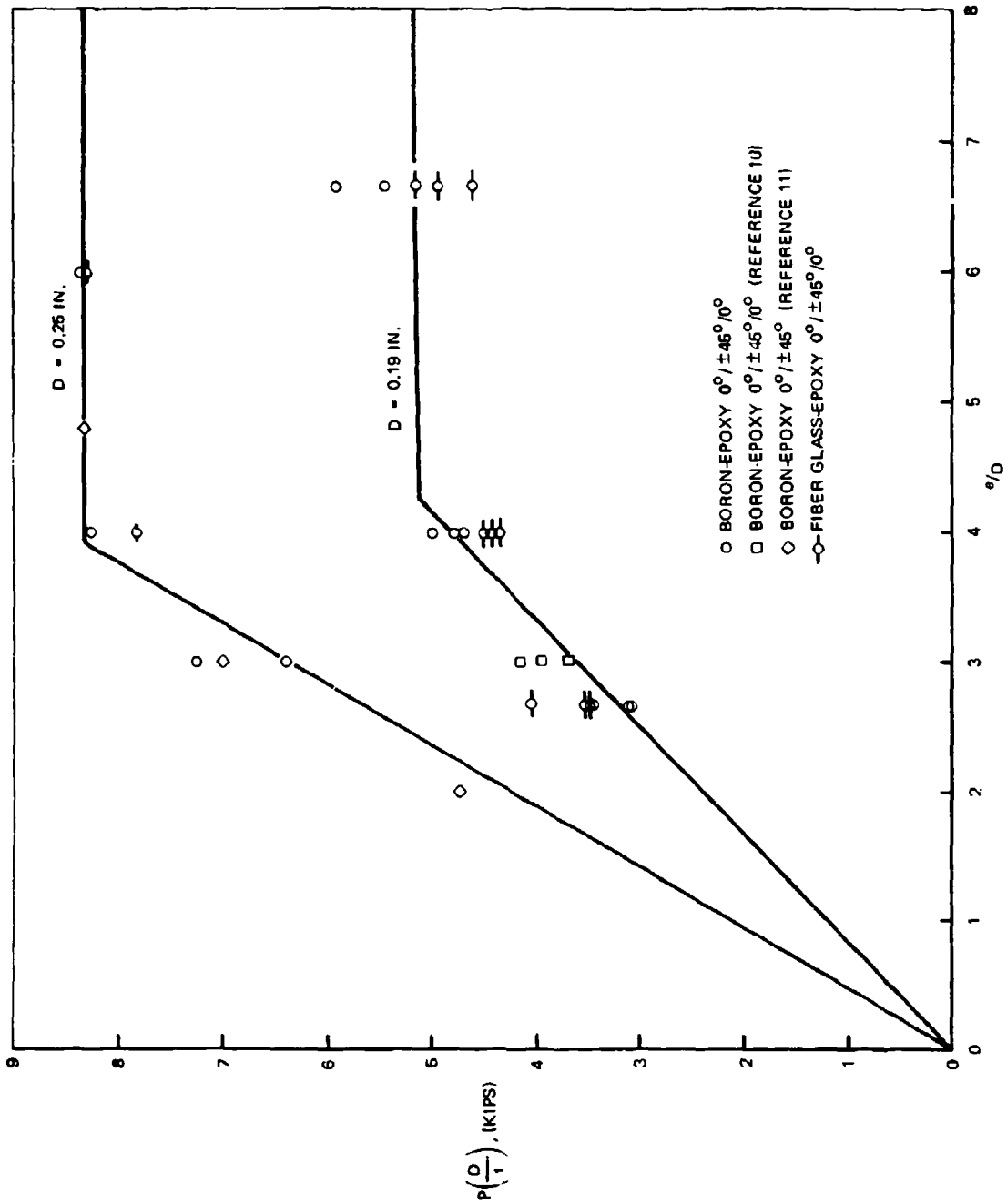


FIGURE 64. BOLTED JOINT STRENGTH VERSUS EDGE DISTANCE RATIO NORMALIZED FOR t/D RATIO

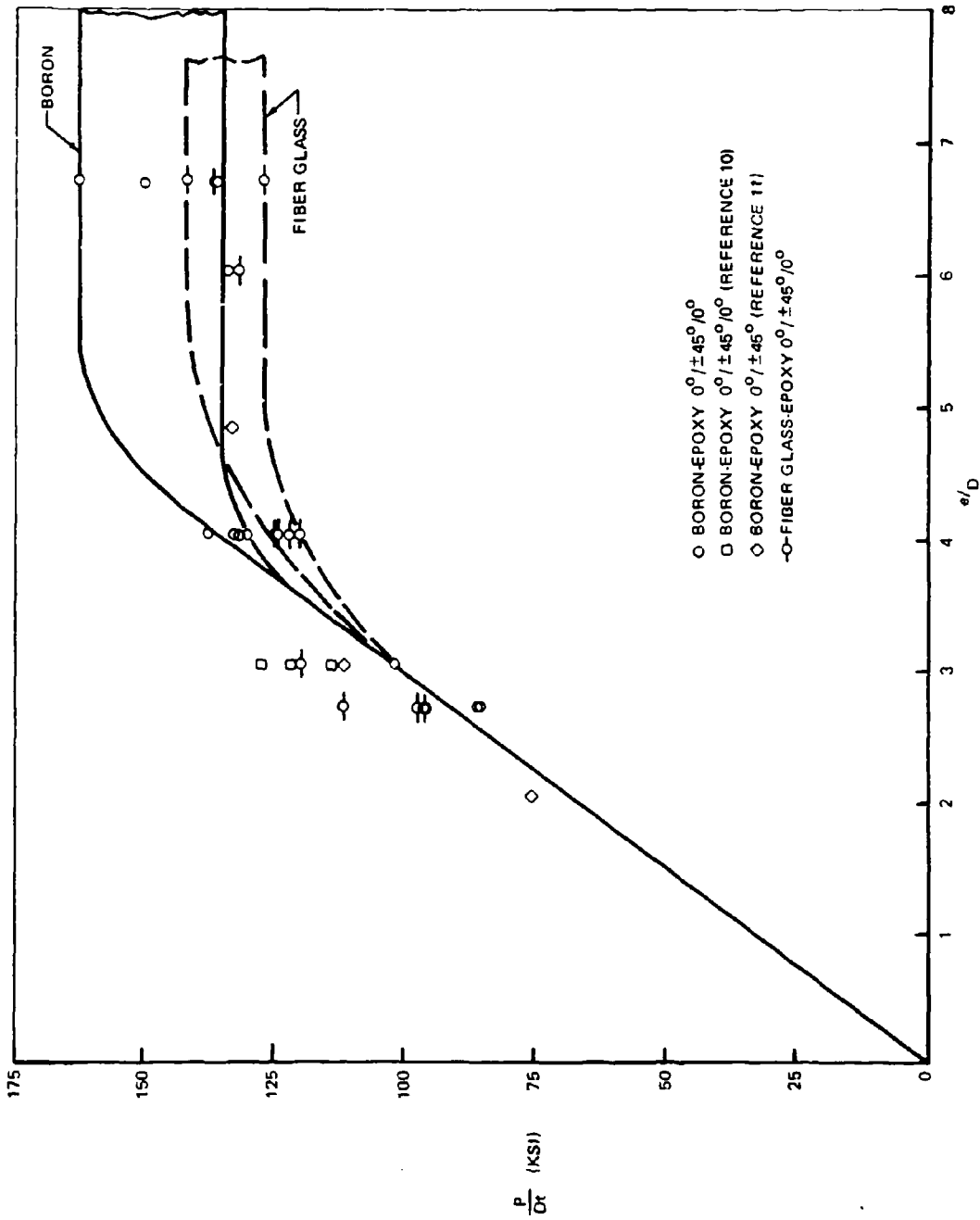


FIGURE 65. BOLTED JOINT BEARING STRESS VERSUS EDGE DISTANCE RATIO

Examination of the failed specimens indicated that the shear-out mode was prevalent in the range $0 < e/D < 4$. There were also physical indications of shear-out and tension failures with $e/D > 4$. However, a study of the actual stresses developed during test indicated that bearing stresses were more instrumental in precipitating failure when e/D exceeded a value of about five.

This behavior may be deduced from Figure 65. The ordinate parameter P/Dt is in fact the bearing stress, and the initial slope of the curve, P/Dt divided by e/D , is P/et . The latter quantity is twice the shear-out stress. In other words, joint strength increased proportionally to twice the allowable shear-out stress (since there are two shearing surfaces) in the region $0 < e/D < 4$. This relationship was valid until e/D was sufficiently large to develop bearing stresses in the composite, which influenced the failure load ($4 < e/D < 5$). Beyond an e/D ratio of about five, the failures were caused primarily by bearing stresses.

When the mode of failure was shear-out, it was observed that the strengths attained by boron and fiber glass-reinforced laminates were comparable. At e/D greater than four, a distinct difference in joint strength was noted between boron and fiber glass-reinforced specimens. From this behavior it was concluded that laminate shear-out strength was essentially a property of the epoxy resin, but bearing strength was dependent on the properties of the reinforcing fibers. The grouping of the data points at e/D equal to four also indicates a zone in the region of about $3 < e/D < 5.5$ in which failure was influenced by an interaction between shear and bearing stresses.

The study of s/D effects was based on test data published by Whittaker (Reference 11) in which e/D and s/D ratios were systematically varied for a $0^\circ/45^\circ/-45^\circ$ boron laminate. Because these parameters were not systematically varied in the present program, the normalizing factor for the ratio s/D was derived from published data.

The nature of the s/D variation was determined from Figure 66. The ratio of test load to predicted load was plotted as the ordinate, and the ratio s/D was plotted as the abscissa. The predicted load was determined from Figure 65 and normalized for the effects of e/D ratio. The ordinate values were multiplied by a constant so the ratio of test to predicted loads was unity at s/D equals two. This constant was subsequently included with other constants in the formulation of the equations for joint strength prediction.

The curve in Figure 66 had the general exponential form

$$y = m e_n^{-nx} + b \quad (7)$$

where e_n is the base of natural logarithms and m , n , and b are constants to be determined from boundary conditions. In terms of the relevant variables

$$\left(\frac{P_{\text{test}}}{P}\right) = m e_n^{-n(s/D - 0.5)} + b$$

The boundary conditions were

$$y = 0 \text{ when } x = 0.5 \text{ (i. e., specimen width = fastener diameter)}$$

$$y = 1 \text{ when } x = 2$$

$$y = 1.1 \text{ when } x \rightarrow \infty$$

from which $m = -b = -1.1$, and $n = 1.6$.

Equation (8) becomes

$$\left(\frac{P_{\text{test}}}{P}\right) = 1.10 \left[1 - e_n^{-1.6(s/D - 0.5)}\right]$$

The evaluation of t/D effects was conducted in the same manner as the evaluation of s/D effects. Figure 67 was plotted with the ratio of test load to predicted load as ordinate and the ratio (t/D) as abscissa. The predicted load was again determined from Figure 65 and normalized for the effects of e/D and s/D ratios. The curve in Figure 67 also has the general exponential form of Equation (7) with the following boundary conditions:

$$y = 0 \text{ when } x = 0 \text{ (i. e., specimen thickness is zero)}$$

$$y = 1 \text{ when } x = 0.9$$

$$y = 1.06 \text{ when } x \rightarrow \infty$$

After evaluation of the constants m , n , and b in Equation (7), the expression relating the t/D ratio to the joint strength ratio is

$$\left(\frac{P_{\text{test}}}{P}\right) = 1.06 \left[1 - e_n^{-3.2(t/D)}\right]$$

With the effects of e/D , s/D , and t/D considered, the equation for bolted joint strength, P , has the form

$$\frac{P}{Dt} = K_n \left(\frac{e}{D}\right) \left[1 - e_n^{-1.6(s/D - 0.5)}\right] \left[1 - e_n^{-3.2(t/D)}\right] \quad (9)$$

where the coefficient K_n includes the various constants and the effects of the variables ϕ and p .

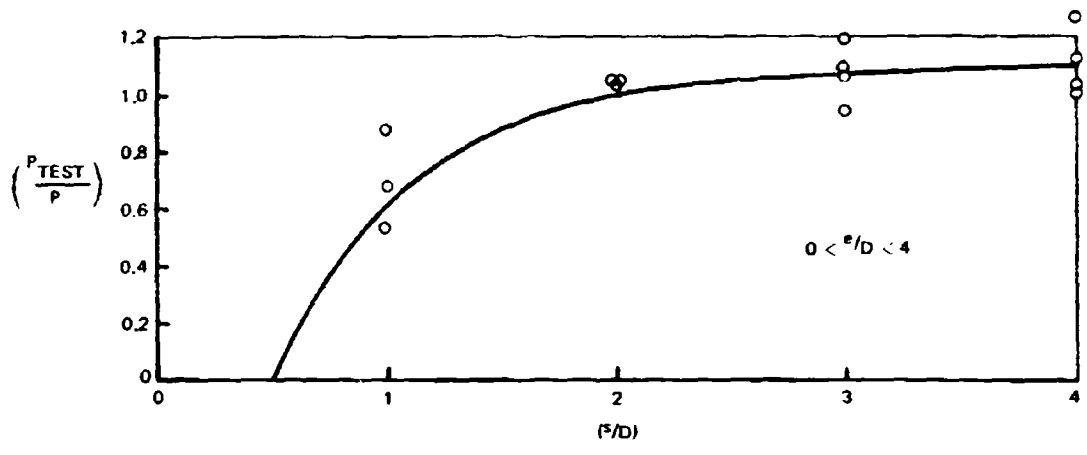


FIGURE 66. BOLTED JOINT STRENGTH RATIO VERSUS s/D RATIO $0 < (e/D) < 4$

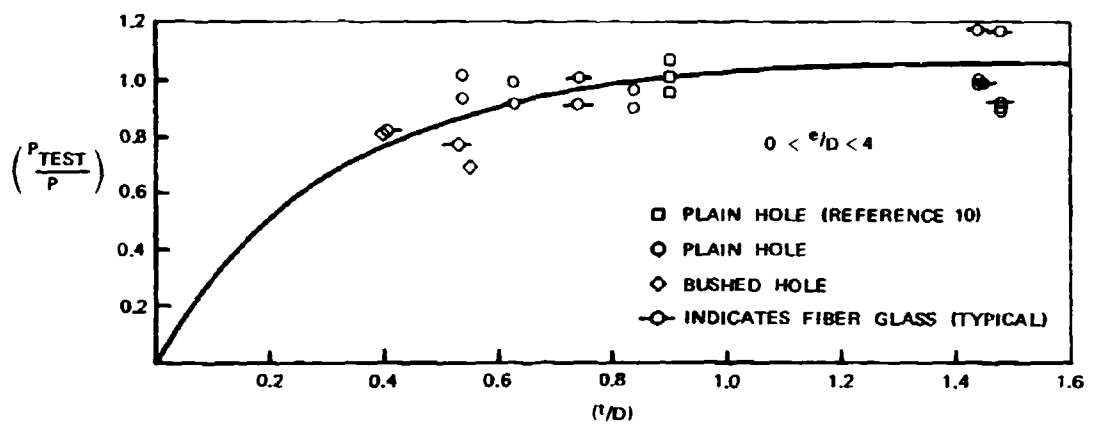


FIGURE 67. BOLTED JOINT STRENGTH RATIO VERSUS t/D RATIO $0 < (e/D) < 4$

The effects of variations in the angle ϕ were evaluated by determination of a coefficient K_ϕ using equation (9).

$$K_\phi = \left\{ \frac{P/Dt}{(e/D) \left[1 - e_n^{-1.6(s/D - 0.5)} \right] \left[1 - e_n^{-3.2(t/D)} \right]} \right\} \quad (10)$$

$$0 < \frac{e}{D} < 4$$

The coefficient K_ϕ was determined using Equation (10) and data from Reference 10, together with experimental results from the present program. The value of K_ϕ as a function of ϕ was thus determined as shown in Figure 68.

In a similar manner a coefficient K_p was determined to normalize the effects of variations in the percentage of layers at an angle $\pm\phi$ to the load axis.

$$K_p = \left\{ \frac{P/Dt}{K_\phi (e/D) \left[1 - e_n^{-1.6(s/D - 0.5)} \right] \left[1 - e_n^{-3.2(t/D)} \right]} \right\}$$

$$0 < \frac{e}{D} < 4$$

Data from References 10 and 11 were used to supplement experimental results from the present program. The value of K_p as a function of p was plotted in Figure 69.

In the range $e/D > 4$, it was concluded previously that laminate failures were influenced primarily by bearing stresses. Thus, failure loads could not be predicted by Equation (6). Bearing failure loads were determined using an equation of the form

$$P = K_n (F_{bru}) Dt, \quad e/D > 4 \quad (11)$$

where F_{bru} is the ultimate bearing strength of the material, and the coefficient K_n accounts for the effects of laminate variables (t/D , p , and ϕ) on bearing strengths.

Ultimate bearing strengths of 130 and 150 ksi were used for the $0^\circ/\pm 45^\circ/0^\circ$ pattern in fiber glass and boron epoxy laminates, respectively. These levels were based on results of the pin bearing tests discussed in Section III.

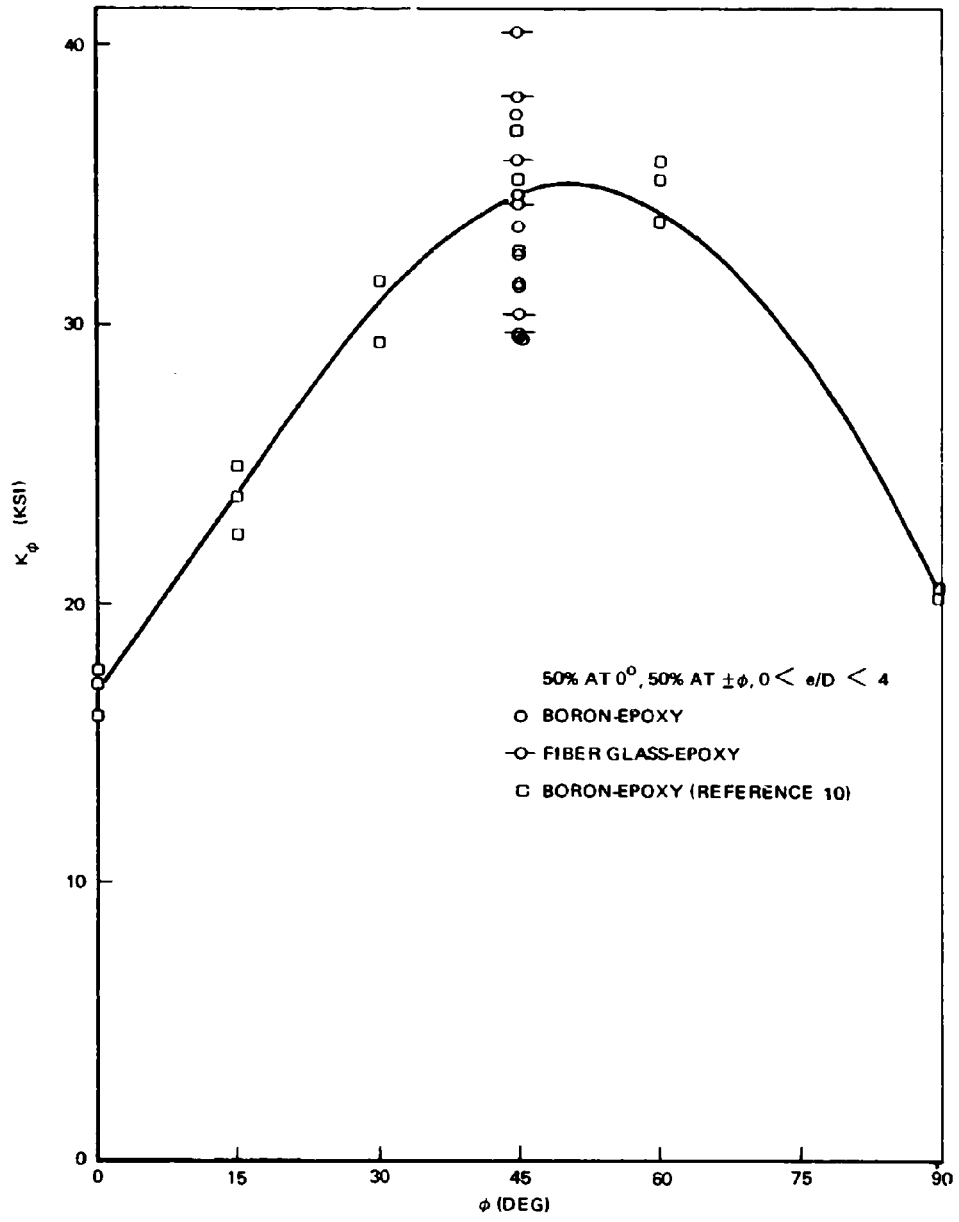


FIGURE 68. COEFFICIENT K_ϕ VERSUS ORIENTATION ANGLE, ϕ $0 < (e/D) < 4$

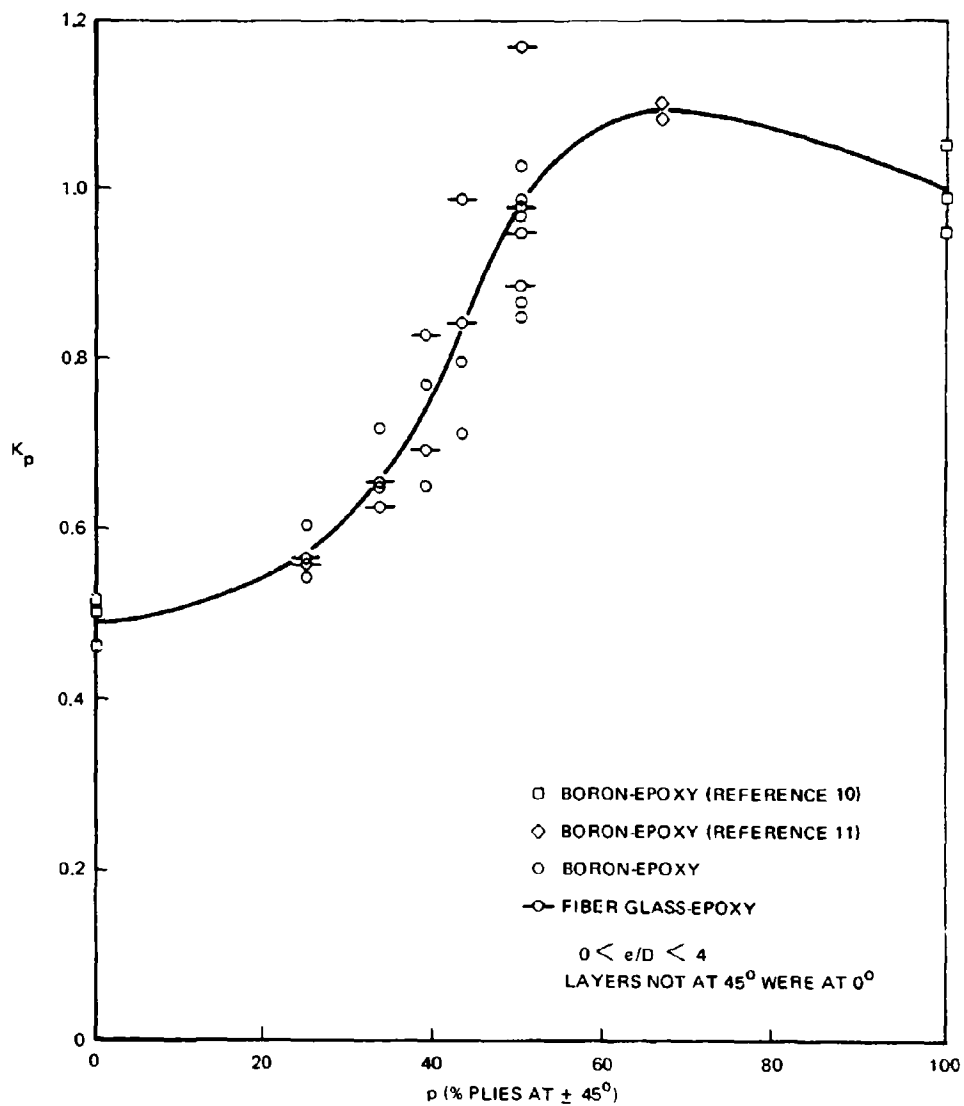


FIGURE 69. COEFFICIENT K_p VERSUS PERCENTAGE OF PLYS AT $\pm 45^\circ$ $0 < (e/D) < 4$

The strength effects of t/D variations were normalized using Figure 70, which was prepared from test data for $e/D > 4$ and 50 percent of the layers at ± 45 degrees to the load axis. This plot differs from the similar plot for $0 < e/D < 4$ (Figure 67), since it reaches a maximum at a t/D ratio of about 0.8 and decreases at larger ratios. There is also a difference between the plots for boron and fiber glass reinforcements, particularly for large values of t/D . This difference is thought to be caused by bolt bending effects in the stiffer boron laminates.

From the experimental data for $e/D > 4$, the coefficient K_p as a function of p was plotted in Figure 71. As noted previously, the bearing properties of the laminate are influenced by the filament material, and hence, fiber glass and boron results are plotted as separate lines. These plots are based on relatively few experimental points, and, thus, their reliability will be increased as more test data are acquired for bearing failures. The coefficient K_ϕ was not varied since the specimens in this group included only combinations of zero-degree and ± 45 -degree layers.

Thus, parametric trends for all the relevant design variables were determined using the semi-empirical techniques of data analysis. The nature of these trends is graphically illustrated in Figures 65 through 71. To consolidate these findings into a bolted joint design technique, a carpet plot, Figure 72, was constructed to summarize the information in Figures 65, 68, and 69. Figure 72 is a plot of the allowable shear-out stress for $0 < e/D < 4$ as a function of the variables ϕ and p . The plot is a good representation of shear-out stresses attained in uniaxial laminates (all zero-degrees), in laminates with all layers at $\pm \phi$ degrees, and in laminates with various percentages of layers at ± 45 degrees. Other combinations of layers and percentages have been spot checked with available data and are believed to depict the proper parametric relationships. They would be verified with more experimental data before being used in design. The allowable shear-out stress from Figure 72 must be corrected for the effects of (s/D) and (t/D) ratios as indicated in Figure 73.

Bolted double lap joint strengths were predicted as follows:

1. Shear-out strength for $0 < e/D < 4$ was calculated

$$P_{so} = 2etRf_{so}$$

where f_{so} is obtained from Figure 72, and R is obtained from Figure 73.

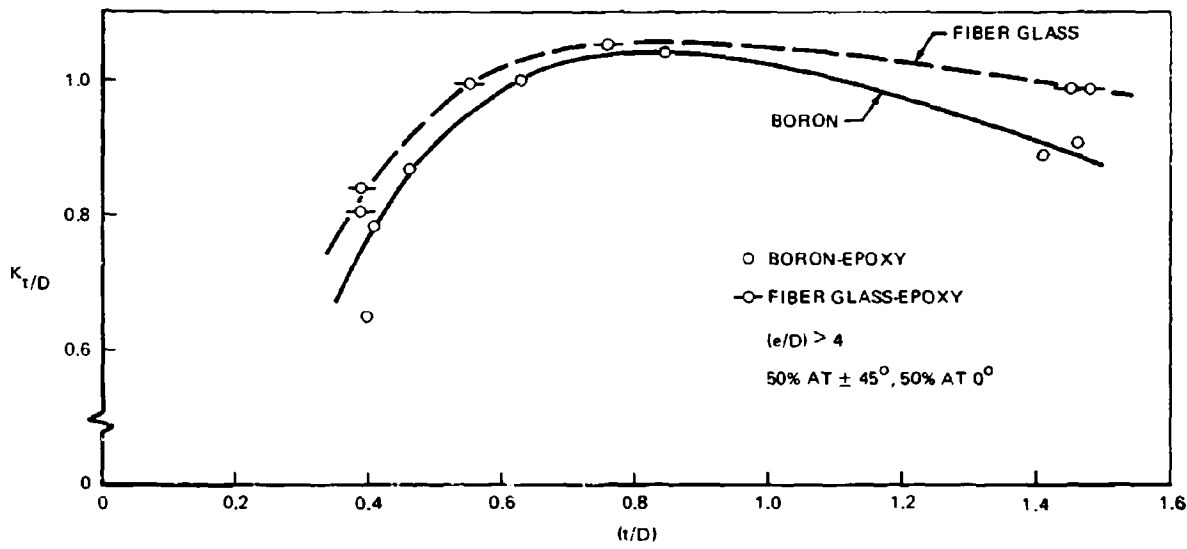


FIGURE 70. COEFFICIENT $K_{t/D}$ VERSUS t/D RATIO ($e/D > 4$)

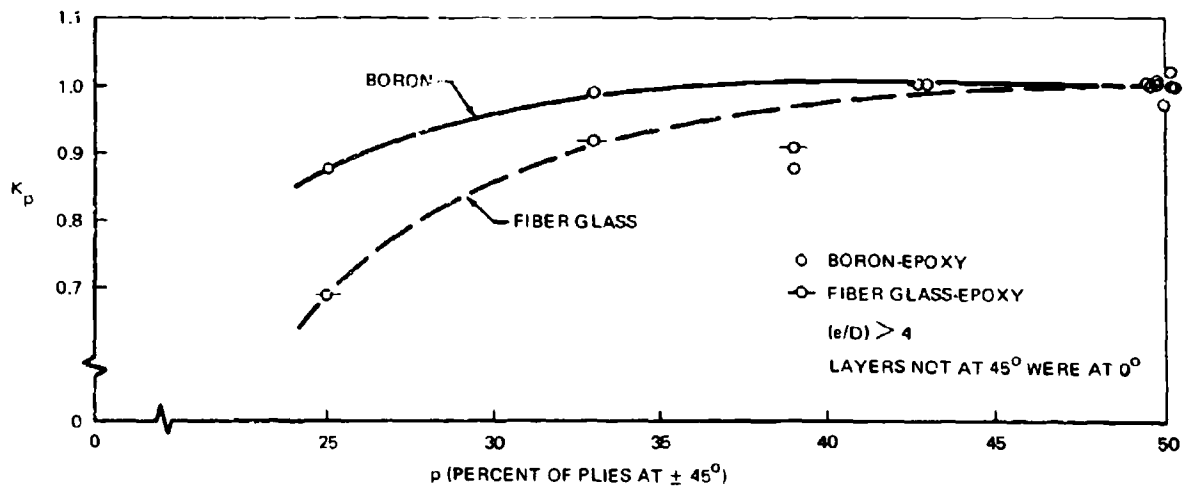


FIGURE 71. COEFFICIENT K_p VERSUS PERCENTAGE OF PLYS AT $\pm 45^\circ$ ($e/D > 4$)

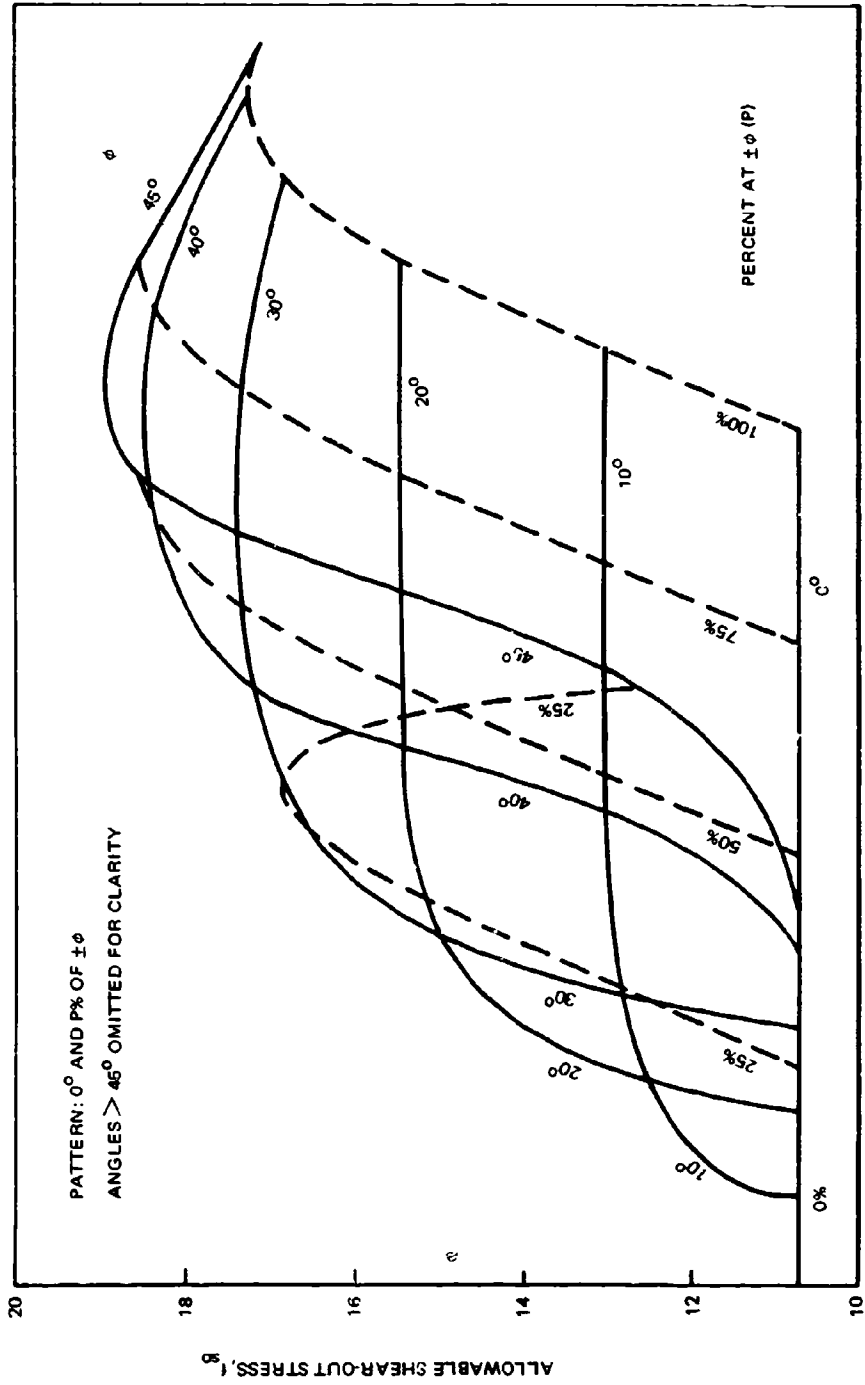


FIGURE 72. BOLTED JOINT ALLOWABLE SHEAR-OUT STRESS

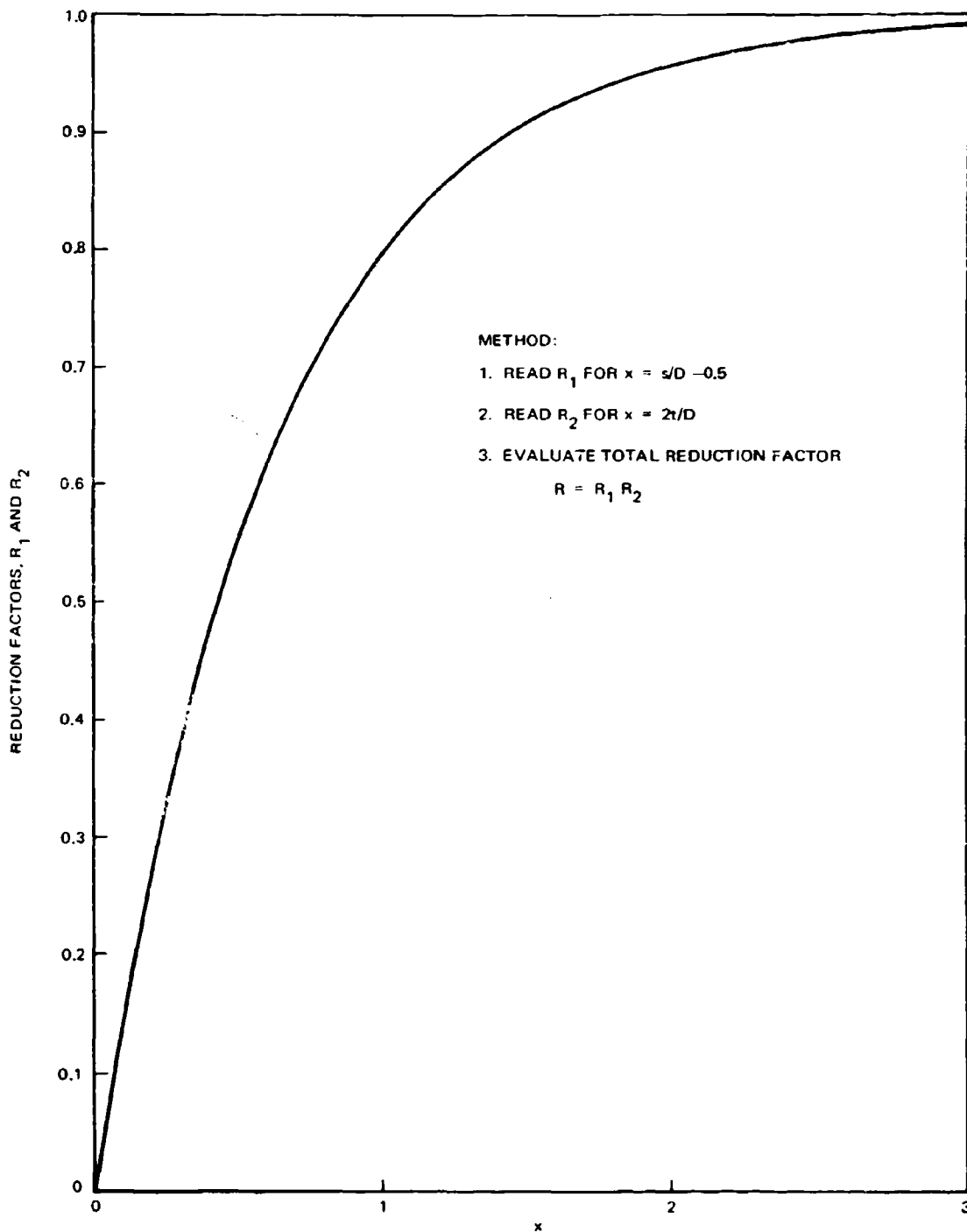


FIGURE 73. BOLTED JOINT CORRECTION FACTORS FOR s/D AND t/D EFFECTS

2. Bearing strength for $e/D \geq 4$ was calculated

$$P_{br} = K_{t/D} K_p (f_{br}) Dt$$

where $K_{t/D}$ and K_p are obtained from Figures 70 and 71, respectively, and

$$f_{br} = 150 \text{ ksi for boron laminates}$$

$$= 130 \text{ ksi for fiber glass laminates}$$

3. The lesser value was selected as the critical strength for $e/D = 4$.

Bearing stresses were critical for some of the fiber glass specimens at $e/D = 4$.

With the exception of the bushed specimen group, agreement between calculated and test loads was very good for most combinations of design variables in the experimental program. This agreement is illustrated in Figure 74. There was relatively more variability in the results for 1/4-inch-diameter bolts, particularly at t/D ratios greater than 1.4. Unconservative strength predictions could be avoided in design by reducing allowable stresses to cover this variability. A reduction of about 12 percent on allowable stresses would have insured predicted loads equal to or greater than test results for all specimens except the bushed joints.

Test results for two specimens containing Al_2O_3 - AlN whisker additives to the resin (at about 2 percent of resin weight) are shown in Figure 74. The results indicate that the whiskers had no effect on joint strength.

Specimens in the experimental program had a minimum s/D ratio of two and fiber orientations of zero degrees and ± 45 degrees only. Values of s/D less than two and angles, ϕ , greater than 45 degrees would tend to produce a third mode of failure in the specimens; namely, tension through the composite section at the fastener hole. No failures of this nature were produced in the experimental program. To make the design method more general, the experimental program should be extended to cover parametric effects on joint strengths for this mode of failure.

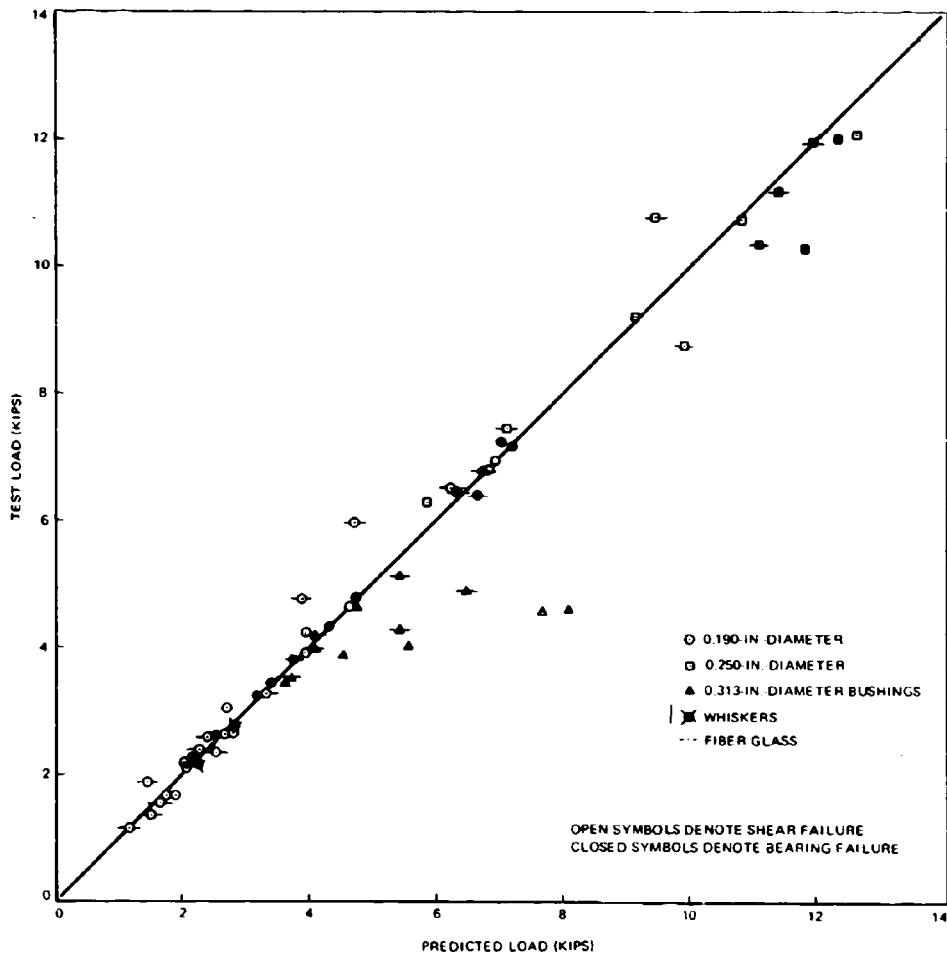


FIGURE 74. BOLTED JOINT - PREDICTED VERSUS ACTUAL STRENGTH

FATIGUE TESTS

In addition to the static tests, selected joints were tested under fatigue conditions. These tests consisted of initial screening of the joint concepts, followed by S-n data tests on two of the adhesive joint configurations.

Screening Tests

Joint configurations tested in the screening phase were the following:

- Bolted joints – single and double lap (Z 3824852)
- Adhesive joints – single and double lap (including variable stiffness) (Z3824849 & Z3824855)
- Adhesive joints – scarf (Z3824851)
- Adhesive joints – stepped lap (Z3824850)

These specimens were tested in constant-amplitude fatigue at a stress ratio of +0.05. The maximum loads during fatigue cycling ranged from approximately 60 to 80 percent of the static load capacities of the joints. The maximum load was arbitrarily selected at a high level to reduce the possibility of fatigue run-out during the screening tests.

Boron-reinforced specimens were cycled at 1800 cycles per minute in a Sonntag testing machine. Most of the fiber glass-reinforced specimens were cycled at 900 cycles per minute in a Krause testing machine to reduce the temperature rise due to hysteresis effects in the specimens. Some of the low-stress, high-cycle fatigue specimens of bolted fiber glass were tested in the Sonntag machine to reduce the test's duration.

The thermocouples were installed on three of the boron bolted specimens, as noted in Table XXV. For the single-lap joints, an appreciable temperature rise (about 50°F) was observed. However, in the symmetrical double-lap joints, the temperature quickly stabilized at about 86°F. One of the fiber glass fatigue specimens cycled at 1800 cycles per minute in the Sonntag testing machine had a thermocouple attached to check temperature conditions at the higher cyclic rate. Due to the relatively low applied loads, no temperature rise was observed in these specimens. Adhesive specimens were not thermocoupled, but they were monitored during the fatigue tests. No temperature rise was detected in the adhesive specimen, not even in those that achieved runouts.

A Typical test setup is illustrated in Figure 75, and results of the screening tests are summarized in Tables XXVI and XXVII. Maximum load for the stepped-lap configurations was considerably greater (8200 pounds) than the other joints, and, consequently, the cycles to failure were quite low. The last two specimens of this configuration were cycled at a maximum load of 6600 pounds to produce an average adhesive stress level comparable to the scarf joint fatigue tests.

**TABLE XXV
TEMPERATURE RISE IN FATIGUE SPECIMENS**

CONFIGURATION Z3824852	SPECIMEN MATERIALS	THERMOCOUPLE LOCATION	ELAPSED CYCLES (10 ³ CYCLES)	TEMPERATURE (°F)
-1 (SPECIMEN NO. 1) BOLTED SINGLE LAP	BORON/ ALUMINUM	ATTACHED TO BOLT HEAD	0	74
			1	80
			2	90
			3	96
			5	100
			7	101
			10	104
			15	105
			20	106
			24 (FAILURE)	118
-503 (SPECIMEN NO. 5) BOLTED SINGLE LAP	BORON/ BORON	ON BORON LAMINATE 5/8- INCH FROM BOLT & ON LOAD LINE	0	74
			1	76
			2	86
			3	94
			4	103
			5	111
			6	118
			7 (FAILURE)	124
-507 (SPECIMEN NO. 5) BOLTED DOUBLE LAP	BORON/ ALUMINUM	ATTACHED TO BOLT HEAD	0	73
			1	78
			2	81
			3	84
			5	85
			8	86
			25	86
			50	85
			100	85

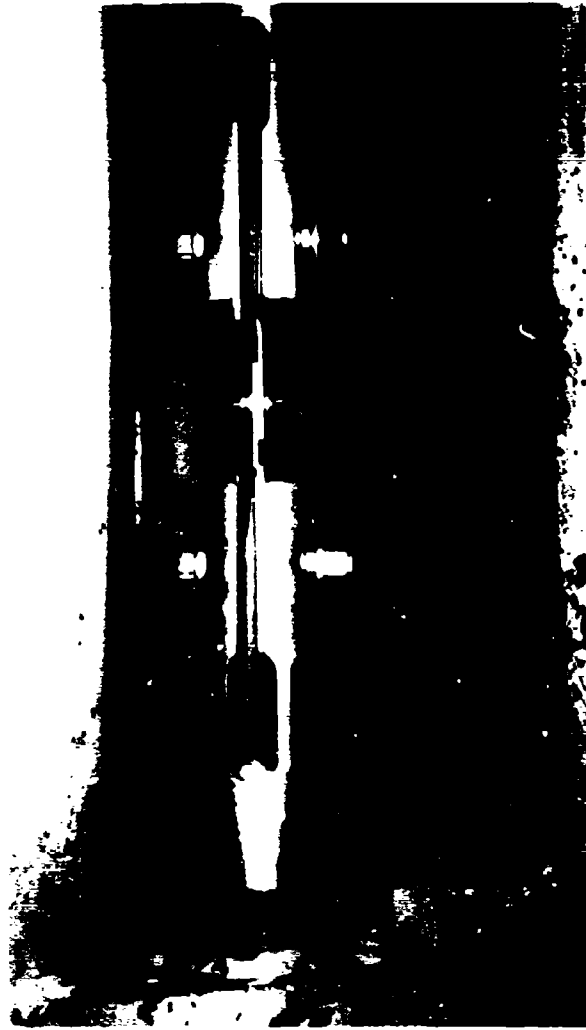


FIGURE 75. FATIGUE TEST SETUP

TABLE XXVI SUMMARY OF BONDED JOINT FATIGUE TEST RESULTS*

JOINT TYPE	MATERIALS AND GAGES (IN.)	OVERLAP LENGTH (IN.)	MAXIMUM LOAD MINIMUM LOAD (LB)	MAXIMUM LOAD % OF STATIC ULTIMATE	TESTS	ADHESIVE STRESS AT MAXIMUM LOAD (PSI)	APPROXIMATE BCF IN ADHESIVE	(SCF) X AVERAGE STRESS AT MAXIMUM LOAD (PSI)	RANGE OF CYCLES TO FAILURE	FAILURE MODE
SINGLE LAP	BORON/ALUMINUM (0.040)/(0.083)	1	1800/80	72	5	1,800	4.8	8,600	8,000 TO 36,000	ADHESIVE
	FIBER GLASS/ALUMINUM (0.040)/(0.083)	1	1600/80	69	6	-	-	-	10,700 TO 19,400	ADHESIVE
DOUBLE LAP	BORON/ALUMINUM (0.080)/(0.126)	1	6400/260	70	8	3,200	3.4	10,900	480 TO 1,880	ADHESIVE
	FIBER GLASS/ALUMINUM (0.080)/(0.126)	1	4200/200	73	2	-	-	-	1,700 TO 2,300	ADHESIVE
	BORON/ALUMINUM (0.160)/(0.160)	1	3400/170	60	3	-	-	-	1,600 TO 8,500	ADHESIVE
FOUR-STEP LAP	BORON/ALUMINUM (0.160)/(0.160)	2	6600/330	66	3	3,300	3.6	11,900	1,000 TO 6,000	ADHESIVE
	BORON/ALUMINUM (0.160)/(0.160) PATTERN C	2	8200/410	70	2	4,100	3.8	14,700	750 TO 2,800	ADHESIVE
	FIBER GLASS/ALUMINUM (0.160)/(0.160)	2	6600/330	57	7	3,300	3.8	11,900	7,500 TO 12,720	ADHESIVE
	BORON/ALUMINUM (0.160)/(0.160)	2	6600/330	78	6	-	-	-	200 TO 300	ADHESIVE
SCARF	BORON/ALUMINUM (0.160)/(0.160)	1	3300/165	70	6	3,300	1.4	4,600	15,000 TO 119,000	ADHESIVE
	FIBER GLASS/ALUMINUM (0.160)/(0.160)	1	3800/190	70	6	-	-	-	1,400 TO 20,000	ADHESIVE

* STRESS RATIO, R = 0.05
SHELL 951 ADHESIVE 1-INCH SPECIMEN WIDTH
LAMINATE PATTERN A

TABLE XXVII
SUMMARY OF BOLTED JOINT FATIGUE TEST RESULTS*

JOINT TYPE	MATERIALS AND GAGES (IN.)	EDGE DISTANCE (IN.)	MAXIMUM LOAD MINIMUM LOAD (LB)	MAXIMUM LOAD % OF STATIC ULTIMATE	TESTS	RANGE OF CYCLES TO FAILURE	FAILURE MODE
SINGLE LAP	BORON/BORON (0.120)/(0.120)	0.750	1800/90	70	5	4,000 TO 13,000	BEARING AND SHEAR-OUT
	BORON/7075-T6 (0.120)/(0.160)						
	FIBERGLASS/ FIBERGLASS (0.120)/(0.120)						
	FIBERGLASS/7075-T6 (0.120)/(0.160)						
DOUBLE LAP	BORON/7075-T6 (0.120)/(0.200)		2100/105	70	5	130,000 TO 2,877,000	ALUMINUM THROUGH FASTENER HOLE NONE (RUNOUTS)
	FIBER GLASS/7075-T6 (0.120)/(0.200)						
DOUBLE LAP BOLTED AND BONDED	BORON/7075-T6 (0.120)/(0.200)	0.750	4950/248	38	5	101,000 TO 176,000	LAMINATE AND ALUMINUM THROUGH HOLE ALUMINUM THROUGH BASIC SECTION
	FIBERGLASS/7075-T6 (0.120)/(0.200)						

*STRESS RATIO, R = +0.05
BOLT DIAMETER, D = 0.190 IN.
1-INCH SPECIMEN WIDTH
LAMINATE PATTERN A

The bolted double-lap specimens produced the longest fatigue life of the screening specimens and resulted in each case in failure of the aluminum alloy details through the bolt hole. Figure 76 illustrates the hole condition in the boron laminate details at failure. In general the lower the fatigue life the worse the appearance of the hole. Specimen Z3824852-507 accumulated 2.677 million cycles without failure, and the hole condition was excellent when the test was suspended. At the suspension of this test, no relaxation of the bolt torque was detected. Figure 76 indicates considerable damage at the unloaded edge of the bolt holes in the composite. No specific reason for this damage was observed during the tests. It was theorized that the back edge of the hole in the metal element damaged the laminate as the metal deformed under load at the bearing surface.

For two of the longer life joint configurations (double-lap bolted and scarf adhesive), the boron laminate was not the critical element in the joint failure. In the bolted joint, the aluminum alloy members failed through the fastener hole; in the scarf joint (and in the other adhesive joint concepts), the adhesive or the resin adjacent to the adhesive failed. Laminate failures in tension and interlaminar shear occurred in the combination bolted and bonded specimens.

The combination bolted and bonded joint in boron performed well in fatigue. Cycles to failure ranged from 101,000 to 176,000 at a maximum load of 4950 pounds. This was the only non-eccentric joint in which laminate fatigue failures were produced during the screening tests. Three of these specimens failed in the laminate through a section at the bolt hole. In two of the specimens, the aluminum alloy failed through the basic section (not at the bolt hole).

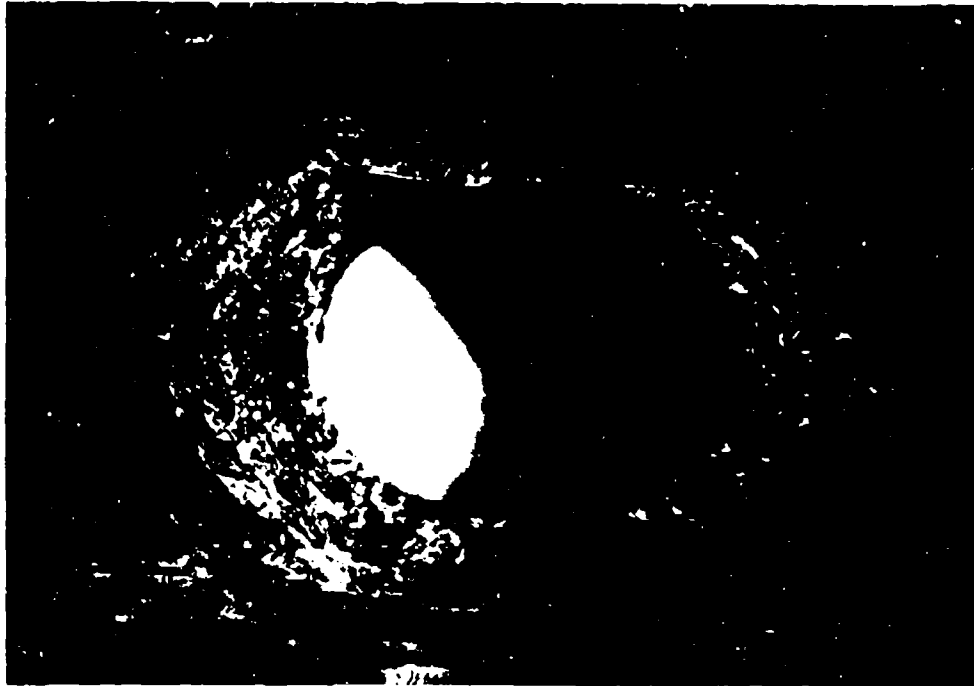
Fatigue test results of the composite-to-aluminum alloy joints are summarized in Figure 77. The bolted double-lap joints in fiber glass each exceed one million cycles, and no failure occurred in the laminates. In one specimen the aluminum alloy failed through the fastener hole. Maximum load for these tests was 1890 pounds, which was 80 percent of the joint's static load capacity.

Although the scarf joint had one of the higher average adhesive stresses of the group tested, its fatigue life was roughly one order of magnitude better than the other adhesive joints. This superiority can be explained by considering the stress concentrations in the adhesives of the various joint concepts. Adhesive stress concentration factors (SCF) were calculated using discrete element analyses and linear-elastic theory. These SCF's are shown in Table XXVI, together with the resulting relative stress levels in the adhesive. When stress concentrations were considered, it was concluded that actual adhesive stresses were less severe in the scarf joint. The expected trend of reduced life with increased stress was also indicated. Analytical determination of the stress concentration factors is discussed in Section VI.

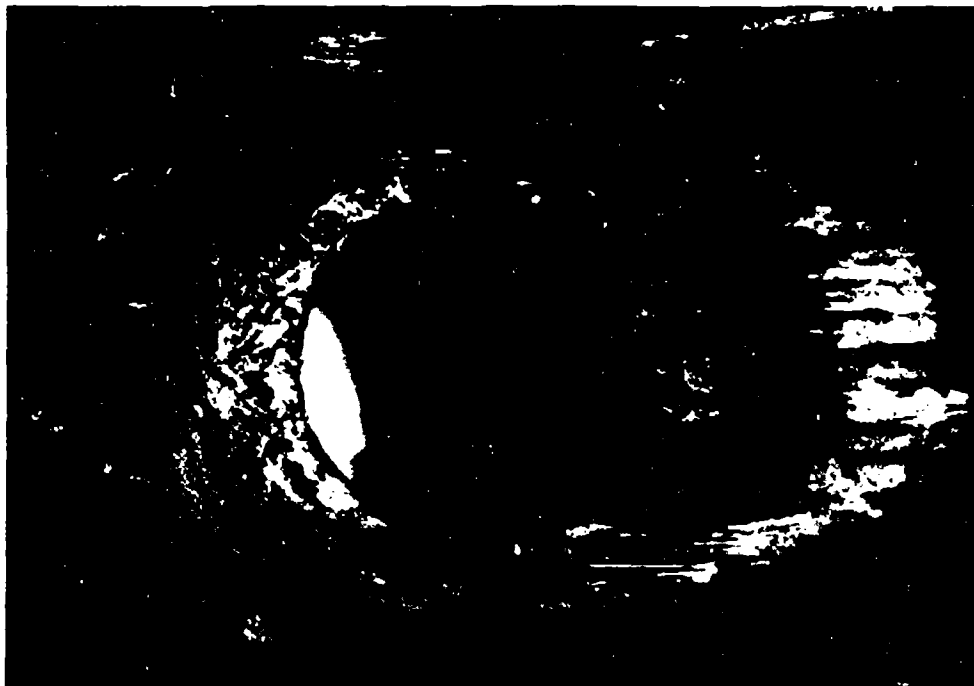
S-n Data Tests

The two joint concepts selected for S-n data tests were the scarf and double-lap adhesive joints. These specimens were also tested at a stress ratio of + 0.05. Drawings Z3824858 and Z3824860 were prepared for the

LOAD DIRECTION



130,000 CYCLES



230,000 CYCLES

FIGURE 76. BOLTED JOINT - HOLE CONDITIONS AFTER FATIGUE CYCLING - 10X

LOAD DIRECTION



1,693,000 CYCLES



2,677,000 CYCLES

FIGURE 76. BOLTED JOINT - HOLE CONDITIONS AFTER FATIGUE CYCLING - 10X (Continued)

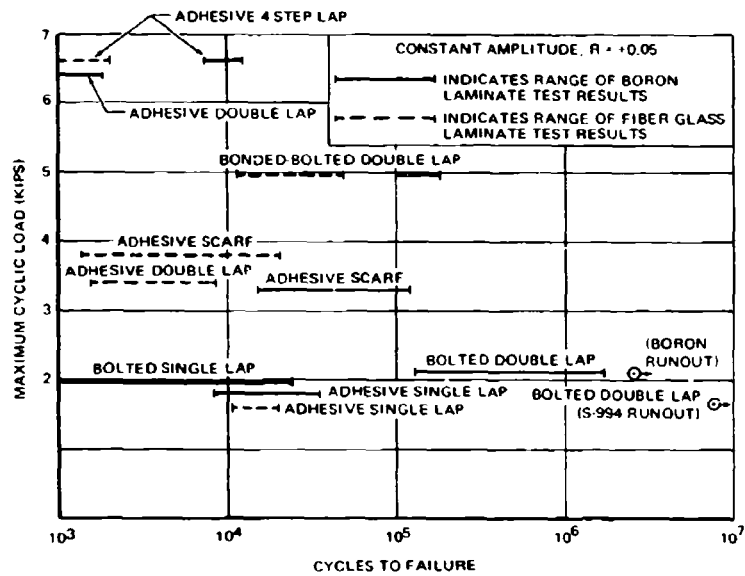


FIGURE 77. FATIGUE PERFORMANCE COMPARISONS FOR COMPOSITE TO ALUMINUM ALLOY JOINTS

scarf and double-lap specimens, respectively, and are included in Volume II. The grip ends of these specimens were redesigned to incorporate stainless steel shims within the composite elements. This change was intended to strengthen the grip ends of the specimens and to conserve boron. Test variables for these specimens are summarized in Table XXVIII. Primary variables are lap lengths and/or fiber patterns.

Four specimens of each fatigue joint configuration were static tested to failure to determine static load capacity of the exact specimen configuration used in the S-n data tests. Static loads were introduced through the 1/2-inch-diameter pin holes to be consistent with fatigue loading conditions. In general, the static load capacity of the scarf joint fatigue specimens exceeded the corresponding static test configurations (Z3824829), and the double lap joint fatigue specimens indicated reduced static strength compared to the corresponding static test configurations (Z3824827). Test results are shown in Table XXIX.

The increased static load capacity for the scarf joint fatigue specimens was attributed to improved bond line thickness control and more uniform distribution of loads to the bonded joint area through the shim design in the grip ends. Bond line thicknesses for the fatigue specimens were consistently measured at about 0.003 inch, compared to thicknesses varying from 0.004 to 0.008 inch for the original static load specimens. The reduced static load capacity of the double lap joint fatigue configurations resulted from the close proximity of the grip reinforcing shims to the adhesive joint. Stress concentrations at the end of the shims caused static failures in that region on five of the specimens using Pattern A. This mode of failure did not occur in the fatigue tests.

Fatigue test results for the S-n data specimens are summarized in Table XXX. The specimens were cycled to failure or to a runout value of at least one million cycles. Residual static strength was determined for each of the runout specimens as noted in Table XXX.

The fatigue failures were generally caused by shear failures of the adhesive and/or the epoxy resin adjacent to the adhesive. Thus, the S-n curves were plotted with average adhesive stress (at maximum cyclic load) as the ordinate and cycles to failure as the abscissa. These curves are shown in Figures 78 and 79. A similar plot using percent of static ultimate load as the ordinate parameter is shown in Figure 80. The adhesive joints made a transition from relatively early failures to runout conditions over a narrow range of stress levels. The residual strengths of the runout specimens were greater in each case than the average strength of the static load specimens.

The proportional limit stress in shear for Shell 951 adhesive was approximately 3000 psi in the torsion ring adhesive tests (Section III). Considering the stress concentration factors in the scarf and double lap joints, this was very near the peak stress level of the adhesive in the joints that achieved runouts. Thus, it was theorized that above this stress level cracks were initiated in the highly stressed regions of the adhesive (or resin). These cracks changed the effective joint geometry and quickly propagated the failure through the joint.

TABLE XXVIII
SUMMARY OF S-N DATA FATIGUE TEST VARIABLES

DRAWING NUMBER	JOINT TYPE	NOMINAL OVERLAP LENGTH (IN.)	FIBER PATTERN	STRESS LEVELS*	NUMBER OF REPLICATES	NUMBER OF SPECIMENS	CUMULATIVE TOTAL
Z3824858-1	SCARF	1.5	A	5	4	20	20
Z3824858-501		1.0	A	5	4	20	40
Z3824860-1	DOUBLE LAP	2.0	A	5	4	20	60
Z3824860-501		2.0	B	5	4	20	80
Z3824860-503		1.0	A	5	4	20	100

*ONE STRESS LEVEL WAS STATIC ULTIMATE STRESS IN EACH CASE.

TABLE XXIX
SUMMARY OF STATIC TEST RESULTS ON
FATIGUE SPECIMEN JOINT CONFIGURATIONS

JOINT CONFIGURATION	STATIC TEST RESULTS ON FATIGUE SPECIMEN CONFIGURATION				ORIGINAL STATIC TEST RESULTS			
	ULTIMATE LOAD (LB)	AVG ADHESIVE STRESS AT (PSI)	AVG ADHESIVE THICKNESS (IN.)	AVG ADHESIVE THICKNESS (IN.)	ULTIMATE LOAD (LB)	AVG ADHESIVE STRESS AT (PSI)	AVG ADHESIVE THICKNESS (IN.)	AVG ADHESIVE THICKNESS (IN.)
1-1/2-INCH SCARF BORON (PATTERN A) TO ALUMINUM	9175	5688	0.0030		7315	5100	0.0040	
	8900	5443			6900	4840	0.0050	
	9450	5363			6675	4620	0.0070	
	8275	5052						
	AVG 8750	AVG 5386	AVG 0.0030	AVG 6863	AVG 4855	AVG 0.0053		
1-INCH SCARF BORON (PATTERN A) TO ALUMINUM	6100	5744	0.0030		5030	5295	0.0040	
	6026	5579	0.0040		4550	4695	0.0070	
	5200	4938	0.0030		4470	4795	0.0080	
	6550	6110	0.0030					
	AVG 5969	AVG 5593	AVG 0.0032	AVG 4683	AVG 4930	AVG 0.0063		
2-INCH DOUBLE LAP BORON (PATTERN A) TO ALUMINUM	4650	1162	0.0020		9150(2)	2280	0.0010	
	4505(1)	1147			9250(3)	2310		
	5425	1340			9605(2)	2400		
	6000(1)	1500			9315(2)	2330		
	AVG 5185	AVG 1297	AVG 0.0020	AVG 9378	AVG 2340	AVG 0.0010		
2-INCH DOUBLE LAP BORON (PATTERN B) TO ALUMINUM	5500	1312	0.0020		5050(3)	1260	0.0015	
	5495	1349			6125(3)	1530	0.0010	
	4980	1205			7825(4)	1950	0.0015	
	4875	1157			6700(3)	1670		
	AVG 5215	AVG 1256	AVG 0.0020	AVG 6180	AVG 1540	AVG 0.0014		
1-INCH DOUBLE LAP BORON (PATTERN A) TO ALUMINUM	6950(1)	3440	0.0020		9150	4507	0.0010	
	5335(1)	2712			9275(2)	4640	0.0010	
	6050(1)	3066			9360(2)	4680	0.0020	
	7825	3653			9410	4640	0.0010	
	AVG 6515	AVG 3218	AVG 0.0020	AVG 9104	AVG 4406	AVG 0.0012		

- (1) FAILED IN LAMINATE AT BASE OF REINFORCING SHIMS
- (2) FAILED IN ALUMINUM ALLOY ADHERENDS
- (3) FAILED IN ALUMINUM ALLOY ON ONE SIDE AND IN ADHESIVE OR INTERLAMINAR SHEAR ON OTHER SIDE
- (4) FAILED IN BORON LAMINATE ADHEREND

PATTERN A - 0°/45°/45°/0°
PATTERN B - 45°/0°/0°/45°

**TABLE XXX
SUMMARY OF S-n FATIGUE DATA**

SPECIMEN NUMBER	NOMINAL LAP LENGTH (IN.)	MAXIMUM FATIGUE LOAD (LB)	PERCENT OF STATIC LOAD	AVERAGE ADHESIVE STRESS AT MAXIMUM LOAD (PSI)	CYCLES TO FAILURE	FAILURE MODE**	RESIDUAL STRENGTH	
							ULTIMATE STRESS (PSI)	PERCENT OF STATIC LOAD
Z3824851-1 SCARF (0°/45°/-45°/0°)	1.5	5000	57	3340	12,000	3		
					42,000	3		
					44,000	3		
					190,000	3		
		4600	52.5	3100	85,000	3		
	95,000				3			
	132,000				1 & 3			
			890,000	3				
		4220	48	2830	17,000	3		
	189,000				1			
	191,000				1			
					1,000,000	RUNOUT	6835	127
	3830	43.7	2560	798,000	3			
1,000,000				RUNOUT	6690	124		
1,039,000				RUNOUT	6250	116		
				1,061,000	RUNOUT	5700	124	
Z3824858-501 SCARF (0°/45°/-45°/0°)	1.0	3100	52	3110	57,000	3		
					96,000	3		
					926,000	3		
	2950	49.5	2970	19,000	2			
34,000				2, 3				
70,000				2				
				1,000,000	RUNOUT	6825	122	
Z3824858-1	1.0	2800	47	2820	971,000	3		
					1,000,000	RUNOUT	6930	124
					1,000,000	RUNOUT	6910	124
					1,408,000	RUNOUT	6838	124
		2670	45	2720	1,674,000	RUNOUT	6460	116

*STRESS RATIO, R = 0.05

**FAILURE MODES

- (1) ALUMINUM ALLOY FAILED
- (2) ADHESIVE OR COHESIVE
- (3) INTERLAMINAR SHEAR
- (4) COHESIVE ONE SIDE AND ALUMINUM ALLOY FAILURE OTHER SIDE

TABLE XXX
SUMMARY OF S-n FATIGUE DATA* (Concluded)

SPECIMEN NUMBER	NOMINAL LAP LENGTH (IN.)	MAXIMUM FATIGUE LOAD (LB)	PERCENT OF STATIC LOAD	AVERAGE ADHESIVE STRESS AT MAXIMUM LOAD (PSI)	CYCLES TO FAILURE	FAILURE MODE **	RESIDUAL STRENGTH	
							ULTIMATE STRESS (PSI)	PERCENT OF STATIC LOAD
Z3824880-501 (CONTINUED)	2.0	1900	36	480	46,000	3	1784	142
					52,000	3		
					1,575,000	1, 3		
		1,000,000	RUNOUT					
		1800	31	402	354,000	1, 3		
					1,001,000	RUNOUT		
1,293,000	RUNOUT							
Z3824880-503 DOUBLE LAP (90°/45° / -45°/90°)	1.0	2300	34	1110	19,000	2	3000	93
					29,000	2		
					30,000	2		
					84,000	2		
					64,000	2		
		1900	29	960	74,000	2		
					101,000	2		
					1,000,000	RUNOUT		
		1550	24	780	1,000,000	RUNOUT		
					1,400,000	RUNOUT		
					1,542,000	RUNOUT		
		1200	18	610	1,000,000	RUNOUT		
					1,060,000	RUNOUT		
					1,017,000	RUNOUT		
					1,142,000	RUNOUT		

*STRESS RATIO, R = +0.05

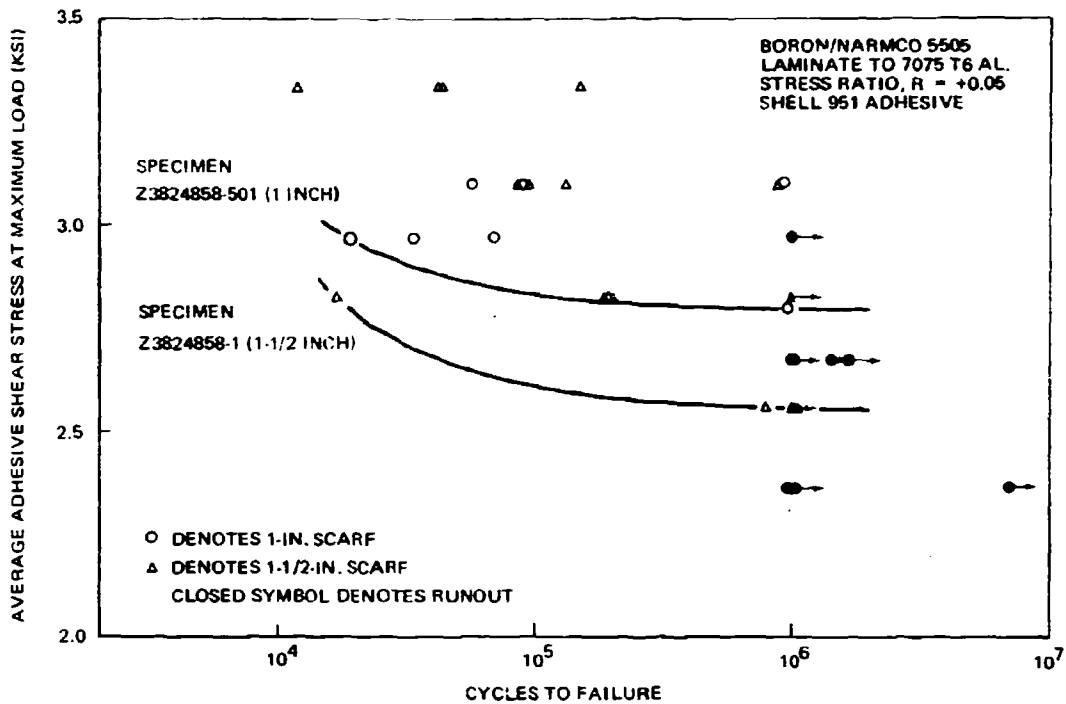


FIGURE 78. FATIGUE DATA FOR ADHESIVE SCARF JOINTS

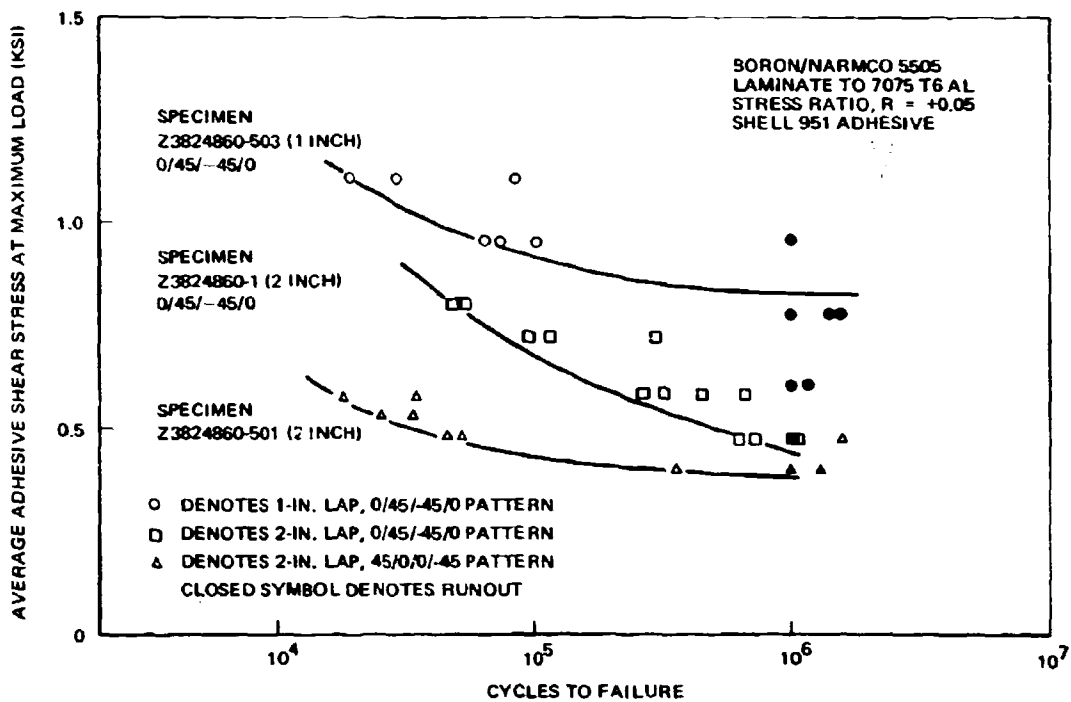


FIGURE 79. FATIGUE DATA FOR ADHESIVE DOUBLE LAP JOINTS

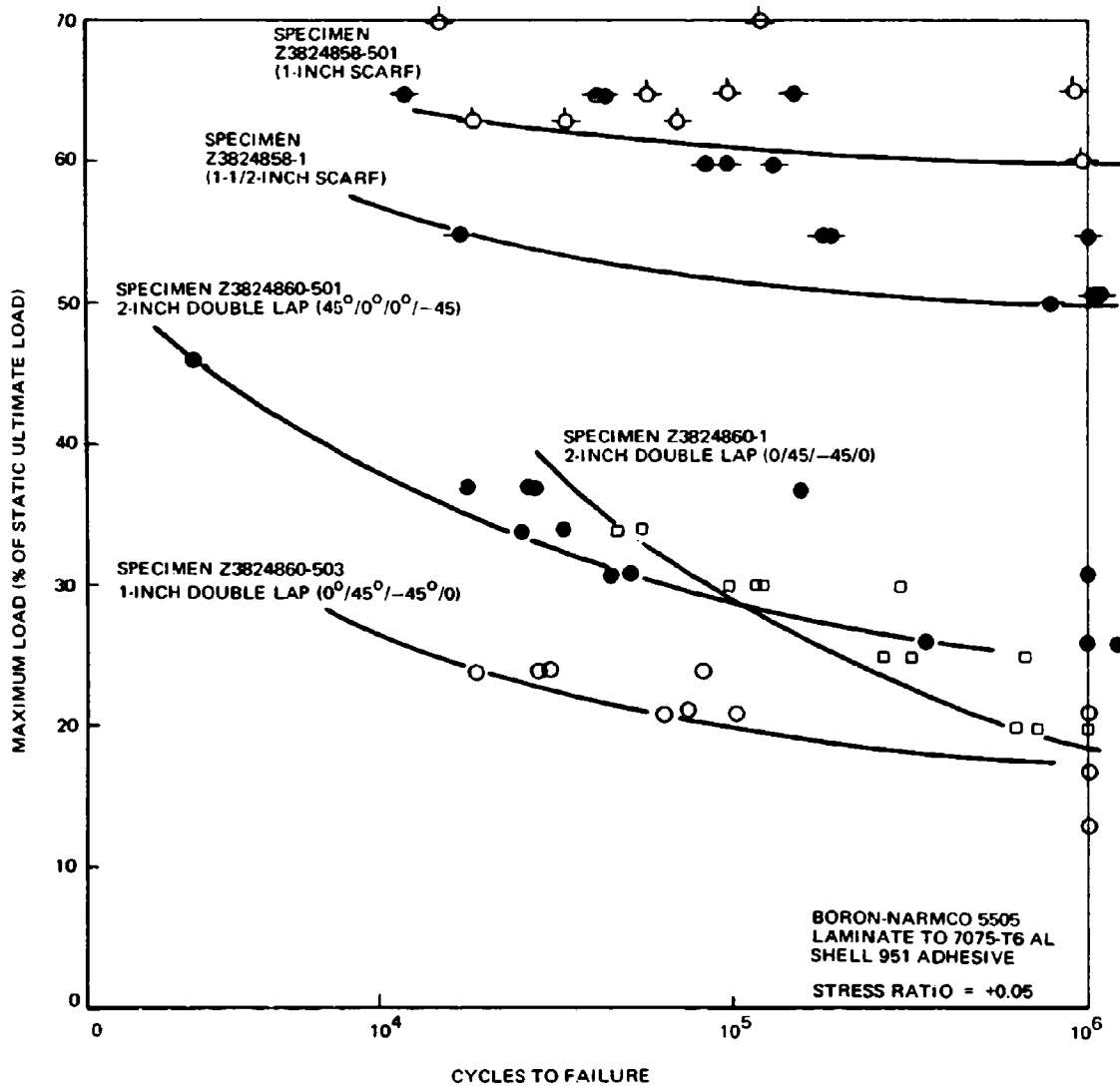


FIGURE 80. FATIGUE STRENGTH FOR ADHESIVE JOINTS

Failures of the scarf joints are illustrated in Figures 81 through 83. Broken fiber ends were visible to some degree in each failure, indicating that interlaminar shear near the fiber ends was instrumental in causing failure.

In the 2-inch double lap joints, progressive failures of the adhesive (in Pattern A) or the resin between the first and second layers of the laminate (in Pattern B) were observed during the fatigue cycling. These progressive failures continued in some cases through about 70 percent of the lap length. The specimens after failure are shown in Figures 84 and 85. Residual strengths of the double lap specimens after fatigue cycling ranged from 74 to 142 percent of the static load capacity. Two of the five residual strength specimens that failed at less than 100 percent static strength incurred visible damage (adhesive or resin cracks) during the fatigue cycling.

A 1-inch lap joint fatigue failure is shown in Figure 86. This specimen clearly indicates that fatigue failure was initiated in the adhesive at the ends of the lap.

Two each of the scarf and double lap specimens failed in fatigue through the basic aluminum alloy specimens. The balance of the aluminum fatigue failures in the double lap joints were regarded as secondary, occurring after an adhesive or interlaminar shear failure had occurred at the opposite adherend.

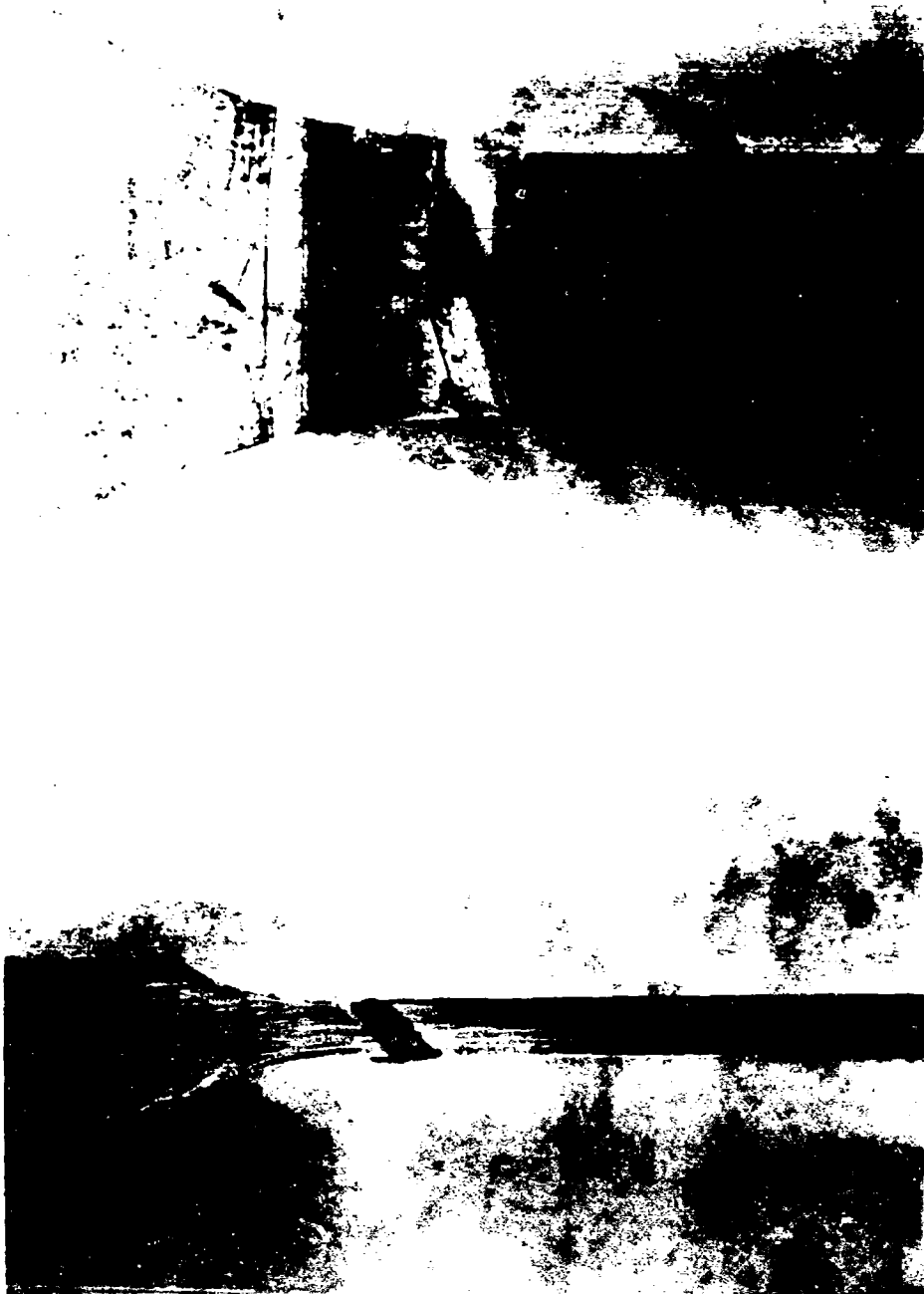


FIGURE 81. FATIGUE FAILURE OF ALUMINUM ALLOY ADHEREND - 1.5-INCH ADHESIVE SCARF JOINT



FIGURE 82. FATIGUE FAILURE IN ADHESIVE AND INTERLAMINAR SHEAR – 1.5-INCH ADHESIVE SCARF JOINT

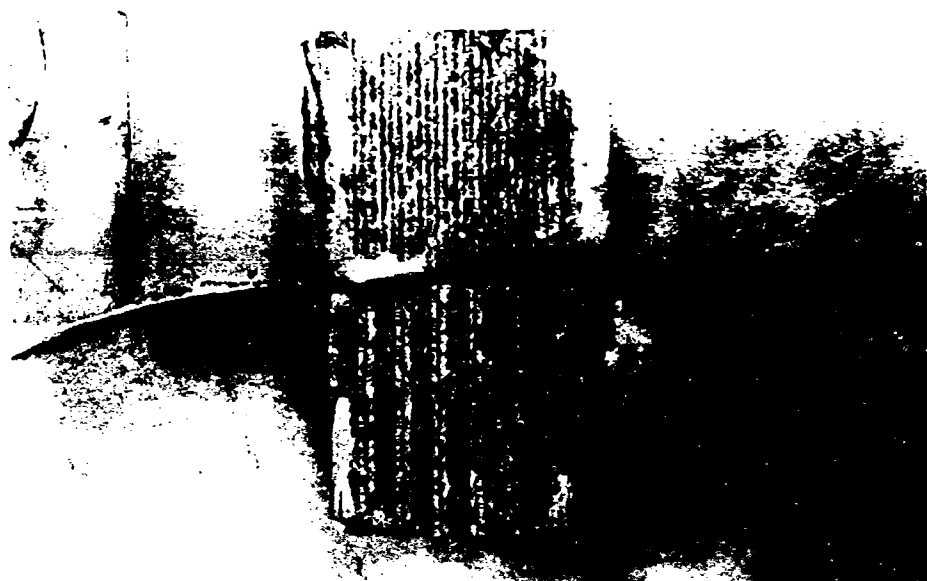


FIGURE 83. FATIGUE FAILURE IN ADHESIVE AND INTERLAMINAR SHEAR – 1-INCH ADHESIVE SCARF JOINT



FIGURE 84. FATIGUE FAILURE IN ADHESIVE - 2-INCH DOUBLE LAP JOINT (PATTERN A)



FIGURE 85. FATIGUE FAILURE IN INTERLAMINAR SHEAR - 2-INCH DOUBLE LAP JOINT (PATTERN B)



FIGURE 86. FATIGUE FAILURE IN ADHESIVE – 1-INCH DOUBLE LAP JOINT (PATTERN A)

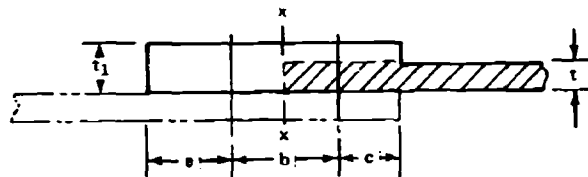
SECTION V

WEIGHT STUDIES

The most efficient structures are those that are continuous and have no joints. Because joints cannot be completely eliminated in most aircraft applications, the designer must make the necessary joints as efficient as possible. Many investigators define joint efficiency as the ratio of joint strength to basic panel strength. However, it is possible to achieve an efficiency of 100 percent with a badly balanced joint configuration, so this criterion was not used in the present analysis. Rather an efficiency criterion based on minimum total weight of the complete structure was used.

In this investigation, uniformly loaded tension panels having joints at each end were considered. A range of load intensities between zero and 20,000 pounds per inch and a panel width of 20 inches were arbitrarily selected. A panel aspect ratio of 3 was used, giving a panel length of 60 inches. These values are typical of aircraft design conditions.

The joint weight increment for these studies was defined as shown in the following sketch. A bolted joint is shown, but the definition of weight increment applies equally well to bonded joints. The following sketch shows a panel of basic thickness, t , joined by two rows of bolts. The edge of the panel is reinforced to thickness t_1 .



All weight additional to the shaded area of the basic panel was defined as the weight penalty. Note that when the two sides of the joint are considered together, the basic panels meet at Section $x-x$ to form the equivalent of a panel without a joint.

For bolted joints, weights of bolt heads, nuts, washers, and the parts of the bolt standing clear of the members being joined are shared equally between the two sides of the joint. This enabled each side to be considered separately, which is necessary when the joined panels are not identical.

In formulating a weight-efficiency criterion, the basic panel must itself be defined since it is a reference datum for the weight penalty. The concept of a basic panel thickness is of prime importance. If panel thickness is increased, the weight of the joint with respect to the new thickness is decreased. This results in an apparent reduction in weight penalty, despite the fact that joint strength may be unchanged and the total weight increased. For purposes of comparison, all the joints considered in the present study were assumed to be loaded in tension and the basic panel thickness was the minimum required to give adequate tensile strength.

For purposes of comparison, panel and joint strengths were calculated for both boron/epoxy and 7075-T6 aluminum alloy panels. The strengths of the boron/epoxy laminate joints were calculated using the strength prediction methods described in Section IV. Material properties and strength allowables used in the weight studies are summarized in Table XXXI.

BONDED JOINTS

Bonded joints considered in the weight study included single and double lap, scarf, and stepped lap joints. Strength and weight comparisons for these joint configurations were determined from tests results using Shell 951 adhesive (see Figure 87). Lap joint strengths were based on the strength prediction methods described in Section IV. Scarf and stepped-lap joint strengths were based on adhesive stresses attained in test (4650 and 6000 psi, respectively). As a practical limitation, a minimum scarf angle of 4° was used. To transmit the maximum tensile load possible in the adherends, a local thickening of the joint was necessary to produce the required bond area. In the weight studies, an adhesive density of 0.043 pounds per cubic inch and an adhesive thickness of 0.010 inch were used.

Lap Joints

The strength of lap joints depends primarily on lap length and the extensional stiffnesses of the adherends. Because an Et ratio of unity yielded the highest strength, this condition was assumed for the weight analysis. Average adhesive shear stress attained in the joint tests is plotted as a function of length in Figure 88. Variations of E and t did not affect this relationship. The strength of the joint is plotted against lap length in Figure 89.

Using joint strengths from Figure 89 and the previously defined weight increment (including both halves of the joint), the weight-strength relationships for bonded lap joints were plotted and are shown in Figure 90.

TABLE XXXI
MATERIAL PROPERTIES AND ALLOWABLE STRESSES
USED IN WEIGHT STUDIES

MATERIAL PROPERTY	BORON LAMINATE 0°/45°/-45°/90°	ALLUMINUM ALLOY 7075-T6 CLAD SHEET	ALLOY STEEL BOLT MATERIAL
ULTIMATE TENSILE STRENGTH, f_{tu} (PSI)	110,000	78,000	160,000 TO 180,000
ULTIMATE BEARING STRENGTH, f_{bru} (PSI)	150,000	148,000	AMPLE
SHEAR-OUT STRESS, f_{90} (PSI)	18,420 MAX.*	47,000	100,000
TENSILE STRENGTH BETWEEN FASTENER HOLES, f_{th} (PSI)	40,000	26,000	NOT APPLICABLE
DENSITY, ρ (LB/CU IN.)	0.072	0.102	0.283

*THE LAMINATE SHEAR-OUT STRESS MUST BE REDUCED FOR t/d AND s/d EFFECTS IN ACCORDANCE WITH FIGURE 73, SECTION IV.

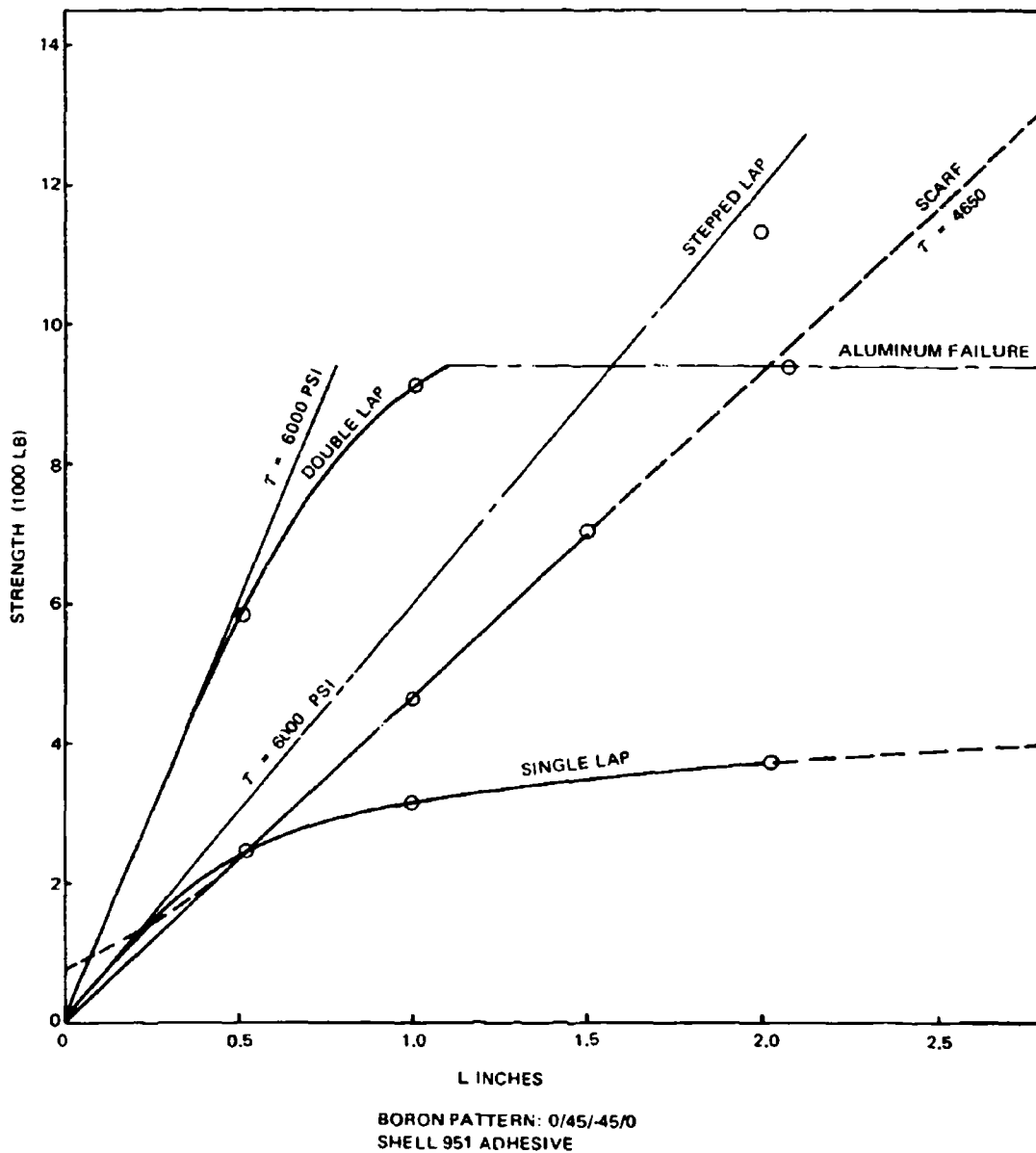


FIGURE 87. BORON-TO-ALUMINUM BONDED JOINT STRENGTHS

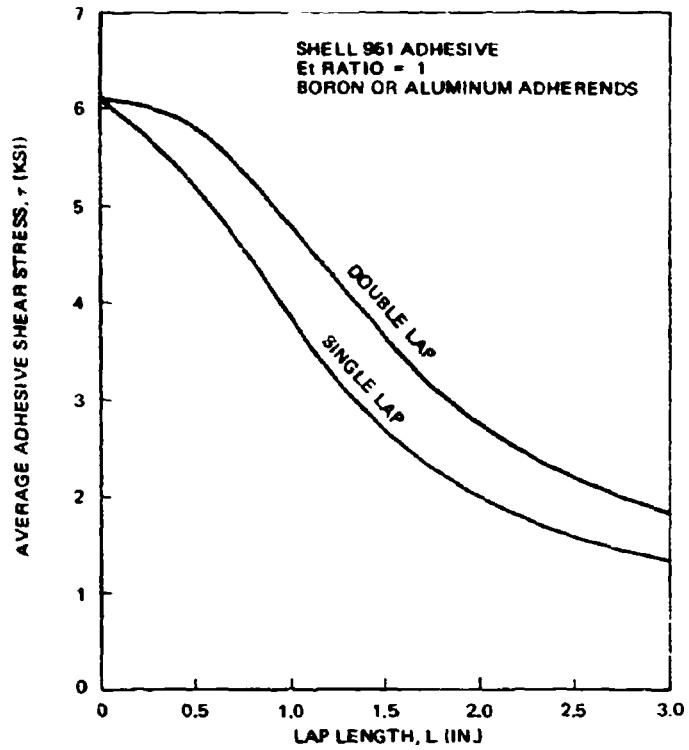


FIGURE 88. AVERAGE ADHESIVE SHEAR STRESS IN BONDED LAP JOINTS

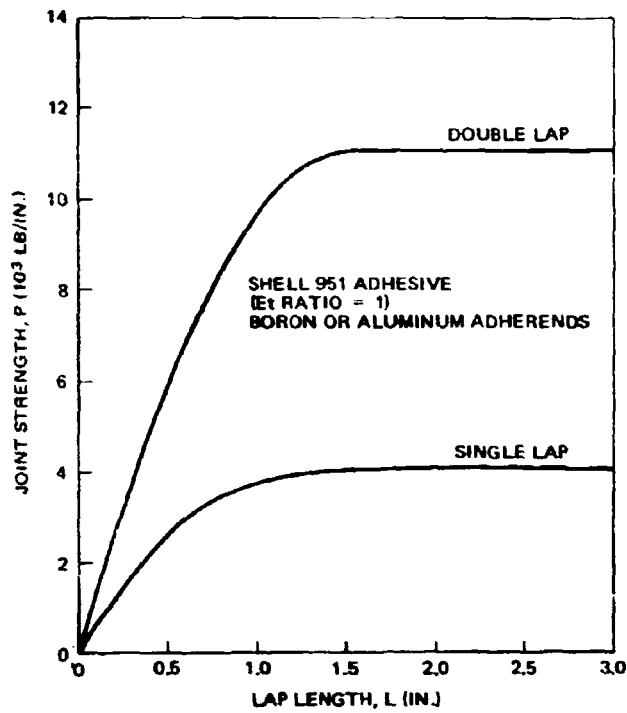


FIGURE 89. BONDED LAP JOINT STRENGTHS

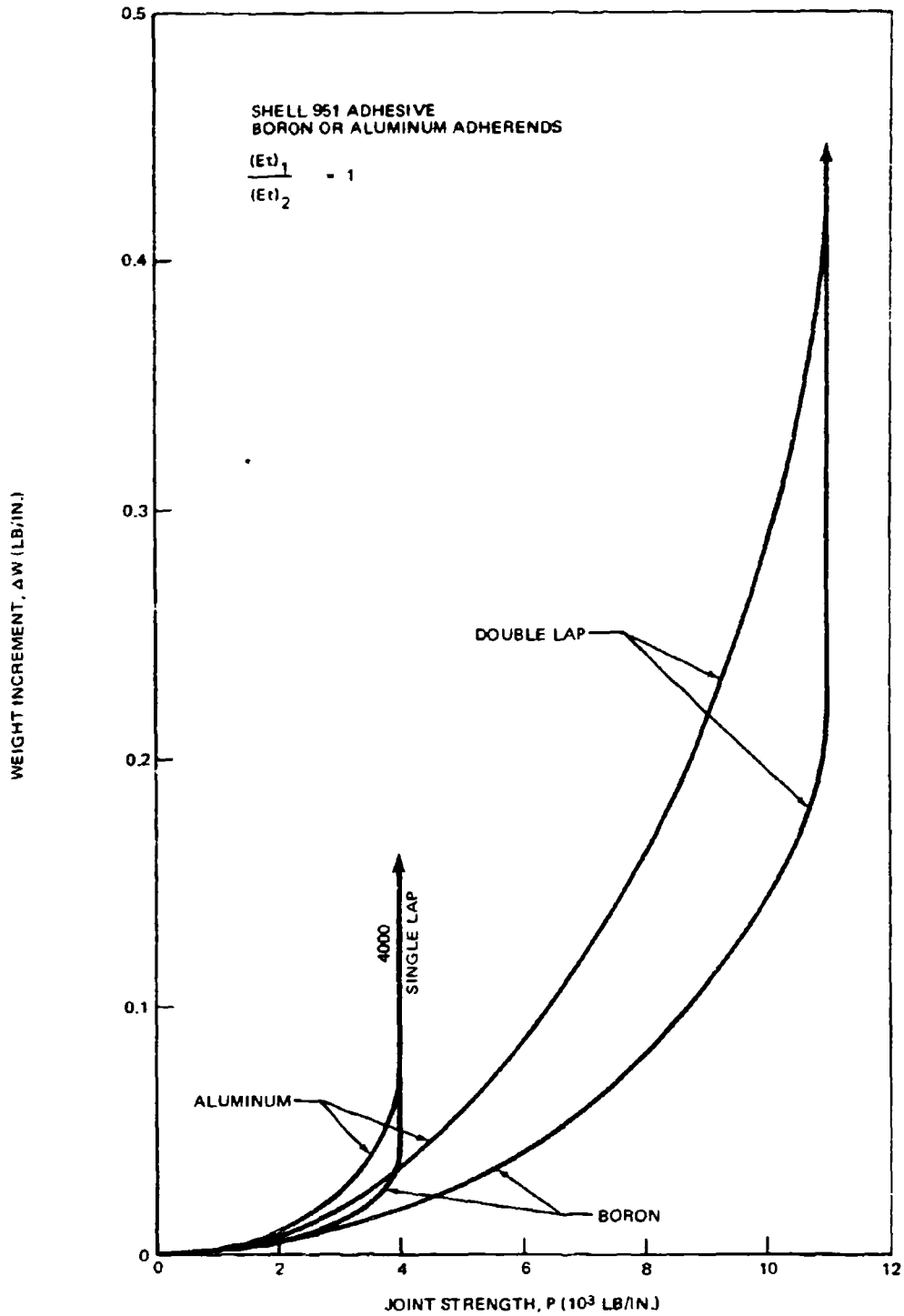
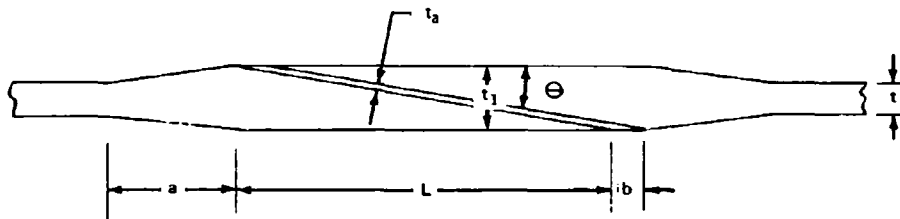


FIGURE 90. WEIGHT INCREMENTS FOR BONDED LAP JOINTS

Scarf Joints

For the range of scarf angles likely to be used in practical applications, the average adhesive shear stress was 4650 psi for Shell 951 adhesive joining boron and aluminum adherends. Using four degrees as the minimum practical angle for machining, it was necessary to add local thickening in the scarf joint to provide adequate lap length for the maximum load possible in the adherends. The local thickening is shown in the following sketch.



To eliminate the dimension "a" as an unknown, it was assumed to be $6(t_1 - t)$. The weight increment for both halves of the joint (neglecting the cosine term for the bond line) is given by the equation

$$\Delta W = (L+a+b)(t_1 - t) - (\rho - \rho_a)Lt_a$$

Weight increments for joints in both boron and aluminum panels are shown in Figure 91. Note that the aluminum joint had a lower penalty because of the thicker basic aluminum panel.

Stepped Lap Joint

For boron and aluminum joints with Shell 951 adhesives, the stepped-lap joint developed an average shear stress of 6000 psi. The strength of the joint was not significantly affected by the number of steps. However,

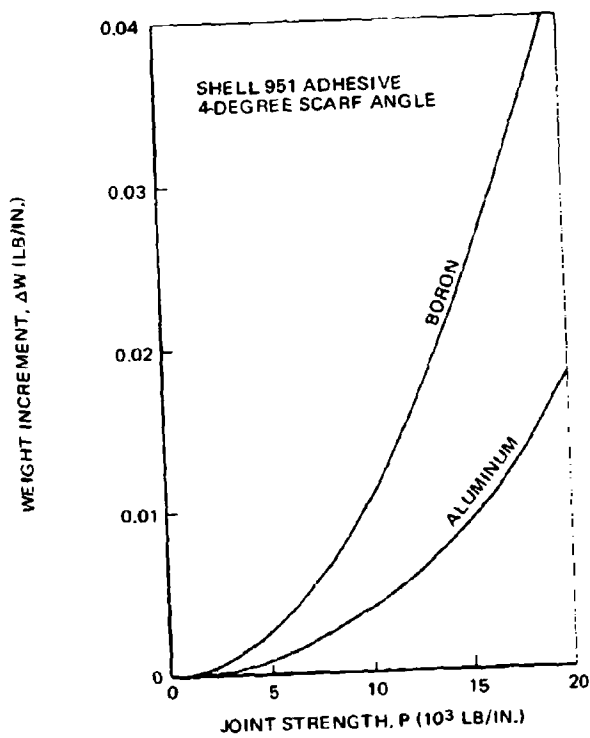
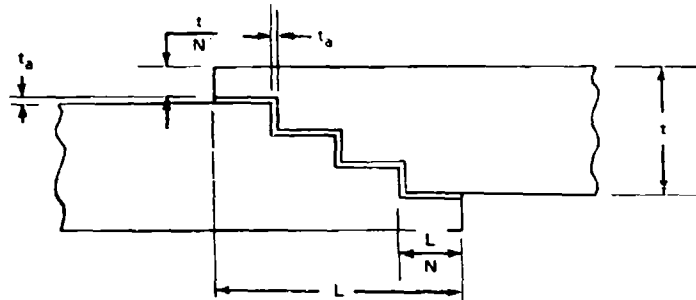


FIGURE 91. WEIGHT INCREMENTS FOR BONDED SCARF JOINTS

weight penalty increased as the number of steps was reduced because of the offset configuration shown by the following sketch.



The adverse weight effect of the offset configuration was compensated for by the fact that no local laminate thickening due to loss of area was required in the region of the joint. Weight increment for both joint halves was calculated using the following equation:

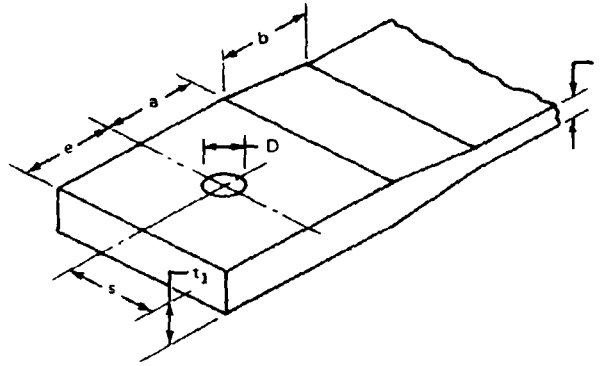
$$\Delta W = \left(\frac{\rho L t}{N}\right) + (0.00043 L) - (\rho - \rho_a) t_a \left(\frac{N-1}{N}\right)$$

Weight increment is plotted in Figure 92 against load intensity (P) and number of steps (N) for boron panels. Boron and aluminum joints are compared in Figure 93 for four-step joint configurations. The four types of bonded joints are compared in Figure 94. The stepped lap joint was superior for all load levels.

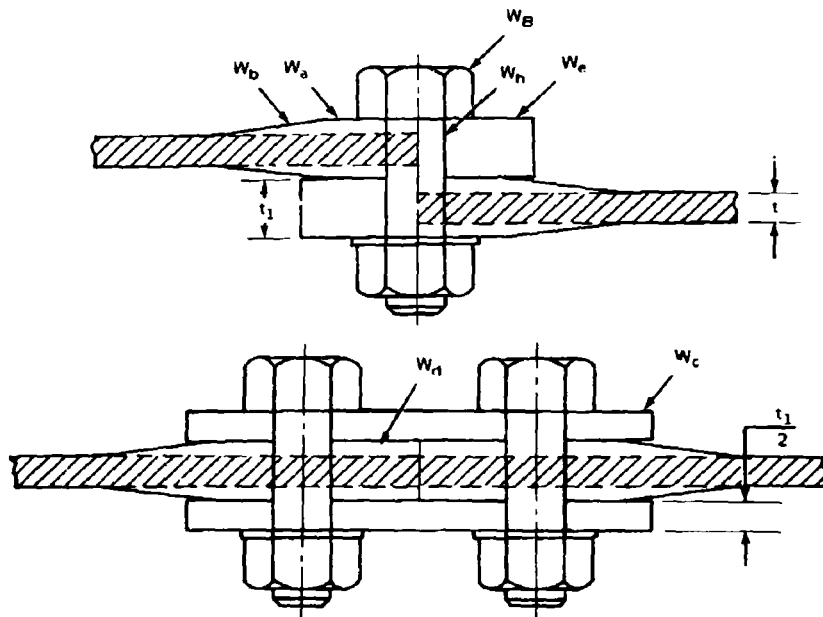
BOLTED JOINTS

The weight increments of bolted joints are plotted against joint strength in Figure 95 for boron laminates having a $0^\circ/45^\circ/-45^\circ/0^\circ$ pattern. The various types of bolted joints tested in this program were compared. The use of bushings to reinforce the hole was less effective than reinforcing the end of the joint by increasing laminate thickness or by inserting metal shims. Of the latter two methods, the thickened-end joint was easier to fabricate, but shims can be used to advantage where space is limited.

The joint selected for the weight study was the single-bolt, reinforced-end configuration in which the layers of reinforcement retained the basic $0^\circ/45^\circ/-45^\circ/0^\circ$ pattern. Relevant joint geometry is shown in the following sketch.



The configurations for single and double lap joints and the elements that comprise the weight increment are the following.



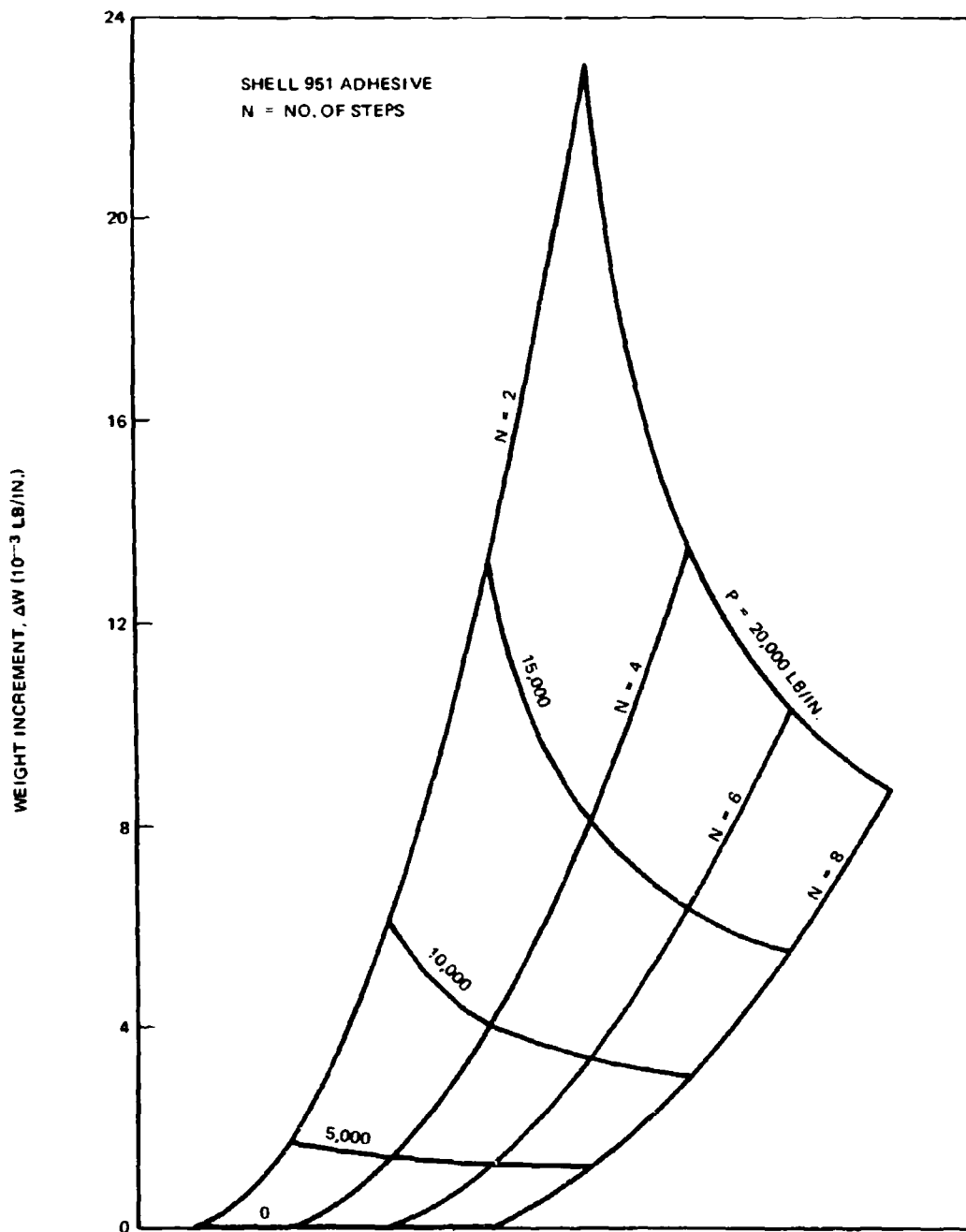


FIGURE 92. WEIGHT INCREMENTS FOR STEPPED LAP JOINTS IN BORON PANELS

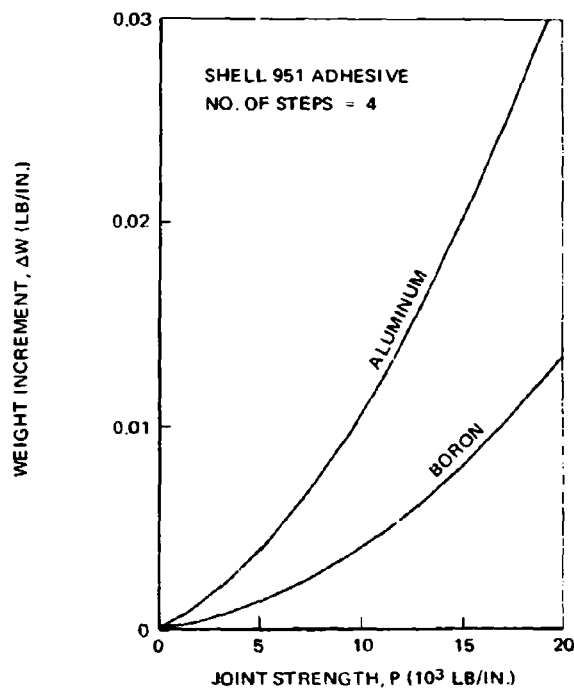


FIGURE 93. COMPARISON OF WEIGHT INCREMENTS FOR STEPPED LAP JOINTS

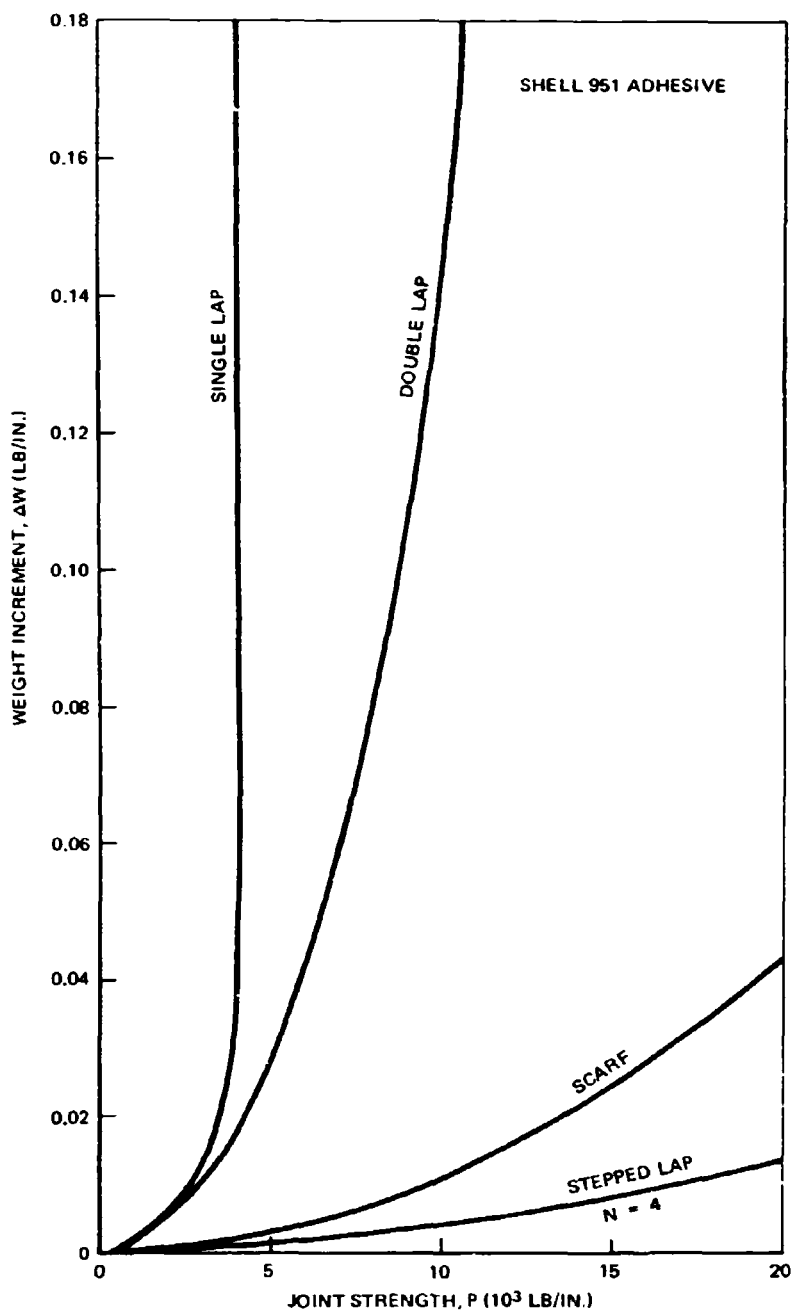


FIGURE 94. WEIGHT INCREMENTS FOR BONDED JOINTS IN BORON PANELS

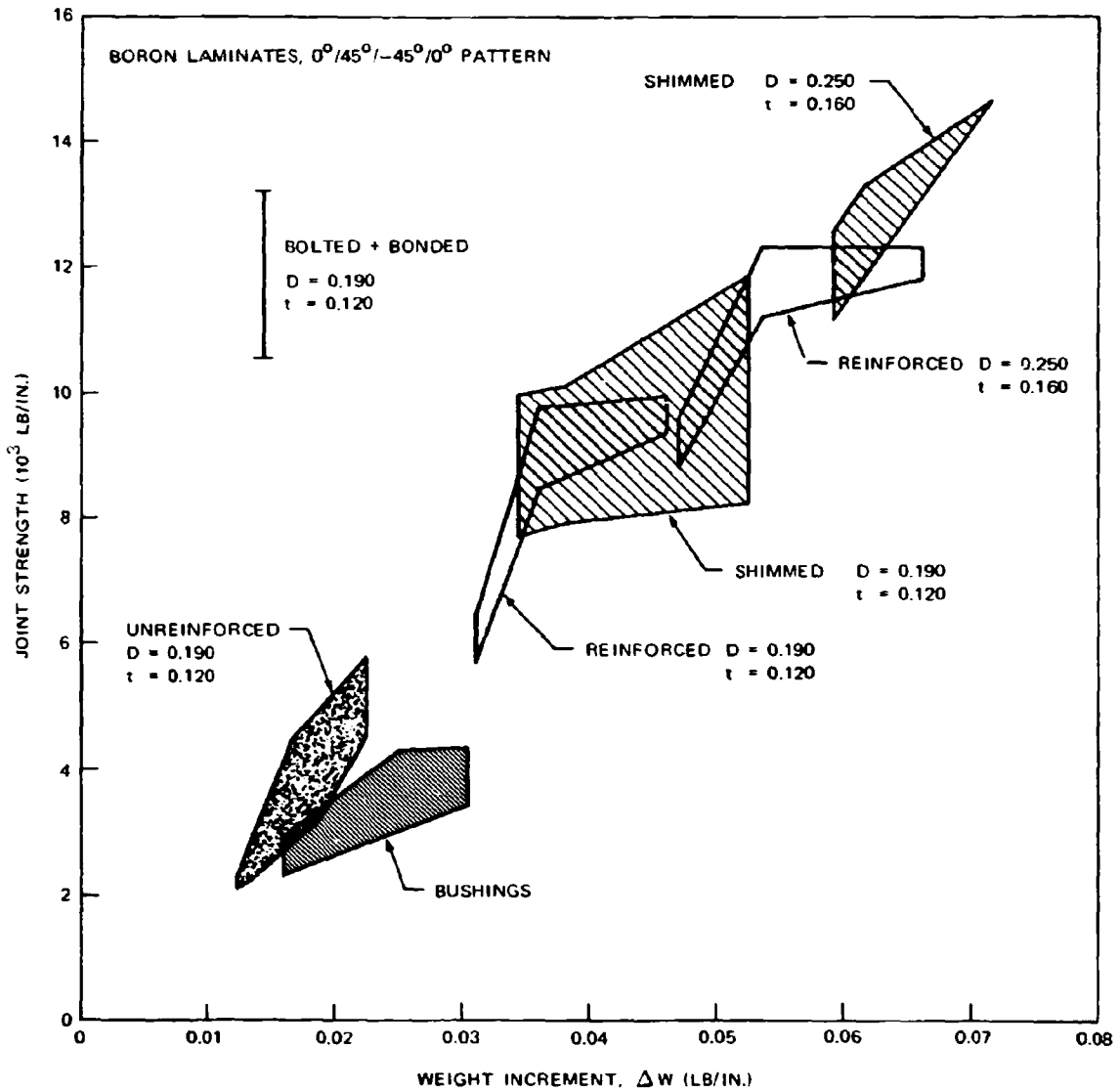


FIGURE 95. STRENGTH-WEIGHT RELATIONSHIPS FOR BOLTED JOINTS

The weight of the bolt assembly external to joint thickness was designated W_B . In practice, bolt weights would be read from catalog values. For this analysis the following approximation was used:

$$W_B = 0.15 D^2/s$$

Weight increments for the single and double lap bolted joints were calculated by summing up the appropriate weights elements as follows:

For single lap joints

$$\Delta W = W_a + W_b + W_e + W_h + W_B$$

For double lap joints

$$\Delta W = W_a + W_b + W_c + W_d + 2W_h + 2W_B$$

In the design of the bolted joints for the weight study, the number of unknowns was reduced to five (D , e , s , t , and t_1) by assuming the following relationships:

$$a = 1.5D$$

$$b = 6(t_1 - t)$$

Additional restrictions of minimum edge distance ratio (e/D) and side distance ratio (s/D) equal to two were also imposed. The following stress relationships were written:

$$\text{Bolt Shear Stress, } \sigma_s = \frac{2sP}{(\pi/4)D^2n} = \frac{8sP}{\pi D^2n}$$

$$\text{Shear-Out Stress, } \sigma_{so} = \frac{2SP}{2R_e t} = \frac{sP}{R_e t}$$

$$\text{Bearing Stress, } \sigma_{br} = \frac{2sP}{Dt}$$

$$\text{Stress Through Hole, } \sigma_{th} = \frac{2sP}{(2s-D)t}$$

Where:

$n = 1$ for Single Shear

$n = 2$ for Double Shear

$R_e =$ Effective Shear-Out Length

Weight increments were calculated for joints having a "balanced design" in which all modes of failure occurred simultaneously (i. e., bolt shear, laminate shear-out, bearing, and tension at a section through the fastener

hole as determined for the foregoing equations). These weight increments are shown in Figure 96. However, it was found that the balanced design is not necessarily minimum weight, because the weights of the attaching hardware were more penalizing for larger diameter bolts. Thus, the joint geometries determined for the "balanced design" were modified by investigating weight increments for smaller diameter bolts (to a minimum diameter of 0.190 inch). Joint strengths were consistent in each case with Figures 72 and 73 in Section IV. The results of these investigations are shown in Figures 97 and 98, respectively, for single and double lap bolted joints.

PANEL AND JOINT WEIGHT COMPARISONS

The significance of the weight increments for different joint configurations becomes more apparent when seen in relation to total panel weights. Basic panel weights, W_p , were calculated for both boron laminate and 7075-T6 aluminum alloy panels for various load intensities. The panel weights were calculated using the following equation:

$$W_p = \rho b l t = \frac{\rho b l P}{\sigma_t}$$

where:

ρ = Material Density (pounds/cubic inch)

b = Panel Width (inches)

l = Panel Length (inches)

P = Load Intensity (pounds/inch)

σ_t = Allowable Tensile Stress (pounds/square inch)

The resulting panel weights were used in conjunction with appropriate joint weight increments to construct the weight comparisons of Figure 99 through 101.

Total panel and joint weights are shown in Figure 99 for boron laminate and aluminum alloy. The boron laminate panel weights ranged from 50 percent of aluminum alloy for the four stepped lap joints to 55 percent of aluminum alloy for the bolted double lap joint. In the case of the scarf joint, where aluminum joints had the lower weight increments, the difference in joint weight increment was insignificant in comparison with the basic panel weights. The scarf and the stepped lap joint had small weight increments compared with the lap joints and, because the increments were small in comparison to panel weights, there was little difference in total weight between them.

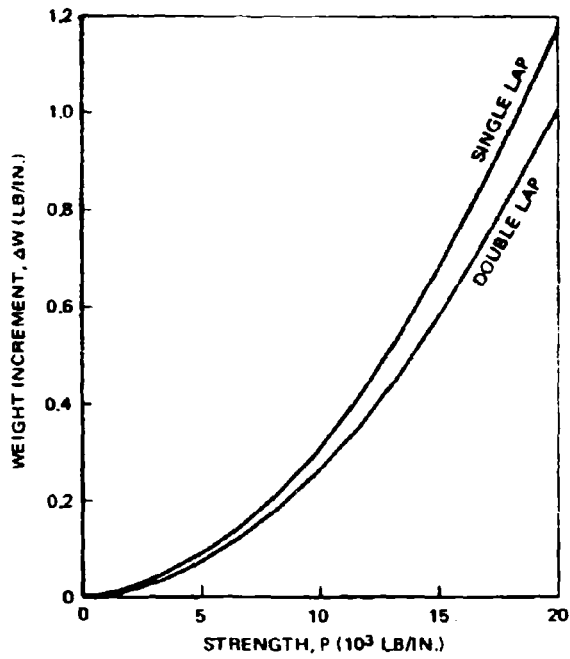


FIGURE 96. WEIGHT INCREMENT FOR BOLTED JOINTS IN BORON PANELS - BALANCED DESIGN

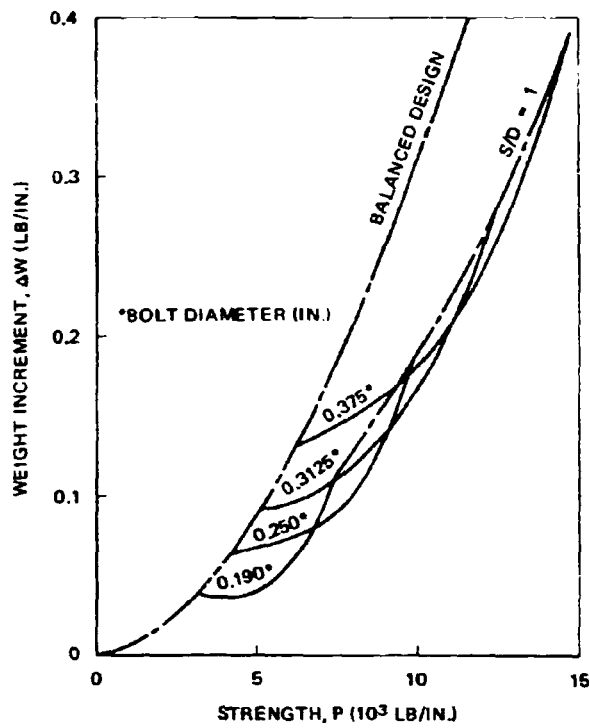


FIGURE 97. WEIGHT INCREMENTS FOR BOLTED SINGLE LAP JOINTS IN BORON PANELS

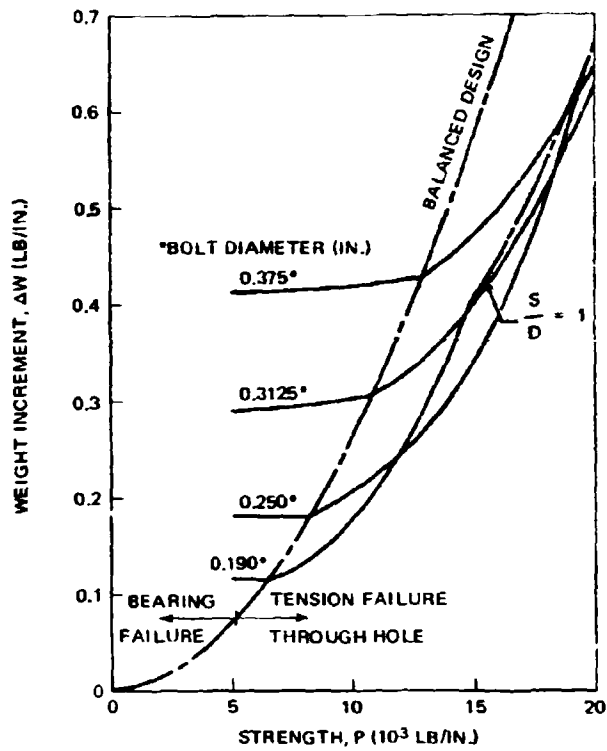


FIGURE 98. WEIGHT INCREMENTS FOR BOLTED DOUBLE LAP JOINTS IN BORON PANELS

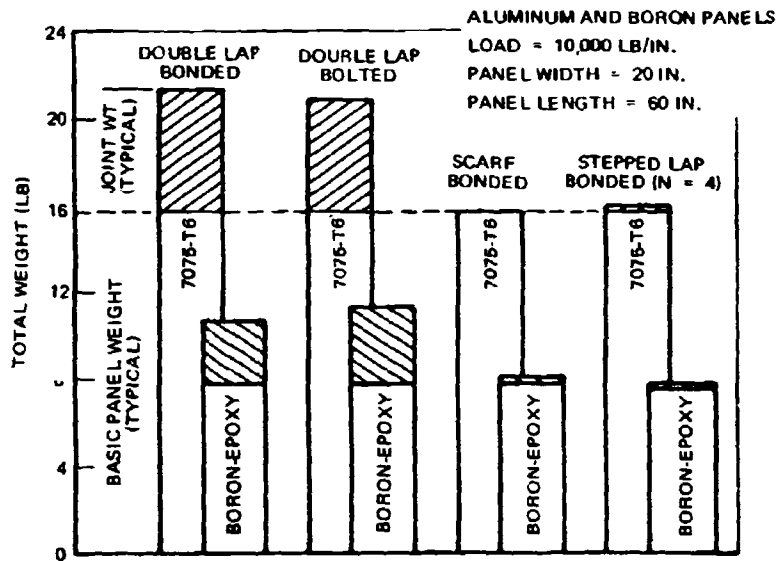


FIGURE 99. TOTAL WEIGHT COMPARISONS FOR PANELS AND JOINTS

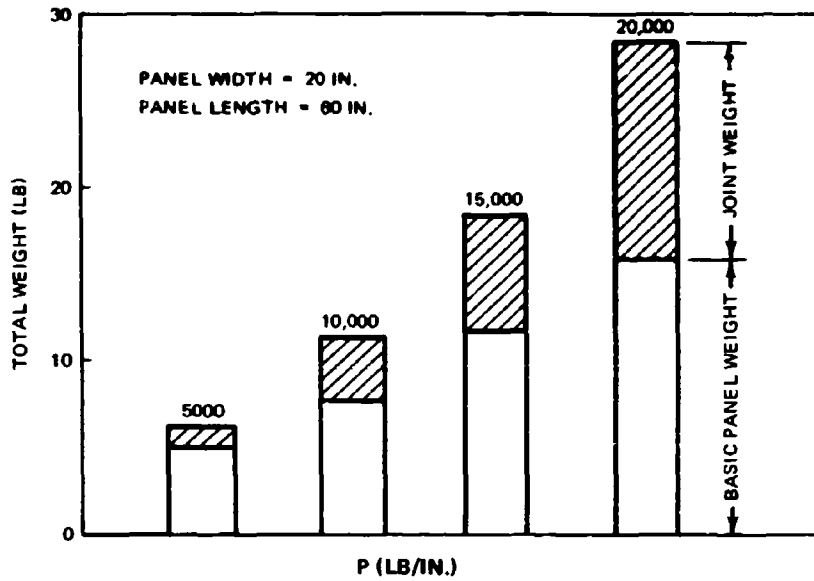


FIGURE 100. WEIGHT OF BORON PANELS WITH DOUBLE LAP BOLTED JOINTS AT VARIOUS LOAD INTENSITIES

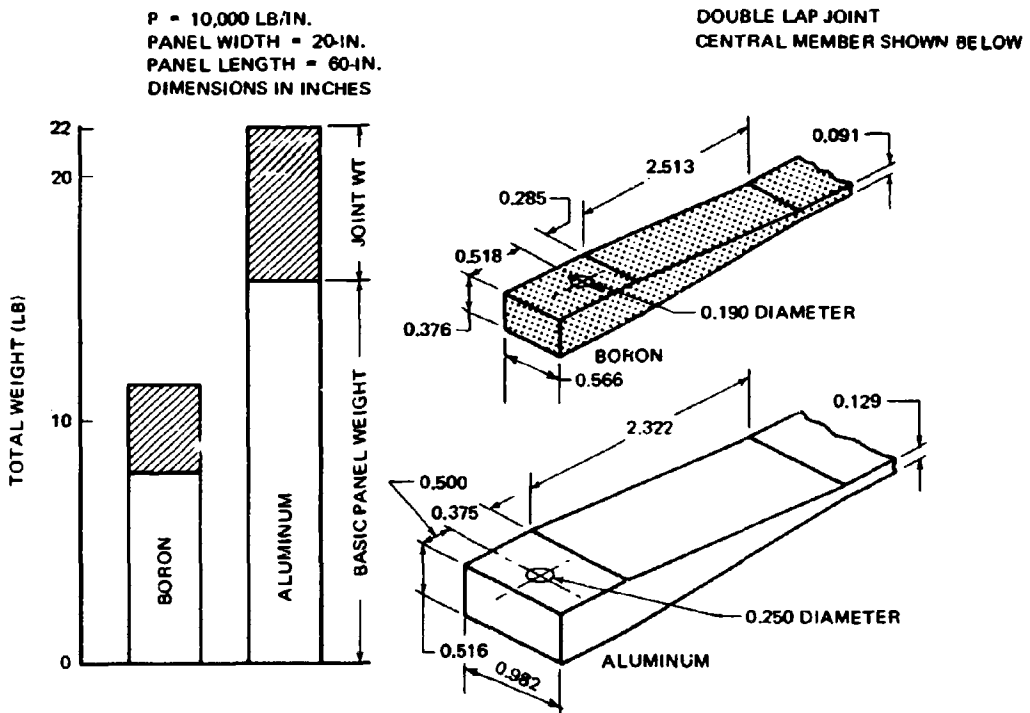


FIGURE 101. COMPARISON OF BORON AND ALUMINUM BOLTED JOINTS

The relative amounts of panel and joint weights are shown in Figure 100 for double lap bolted joints at load intensities up to 20,000 pounds per inch. Joint weight increments were a greater proportion of the total weights as load intensity increased. At a load intensity of 5000 pounds/inch, the joint weight increment was 23 percent of the total weight. At 20,000 pounds/inch, the joint weight increment increased to 45 percent of the total. Design details for double lap bolted joints at 10,000 pounds per inch load intensity are shown in Figure 101.

SECTION VI

ANALYTICAL STUDIES

The basic joint configurations in the experimental program were studied analytically to evaluate available analysis methods and to provide insight into the experimental results. The analytical studies consisted primarily of linear matrix computer analysis using lumped parameter modeling (References 16 and 17).

The results of the linear digital analyses of bonded joints were evaluated in two ways.

- Stress concentration factors from the linear digital analyses were used to normalize the results of fatigue screening tests. The fatigue data included single lap, double lap, stepped lap and scarf joints, with stress concentration factors ranging from 1.7 to 8.6. The correlation of data was very satisfactory in spite of the broad scope of data.
- Stress distributions from the linear digital analyses of double lap bonded joints were modified by an approximate plasticity method (Reference 18) to predict the ultimate strength of joints. The predictions agreed very well with adhesive and adherend failures.

In the correlation of the fatigue screening data, several of the digitally computed stress concentration factors were scaled to account for differences in the experimental and analytical configurations. The data were scaled using a one-dimensional, linear, analytic solution for shear stresses in bonded joints (Reference 19). The satisfactory correlation of the fatigue data, therefore, also verified this method.

The linear matrix computer analysis method was also used to analyze bolted joints. The results were unsatisfactory. However, the approach is summarized in this document for the benefit of future investigations.

Double lap bonded joints were also analyzed by a nonlinear digital method (References 20 and 21). The method and representative results are discussed in this section to indicate the potential of nonlinear analyses in the prediction of strength of joints in composite structures.

LINEAR ANALYSIS OF BONDED JOINTS

Seventeen joint configurations were analyzed by the linear matrix computer method (Table XXXII). Variations included joint type, adherends, adhesive, lap length, and reinforcement pattern.

The idealization in Figure 102 is representative of the modeling of bonded joints. The grid lines represent centerlines of bars that carry axial loads, and the grid intervals represent rectangular panels that carry shear loads only. In the analysis, bars were assigned properties that represented those characteristics of the real structure that are associated with normal stresses, and panels were assigned properties that represented those

TABLE XXXII
LINEAR MATRIX COMPUTER ANALYSES - BONDED JOINTS

ANALYSIS	JOINT TYPE*	ADHEREND GAGE AND MATERIAL**		ADHESIVE	LAP LENGTH (INCHES)	SCF (SHEAR)
		BASE	SPLICE			
1	SL	0.072 FG	0.102 AI	0.005 FM-47	1.375	7.4
2	DL	0.144 FG	0.102 AI	0.005 FM-47	1.375	6.8
3	DL	0.120 FG	0.160 AI	0.005 MB-408	1.5	5.2
4	DL	0.080 BO	0.040 BO	0.005 MB-408	1.5	4.2
5	DL	0.120 BO	0.160 AI	0.005 MB-408	0.5	1.5
6	DL	0.120 BO	0.160 Ti	0.005 MB-408	0.5	1.55
7	DL	0.120 BO	0.160 St	0.005 MB-408	0.5	1.6
8	SC	0.080 BO	0.080 BO	0.00525 MB-408	0.25	1.4
9	SC	0.080 BO	0.080 AI	0.00525 MB-408	0.25	1.4
10	2S	0.040 BO	0.040 AI	0.005 SHELL 951	2.0	8.1
11	SC	0.080 BO	0.080 AI	0.00525 SHELL 951	0.25	1.4
12	SC	0.080 BO	0.080 AI	0.00525 SHELL 951	0.75	1.7
13	4S	0.080 BO	0.080 AI	0.005 SHELL 951	2.0	3.6
14	SL	0.040 BO	0.063 AI	0.005 SHELL 951	2.0	9.6
15	SL	0.040 BO	0.063 AI	0.005 SHELL 951	2.0	12.3(†)
16	DL	0.080 BO	0.063 AI	0.005 SHELL 951	2.0	3.9
17	SC	0.160 BO	0.160 AI	0.00525 SHELL 951	2.0	1.4

- | | |
|---|--|
| <ul style="list-style-type: none"> *SL - SINGLE LAP DL - DOUBLE LAP SC - SCARF 2S - TWO-STEP LAP 4S - FOUR-STEP LAP (†) - PATTERN B | <ul style="list-style-type: none"> **FG - FIBER GLASS LAMINATE BO - BORON LAMINATE AI - ALUMINUM ALLOY 7075-T6 TI - TITANIUM ALLOY 6 Al-4V SI - STAINLESS STEEL |
|---|--|

characteristics of the real structures that are associated with tangential stresses. Assigned properties were based on the effective properties of the individual laminae in the plane of the idealization. Poisson coupling was included in all but the earliest analytical cases (analyses 1 through 9 in Table XXXII). The digital solutions were computed using a matrix displacement computer program that takes advantage of the regularity of the grid and the symmetry and banding of the stiffness matrix.

The shear stress distribution in the adhesive of the two-step lap joint is shown in Figure 103. The curve includes the peak stresses at the ends of adhesive that are characteristic of bonded joints. It also includes stress concentrations at the central discontinuity. This curve also demonstrates another characteristic of bonded joints: In relatively long joints, the central zone of the adhesive is virtually ineffective, and peak stress is independent of the joint length. One implication of this characteristic is that a critical lap length exists, beyond which increased lap length does not substantially increase fatigue life. For the adhesive/adherend combinations in this investigation, the critical length was less than 1 inch.

The stress concentration factors determined by digital analysis (Table XXXII) were used to normalize the results of the fatigue screening tests to evaluate reliability of the computed stress concentration factors. The results of the normalization process are shown in Figure 104. The ordinate scale represents peak adhesive shear stress, which is the product of the average shear stress level in the fatigue screening test and stress concentration factor as determined by analysis. Not all joint configurations were analyzed digitally, and therefore some of the digitally computed stress concentration factors were scaled to correct for the configuration differences.

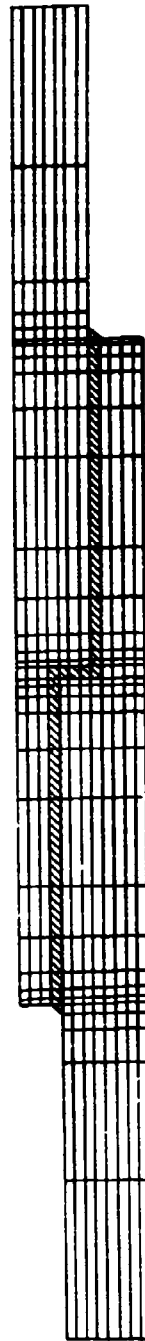
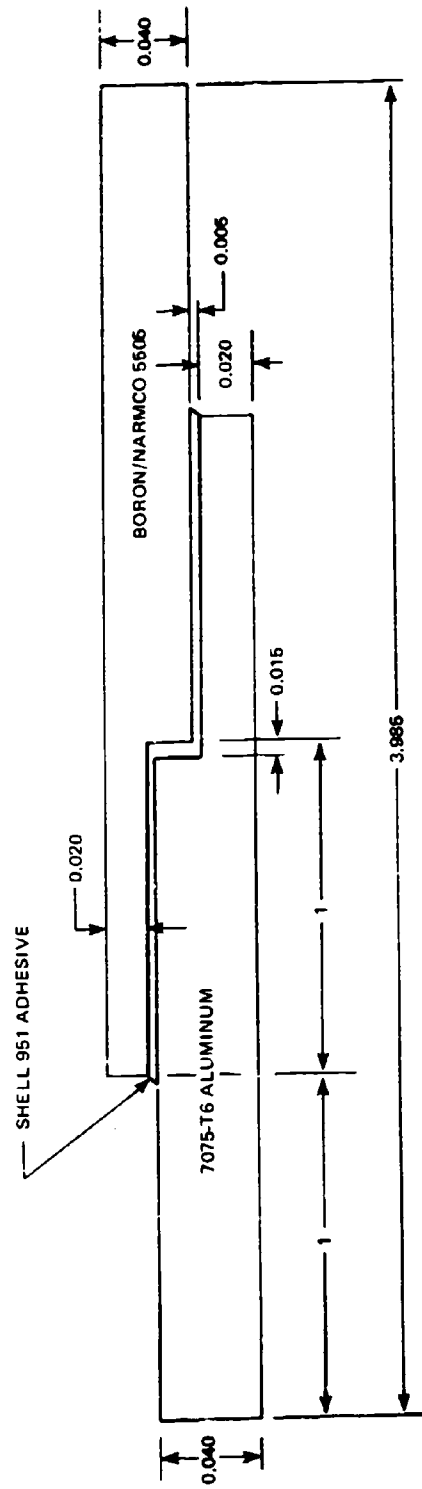


FIGURE 102. IDEALIZED TWO-STEP LAP JOINT

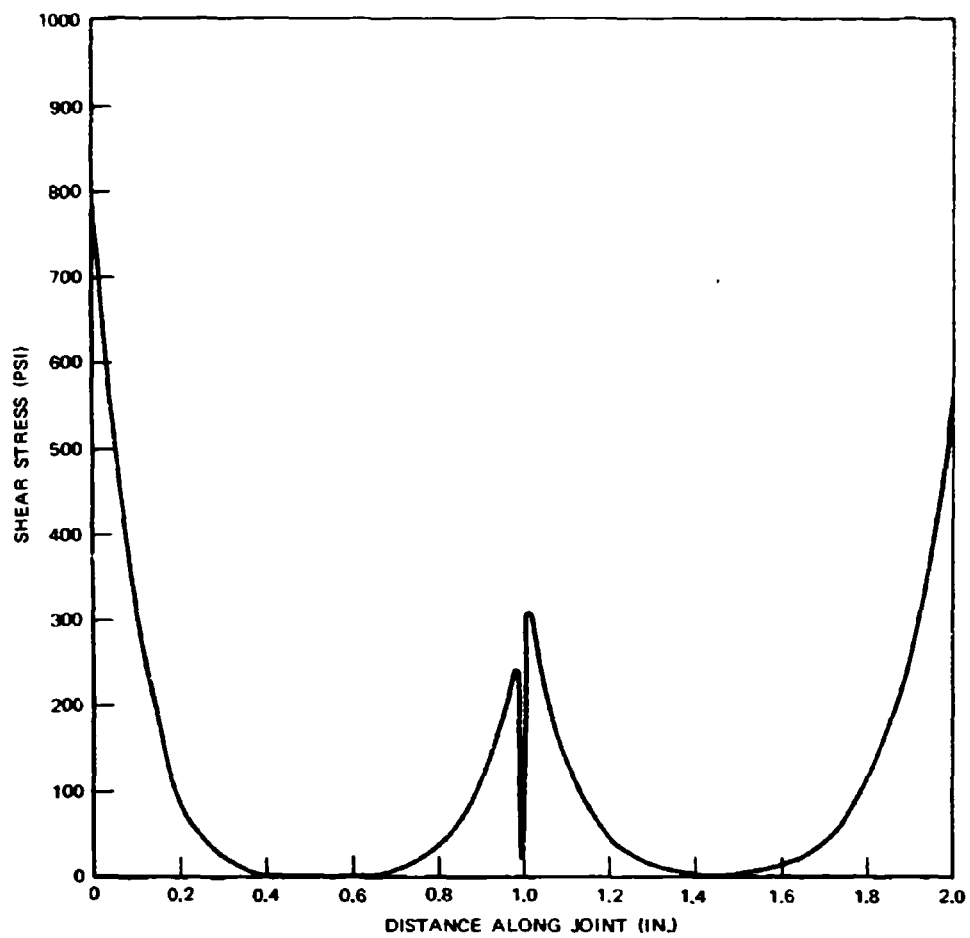


FIGURE 103. STRESS DISTRIBUTION IN THE ADHESIVE OF A TWO-STEP LAP JOINT

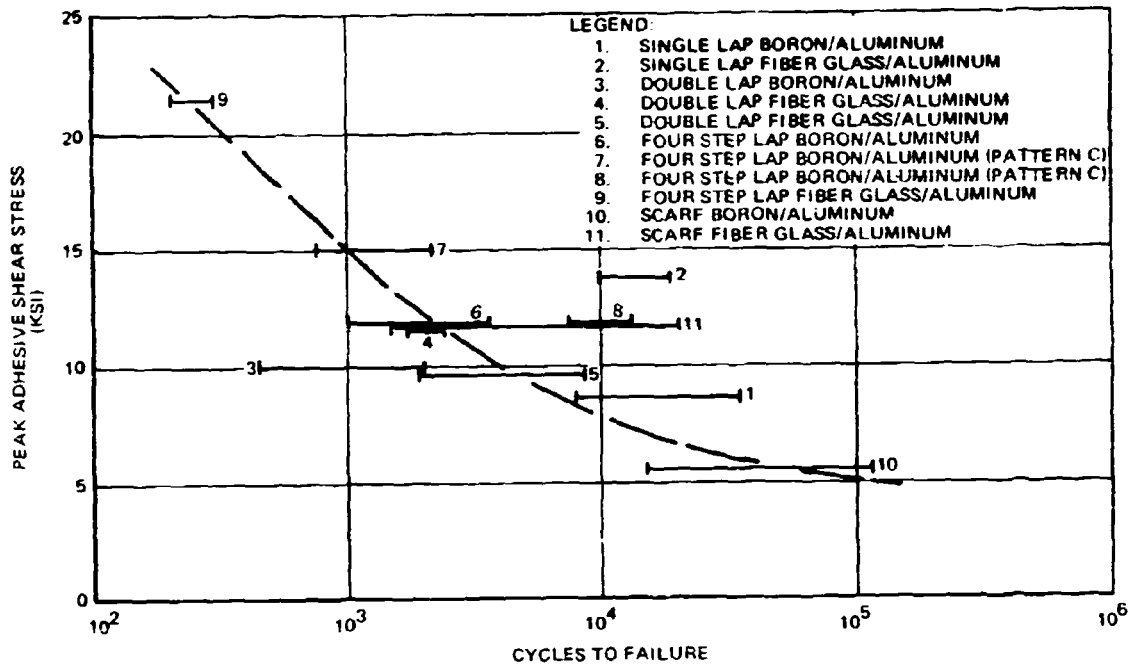


FIGURE 104. FATIGUE STRENGTH OF BONDED JOINTS

The scaling was based on a linear, one-dimensional, analytic solution for shear stresses in a symmetric, double lap, bi-modular joint (Reference 19). For joints longer than 1/2 inch (for the adhesive/adherend combinations in this study), the stress concentration factor was given by

$$F = \frac{L}{t} \left(\frac{K_a K_2}{K_1 (K_1 - K_2)} \right)^{1/2}$$

where

F is the stress concentration factor

L is the lap length

t is the thickness of the adhesive

K_a is the product of thickness and shearing modulus of the adhesive

K_1 is the product of the thickness and direct stress modulus of the basic adherend

K_2 is the product of the thickness and direct stress modulus of the splice adherend

(For K_1 and K_2 , the thickness is for a symmetric half of the joint)

For example, the stress concentration factor is proportional to the lap length, inversely proportional to the thickness of the adhesive, proportional to the square root of the shearing modulus of the adhesive, etc. Using this expression as a guide, the most applicable stress concentration factors from Table XXXII were corrected for the test specimen configurations and used as factors on the stress levels in the fatigue screening tests. The results (Figure 104) were very satisfactory in spite of the broad scope of data. These results verify, for design purposes, that (1) the peak shear stress concept is valid for evaluation of relative fatigue life of bonded joints, and (2) linear analysis methods can be useful in predicting relative fatigue life of bonded joints in composite structures.

Stress distributions in the adhesive, determined by linear matrix computer analyses, were modified by an approximate method to account for plasticity and estimate ultimate strength (Reference 18). The approximate method is based on the assumptions that (1) the adhesive is an elastic/perfectly plastic material, and (2) at failure, the width of the plastic zones at the ends of the adhesive is constant for a given joint type, adhesive, and overlap length. This approximation was applied successfully in an investigation of brazed joints (Reference 18). In this investigation the width of the plastic zone was determined by analysis of test data for a joint with a 1-1/2-inch lap. A test-theory comparison of ultimate strength for double lap bonded joints is shown in Figure 105. The correlation is good for both adhesive and adherend failures, verifying the value of linear analysis, with the approximate plasticity technique, as a valuable design tool for double lap joints.

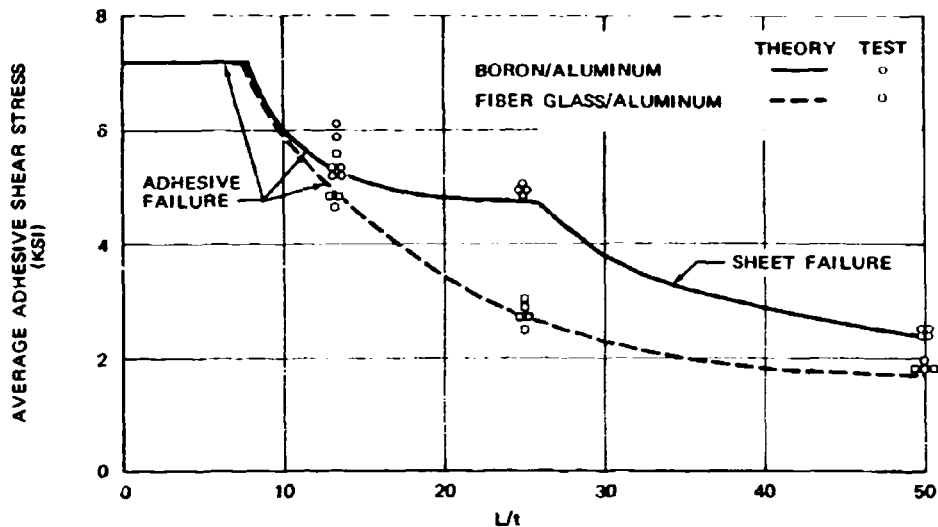


FIGURE 105. ULTIMATE STRENGTH OF DOUBLE LAP BONDED JOINTS

LINEAR ANALYSIS OF BOLTED JOINTS

A three-phase approach was used to analyze bolted joints (Figure 106). First, a pin-loaded strip was analyzed as a plane stress problem to determine stress and deflection influence coefficients. Second, the pin-bending effect was analyzed using influence coefficients from the first step to determine force and deflection influence coefficients for a basic fastener unit. Third, the multiple-fastener system was analyzed using the influence coefficients from Step 2 to determine the distribution of loads between fasteners. The detail behavior of the joint (e. g., bearing stress in different laminae) were then defined by the fastener loads and the influence coefficients from Steps 1 and 2.

This three-phase approach was applied successfully to metallic joints (Reference 22); however, the results were unsatisfactory for bolted joints in composite structures. The difficulty was a severe material nonlinearity in the first step. The mechanism apparently consisted of three basic nonlinearities:

- o Variable contact area in bearing
- o Plastic deformation of the matrix material
- o Local buckling of the fibers

An extremely sophisticated nonlinear analysis capability will be required to account for these mechanisms in predicting force-deformation characteristics.

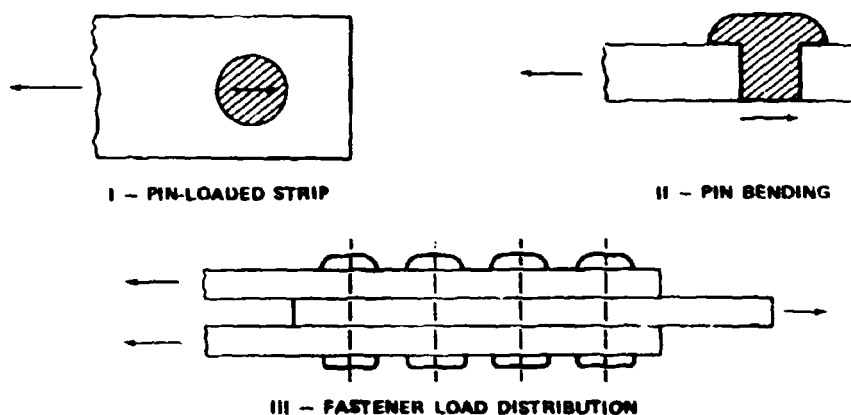


FIGURE 106. BOLTED JOINT ANALYSIS

NONLINEAR ANALYSIS OF BONDED JOINTS*

A 1/2-inch double lap bonded joint consisting of a boron/epoxy laminate (Pattern A) and aluminum alloy splice plates was analyzed to evaluate the effects of nonlinear material behavior in appropriate elements of the joint.

Joint Idealization

The joint was modeled as a two-dimensional idealization similar to the one shown in Figure 102. Behavior associated with normal stresses was represented by bars that carry only axial loads, and behavior associated with tangential stresses was represented by rectangular panels that carry only shear loads. Taking advantage of symmetry about the midplane of the basic adherend, one-half of the joint was represented by 773 bars and panels, of which 150 exhibited nonlinear behavior during the analysis. The idealized aluminum and composite adherends were extended beyond the ends of lap to minimize the effects of assumed loading distributions at the adherend ends (St. Venant principle). This distance was 0.160 inch, which was twice the thickness of the composite (0.080 inch) and 2.5 times the thickness of the aluminum (0.063 inch). The external load was applied uniformly at the ends of the adherends.

Bars oriented in the load direction and representing the laminae with fibers oriented at zero degrees were assigned an elastic modulus of E_L , whereas bars normal to the load direction and within the same laminae had an elastic modulus of E_T . Bars representing the other laminae (fibers oriented 45 degrees to the load direction) were assigned elastic moduli of 2.6035×10^6 psi and 2.44×10^6 psi, as obtained from the stiffnesses of the 45-degree laminae in directions parallel and normal to the load direction, respectively. Poisson coupling for deformations between these two sets of lumped parameters was designated as ϵ_{LT}/ϵ_L . All shear panels were assigned an elastic modulus of G_{LT} .

Nonlinear Material Representations

The joint consisted of aluminum alloy (7075-T6) and boron/epoxy adherends, with Shell 951 adhesive. Nonlinear behavior was considered in the aluminum alloy, in the adhesive, and in the resin of the composite in interlaminar shear. Only elastic behavior was considered for bars representing composite behavior parallel and normal to the load direction. This type of behavior is justified for bars parallel to the load direction because the fibers which provide most of the stiffness exhibit elastic behavior only. Test data substantiate this approximation. Inelastic strains in the composite

* These studies were conducted under the contractor's Independent Research and Development Program, and are documented in References 20 and 21. Results are summarized in this report because of their particular relevance.

in the direction normal to the load were considered secondary and were ignored. Inelastic deformation was considered for shear panels representing interlaminar behavior. Nonlinear response in interlaminar shear was deduced from inplane shear tests of unidirectional laminates (see Table V, Section III).

The coupling of strain in the aluminum and the adhesive was defined using the Prandtl-Reuss stress-strain relationships. The equivalent stress-strain diagrams required by these relationships were represented with curves having linear segments as shown in Figure 107. Equivalent stress-strain data were obtained from simple tensile test data for the aluminum and from torsion ring shear test data for the adhesive. The uncoupled stress-strain properties in interlaminar shear were also represented by linear segments (Table XXXIII).

Method of Analysis

The matrix force method implemented in FORMAT (Reference 23) was used to compute elastic stresses in each lumped parameter element due to unit external loads and unit plastic strains in each of the structural elements.

The increments of stresses due to loads and plastic strains were obtained by superimposing the two elastic solutions ($\dot{\sigma}_L$ and $\sigma_\epsilon \dot{\epsilon}^{(P)}$) in a manner that maintained the appropriate relationships between stress and strain increments. The analysis method may be formulated in matrix notation as follows.

$$\dot{\sigma} = \dot{\sigma}_L + \sigma_\epsilon \dot{\epsilon}^{(P)}$$

where

$\dot{\sigma}$ is a column matrix of element stress increments

$\dot{\sigma}_L$ is a column matrix of the component of the element stress increments due to external loads

σ_ϵ is a matrix of influence coefficients for member stresses due to unit member strains

$\dot{\epsilon}^{(P)}$ is a column matrix of element plastic strain increments.

From the governing stress-strain relationships,

$$\dot{\epsilon}^{(P)} = D \dot{\sigma}$$

where

D is the plastic flexibility matrix.

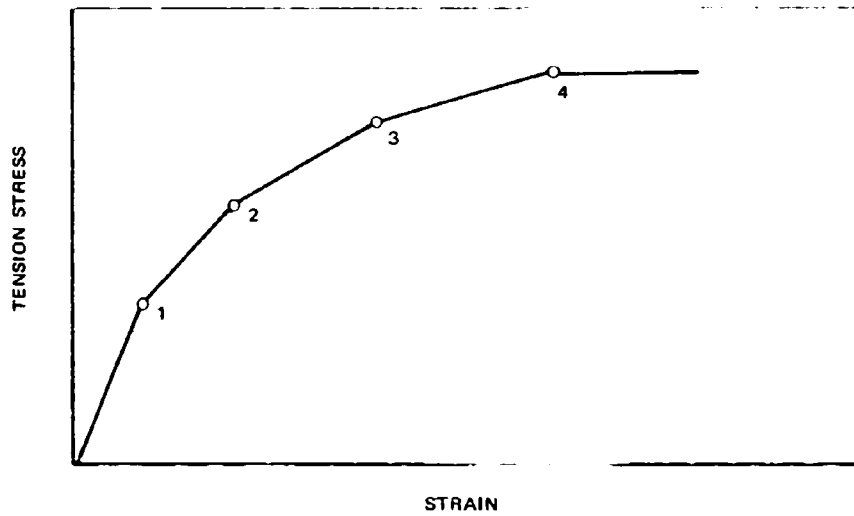


FIGURE 107. NONLINEAR MATERIAL REPRESENTATION

TABLE XXXIII
NONLINEAR STRESS-STRAIN CHARACTERISTIC USED IN BONDED JOINT ANALYSIS

	ALUMINUM ALLOY (7075-T6)		SHELL 951 ADHESIVE		BORON LAMINATE (UNIDIRECTIONAL)		
ELASTIC PROPERTIES							
E (10^6 PSI)	10.0		0.208		33.5 (LONGITUDINAL) 2.32 (TRANSVERSE)		
G (10^6 PSI)	3.76		0.075		0.70		
μ	0.33		0.387		0.244 (LT) 0.250 (TZ)		
STRESS-STRAIN CHARACTERISTICS	TENSION PROPERTIES		SHEAR PROPERTIES		INTERLAMINAR SHEAR PROPERTIES		
	POINT*	STRESS (KSI)	STRAIN (INCH/INCH)	STRESS (KSI)	STRAIN (INCH/INCH)	STRESS (KSI)	STRAIN (INCH/INCH)
	1	59.0	0.0059	3.00	0.04	0.98	0.0014
	2	66.0	0.0074	3.85	0.15	3.00	0.0057
	3	69.0	0.0088	4.45	0.38	6.00	0.0141
	4	70.2	0.0106	5.40	1.08	10.00	0.0334
	5	70.2	0.0106	6.00	1.88	12.00	0.0600
	C	-	-	6.00	≥ 1.88	12.00	≥ 0.0600

*SEE FIGURE 107

Combining equations

$$\dot{\sigma} = \dot{\sigma}_L + \sigma_{\epsilon} D \dot{\sigma}$$

or

$$\dot{\sigma} = (I - \sigma_{\epsilon} D)^{-1} \dot{\sigma}_L$$

where

I is the identity matrix.

The plastic flexibility matrix D is nonlinear and depends on the slope of the equivalent stress-strain diagram at the "current" state of stress. The computer program used in the analysis automatically incremented the loading, recomputed the matrix D, and printed a history of stresses and strains through the loading range to failure.

Test-Theory Correlation

Results of the nonlinear analysis of the 1/2-inch double lap joint are shown in Figure 108. Normalized adhesive shear stresses (shear stress divided by external load) are plotted as ordinates at stations along the lap length (abscissa). Linear analysis was valid to an external load level of 221 pounds, which was only 8.5 percent of ultimate strength of the joint. At this point, a shear panel in the adhesive reached its proportional limit stress (i. e., point 1 in Figure 107).

A load of 2851 pounds was determined analytically as the ultimate strength of the joint. This load was considered as ultimate because critical elements of the adhesive were developing shear strains comparable to experimental failure strains, and several structural elements unloaded as the external loads were increased. This indicated that a maximum (or relative maximum) joint stiffness has been achieved. As noted on Figure 108, this ultimate load agreed with experimental results within 2 percent.

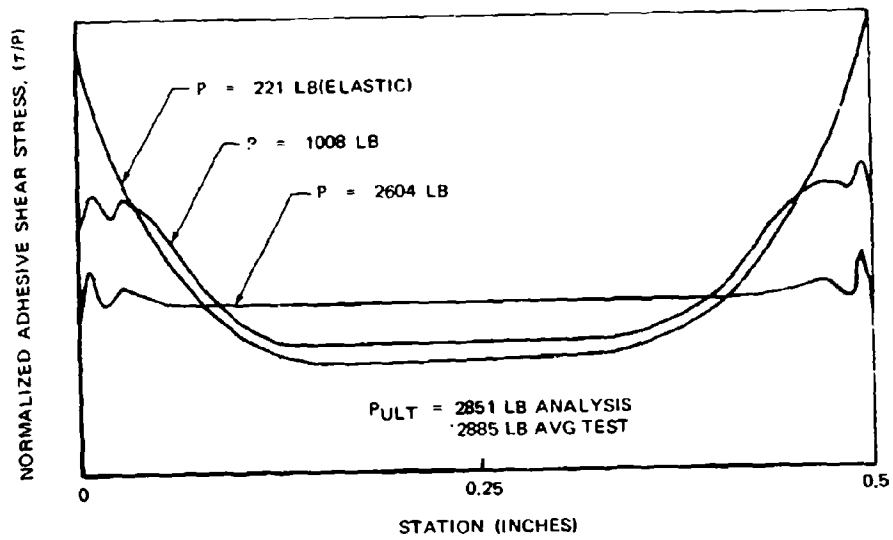


FIGURE 108. NONLINEAR ANALYSIS - 1/2-INCH DOUBLE LAP JOINT

SECTION VII

CONCLUSIONS

Joint weight penalties less than current state-of-the-art penalties in aluminum alloy are feasible for mechanical joints in composite structures. Design practices for composite joints can generally follow the practices established for mechanical and bonded joints in isotropic materials. However, the relatively low shear strength of epoxy resin composites makes this property limiting in the design of many composite joints, both mechanical and bonded.

In terms of weight efficiency, bonded joints are superior to bolted joints, reducing the weight penalty by one order of magnitude. For highly loaded joints, mechanical properties of the adhesive are of prime importance. However, it was found that ultimate shear strength alone was not a good criterion for selection of an adhesive. In cases of strain incompatibility in the adherends, it was demonstrated that improved strength was obtained using an adhesive that exhibited considerable ductility.

In bonded joints of epoxy resin composites with L/t ratios of about 25, interlaminar shear strength of the laminate is the limiting strength. When a ductile adhesive of moderate shear strength (about 6000 psi ultimate) is used, these interlaminar shear failures occur after the adhesive is stressed well into the plastic range. Thus, improvements in interlaminar shear strength of the laminates must be accompanied by improvements in adhesive shear strength for significant gains in bonded joint performance.

Scarf and stepped lap adhesive joints may be scaled up to react the static loads needed in primary structural joints. The scarf joint is superior to the stepped lap joint (and other bonded configurations) in fatigue because of lower stress concentrations in the adhesive. The scarf joint, in theory, has no inherent weight penalty. From a practical design standpoint, however, precision scarf angles less than about 4 degrees are difficult to produce. Therefore, some weight penalty is incurred in local thickening of the joint area to produce the required lap lengths for currently available adhesives and practical scarf angles.

Mechanical fastening is required in demountable joints and numerous stressed and unstressed access doors. In mechanical joints optimum relationships between e/D , s/D , and D/t ratios vary for different laminate patterns because composite strength in shear, tension, and bearing are functions of laminate pattern. For laminates consisting of 50 percent zero-degree plies and 50 percent ± 45 -degree plies, an e/D ratio of about 4.5 is required to develop consistent shear and bearing stresses in unreinforced laminates. This ratio compares to an e/D ratio of about 2 for common structural metals. The composite joint ratios of s/D and D/t are more consistent with metal joint design practices because laminate strengths in tension and bearing are more comparable to metal properties than is shear strength.

Laminate reinforcing, such as metallic shims or laminate buildups, are required in mechanically fastened joints to develop the load intensities required in primary structures for aircraft. Shear-out failures predominated

in plain laminate bolted joints, even when thickness and edge distances were unrealistically large. At low load intensities (about 2000 pounds per inch), double lap bolted joints performed well in fatigue, resulting in fatigue run-outs (10^6 cycles) in many tests. Additional fatigue data are needed for shim-reinforced joints at higher load intensities.

The combination bolted/bonded joint performed well under both static and fatigue load conditions. The presence of the bolt enhanced the performance of the bond, and vice versa. This synergistic effect resulted from a fundamental change in the mode of failure of the joint from the modes observed in similar joints using bolting and bonding separately. The combination joint failed in interlaminar shear and in tension in the laminate at a section through the fastener hole. Similar joints using only bolts failed in shear-out, and similar bonded joints failed in a shear mode at the adhesive/resin interface.

Theoretical techniques for determination of elastic and strength properties of laminates and adhesive joints are in substantial agreement with total results. However, better definitions of material properties and failure criteria are required for adhesives and laminates (especially in interlaminar shear of compound patterns) before analytical techniques can be used with confidence in joint design. Load-deformation characteristics of bolted joints in composites cannot be adequately predicted with linear analysis. These load-deformation characteristics are needed for minimum weight design of multiple fastener joints. At present, semi-empirical methods are the most effective approach to rational joint design in composite structures.

APPENDIX I

SPECIMEN FABRICATION PROCEDURES

Processing and machining methods used in specimen fabrication are described in this appendix under the headings Laminate Processing, Machining and Drilling, and Adhesive Bonding.

LAMINATE PROCESSING

Laminates required in the joint and data specimens fell into four categories: flat panels, tubular laminates, stepped or tapered laminates, and steel shim-reinforced laminates. Some specimens in the first two categories included small amounts of whisker additives to the resin (1 or 2 percent of resin weight). Fabrication procedures used in preparing these laminates are described in the following subsections.

Flat Panels

Flat panels were laminated on a 1/4-inch aluminum alloy plate. The surface of the plate was free of surface scratches and other defects. Most of the panels were made using 0.004-inch Teflon film as a surface parting agent, but acceptable results were also obtained using Ram 225 or Prekote 87-X76 from the Ram Chemical Company or MS-122 Fluorocarbon from the Miller-Stephens Company as mold release agents.

The packages of 3-inch prepregged boron tape were removed from cold storage (0°F) and allowed to stand a minimum of two hours (usually overnight) at room temperature before opening. (This precaution was taken to avoid moisture condensation on the tape.) After opening the packages, sections of tape were cut to proper length and placed face down on clear Teflon film. The paper backing was removed from the tape to expose the 104 glass scrim cloth carrier surface. This surface was laminated face down on the mold. The clear Teflon film allowed close visual location of the butting edges of the 3-inch tape in desired locations. The tape had good tack and retained its position after light pressure was applied. The Teflon film was easily removed prior to locating the next layer of fibers. The 45-degree layers were trimmed to match the edges of the panel. The specified number of plies were laminated by this procedure to meet the drawing requirements.

After completion of layup, an edge dam was located against the edges of boron layup to help control the flow of resin as the material was cured. An aluminum "picture frame" coated with MS-122 Fluorocarbon mold release was used as an edge dam for most of the panels. Silicone rubber and cork rubber sheet were also used successfully as edge dam materials.

As many as 32 plies were required for some specimens, so special care was taken to ensure that the proper sequence and orientation of layers was maintained. A layer check-off sheet was prepared for each laminate that identified the specimens to be made and the fiber orientation for each ply of material. The laboratory technician fabricating the panel recorded each ply of laminate as it was applied to the tool.

BLANK PAGE

One layer of Armalon, a Teflon-coated fabric perforated on approximately 1/2-inch centers, was placed on top of the laminate as a parting film. Glass fiber bleeder cloths were added next to the Armalon in amounts depending on panel thickness. Bleeder cloths were added as follows:

PANEL THICKNESS (IN.)	BLEEDER CLOTH REQUIRED
0.020	1 LAYER 120 GLASS CLOTH
0.040	2 LAYERS 120 GLASS CLOTH
0.060 TO 0.100	1 LAYER 181 GLASS CLOTH
0.100 TO 0.120	1 LAYER 120 GLASS CLOTH 1 LAYER 181 GLASS CLOTH

The perforations in the Armalon allowed volatiles to escape and resin to flow into the bleeder cloth uniformly across the surface of the panel.

One layer of Mylar film was placed over the bleeder cloth and the edge dams. Silicone pressure-sensitive tape was used to secure the edges of the Mylar film to the dam, and the edges of the dam to the mold surface. This was done to restrict resin flow at the panel edges and ensure resin flow only into the glass bleeder cloths. A 0.060-inch-thick aluminum pressure plate, coated with MS-122 Fluorocarbon mold release was placed over the mylar film.

The layup assembly was placed in a Mylar vacuum bag (as illustrated in Figure I-1), evacuated, and checked for leaks. This unit was placed in the autoclave, the pressure was raised to 100 psi, and the vacuum line was opened to the atmosphere. The following curing pressure and temperature cycle was used:

1/2 hour	Atmospheric Pressure	Room Temperature
2 hours	100 psi	200° F
2 hours	100 psi	300° F
1 hour	Post Cure	350° F

The panels were cooled under pressure to below 200° F before removal from the autoclave.

Preceding Page Blank

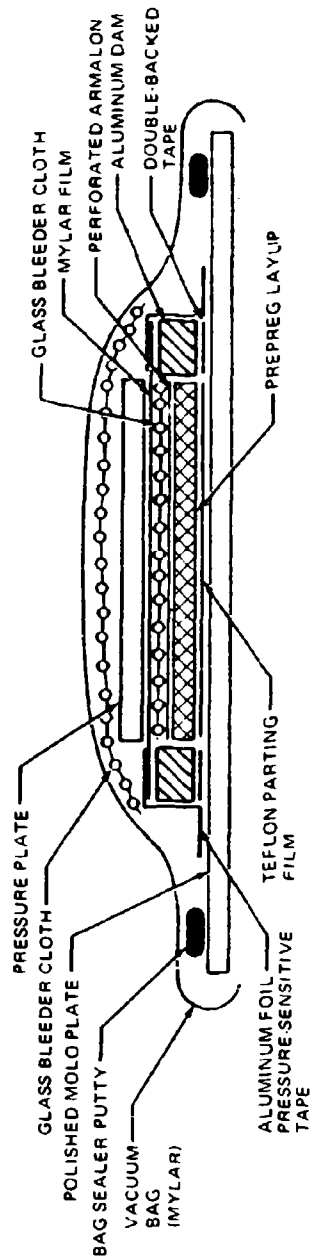


FIGURE I-1. CONTROLLED RESIN BLEED LAYUP DETAIL

Glass laminate specimens were fabricated from 20-end S-HTS glass roving impregnated with the "B"-staged 5505 epoxy resin. The roving was wound on an 11-inch-diameter drum (over a Teflon parting film) to produce broad-goods. A fiber spacing of 0.072 inch per revolution was used. This fiber spacing gave a cured laminate thickness of approximately 0.010 inch per ply. The single layer of roving was cut from the mandrel and laid flat to produce a collimated sheet 10 inches wide and approximately 34 inches long. The flat fiber glass panels were laminated from this material. The specimen fabrication procedure was similar to the boron laminates with the exception of number of layers of material, as specified on the engineering drawings.

Selected specimens contained small amounts of whisker additions to the resin. Two types of whisker mixtures were used as noted in Table I, Section III. These specimens were included in the test program to determine the effects of high-modulus whisker additives on the properties of the composites.

The desired whisker content (1 or 2 percent of resin weight) was obtained as follows:

- The weight of resin (based on an estimated composite resin content of 30 percent) was calculated.
- Whiskers were measured into a tray totaling 1 or 2 percent of this calculated value, as appropriate.
- The whiskers were divided into 23 equal volumes.
- The 23 equal volumes were applied, in turn, between each layer of the 24-ply laminate. A small, stiff brush was used to disperse the whiskers uniformly over the desired area.
- The laminate was cured using the procedure described previously for flat laminates.

After curing, the laminates were examined under a microscope at magnification up to 500X to check the dispersion of whiskers during cure. The whisker dispersion was quite uniform (see Figure 3, Section III).

Tubular Laminates

The compression specimens were fabricated in a tubular configuration in accordance with Drawing Z3824818, Volume II. The specimens were layed up individually on a precision-ground, hard-anodized, aluminum alloy mandrel with an outside diameter of 2.960 inches. The surface of the mandrel was prepared with a layer of polished Simonize wax and a coat of Ram 225 mold release before each layup was begun.

Specimens were fabricated using boron and/or fiber glass-reinforced epoxy laminates. Three-inch tape per DMS 1919A was used for the boron-reinforced specimens. The cutting and layup of the tapes to the prescribed patterns were similar to the flat laminate panels. The major change in

fabrication procedure was a step densification process used during the lamination buildup. After each four layers of lamination were applied to the mandrel, a layer of Armalon parting film was placed around the cylinder. The partial layup was then vacuum bagged and heated to 150° F. This process densified the four-layer laminate and minimized the chance of wrinkles in the completed cylinder. The partial layup was cooled under vacuum pressure, and the vacuum bag and Armalon were removed. This process was repeated until the specimen wall was built up to the desired pattern and thickness. After the final layer was applied, Armalon parting film was placed over the part and 1-inch Mylar shrink tape was wrapped around the Armalon. The cylinder was placed in a vacuum bag and cured in the autoclave using the standard curing cycle. Fiber glass-reinforced cylinders were fabricated in a similar manner using the drum-wound broad-goods described previously.

The combination boron-fiber glass cylinders were also fabricated in a similar manner, but materials of a different form were used. The fiber glass layers were circumferential wraps using prepregged 20-end roving as supplied by the vendor. These layers were applied directly to the cylinder with 5 pounds tension in the roving and a spacing of 0.072 inch per revolution.

A 1/8-inch-wide collimated boron tape (without glass scrim) was wrapped onto the 11-inch-diameter drum at a spacing of 0.104 inch per revolution. This spacing resulted in a slight overlap (no gaps) in the parallel boron fibers. The wound tape was cut from the mandrel and laid flat, as with collimated boron fiber sheet. This sheet material was cut to size for each layer of material required in the cylinder. The step-densification procedure was used for each four layers. The bagging and curing techniques were the same as for the other cylinders.

Whiskers were applied in selected configurations of the compression specimens as specified on the engineering drawing. These whiskers were applied using the technique described previously for the flat laminate panels.

Stepped or Tapered Laminates

Stepped or tapered laminates were required on several of the joint specimens. Stepped lap joints were called for on Drawings Z3824830 and Z3824850 (Volume II). Tapered laminates were required on the composite-reinforced bolted specimens (Drawings Z5824838 and Z5824839) and at the grip ends of the fatigue specimens (Drawings Z3824849 through Z3824852). These specimens were laminated on machined aluminum alloy molds to maintain dimensional accuracy throughout the specimen thickness.

The stepped lap specimens were laminated in place on aluminum alloy plates with precision-machined step length and depth dimensions. Ram Prekote 87-X76 mold release was used as a parting agent. The layup procedure was similar to the flat panels, except that special care was taken to butt the individual layers snugly against the machined steps of the layup tool. Edge dams were placed on three sides of the completed layup, and the stepped tool served as the fourth side. The layups were prepared for curing using bleeder cloths and vacuum bagging as described previously.

Two-piece aluminum molds were machined to match the tapered end built-up areas for each tapered specimen configuration. The molds were of sufficient length to make the required number of specimens with adequate trim allowances between specimens and at the panel edges.

The mold surface preparation consisted of two coats of polished Simonize wax and one coat of Ram Prekote 87-X76 mold release to ensure laminate release from the tool after curing. One-half of the layup was made on each half of the two-piece mold. The layups were made using 3-inch prepregged boron tape or drum-wound fiber glass broad-goods described previously. A layer check-off sheet was prepared for each panel to ensure that the plies were applied in the proper orientation and sequence. The laboratory technician recorded each ply of the laminate on the check-off sheet as it was applied to the layup.

The layers in the built-up areas were uniformly stepped in length for a smooth transition in specimen thickness. A typical taper consisted of an 0.080-inch change in thickness over a 1.5-inch length. Because this change in thickness involved 16 layers of boron tape, each layer of buildup was made 3/32-inch longer than the previous one.

Upon completion of the layup halves, the laminates were trimmed flush with the edges of the laminating tools and the two halves mated. The edges of the tools were aligned to coordinate the locations of the tapered areas in the layup halves. End plates were coated with MS-122 Fluorocarbon mold release and located at the four edges of the tool to cover the exposed edges of the layup. This was equivalent to the dam around the edges of the flat laminate panels. The edges were sealed with masking tape to maintain the alignment and minimize resin flow from the edge of the panel during cure. The assembly was vacuum bagged as shown in Figure I-2 and cured in the conventional manner. Post cure of the panels was always accomplished on the laminating tool.

Steel Shim-Reinforced Laminates

Steel shim reinforcing was specified on Drawings Z5824840, Z5824841, Z3824858, and Z3824860 (Volume II). The shim materials were 17-7PH, PH15-7 Mo, and Type 301 full-hard stainless steel.

The PH steels were heat treated to 210,000 psi, cleaned by sandblast, and rinsed in MEK. The Type 301 stainless steel was cleaned by acid etch. The shim surfaces were primed with Shell 9261 Epon R primer and dried at 150°F for one hour before installation in the laminates. In these specimens the outer plies of material were continuous across the steel shims. The stainless steel comprised the entire change in specimen thickness in the built-up area. This is in contrast to the tapered buildup of the outer layers in the tapered composite specimens.

The preparations for curing the panel were similar to the tapered laminates described previously. The vacuum bagged assembly, ready for autoclave cure, is illustrated in Figure I-3. Post cure was accomplished on the laminating tool.

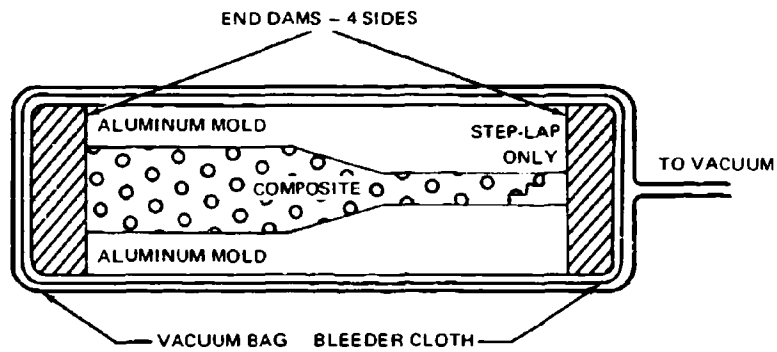


FIGURE I-2. COMPOSITE-REINFORCED PANEL LAYUP READY FOR AUTOCLAVE CURE

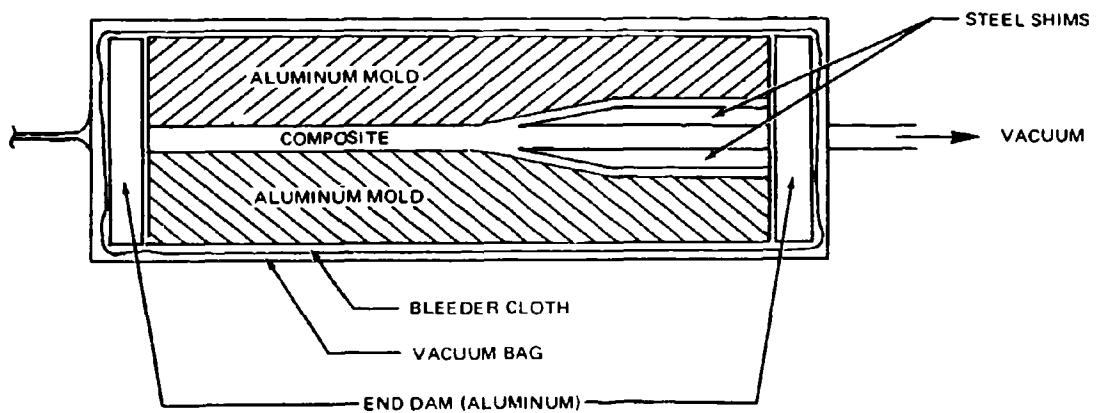


FIGURE I-3. STEEL SHIM-REINFORCED PANEL LAYUP READY FOR AUTOCLAVE CURE

MACHINING AND DRILLING

Each of the laminate details required machining at the boundaries for compliance with drawing dimensions. The bolted joint specimens also required fastener holes. Methods used to machine and drill the laminates, both with and without steel shim reinforcing, are described in this section.

Machining

Straight cuts in both plain and steel shim-reinforced laminates were made using a 12-inch-diameter diamond abrasive wheel at 1500 rpm. A continuous spray of water soluble oil was used as a coolant and lubricant. The specimens were hand-fed past the wheel at a slow rate. The specimens containing steel shims were difficult to cut using hand-feed methods, but satisfactory cuts were obtained as shown in Figure I-4. Improved cuts were obtained using machine feed at a rate of 1-1/8 inches per minute.

The scarf joint coupons of boron and glass reinforcement were machined to the proper scarf angle using a six-inch-diameter electro-bonded diamond wheel on a horizontal bed mill. A water soluble oil was sprayed over the cutting surface and wheel to act as a coolant and lubricant. The wheel was turned at 1330 rpm with a feed rate of 7 inches per minute. The machining setup is shown schematically in Figure I-5, and finished details are shown in Figure I-6.

The compression cylinders were initially cut to approximate length using a water cooled diamond cutoff wheel. The cylinders were then mounted on lathe centers using an expanding internal holding fixture. While the cylinder was rotated on the lathe centers the ends were machined square and parallel (within the precise drawing tolerance) with a water cooled diamond abrasive wheel turning at 1500 rpm.

The fatigue specimens were designed with reinforced gripping provisions for a Sonntag (or Krause) fatigue machine to ensure failures in the joint areas. For increased strength, the grip areas were tapered in both thickness and width dimensions. The taper in thickness was provided by two-piece machined aluminum alloy molds described earlier. Dimensional control of the composite specimen width was provided with a machined profiling setup in a conventional vertical milling machine, as shown in Figure I-7. The specimen shape was controlled by following a metal pattern with a tracing stylus as shown. The cured composite laminate stock was removed with a 6-inch-diameter diamond cutter, as shown in Figure I-8. A spindle speed of 3400 rpm and a feed rate of 30 inches per minute resulted in excellent machine cuts. Typical finished details are shown in Figure I-9. The profiling was originally accomplished using a vaporized coolant spray, (Figure I-8). This technique did not adequately confine the abrasive cutting dust, which could damage the machine's working surfaces, from the boron laminates. A coolant-flood technique was used to confine the cutting dust in subsequent profiling operations.



FIGURE I-4. EDGE DETAILS FOR STEEL SHIM-REINFORCED SPECIMEN

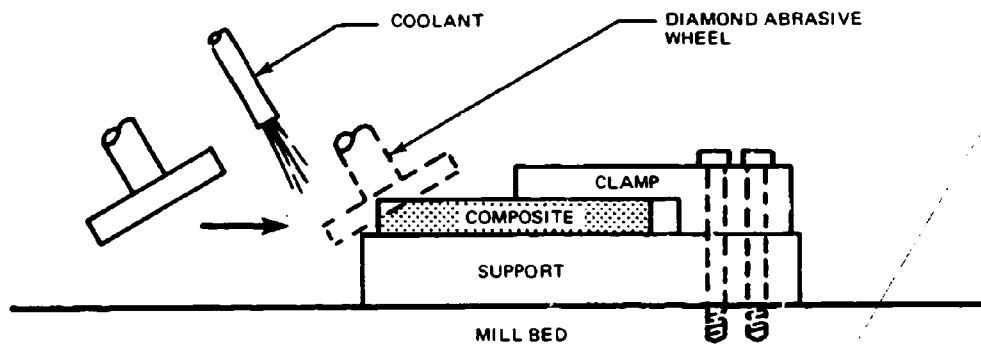


FIGURE I-5. SCARF JOINT MACHINING SETUP



FIGURE I-6. SCARF JOINT SPECIMEN DETAILS AFTER MACHINING

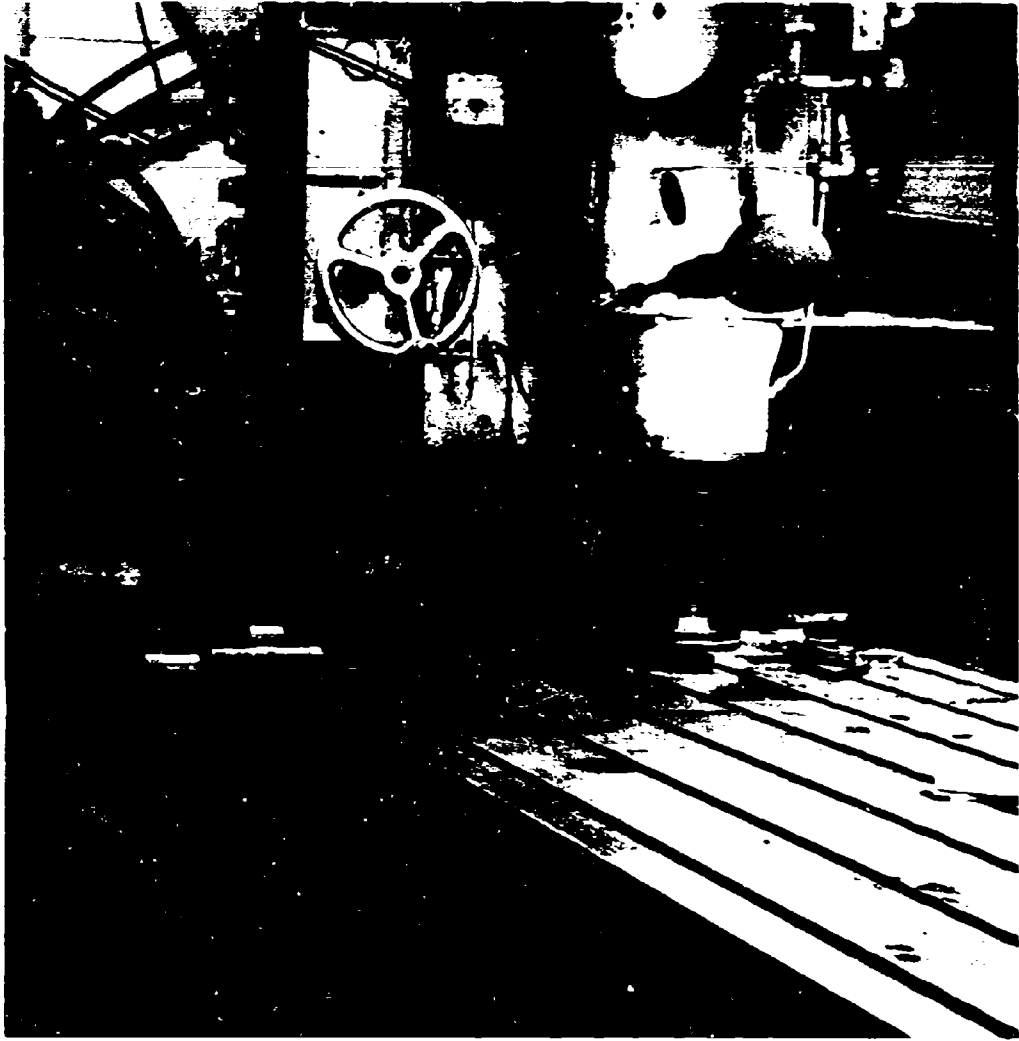


FIGURE I-7. PROFILING SETUP FOR FATIGUE SPECIMEN MACHINING

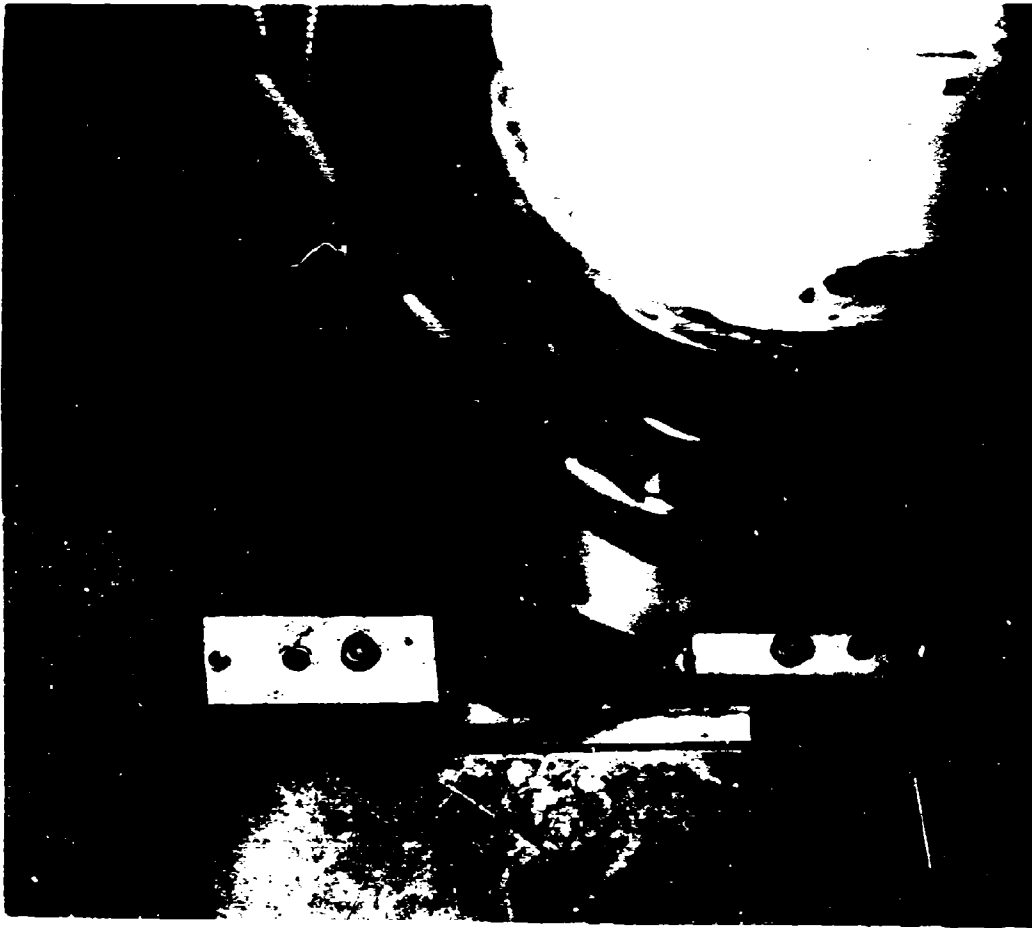


FIGURE I-8. FATIGUE SPECIMEN PARTIALLY MACHINED



FIGURE I-9. FINISHED DETAILS FOR STEPPED-LAP FATIGUE SPECIMEN

Radius cuts on laminates containing steel shims were produced on a surface grinder. A silicon carbide wheel (GC 100-H11-VR manufactured by Carborundum) was used to rough cut the required shape, and a resin-bonded diamond wheel (BT-71-CX-80/100) was used for finished dimension cuts. The wheels were turned at 1800 rpm and cooled with a water-soluble oil. The removal rate was 0.002 to 0.005 inch of depth per pass across and/or along the specimen edge. The grinding wheels were moved constantly back and forth across a stack of four to six specimens that were machined simultaneously. The traverse feed rate was by hand. This technique produced an excellent finish as shown in Figure I-10.

Drilling

Composite laminate specimens (without steel shims) were drilled on a conventional drill press using water cooled diamond core drills of proper diameter from the Felker Manufacturing Company. Drill jigs were used to locate the holes and center the core drills. Plate glass was used as a backup member to minimize edge delamination due to drill breakout.

For 0.190- and 0.250-inch-diameter holes, reasonable hole quality was produced in both fiber glass and boron/epoxy steel-shimmed specimens using a solid carbide twist drill in a Bridgeport milling machine at 2000 rpm. A manual feed and water coolant were used. The specimens were clamped firmly in a special drill jig with a bushing to locate the hole and support the drill bit. A mild steel backup member, 1/16-inch thick, was also clamped in the setup to prevent delamination of the specimen at drill breakout. The surface of each specimen was first center-drilled, using a full-size drill in the locating bushing. An undersize drill was then centered in the hole and used to penetrate the buildup composite and the 1/16-inch steel backup sheet. A full-size drill was then carefully fed through for final sizing of the hole.

Examination of the holes after drilling showed slight damage in some instances in the form of minor delamination and chipped fibers adjacent to the hole. These imperfections did not adversely affect the strength of the joints during test. An enlarged picture of a hole condition after drilling is shown in Figure I-11.

The 1/2-inch-diameter holes in the steel shim-reinforced fatigue specimens were produced using a 118-degree included angle, high-speed steel drill. Both surfaces of the specimen were supported by in-line drill bushings to minimize edge delamination of the hole. The holes were drilled at 110 rpm using a flood of water-soluble oil as a coolant and a feed rate of 0.005 inch per revolution.

The hole quality was acceptable for this application, since no failures occurred at the hole during test. However, burrs were produced in the steel shims as shown in Figure I-12.



FIGURE I-10. EDGE DETAIL OF STEEL SHIM-REINFORCED FATIGUE SPECIMEN



FIGURE I-11. DETAILS OF HOLE DRILLED WITH CARBIDE BIT IN STEEL SHIM-REINFORCED SPECIMEN



FIGURE I-12. DETAILS OF HOLE DRILLED WITH HIGH-SPEED STEEL DRILL IN STEEL SHIM-REINFORCED SPECIMEN

ADHESIVE BONDING

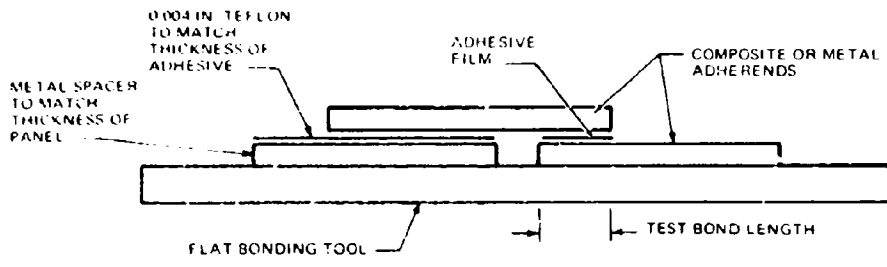
During fabrication of the adhesive specimens, special attention was devoted to cleaning the detail parts. The metal components were cleaned with a hot alkaline cleaner and a sulfuric acid-sodium dichromate etch. The laminate bonding surfaces were cleaned in a three-step process as follows:

1. The surface was cleaned with a solution of Ajax household cleanser and rinsed with water.
2. The bonding surface was scuff-sanded.
3. The surface was washed with MEK and dried in an oven.

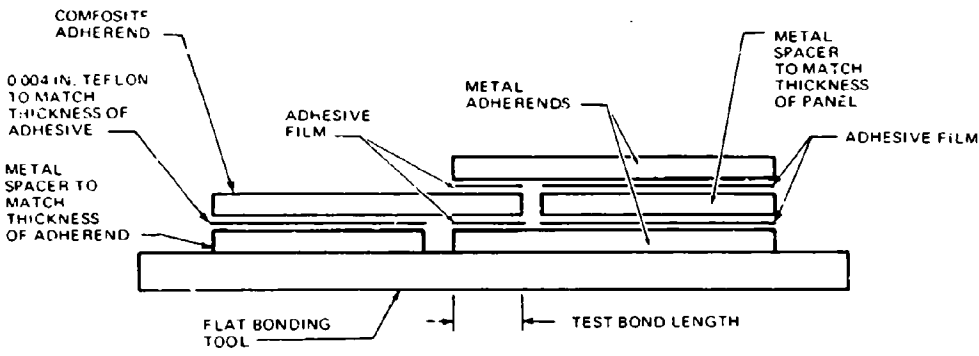
Special bonding tools were used for each type of specimen to locate the details in correct position during the cure cycle. The bonding tools are shown schematically in Figure I-13 for each type of adhesive joint specimen. The Shell 951 adhesive, used in most of the specimens, was cured in the autoclave at 50 psi and 350°F for one hour.

The variable stiffness adhesive specimens (Z3824854) were designed using a ductile adhesive (Shell 951) at the joint extremities, and a high-strength adhesive (AF130) in the joint center. These adhesives were chosen both for their engineering properties and their common curing cycles (i. e., 50 psi, 350°F for one hour). The AF130 adhesive was cut to size for each coupon and located in position on the metal detail. The adhesive had adequate tack and remained in position. The Shell 951 adhesive was cut to 3/8-inch width to allow a 1/8-inch lap outside the 1/4-inch bond area. The adhesive did not have adequate tack and was secured in position on the metal details by a spot heat tack with the tip of a warm soldering iron. The rest of the coupon details were assembled, placed under a vacuum bag, and cured in an autoclave at 50-psi pressure for one hour at 350°F.

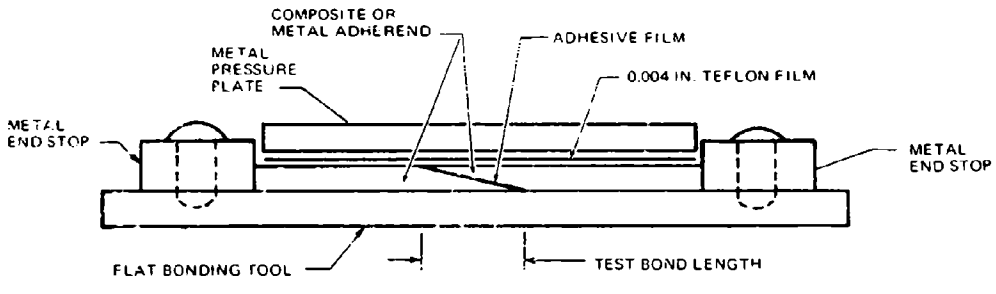
Aluminum tabs were secondarily bonded to the composite surfaces that were gripped in the test machine. The tabs were cleaned by standard metal bond procedures. The surface of the composite was recleaned with MEK solvent wipe. Initially, Lefkowitz 109 cold-set epoxy was used as the adhesive system, and the bonds were cured at room temperature. Some of these bonds failed during test, so the remainder of the tabs were bonded using Narmco 252 adhesive systems for higher strength. This adhesive was cured at 250°F for 90 minutes under 50 psi autoclave pressure.



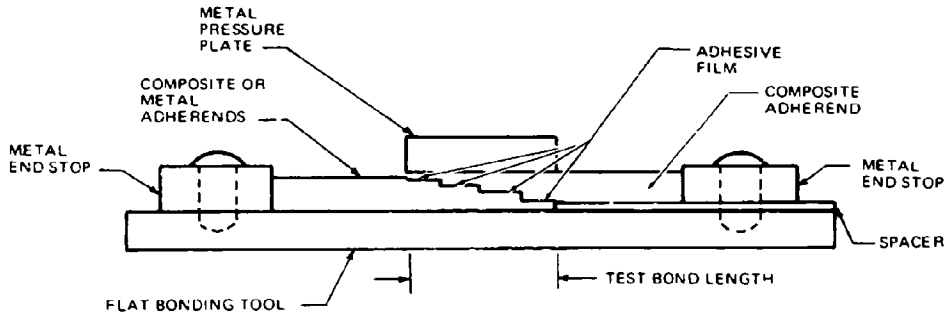
SINGLE LAP JOINT



DOUBLE LAP JOINT



SCARF JOINT



STEPPED-LAP JOINT

FIGURE I-13. ADHESIVE JOINT BONDING TOOLS

APPENDIX II

SHELL 951 ADHESIVE CHARACTERISTICS

Shell 951 adhesive was supplied by the Shell Chemical Company, Adhesives Department, Pittsburg, California. This adhesive has been thoroughly evaluated and has established a long and successful production background. The adhesive for the program was ordered, purchased, and tested by standard quality control procedures to meet the requirements of Douglas Materials Specification (DMS) 1808C Adhesive, Epoxy-Nylon. It is a nontacky, unsupported epoxy-nylon film with a nominal thickness of 10 mils. The material meets the requirements of Federal Specification MMM-A-132, Type I, Class I, and resists common aircraft fluids, salt water spray, water, and high humidity. The film can be stored in a sealed container at 40° F for six months and meet all of the requirements of DMS1808C.

The surfaces to be bonded must be thoroughly cleaned by established procedures. The bonding pressure must be sufficient to give positive contact between the surfaces being joined. Extra pressure will squeeze out the melted adhesive and thus, affect bondline thickness and strength. The pressure required for acceptable curing varies from as low as 10 psi for well matched small details to 100 psi for larger parts that require some force to obtain bond line contact. Pressure over 100 psi may cause excessive adhesive flow and is not advised.

The normal curing cycle for Shell 951 is 350° F bond line temperature for one hour in an autoclave at 50 psi pressure. The adhesive melts at 315° F, flows, and wets the bonding surfaces. The rate of polymerization is very slow. Curing is not recommended below 325° F. Curing temperatures up to 400° F are acceptable if the materials being bonded are not degraded by the higher temperature.

Heat-up time is not critical in developing high-strength properties in faying surface bonds. However, honeycomb to skin bond line temperature must be raised to 350° F within 30 minutes. The strength of a sandwich bond is significantly reduced by a slow heat-up rate.

DMS1808C requirements and producers data for strength, creep properties, and environmental resistance are shown in Table II-1.

TABLE II-1.
STRENGTH CHARACTERISTICS FOR SHELL 951 ADHESIVE

TEST	EXPOSURE CONDITIONS			DMS 1808C MINIMUM REQUIREMENT	SHELL CHEMICAL COMPANY DATA	TEST SPECIMEN CONFIGURATION
	TEMP (°F)	TIME (HR)	STRESS (PSI)			
LAP SHEAR STRENGTH (PSI)	-67	-	-	2000	6500	1/2 INCH SINGLE LAP (MIL-A-5090)
	0	-	-	-	7200	
	75	-	-	3600	6300	
	180	-	-	-	4270	
PEEL STRENGTH (LB/IN.)	250	-	-	1000	2170	"TEE" PEEL SPECIMEN (MIL-A-5090)
	-67	-	-	3	38	
	0	-	-	-	63	
	75	-	-	55	86	
MAXIMUM CREEP DEFORMATION (INCH)	160	-	-	-	60	1/2 INCH SINGLE LAP (MIL-A-5090)
	180	-	-	8	-	
	75	200	250	0.00025	-	
	180	200	250	0.00100	-	
ENVIRONMENTAL RESISTANCE - STRENGTH AFTER EXPOSURE (PSI) MIL-H-3136	75	200	250	-	0.0022	1/2 INCH SINGLE LAP (MIL-A-5090)
	75	192	1600	-	0.0042	
	75	192	800	-	-	
	75	2400	-	2000	-	
	75	188	-	-	6250	
	75	2400	-	2250	-	
	75	188	-	-	6300	
	75	720	-	2250	6200	
	100 (90% RH)	720	-	2250	6600	
	120 (95% RH)	1440	-	2250	-	
SKYDROL 500 FLUID HYDRAULIC FLUID MIL-H-5650	75	720	-	-	5950	1/2 INCH SINGLE LAP (MIL-A-5090)
	160	720	-	2250	-	
	75	188	-	-	6400	
	75	2400	-	2250	-	

REFERENCES

1. Tsai, S. W., "Strength Characteristics of Composite Materials," NASA Report CR-224, 1965
2. Hill, R., The Mathematical Theory of Plasticity, Oxford University Press, England, 1950
3. Schofield, B. E., "A Computer Program for Performing a Stress or Strength Analysis on Multilayered Laminated Composites," Douglas Aircraft Company Technical Report DAC 33893, August 1967
4. Noyes, J. V., and B. H. Jones, "Crazing and Yielding of Reinforced Composites," Technical Report No. AFML-TR-68-51, March 1968
5. "Structural Airframe Application of Advanced Composite Materials," Fourth Quarterly Progress Report for Contract AF33(615)-5257, June 1967
6. Ashizawa, M. "Compendium of Boron Composite Test Data," Douglas Aircraft Company Report DAC-66637, 24 May 1968.
7. Lunsford, L. R., "Shear Tests for Adhesive Bonds," Symposium on Standards for Filament-Wound Reinforced Plastics, ASTM Special Technical Publication No. 372, published by the American Society for Testing and Materials, Philadelphia, Pennsylvania, June 1962
8. Franzblau, M. C., and J. L. Rutherford, "Study of Micromechanical Properties of Adhesive Bonded Joints," Second Quarterly Progress Report; Contract DAAA 21-67-C-0500, December, 1967
9. Clark, G., "Fabrication Techniques for Advanced Composite Attachments and Joints," Quarterly Report for Contract No. F33615-67-C-1802, September 1967
10. "Structural Airframe Application of Advanced Composite Materials," General Dynamics Fifth Quarterly Progress Report for Contract AF33(615)-5257, September 1967
11. Wilson, F., "Research on Resin-Impregnated, Collimated Boron Filaments and Improved High-Modulus, High-Strength Filaments and Composites," Whittaker Corporation, AFML-TR-67-20, January 1967
12. Saffire, V. H., "Application of Advanced Fibrous Reinforced Composite Materials," General Electric, AFML-TR-66-272, September 1966

REFERENCES (Continued)

13. "Exploratory Application of Filament-Wound Reinforced Plastics for Aircraft Landing Gear," Bendix Corporation, AFML TR 66-309, December 1966.
14. Kutscha, D., and K. E. Hofer, "Feasibility of Joining Advanced Composite Flight Vehicle Structures," IIT Research Institute Reports published under Contract No. AF33(615)-3962, 1 May 1966 through 1 July 1967.
15. Nadler, M. A., and S. Y. Yoshino, "Adhesive Joint Strength as a Function of Geometry and Material Parameters," SAE paper No. 670856, 1967.
16. Warren, D. S., R. A. Castle, and R. C. Gloria, "An Evaluation of the State of the Art of Thermo-Mechanical Analysis of Structures," Technical Report No. WADD-TR-61-152, Aeronautical Systems Division, Air Force Systems Command, Wright-Patterson Air Force Base, Ohio, January 1962.
17. Lobbett, J. W., and E. A. Robb, "Thermo-Mechanical Analysis of Structural Joint Study," Technical Report No. WADD-TR-61-151, Aeronautical Systems Division, Air Force Systems Command, Wright-Patterson Air Force Base, Ohio, January 1962.
18. Goodwin, J. F., "Research on Thermo-Mechanical Analysis of Brazed or Bonded Structural Joints," Technical Report No. ASD-TDR-63-447, Aeronautical Research Division, Air Force Systems Command, Wright-Patterson Air Force Base, Ohio, September 1963.
19. Hahn, K. F., and D. F. Fouser, "Methods for Determining Stress Distribution in Adherends and Adhesives," Symposium of Adhesives for Structural Applications, M. J. Bodnar, 1961.
20. Teodosiadis, R., D. S. Warren, and P. H. Denke, "Matrix Methods for Inelastic Structures," Report No. LB-31941, Douglas Aircraft Company, November 1964.
21. Teodosiadis, R., "Plastic Analysis of a Bonded Composite Lap Joint," Report No. DAC-67836, Douglas Aircraft Company, May 1969.
22. Hille, A. A., "Joint Design Optimization by Discrete Element Computer Techniques," Report No. LB-33964, Douglas Aircraft Company, October 1967.
23. Pickard, J., et al., "FORMAT - Fortran Matrix Abstraction Technique," AFFDL-TR-66-207, Volumes V, VI and VII. Air Force Flight Dynamics Laboratory, Wright-Patterson Air Force Base, Ohio, 1968.

BIBLIOGRAPHY

1. August, A., "Advanced Composite Wing Structures," Grumman Aircraft Engineering Corporation, Contract No. F33615-68-C-1301, First, Second and Third Quarterly Reports, May 1968, August 1968, and November 1968. Also sub-report "Preliminary Analysis and Optimization Methods," Report No. AC-SM-7843, August 1968.

Theory and test results are given for bonded lap joint, flatwise tension, and short-beam sandwich specimens. The design of a multiple plate stepped shim joint is included.

2. Bodnar, M. J., "Symposium on Adhesives for Structural Applications," held at Dover, N. J., September 1961, Picatinny Arsenal.
3. Bodnar, M. J., "Structural Adhesives Bonding," 1966, Interscience Publishers, (John Wiley & Sons, New York), Symposium held at Stevens Institute of Technology, Hoboken, N. J., September 1965, sponsored by Picatinny Arsenal.
4. Brinchmann, A., "Segmented Fiberglass Motor Case Joint Design and Analysis," Thiokol Chemical Corporation, AIAA 6th Structure and Materials Conference, 1965.

A multishim joint is described and analyzed.

5. Broutman, L. J., "Glass-Resin Joint Strengths and Their Effect on Failure Mechanisms in Reinforced Plastics," IITRI, Society of Plastic Engineers Regional Technical Conference, Seattle, July 1965.
6. Bryant, R. W., and Dukes, W. A., "The Effect of Joint Design and Dimensions on Adhesive Strength," SAE Paper 670855, Aeronautic and Space Engineering and Manufacturing Meeting, Los Angeles, October 1967.

Includes investigation of adhesive thickness and strain-rate.

7. Clark, G. A., and K. I. Clayton, "Structural Techniques for Joining Filamentary Composites," North American Rockwell Paper No. 68-1038, Columbus Division, AIAA 5th Annual Meeting and Technical Display, Philadelphia, October, 1968.
8. Clark, G. A., "Structural Composites - Fabrication Techniques for Advanced Composite Attachments and Joints," North American Rockwell Technical Management Reports, Nos. 1 through 4, Columbus Division, Contract No. F33615-67-C-1802, October 1967 - July 1968.

Particular major joints are discussed, together with lap and scarf bonded joints and bolted lap joints. Test results for variable adhesive joints are given.

9. Cole, B. W., J. P. Wong, and A. L. Courtney, "Development of the Shim Joint Concept for Composite Structural Members," The Bendix Corporation, Technical Report No. AFFDL-TR-67-116, August 1967.

Theoretical and test results are given for multishim joints. Parametric studies yield empirical design data. Photographs of failed specimens are included.

10. Crilly, E. R., "Producibility Considerations in Adhesive Bonded Structures," Lockheed-California Company, SAE Paper No. 670857, Aeronautic and Space Engineering and Manufacturing Meeting, Los Angeles, October, 1967.
11. Dallas, R. N., "Mechanical Joints in Structural Composites," Lockheed-California Company, 12th National SAMPE Symposium, October, 1967.

Test results are given for glass laminates reinforced by a variety of shim materials. Riveted and bolted joints were tested.

12. DeBruyne, N. A., and R. Houwink, "Adhesions and Adhesives," Elsevier Publishing Company, 1951.
13. Eickner, H. W., "Basic Shear Strength Properties of Metal-Bonding Adhesives as Determined by Lap-Joint Stress Formulas of Volkerson, Coland and Reissner," Forest Products Laboratory Report No. 1850, August 1955.
14. Eickner, H. W., "Weathering of Adhesive-Bonded Lap Joints of Clad Aluminum Alloy," Forest Products Laboratory, WADS Technical Report 54-447, Part II, December 1956.
15. Forest, J. D., and J. L. Christian, "Development and Application of Aluminum-Boron Composite Material," General Dynamics - Convair Division Paper No. 68-975, AIAA 5th Annual Meeting and Technical Display, Philadelphia, October, 1968.

Strength of rivets, spotwelds, and lockbolts in aluminum-boron composites are given.

16. Frocht, M. M., and H. N. Hill, "Stress-Concentration Factors Around a Central Circular Hole in a Plate Loaded Through a Pin in the Hole," Transactions of the American Society of Mechanical Engineers, 62: A-5, March 1940.
17. Gehring, R. W., and C. H. Maines, "A Redundant-Force Method for the Inelastic Analysis of Mechanically Fastened Joints," Report NAEC ASL 1103, Aeronautical Structure Laboratory, Naval Air Engineering Center, Philadelphia, January, 1967.
18. Goberdhan, C. B., "Advanced Composites for RA-5C Leading Edge," North American Rockwell, Columbus Division, Cooperative IR&D Program, Status Report No. 6 (NR 68H-261), January, 1968.
19. Goland, M., and E. Reissner, "The Stresses in Cemented Joints," Journal of Applied Mechanics, March 1944.

20. Gorman, F., "Review of Motor Case Materials and Fabrication Techniques for Large Solid Motors," AIAA/ASME 8th Structures, Structural Dynamics and Materials Conference, Aerospace Corporation, March 1967.

This report reviews composite segmented joints under development by various companies.

21. Gnapp, J. I., "Measurements of Moments at Edges of Adhesive Lap Joints Between Glass-Reinforced Plastic Laminates," Picatinny Arsenal Technical Memorandum 1932, September, 1965.
22. Grimes, G. C., "Investigation of Structural Design Concepts for Fibrous Aircraft Structures," Southwest Research Institute, Contract No. AF 33(615)-2502, Report No. AFFDL-TR-67-29, Vol. I, February, 1968.
23. Hahn, K. F., "Stress Distributions in the Adherends of Bonded Lap Joints," Douglas Aircraft Company Report No. SM-410010, March 1961.
24. Harvill, W. E., "Development Program for Boron Leading Edge Slat for C-5A Aircraft," Lockheed Georgia Company, Contract No. F33657-68-C-0900, First through Fourth Quarterly Reports, May 1968 - February 1969.
25. Hoffstedt, D., "Research and Development of Helicopter Rotor Blades Utilizing Advanced Composite Materials," Boeing-Vertol Division, Contract No. AF33(615)-5275, First through Sixth Quarterly Reports, Nos. D8-0471-1 through D8-0471-6, to December 1967.
26. Hughes, E. J., and J. L. Rutherford, "Study of Micromechanical Properties of Adhesive Bonded Joints," General Precision Systems Inc., Contract No. DAAA21-67-C-0500, First through Third Quarterly Progress Reports.

Contains accurate measurements of bulk adhesive properties.

27. Hughes, E. J., "On Measuring the Properties of Adhesives in Bonded Joints," 14th National SAMPE Symposium, November 1968.
28. Jacobson, H. R., "Development of a Fiberglass Segmented Rocket Motor Case," Douglas Aircraft Company, MSSD, Contract No. AF 04(611)-8184, Report No. AFRPL-TR-65-79, July 1965.
29. Kuenzi, E. W., and G. H. Stevens, "Determination of Mechanical Properties of Adhesives for Use in the Design of Bonded Joints," Forest Products Laboratory Report No. FPL-011, September 1963.
30. Kutscha, D., "Mechanics of Adhesive Bonded Lap-type Joints: Survey and Review," IIT Research Institute, Contract No. AF33(657)63-358, Technical Report No. ML-TDR-64-298, December 1964.

31. Lackman, L. M., "Aircraft Structural Design Manual - Advanced Composites," North American Rockwell - Los Angeles Division, Contract No. F33615-68-C-1489, First through Fourth Quarterly Progress Reports, to March 1969.
32. Lubkin, J. L., "The Stress Distribution in Adhesive Joints," Final Report for Contract NOrd-13383, Department of the Navy, Bureau of Ordnance, September 1953.
33. Lunsford, L. R., "Shear Tests for Adhesive Bonds," Symposium on Standards for Filament Wound Reinforced Plastics, ASTM Special Technical Publication No. 327, published by the American Society for Testing and Materials, Philadelphia, Pennsylvania, June 1962.
34. McClaren, S. W., C. E. Swindlehurst, and G. Pascador, "Investigation of Boron Composite Integrally Stiffened Panels and Power Transmission Shafting," LTV, Vought Aeronautics Division, Technical Memorandum 2-53420/8TM-10, Presented to AFML IR&D Status Review, March 1968.
35. Palmer, R. J., "Bolted Joint Strength of Filament Wound Flat Panels," Douglas Aircraft Company Laboratory Report LR-AD-2075, May 1964.
36. Palmer, R. J., "Preliminary Report on Fiberglass Joint Strength," Douglas Aircraft Company Report No. LB-32467, November 1965.

A number of means of reinforcing bolted joints in composites were evaluated. Bushed, shim-reinforced, and built-up edge joints were tested. The most successful method was that of increasing edge thickness by the addition of ± 45 degree layers.

37. Pinckney, R. L., "Fabrication Techniques and Materials for High-Modulus, Filament-Reinforced Composites," The Boeing Company, Contract No. AF33(615)-3319, Report No. AFML-TR-67-399, December 1967.

Contains pin-bearing specimens and designs of particular joints.

38. Reinhart, T. J., G. Y. Young, and J. A. Cherry, "Laminated Adhesive Bonded Structures," 14th National SAMPE Symposium, November 1968.
39. Richards, W. J., "Development of Analysis Methods for Composite Structural Joints," Douglas Aircraft Company Report DAC-67114, September 1968.
40. Ris, D., "Future Requirements for Adhesive Systems," C.I.B.A. Bonded Structures Division, Aircraft Engineering, November 1967.
41. Rogers, C. W., et al., "Structural Airframe Application of Advanced Composite Materials," General Dynamics - Fort Worth Division, Contract No. AF33(615)-5257, First through Eighth Quarterly Progress Reports, July 1966 - June 1968.

An important source of bolted joint test result information.

42. Schaefer, W. H., "Evaluation of the Structural Behavior of Filament-Reinforced Metal Matrix Composites," General Dynamics - Convair Division, Contract No. F33615-67-C-1548, Progress Reports 1 through 5, Report No. GDC-AVP 67-001, June 1967 - July 1968.
43. Shuford, D. M., J. F. Rudy, and J. J. Damico, "A New Method of Pressure Control for Adhesive Bonding," Martin Marietta Corporation, 14th National SAMPE Symposium, November 1968.
44. St. Germain, F., and R. E. Helm, "Boron Epoxy Composite F-5 Main Landing Gear Strut Door," Northrop Norair, Cooperative IR&D Program Status Report No. 2, March 1968.

Test results are given for lap, scarf, and butt joints.

45. Szepe, F., "Strength of Adhesive-Bonded Lap Joints with Respect to Change of Temperature and Fatigue," Second SESA International Congress on Experimental Mechanics, Washington, D. C., September 1965.
46. Watson, J. C., "Boron-Epoxy Rudder Program Interim Report," The McDonnell Company Report G. 100, Revised October 1968.

Contains test results for lap joints bonded with FM-96.

47. Wegman, R. F., and A. T. Devine, "Adherend Mechanical Properties Limit Adhesive Bond Strength," Picatinny Arsenal, 14th National SAMPE Symposium, November 1968.

A plateau in the Load vs. (L/t) curve is shown to occur at 55 percent of the yield strength of the adherend.

48. Wilson, F. M., "Further Research on Resin-Impregnated, Collimated Boron Filaments and Improved High-Modulus, High-Strength Filaments and Composites," Whittaker Corporation, Contract No. F33615-67-C-1607, First through Fourth Quarterly Progress Reports, June 1967 - March 1968.
49. Yurenka, S., "Investigation of Advanced Filament Wound Aircraft Landing Gear Structures," Douglas Aircraft Company, Contract No. F33615-67-C-1717, First through Third Quarterly Reports, August 1967 - February 1968.
50. Yurenka, S., "Douglas Boron Flap," Douglas Aircraft Company Report No. DAC-66929, December 1968.

Contains test results for bonded double lap joints.

51. "Analytical Design Methods for Aircraft Structural Joints," LTV, Vought Aeronautics Division Progress Reports for Contract F33615-17-C-1339.

52. "Evaluation of Test Techniques for Advanced Composite Materials," Avco Corporation, Contract No. F33(615)-67-C-1719, Quarterly Report No. 2, January 1968.
53. "Filament Wound Joint Design Study," ACF Industries, Inc., ACF-412-256, October 1965.

Fabrication, processing, and testing details are given for both bonded and bolted joints. Joint configurations include double lap, scarf, stepped lap, interlocked, and multishim designs. A number of materials were inserted at bondlines, and the addition of tungsten filaments increased the bond strength of these. Maraging steel shims required careful processing, but stainless steel shims yielded successful joints. Results of tests are given as arithmetic means and standard deviations.

54. MIL-Hdbk-17, "Plastics for Flight Vehicles, Part 1, Reinforced Plastics," May 1964.

This handbook summarizes design information to its date of publication. It deals mainly with glass fiber woven cloths, with only brief mention of parallel filament composites.

Unclassified
Security Classification

DOCUMENT CONTROL DATA - R&D		
<i>(Security classification of title, body of abstract and indexing annotation must be entered when the overall report is classified)</i>		
1 ORIGINATING ACTIVITY (Corporate author) Douglas Aircraft Company McDonnell Douglas Corporation		2a REPORT SECURITY CLASSIFICATION Unclassified
		2b GROUP
3 REPORT TITLE Investigation of Joints in Advanced Fibrous Composites for Aircraft Structures		
4 DESCRIPTIVE NOTES (Type of report and inclusive dates) Final report of work conducted between 25 April 1967 and 28 March 1969		
5 AUTHOR(S) (Last name, first name, initial) Lehman, George M. Hawley, Arthur V. et al.		
6 REPORT DATE June 1969	7a TOTAL NO OF PAGES 240	7b NO OF REFS 23
8a CONTRACT OR GRANT NO. F33615-67-C-1582	9a ORIGINATOR'S REPORT NUMBER(S) DAC 68498	
b. PROJECT NO. c. d.	9b OTHER REPORT NO(S) (Any other numbers that may be assigned this report) AFFDL-TR-69-43, Vol. I	
10 AVAILABILITY/LIMITATION NOTICES This document is subject to special export controls, and each transmittal to foreign governments or foreign nationals may be made only with prior approval of AFFDL (FDTIC) Wright-Patterson AFB, Ohio 45433.		
11 SUPPLEMENTARY NOTES	12 Structures Division Air Force Flight Dynamics Laboratory Wright-Patterson AFB, Ohio 45433	
13 ABSTRACT To find ways of efficiently joining composite materials, an investigation was undertaken to explore design philosophies, identify parameters affecting joint strength and life, establish design approaches for aircraft applications, and compile design data. Properties of boron and S-994 fiber glass laminates using Narmco 5505 resin were determined in tension, compression, in-plane shear, interlaminar shear, and pin-bearing tests. In comparing six adhesives, a nylon-epoxy adhesive was found to have the best combination of shear strength and ductility (except in scarf joints, where ductility is less important). Ultimate strength and fatigue data were determined for a variety of bonded joint and bolted joint test specimens. The bonded joint concepts included single and double lap, stepped lap, scarf, and variable stiffness adhesive joints. The bolted joint concepts included laminates with plain holes and with reinforced holes using either composite or steel shim reinforcing or steel bushings. The effects of design parameter variations on joint failure modes were determined, and parametric strength trends were analyzed. Design parameters influencing bonded joint failures the most were adherend and adhesive properties (strength and stiffness), lap length, adherend thickness, and fiber orientation adjacent to the adhesive. Bolted joint failures were most affected by laminate strength and stiffness, edge distance, fastener pitch, laminate thickness, and fastener diameter. A combination bolted-bonded joint performed better than joints employing either bolting or bonding separately because of a fundamental change in failure mode caused by		

DD FORM 1473 0101-807-6800

Unclassified
Security Classification

Unclassified

Security Classification

14 KEY WORDS	LINK A		LINK B		LINK C	
	ROLE	WT	ROLE	WT	ROLE	WT
Fibrous Composites Boron Fiber Glass Joint Design, Bonded and Bolted Adhesives Analysis, Linear Analysis, Nonlinear						

INSTRUCTIONS

1. **ORIGINATING ACTIVITY:** Enter the name and address of the contractor, subcontractor, grantee, Department of Defense activity or other organization (*corporate author*) issuing the report.
- 2a. **REPORT SECURITY CLASSIFICATION:** Enter the overall security classification of the report. Indicate whether "Restricted Data" is included. Marking is to be in accordance with appropriate security regulations.
- 2b. **GROUP:** Automatic downgrading is specified in DoD Directive 5200.10 and Armed Forces Industrial Manual. Enter the group number. Also, when applicable, show that optional markings have been used for Group 3 and Group 4 as authorized.
3. **REPORT TITLE:** Enter the complete report title in all capital letters. Titles in all cases should be unclassified. If a meaningful title cannot be selected without classification, show title classification in all capitals in parenthesis immediately following the title.
4. **DESCRIPTIVE NOTES:** If appropriate, enter the type of report, e.g., interim, progress, summary, annual, or final. Give the inclusive dates when a specific reporting period is covered.
5. **AUTHOR(S):** Enter the name(s) of author(s) as shown on or in the report. Enter last name, first name, middle initial. If military, show rank and branch of service. The name of the principal author is an absolute minimum requirement.
6. **REPORT DATE:** Enter the date of the report as day, month, year, or month, year. If more than one date appears on the report, use date of publication.
- 7a. **TOTAL NUMBER OF PAGES:** The total page count should follow normal pagination procedures, i.e., enter the number of pages containing information.
- 7b. **NUMBER OF REFERENCES:** Enter the total number of references cited in the report.
- 8a. **CONTRACT OR GRANT NUMBER:** If appropriate, enter the applicable number of the contract or grant under which the report was written.
- 8b, 8c, & 8d. **PROJECT NUMBER:** Enter the appropriate military department identification, such as project number, subproject number, system numbers, task number, etc.
- 9a. **ORIGINATOR'S REPORT NUMBER(S):** Enter the official report number by which the document will be identified and controlled by the originating activity. This number must be unique to this report.
- 9b. **OTHER REPORT NUMBER(S):** If the report has been assigned any other report numbers (*either by the originator or by the sponsor*), also enter this number(s).
10. **AVAILABILITY/LIMITATION NOTICES:** Enter any limitations on further dissemination of the report, other than those

imposed by security classification, using standard statements such as:

- (1) "Qualified requesters may obtain copies of this report from DDC."
- (2) "Foreign announcement and dissemination of this report by DDC is not authorized."
- (3) "U. S. Government agencies may obtain copies of this report directly from DDC. Other qualified DDC users shall request through _____."
- (4) "U. S. military agencies may obtain copies of this report directly from DDC. Other qualified users shall request through _____."
- (5) "All distribution of this report is controlled. Qualified DDC users shall request through _____."

If the report has been furnished to the Office of Technical Services, Department of Commerce, for sale to the public, indicate this fact and enter the price, if known.

11. **SUPPLEMENTARY NOTES:** Use for additional explanatory notes.

12. **SPONSORING MILITARY ACTIVITY:** Enter the name of the departmental project office or laboratory sponsoring (*paying for*) the research and development. Include address.

13. **ABSTRACT:** Enter an abstract giving a brief and factual summary of the document indicative of the report, even though it may also appear elsewhere in the body of the technical report. If additional space is required, a continuation sheet shall be attached.

It is highly desirable that the abstract of classified reports be unclassified. Each paragraph of the abstract shall end with an indication of the military security classification of the information in the paragraph, represented as (TS), (S), (C), or (U).

There is no limitation on the length of the abstract. However, the suggested length is from 150 to 225 words.

14. **KEY WORDS:** Key words are technically meaningful terms or short phrases that characterize a report and may be used as index entries for cataloging the report. Key words must be selected so that no security classification is required. Identifiers, such as equipment model designation, trade name, military project code name, geographic location, may be used as key words but will be followed by an indication of technical context. The assignment of links, roles, and weights is optional.

Unclassified

Security Classification